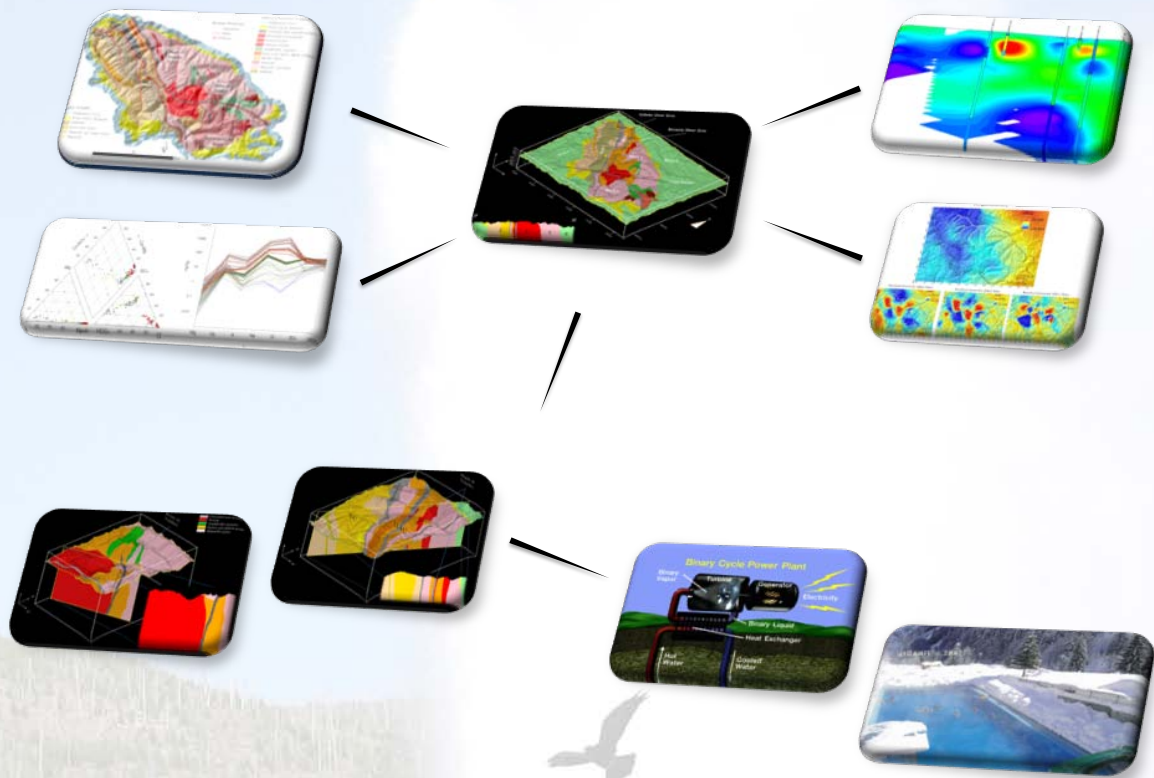


Multidisciplinary Approach of Geothermal Prospection in the Argentera Massif (South-Western Alps)



Luca Guglielmetti

PhD thesis, University of Neuchatel, Switzerland, 2012

Multidisciplinary Approach of Geothermal Prospection in the Argentera Massif (South-Western Alps)

by

Luca Guglielmetti

PhD thesis in co-tutoring between the Faculty of Sciences of the University of Turin (Italy) and the Faculty of Sciences of the University of Neuchâtel (Switzerland) to satisfy the requirements of the degree of Doctor of Philosophy in Science

PhD thesis evaluation committee:

| | |
|-----------------------|---|
| Prof. Eva Schill | Thesis director (Université de Neuchâtel, Centre D'Hydrogéologie et Géothermie, Neuchâtel, Switzerland) |
| Dr. Giuseppe Mandrone | Thesis director (Università di Torino, Dipartimento di Scienze della Terra, Torino, Italy) |
| Prof. Francesca Verga | Examiner (Politecnico di Torino, Dipartimento di Ingegneria del Territorio, dell'Ambiente e delle Geotecnologie, Torino, Italy) |
| Prof. Thomas Kohl | Examiner (Karlsruher Institut für Technologie Institut für Angewandte Geowissenschaften, Karlsruhe, Germany) |
| Dr. Isabella Nardini | External Referee (Centre of Excellence for Geothermal Energy Larderello, Lardarello, Italy) |

IMPRIMATUR POUR LA THESE

Multi-disciplinary approach for geothermal prospection in the Argentera Massif (South-Western Alps)

Luca GUGLIELMETTI

REALISEE EN COTUTELLE AVEC

L'UNIVERSITE DE TURIN (I)

et

L' UNIVERSITE DE NEUCHATEL (CH)

FACULTE DES SCIENCES

La Faculté des sciences de l'Université de Neuchâtel,
sur le rapport des membres du jury

Prof. Eva Schill (co-directrice de thèse), UniNe
Prof. Giuseppe Mandrone (co-directeur de thèse), Université de Turin
Prof. Francesca Verga, DITAG, Turin
Prof. Thomas Kohl, Karlsruhe Institute of Technology

autorise l'impression de la présente thèse.

Neuchâtel, le 5 juin 2012

Le doyen :
P. Kropf

Thesis jury defence date: February 22nd, 2012
Public presentation date: June ,2012

to my parents

Acknowledgements

A PhD is something that will always be engraved in the memory of each Doctor.

It requires a lot of energies, sometimes it's fun (most of the time actually), sometimes it's just troubles and frustration.

To me the doctorate has been an incredible opportunity to learn from many many many people in Turin and in Neuchatel.

For this reason I would like to thank my supervisors Giuseppe, Eva and Cesare for their constant support and for giving me the chance and the freedom to develop the project how I wanted to be. I also would like to thank Romain for helping me in water sampling, Enrico and Vittorio for the geochemical analyses, Adele Manzella, Serena and Carlo (CNR, Pisa) and Pascal Sailhac (EOST, Strasbourg) for providing the instruments and some strong arms for the magnetotelluric surveys. I would like to also thank my "personal" assistant Patrizio who shared with me the most part of the field work, hiking with many kilos of instruments in our backpacks. Of course a big of thank you to Roberta for making me laugh and breaking the quiet of the rough mountains with a LOT of words.

Two years in Neuchatel have been simply great, mostly thanks to my coworkers at CHYN. A special thanks to Francois-David for being a living geothermal database and for being always there when I needed suggestion, to Yassine for teaching me so much, not only about geophysics, to Francois "Paco" who helped me a lot, especially in the field and for introducing me to the "wild" nightlife in Neuchatel.

A great time is so because of great people.

People like Paul, Geoffrey, Lilou and Gennaro.

People like Giulia, Valerio&Giulia, who are really special people.

Thanks to ALL

EXTENDED ABSTRACT

Keywords: Argentera Massif, Geothermics, Geochemistry, 3D Modelling, Gravity, Magnetotelluric, Geothermal Potential

PART I - Introduction

The present thesis was developed in co-tutoring between the Dipartimento di Scienze della Terra of the University of Turin in Italy and the Centre d'Hydrogéologie et Géothermie of the University of Neuchâtel in Switzerland. Thanks to this collaboration, the project benefit from the geological and geophysical understanding of the study region from the Turin department and of the geochemical, geophysical and 3D modelling knowledge from the Swiss institution.

This thesis aims at developing a new multi-disciplinary concept to characterize geological and structural subsurface condition relevant to geothermal exploitation of local reservoirs in Alpine environment. In the past, most of the information of such type of reservoirs was gained through geochemical analysis of thermal fluids, which may provide indication for the infiltration area, the circulation path, and the reservoir temperature. In this study, additionally to new geological observations and fluid chemical data, new prospection methods were employed. 3D geological modelling and gravity and magnetotelluric geophysical methods were used to investigate the subsurface and constrain the region where thermal waters might circulate down to several kilometres in depth. The integration of the data from the different approaches allowed estimating the parameters (e.g. rock density and porosity, reservoir volume and temperature, flow rate), relevant to determine the geothermal potential of the study areas and suggest optimized exploitation of the geothermal resource for power and/or heat production.

PART I – Geothermal systems in Alpine regions

This chapter describes the different types of geothermal systems and the worldwide present day exploitation of the geothermal resource (power generation and direct uses) with particular focus on the recent development of binary power plants for electric generation, used for power production from low temperature geothermal fluids.

In north-western Italy volcanic activity is absent. Therefore the presence of geothermal anomalies at surface is related to local geological conditions, which allow the water circulation in the subsurface and formation of hot springs. The circulation of these waters is related to deep groundwater systems, which are considered as dynamic, advective low enthalpy geothermal systems. In Alpine regions thermal waters discharge from thermal springs or are pumped from boreholes and are used mainly for spa bathing and sometimes for heating buildings or drinking water.

Two sites were selected as study areas: Bagni di Vinadio and Terme di Valdieri. They were selected because of the observed geothermal conditions and the availability of geological and geochemical data. Moreover these two sites shows the highest concentration of thermal springs related to fault networks, and the highest natural flow rates and temperatures of the entire Alpine chain. The hydrothermal area of Bagni di Vinadio is located at about 1350 m a.s.l. The hot springs of Bagni di Vinadio are located within an area of 500 m². Three shallow

wells were drilled and catch thermal waters at about 80 m in depth with temperature up to 70°C. Part of the hot springs is located within the thermal baths buildings and hot waters discharging from these springs are directly used for the spa. The thermal springs of Terme di Valdieri are located at 1370 m a.s.l. At Terme di Valdieri the thermal springs are mainly located in a cave of about 100 m². The temperature ranges between 28 and 65°C within few meters of distance. Most of the hot springs are located in three caves and are used for thermal baths.

PART II – Geological setting

The Argentera Massif is the southernmost of the External Crystalline Massifs ECM of the Western Alps and it represents a portion of deep crust cropping out as a pop-up structure thanks to the complex tectonic condition of the region. It is mainly composed by high-grade metamorphic rocks (schist, migmatitic paragneiss, amphibolites, diatexite and anatexitic granitoid), locally intruded by post metamorphic granitic bodies. The crystalline rocks are unconformably overlaid by Triassic to Early Cretaceous carbonates that are mostly detached above the Late Triassic evaporite. The Alpine structures cross-cutting the AM are represented mainly by ductile shear zones, strike-slip and reverse faults, often reactivating pre-Alpine and early-Alpine structures.

At Bagni di Vinadio thermal springs discharge through intensely fractured leucogranites and migmatitic gneiss. The hot springs are located at the step-over zone between two brittle shear zones with dextral sense of shear. The thermal springs of Terme di Valdieri are located in correspondence of the northern termination of the 200m-wide cataclastic shear zone. The structural setting of Terme di Valdieri is controlled by pervasive en-echelon NW–SE to NNW–SSE directed faults showing evidences of right-lateral displacement and cutting the migmatites and the granitic body with persistence up to 10 km.

The geological observations carried out in this study allowed understanding the complexity of the region in particular of the fault networks and their relations with the surrounding rock formations. Moreover detailed observations in the proximities of the springs showed that the final upflow of the thermal waters at both sites is strictly related to some sets of low angle minor fractures which are connected at depth to the major fault zones.

The geological observations allowed understanding the complexity of the region in particular of the fault networks and their relations with the surrounding rock formations. Moreover detailed observations in the proximities of the springs showed that the final upflow of the thermal waters at both sites is strictly related to some sets of low angle minor fractures which are connected at depth to the major fault zones. Available geological data (field observations, geological maps and cross sections) were used as main data source for the starting geological model.

PART III – Geochemical investigations

In this part the methods of water sampling and analyses are described and the results of two new sampling campaigns were compared to previous studies. Major ions, trace elements, stable isotopes of Hydrogen and Oxygen and Tritium were analysed.

Geochemical data pointed out the differences in terms of chemical composition of the thermal waters discharging at the two sites. These differences suggest that thermal springs are recharged by two separate geothermal systems. At Vinadio the hot waters probably have

a circulation path and residence time longer than those at Valdieri, as suggested by the increased salinity and the higher temperature of the reservoir. In particular the high salinity was studied using the Cl/Br molar ratio and highlighted that the contribution of fluid inclusions which are rich in Chloride can't be neglected but at the same time can't totally justify the high salinity. In fact the Cl/Br ratio values for Vinadio are characteristic of waters interacting with evaporite formations which, in the study area, entirely surround the Argentera Massif and are locally pinched in main structures of the massif.

Geochemical investigations also provided the average elevation of the recharge basins, the reservoir temperature (130°C at Vinadio and 100°C at Valdieri), the residence time and the depth of the circulation paths (up to 5km)

PART IV – 3D geological modelling

The utilization of 3D models has been an important tool employed in the thesis because it allowed collecting all the scattered geological data to build *a-priori* 3D geological models according to geological information. Moreover the models were calibrated and validated according to geophysical data by means of forward modelling and 2D inversion processing. The software employed in the thesis, 3D-Geomodeller[®] by INTREPID Geophysics, was developed with the goal to infer 3D geological models taking into account the usually scarce and scattered field data, which are usually available to geologists.

The goal of the preliminary phase was to keep the geological complexity on the basis of strict interpretations but at the same time to produce models which can be used as the basic tool to integrate geology and geophysical data. A model of the entire Argentera Massif was computed to understand the efficacy of the modelling software and then 2 more detailed models were created for the two study sites. The two latter models were then employed to integrate the results of the geophysical surveys.

PART V – Geophysical surveys

Gravity and magnetotelluric MT methods were employed to investigate the subsurface and provided important information on density and electrical resistivity distribution at depth.

Two gravity surveys were carried out in summer 2010 and spring 2011 on the entire Italian side of the Argentera Massif collecting 403 stations, which were tied to the International Gravimetric Bureau BGI stations which covered to outer regions. Gravity data were reduced to complete Bouguer gravity anomalies with a reduction density of 2.67 g/cm³ by applying the reductions and corrections to a 167 kilometres radius. Moreover the Bouguer Anomaly was filtered using a high-pass Butterworth filters at 50, 20 and 10 kilometres. The application of a high-pass filter to a Bouguer Anomaly produces *residual anomalies* removing the wavelengths related to regional trend and to the effect of deep and regional masses emphasizing the effect of shallow structures in the subsurface. This is a crucial step if gravity data will be integrated into a 3D geological model.

Two MT surveys were accomplished in summer 2010 and spring 2011 in the Italian side of the Argentera to detect the electrical resistivity distribution up to 10 kilometres in depth and to figure out any relationship between resistivity variations and geological structures. The time series of each station were elaborated to come out with satisfying transfer functions removing the known sources of noise (e.g. 50 and 150 Hz). Then entire spectrum of frequencies

was processed and the MT data were finally edited and modelled. Even though 2D inverted models have been obtained, they resulted poorly indicative for such complex and three-dimensional geologic context. Therefore the interpretations are limited to inverted 1D profiles and interpolated to produce 2D sections of apparent resistivity.

The comparison of the results of both methodologies on 2D cross sections suggested that the correlation between some low density regions can be coupled to low resistivity distributions suggesting enhanced fracture conditions in the subsurface where thermal waters might circulate.

PART V – Integration between 3D models and geophysical results

The goal of this part was to integrate geophysical observations, in particular gravity, into the 3D models of the Bagni di Vinadio and Terme di Valdieri areas to eventually improve the geological models in the subsurface in terms of density distribution. Hence density values for each formation in the model were set using the employed modelling software and the gravity effect of the model was computed and compared to the residual anomaly. Then the 10km-anomaly was chosen for both regions as it showed the lower misfit compared to the average gravity response of the model. The residual anomaly values were plotted on selected profiles which then were processed using a 2D inversion code which was created during the thesis. The results of inversion show the geometries, the depth and the density variations along the profiles. Hence they were be used in the 3D models to better constrain the geometries and the density values for each formation. As a consequence the 3D models were modified according to the results of the 2D inversion until a satisfying fit with the residual anomaly was reached. This phase also allowed estimating the volume of the low density regions at the thermal springs and its porosity, which was compared that estimated by the MT method (8-11% at Vinadio and 10-15% at Valdieri).

PART VI – Geothermal potential estimation

The geothermal potential of a site can be divided into thermal energy and electrical power outputs, which can be extracted from the geothermal fluid. The former can be assessed using the *Surface Thermal Flux* and the *Volume* methods. The latter can be estimated using the *Net Electric Power* and the *Exergy* methods. These methods requires some parameters, such as temperature at the surface and in the reservoir, flow rate, rock density, reservoir volume and its porosity, which can be inferred by the multidisciplinary approach developed in the thesis.

The results showed that the geothermal resource is only partially exploited according to the present day usages of the thermal waters at both sites. For the two thermal sites it was possible to estimate that, if the thermodynamic conditions of the geothermal fluid in the reservoir are confirmed, electric power production can be envisaged, in particular at Bagni di Vinadio, where the reservoir temperature might be more favourable. Finally, the geothermal potential is estimated to be in the order of $\sim 300\text{kW}_{\text{EL}}$ and heat for about 250 habitants. Moreover such approach can benefit of a cascade approach of utilization, keeping the thermal baths activity as a priority. The deep fluid at high temperature can be used for power generation. Then the fluids can be directly exploited for the spas and then for heating building using heat pumps or de-icing the roads during the winter season. A flexible scenario can be also predicted. In fact, for the higher temperature range, it could be possible to focus

the exploitation of the resource for power generation during summer season and switch to heat production during the winter period when the need of heat is predominant.

PART VII – Discussion and future research

The presented work provided an example on how data from different sources can be integrated and jointly interpreted to come out with an overview of the general geological conditions controlling thermal water circulation in challenging areas such as the Alpine regions. Moreover it has been possible to gather the parameters in terms of flow rate, temperature at depth, reservoir volume, rock density and porosity, which have been used to calculate the geothermal potential.

The geological observations, jointly interpreted with the geochemical investigations allowed understanding the complexity of the region and of the circulation paths of the thermal fluids. In particular fault networks, their relations with the surrounding rock formations and the water-rock interactions allowed constraining the main structures related to the deep circulations and their geometries. Moreover detailed observations in the proximities of the springs showed that the final upflow of the thermal waters at both sites is strictly related to some sets of low angle minor fractures which are connected at depth to the major fault zones

The utilization of 3D models has been the core of the thesis. Thanks to the integration of forward modelling and inversion processing it has been possible to modify the geological models interpreting these anomalies as zones of increased porosity of the rock related to enhanced fracture density in the subsurface where the presence of deep fluid can be hypothesized.

Finally the integration of all these methodologies also allowed extracting the main parameters needed to estimate the geothermal potential of the study areas. Several methods were used to calculate the geothermal potential in terms of heat and power generation and optimized utilization of the geothermal resources were proposed to maximise the exploitation of the thermal waters at the two study sites.

TABLE OF CONTENTS

| | |
|--|--------|
| EXTENDED ABSTRACT | ix |
| TABLE OF CONTENTS | xv |
| ABSTRACT | xix |
| RESUMÉ | xxi |
| 1 INTRODUCTION | - 1 - |
| 1.1. Motivations | - 3 - |
| 1.2. Structure of the Study | - 6 - |
| 1.3. Generalities about the geothermal resource at Bagni di Vinadio..... | - 7 - |
| 1.4. Generalities about the geothermal resource at Terme di Valdieri | - 8 - |
| 2 GEOTHERMAL SYSTEMS IN ALPINE REGIONS | - 11 - |
| 2.1. General introduction to geothermal energy systems and utilizations..... | - 13 - |
| 2.2. Binary plants for geothermal power generation | - 18 - |
| 2.3. Geothermal resources in the Alps | - 19 - |
| 2.4. Geothermal exploration methods applied in Alpine context..... | - 23 - |
| 2.4.1. Structural geology | - 23 - |
| 2.4.2. Exploration wells and alpine tunnels..... | - 25 - |
| 2.4.3. Geochemistry of the fluids | - 28 - |
| 2.4.4. 3D geological modelling..... | - 29 - |
| 2.4.5. Geophysical exploration | - 30 - |
| 3 GEOLOGICAL SETTING AND STRUCTURAL GEOLOGY | - 33 - |
| 3.1. The External Crystalline Massifs of the Western Alps..... | - 35 - |
| 3.2. The Argentera Massif | - 36 - |
| 3.2.1. The Sedimentary Cover of the Argentera Massif..... | - 38 - |
| 3.2.2. The Crystalline Basement and its Structures | - 40 - |
| 3.2.3. Geodynamic Evolution and Exhumation of the Argentera Massif..... | - 42 - |
| 3.3. Relationships between Geomorphology and Structures..... | - 43 - |
| 3.4. Seismicity of the Western Alps and the Argentera Massif | - 44 - |
| 4 GEOLOGICAL FRAMEWORK OF THE INVESTIGATION SITES - | 47 - |
| 4.1. Geology and boreholes at Bagni di Vinadio | - 49 - |

| | | |
|----------|--|----------------|
| 4.1.1. | Geological observations..... | - 49 - |
| 4.2. | Boreholes..... | - 54 - |
| 4.3. | Geological Setting of the Terme di Valdieri Area | - 56 - |
| 4.3.1. | Geological observations..... | - 56 - |
| 4.4. | Boreholes..... | - 60 - |
| 5 | GEOCHEMICAL INVESTIGATIONS..... | - 63 - |
| 5.1. | Geochemical investigations..... | - 65 - |
| 5.1.1. | On site measurements..... | - 65 - |
| 5.1.2. | Chemical analysis..... | - 65 - |
| 5.1.3. | Water chemistry | - 66 - |
| 5.1.4. | Mixing processes | - 66 - |
| 5.1.5. | Water-rock interactions | - 67 - |
| 5.1.6. | Flow Systems..... | - 67 - |
| 5.1.7. | Reservoir Temperature | - 68 - |
| 5.1.8. | Residence Time..... | - 72 - |
| 5.2. | The Bagni di Vinadio Thermal Site..... | - 73 - |
| 5.2.1. | Water Chemistry | - 73 - |
| 5.2.2. | Mixing Processes..... | - 74 - |
| 5.2.3. | Water-Rock Interactions..... | - 79 - |
| 5.2.4. | Origin and Elevation of the Recharge Zone..... | - 81 - |
| 5.2.5. | Reservoir Temperature | - 84 - |
| 5.2.6. | Groundwater Residence Time | - 87 - |
| 5.3. | The Terme di Valdieri Thermal Site..... | - 88 - |
| 5.3.1. | Water Chemistry | - 88 - |
| 5.3.2. | Mixing Processes..... | - 91 - |
| 5.3.3. | Water-Rock Interactions..... | - 94 - |
| 5.3.4. | Origin and Elevation of the Recharge Zone..... | - 94 - |
| 5.3.5. | Reservoir Temperature | - 97 - |
| 5.3.6. | Groundwater Residence Time | - 99 - |
| 6 | 3D GEOLOGICAL MODELLING | - 101 - |
| 6.1. | Concepts and Methods | - 103 - |
| 6.1.1. | Data Type | - 104 - |
| 6.2. | Computing the 3D Models of the study sites..... | - 105 - |

| | | |
|----------|--|----------------|
| 6.2.1. | Definition of the topography..... | - 106 - |
| 6.2.2. | Definition of the extent of the model..... | - 106 - |
| 6.2.3. | Collection of the available data..... | - 106 - |
| 6.2.4. | Modelling criteria..... | - 106 - |
| 6.2.5. | Results..... | - 110 - |
| 7 | GEOPHYSICAL SURVEYS IN THE ARGENTERA MASSIF | - 117 - |
| 7.1. | Concepts and Methods..... | - 119 - |
| 7.1.1. | The gravity method..... | - 119 - |
| 7.1.1.1. | Gravity reductions..... | - 120 - |
| 7.1.1.2. | Application of the GraviFor3D code to calculate the Bouguer Anomaly of the Argentera Massif..... | - 122 - |
| 7.1.1.3. | Inversion processing of the gravity data..... | - 123 - |
| 7.1.1.4. | Laboratory density measurements..... | - 125 - |
| 7.2. | The magnetotelluric method..... | - 127 - |
| 7.3. | Gravity Observations in the Argentera Massif..... | - 130 - |
| 7.3.1. | Comparison between the original data and the results of the GraviFor3D code..... | - 130 - |
| 7.3.2. | Field data collection..... | - 132 - |
| 7.3.3. | Data processing and results..... | - 134 - |
| 7.3.4. | Integration of the computed models to the 3D geology..... | - 137 - |
| 7.3.4.1. | The Bagni di Vinadio area..... | - 138 - |
| 7.3.4.2. | The Terme di Valdieri study area..... | - 145 - |
| 7.4. | The Magnetotelluric campaigns in the Argentera Massif..... | - 153 - |
| 7.4.1. | Data collection in the Argentera Massif..... | - 155 - |
| 7.4.2. | Data treatment..... | - 156 - |
| 7.4.3. | Joint interpretation with gravity models..... | - 161 - |
| 8 | EVALUATION OF THE GEOTHERMAL POTENTIAL AND USAGE PROPOSALS..... | - 167 - |
| 8.1. | Geothermal Potential Estimation Methods..... | - 169 - |
| 8.2. | Surface Thermal Flux method..... | - 170 - |
| 8.2.1. | The Volume method..... | - 170 - |
| 8.2.2. | Net Electric Power Method..... | - 171 - |
| 8.2.3. | The Exergy concept..... | - 171 - |
| 8.3. | Estimations for the Study Areas..... | - 173 - |

| | | |
|----------|---|---------|
| 8.3.1. | Surface Thermal Flux | - 173 - |
| 8.3.2. | Volume Method | - 174 - |
| 8.3.3. | Net Electric Power NEP method | - 175 - |
| 8.3.4. | Exergy | - 175 - |
| 8.4. | Production Proposals..... | - 176 - |
| 9 | DISCUSSION AND FUTURE RESEARCH | - 179 - |
| 9.1. | Results | - 181 - |
| 9.2. | Future Research | - 183 - |
| | REFERENCES | - 185 - |

ABSTRACT

Keywords: Argentera Massif, Geothermics, Geochemistry, 3D Modelling, Gravity, Magnetotelluric, Geothermal Potential

This thesis aims at developing a new multi-disciplinary concept to characterize geological and structural subsurface condition relevant to geothermal exploitation of local reservoirs in Alpine environment. In the past, most of the information of such type of reservoirs was gained through geochemical analysis of thermal fluids, which may provide indication for the infiltration area, the circulation path, and the reservoir temperature. In this study, additionally to new fluid chemical data, three main aspects were included:

- Detailed observation of fracture networks at the surface close to the thermal springs.
- Acquisition of new gravity and magnetotelluric data to gather information about the density and resistivity distribution in the subsurface, which may be indicative for existing fracturation and the occurrence of deep geothermal fluid circulation.
- 3D geological models to integrate the structural and geochemical observations and geophysical data for constraining geological structures that may be involved in the thermal fluid circulation.

The integration of these methods allowed a better understanding of the physical conditions related to thermal anomalies in the deep subsurface of Alpine systems. Two geothermal sites have been chosen to test this concept: Bagni di Vinadio and Valdieri in the Italian Argentera Massif (AM). The findings of this comprehensive approach have been finally used to infer the geothermal productivity of the local reservoirs in these two areas.

The geological observations revealed different sets fractures. Thermal springs at both sites are located along an NE-SW oriented low-angle set of fractures dipping towards SE that is directly connected to the main steep fault systems oriented NW-SE. The vertical upflow of the thermal fluids seems to be related to the intersecting fault systems.

Geochemical investigations point out the differences in terms of chemical composition of thermal waters at the two study areas. The main difference is the anomalous high chloride content in thermal water at Vinadio, where springs reach a temperature of 70°C. In contrast, the Na-SO₄ water type at Valdieri reveals typical water circulating in crystalline massifs. The Cl/Br molar ratio reveals the origin of the salinity at Vinadio: a possible interaction of the thermal water of Vinadio with the evaporitic formations which surround the AM and that can be pinched within the main structures of the massif. Reservoir temperatures were estimated to 130°C at Vinadio and 100°C at Valdieri.

Gravity and magnetotelluric methods were employed to investigate the subsurface and provided important information on density and electrical resistivity distribution at depth. The main result was the identification of low density regions in the area of the thermal springs, which can be related to a reduction of density by fracturation. Three dimensional geological modelling was employed, in particular, to infer the structural setting at depth from the observations at the surface. The two models were then combined to geophysical observations and finally modified to match the geophysical results by means of forward modelling and inversion processing. In this way, the location, the volume and the porosity of the reservoir zones of the thermal springs was estimated.

Finally, several methods of estimating the productivity of these deep reservoirs were compared. The geothermal potential is estimated to be in the order of $\sim 300\text{kW}_{\text{EL}}$ and heat for about 250 habitants under the condition to install a cascade approach.

RESUMÉ

Mots-clés: Massif de l'Argentera Massif, Géothermie, Géochimie, Modélisation 3D, Gravimétrie, Magnétotellurique, Potentiel Géothermique

Cette thèse vise à développer un nouveau concept multidisciplinaire pour caractériser l'état géologique et structural du sous-sol indispensable pour la prospection et l'exploitation des réservoirs géothermiques locaux dans l'environnement alpin. Dans le passé, la plupart des informations de ce type de réservoirs ont été acquises grâce à l'interprétation des données géochimiques des fluides thermaux, qui peuvent fournir des indications sur la zone d'infiltration, les modes de circulation souterraine et la température du réservoir. Dans cette étude, en outre, de nouvelles données chimiques des fluides, trois aspects principaux ont été inclus:

- Observation détaillée des réseaux de fractures en surface à proximité des sources thermales.
- Acquisition de données gravimétriques et magnétotelluriques pour recueillir des informations sur la densité et la distribution de résistivité dans le sous-sol, qui peuvent donner des indications sur la fracturation existante et la présence du fluide géothermique en profondeur.
- Modélisation géologique en 3D pour intégrer les observations structurales, géochimiques et les données géophysiques, pour contraindre les structures géologiques potentiellement impliquées dans la circulation du fluide thermal.

L'intégration de ces méthodes a permis une meilleure compréhension des conditions géologiques liés à des anomalies thermiques du sous-sol dans des systèmes hydrothermaux en milieu alpin. Deux sites géothermiques ont été considérés pour tester ce concept: Bagni di Vinadio et Valdieri dans le Massif de l'Argentera (AM). Les résultats de cette approche ont été finalement utilisés pour déduire le potentiel géothermique de ces deux systèmes.

Les observations géologiques ont révélé différents systèmes de fractures. Les sources thermales des deux sites sont localisés le long d'une direction NE-SO dont les fractures ont un faible pendage vers le SE. Ces fractures (ces sites ?) sont directement relié(e)s aux principaux systèmes de failles décrochantes orientées NW-SE. Les eaux thermales remontent le long les failles principales, mais ce sont les systèmes de failles croisant ces dernières qui contrôlent la sortie des fluides thermaux en surface, ou le mélange entre eaux thermales et eaux froides superficielles.

Les études géochimiques ont souligné les différences de composition chimique des eaux thermales sur les deux sites d'étude. La principale différence est la teneur en chlorure qui est beaucoup plus élevée dans l'eau thermale à Vinadio, de type Na-Cl, où les sources atteignent une température de 70° C. En revanche, le type d'eau Na-SO₄ à Valdieri est typique des circulations profondes dans les massifs cristallins. Le rapport Cl/Br donnent des informations quant à l'origine de la salinité à Vinadio: une interaction de l'eau thermale de Vinadio avec les formations évaporitiques, qui entourent le Massif de l'Argentera, mais qui peuvent aussi être pincées dans les principales structures du massif. Les températures du réservoir ont été estimées à 130 °C à Vinadio et 100 °C à Valdieri.

Les méthodes gravimétriques et magnétotelluriques ont été utilisées pour enquêter sur les informations du sous-sol et ont permis d'obtenir d'importantes informations sur les variations de la densité et de la distribution de la résistivité électrique en profondeur. Le résultat principal a identifié des régions à faible densité dans la zone des sources thermales, qui peuvent être liées à une réduction

de la densité par la fracturation. La modélisation géologique tridimensionnelle a été employée, en particulier, pour contraindre les structures géologiques et leurs paramètres physiques en profondeur à partir des observations en surface. Les deux modèles ont ensuite été combinés aux observations géophysiques et finalement modifiés et validés pour correspondre aux résultats géophysiques, au moyen de la modélisation directe et inverse. De cette façon, l'emplacement, le volume et la porosité des réservoirs hydrothermaux ont été estimés.

Finalement, plusieurs méthodes d'estimation du potentiel géothermique ont été comparées. Le potentiel géothermique est estimé à environ 300kW_{EL} pour la production électrique et aux besoins en chaleur d'environ 250 habitants, à condition d'utiliser une approche en cascade.

1

INTRODUCTION

1.1. Motivations

The present thesis was developed in co-tutoring between the Dipartimento di Scienze della Terra of the University of Turin in Italy and the Centre d'Hydrogéologie et Géothermie of the University of Neuchâtel in Switzerland. Thanks to this collaboration, the project benefit from the geological and geophysical understanding of the study region from the Turin department and of the geochemical, geophysical and 3D modelling knowledge from the Swiss institution.

The increasing need of clean and renewable energy production combined with the social willingness to reduce CO₂ emissions is leading to a growing interest in the deep subsurface. Since different technologies for energy production or CO₂ storage in the subsurface are on the way to be developed, the interest of local administrations, research institutions, private companies and developers in the development of the deep underground exploration is growing.

In north-western Italy volcanic activity is absent. Therefore the presence of geothermal anomalies at surface is related to local geological conditions, such as topography, deep sedimentary aquifers, fault systems, which allow the water circulation in the subsurface and formation of hot springs. The circulation of these waters is related to deep groundwater systems, which are considered as low enthalpy geothermal systems. In fact, in low temperature dynamic geothermal systems, such as those studied in this thesis, thermal waters derive from the circulation of infiltrating waters (usually meteoric), which are heated up due the local geothermal gradient conditions and to possible heat sources in the basement. The heat transfer is dominated by advective processes and the upflow is driven by intersecting fault systems that are characterized by higher permeability than the surrounding formations.

In Alpine regions thermal waters discharge from thermal springs or are pumped from boreholes and are used mainly for spa bathing and sometimes for heating buildings or drinking water. Such geothermal systems have usually been studied for their geological, geochemical and hydrogeological aspects. The main questions raised to understand the deep circulation systems in mountainous regions concern the local geological and structural setting and the geochemical composition of the fluids. These two methods, if analyzed by numerical models provide useful information about the dynamic of such system type. However a detailed description of the geological conditions at depth is necessary and none of the previous methods can characterize the subsurface in details. To answer this question geophysical methods are usually the most effective methods that can provide information about the physical properties of the geological formations in the subsurface, even several kilometres in depth.

The present thesis proposes a new multidisciplinary concept of geothermal exploration combining the more traditional geological and geochemical investigations to 3D geological modelling and self potential geophysical methods such as gravity and magnetotelluric. The final goals of the study is the integration of these different methodologies to better understand the subsurface conditions controlling the thermal waters circulation and to come out with the parameters (e.g. rock density and porosity, reservoir volume and temperature, flow rate), relevant to determine the geothermal potential of the study areas and suggest optimized exploitation of the geothermal resource for power and/or heat production.

In the framework of the thesis geological surveys have been carried out in the proximity of the thermal springs to understand the fault and fracture network and the geological formations related to the final upflow of the thermal waters. Moreover geochemical investigations on waters collected during two sampling campaigns have been carried out to improve the set of available data and propose new interpretations. In addition three dimensional geological models were computed for the study sites as they allow understanding the geometry of the geological formations in the subsurface and were then used to integrate data from the different sources (i.e. geology, geochemistry and geophysics). Furthermore gravity and magnetotelluric MT methods were chosen to investigate the subsurface to a depth of about 5 to 10 km, as their application for geothermal reservoir detection is well proven. In fact density and resistivity anomalies can be related to zones of enhanced fracture density and thermal fluid circulation. In Alpine regions gravity has usually been used to detect deep crustal structures or to estimate the thickness of the quaternary filling of the valleys and MT employed to investigate deep structures for geodynamic and tectonic purposes. For the first time in Alpine regions, geological mapping, geochemical investigations coupled with new interpretations deriving from 3D geological modelling and geophysical surveys are jointly interpreted to finally better constrain the results and come out with a better understanding of the subsurface conditions related to the thermal water circulation in the Argentera Massif.

The integration of these investigation methods can provide a scientific base to plan geothermal projects such as drilling deep boreholes, limit the geological uncertainty and better manage a long term exploitation of the geothermal resource.

Two sites were selected as study areas: Bagni di Vinadio and Terme di Valdieri. As shown in Figure 1-1, they are both located in the south-western Alps, at the border between Italy and France, in the Argentera Massif. The choice of these two sites was driven by the observed geothermal conditions and the availability of geological and geochemical data provided by the several studies carried out in the past. In fact the Argentera Massif shows the highest concentration of thermal springs related to fault networks, and the highest natural flow rates and temperatures of the entire Alpine chain. On the geological point of view the Argentera Massif is the southernmost of the External Crystalline Massifs ECM of the Western Alps and it represents a portion of deep crust cropping out as a pop-up structure thanks the complex tectonic condition of the region (cfr Chapter 3).

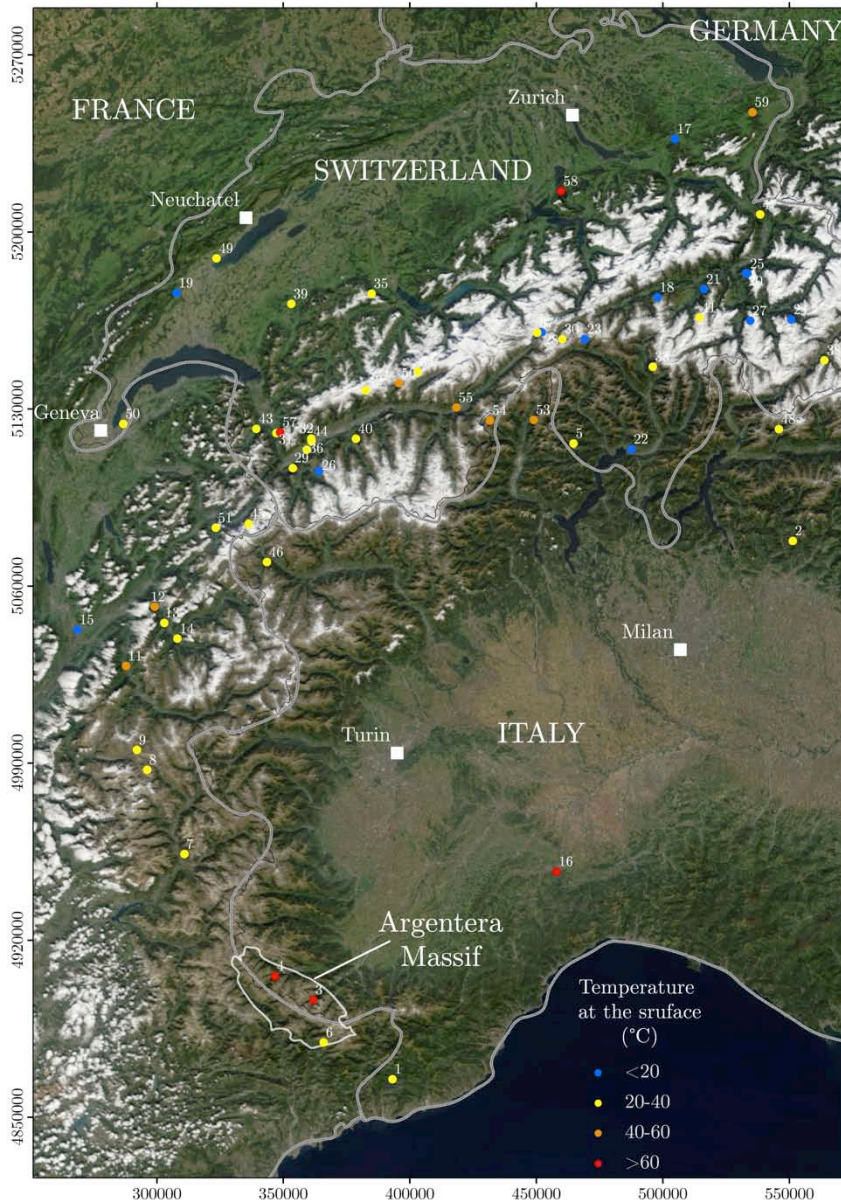


Figure 1-1 Location of the thermal manifestations in the Western Alps and the surrounding regions: 1. Pigna (30.8 °C), 2. Palazzolo (26.1 °C), 3. Valdieri (63.8 °C), 4. Vinadio (65 °C), 5. Bagni di Craveggia (27.5 °C), 6. Berthemont (30 °C), 7. Plan de Phazy (28 °C), 8. Monetier (34 °C), 9. La Liche (24 °C), 10. Uriage (27 °C), 11. Echallon (42 °C), 12. La Lechere (53 °C), 13. Salins (35 °C), 14. Brides (37 °C), 15. Allevard (16 °C), 16. Acqui Terme (71 °C), 17. Ricken (12 °C), 18. Tenigerbad (13.5 °C), 19. Moiry (14.4 °C), 20. Rhaezuens (14.7 °C), 21. Peiden (15.2 °C), 22. Locarno (16 °C), 23. Gotthard (16 °C), 24. Berguen (17 °C), 25. Rothenbrunnen (17.2 °C), 26. Val de Bagnes (17.4 °C), 27. Andeer (18 °C), 28. Gletsch (18.6 °C), 29. Bovernier (21.1 °C), 30. Furka (21.7 °C), 31. Epinassey (21.7 °C), 32. Leytron (24.2 °C), 33. Acquarossa (24.9 °C), 34. Loetschberg (25.8 °C), 35. Weissenburg (25.9 °C), 36. Saxon (26 °C), 37. Grimsel (27 °C), 38. Saint-Moritz (29 °C), 39. Bulle (29 °C), 40. Combioula (29.4 °C), 41. Vals (29.6 °C), 42. Rawyl (29.7 °C), 43. Val d'Illiez (30 °C), 44. Saillon (30.1 °C), 45. Mont-Blanc (34 °C), 46. Pre-Saint-Didier (35.8 °C), 47. Bad-Ragaz (36.5 °C), 48. Masino (37.9 °C), 49. Yverdon-les-Bains (38 °C), 50. Thonex (39.1 °C), 51. Saint-Gervais-les-Bains (39.6 °C), 52. Bormio (42 °C), 53. Piedilago (42.7 °C), 54. Simplon (44.2 °C), 55. Brigerbad (50.2 °C), 56. Leukerbad (51 °C), 57. Lavey-les-Bains (65 °C), 58. Weggis (73 °C), 59. Weissbad (45 °C) ,

1.2. Structure of the Study

Chapter 1 is the introduction to the study sites with a brief overview of the geothermal sites in the Western Alps, location and historical aspects of the study sites of Bagni di Vinadio and Terme di Valdieri sites

Chapter 2 can be divided into three main parts. The first part briefly describes the different types of geothermal systems the present day exploitation of the geothermal resource with particular focus on the recent development of binary power plants for electric generation. The second part concerns the geothermal resource in the Alps and the third describes the geothermal exploration methods that can be used in mountainous regions.

Chapter 3 regards the regional geology of the western Alps and then focuses on the geological setting of the Argentera Massif, the geodynamic evolution of the region, the relations between geomorphology and geological structures and the seismic activity.

Chapter 4 is devoted to the detailed description of the geological setting of the investigation sites with particular focus on the structural setting and fault networks. Moreover some considerations about the fracture networks and their relation with the cropping out rock formations in the proximities of the thermal springs are described on the base of the field observations carried out in this study.

Chapter 5 covers the geochemical investigations taking into account the results of the analyses of two new sampling campaigns and the comparison to previous studies. This chapter is divided into two main sections where the results for the thermal waters at Vinadio and Valdieri are discussed separately. This choice was taken considering the differences in terms of geological setting and chemical composition of the thermal waters discharging at the two sites.

Chapter 6 focuses on the 3D geological modelling. In this chapter both the results and the main issues faced during this phase are presented. The first part describes the criteria employed to model the entire Argentera Massif, while the second and third part are focussed on the modelling of the Vinadio and Valdieri areas with particular attention to the main geological features representative of each area.

Chapter 7 presents the results of the geophysical surveys and the integration between geophysics and 3D models. The first part regards the results of the gravity survey and the selection of the criteria to integrate gravity data and 3D geological models. The second part deals with the magnetotelluric surveys, the problems faced during data collection and the results which were interpreted taking into account gravity and 3D. The final part focuses on the comparison between gravity and magnetotelluric and the relations between density and resistivity anomalies.

Chapter 8 describes the methods employed to calculate the geothermal potential in terms of heat and electricity production estimations for the two sites. On that base some utilization alternative to the current usage, are suggested to eventually optimize the exploitation of the resource

1.3. Generalities about the geothermal resource at Bagni di Vinadio

The hydrothermal area of Bagni di Vinadio is located at about 1350 m a.s.l. in the valley of Corborant torrent, a tributary of Stura di Demonte River, one of the main stream of Cuneo Province. More precisely this site is 10 km west of Vinadio at the intersection between the Corborant, Ischiator and Insciauda valleys (Figure 1-2).

The hot springs of Bagni di Vinadio are located within an area of 500 m² on the right side of the Corborant Valley. Three shallow wells were drilled and catch thermal waters at about 80 m in depth (Chapter 4). Part of the hot springs is located within the thermal baths buildings and so the three wells. Hot waters discharging from these springs are directly used for sauna bathing and those from only one of the wells are used for the swimming pool after mixing with cold fresh waters. Some other hot springs can be found along the riverbed of the Corborant Torrent, few tens of meters far from the spa and are not exploited.

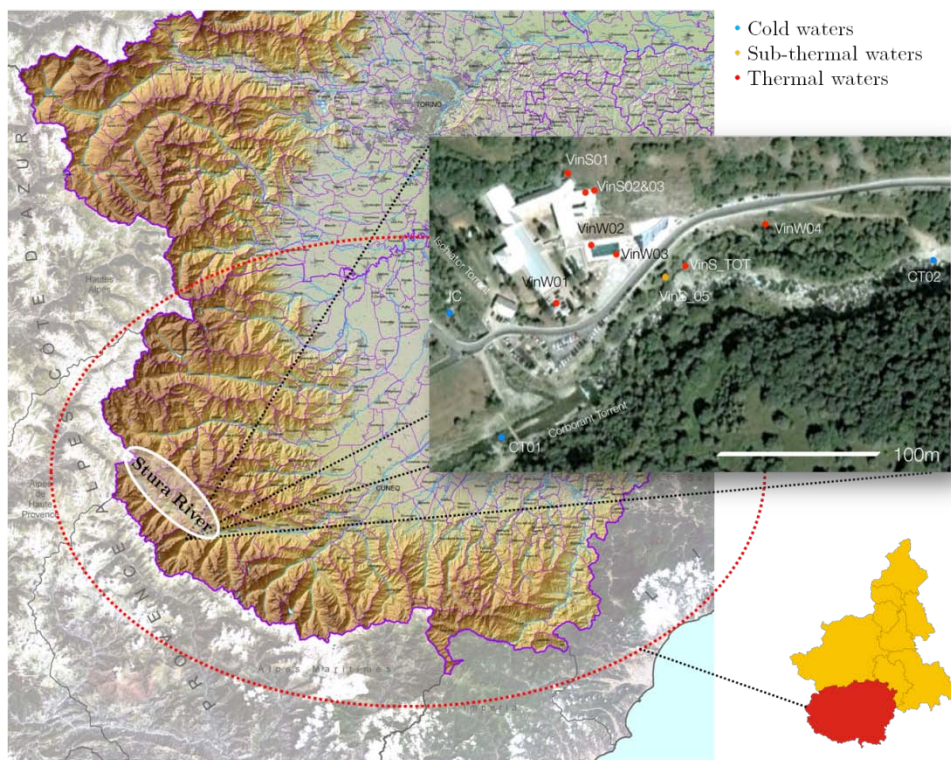


Figure 1-2 Detailed map of the location of the the sampled waters at Bagni di Vinadio

The thermal springs at Bagni di Vinadio are probably known since the Roman age but proven documentation about the usage of the thermal waters for bathing dates back to 1552. The first temperature measurements were carried out by Fontana in 1786 and then by Borelli in the 1850's (Figure 1-3). At that time measured temperatures, in °Reamur, indicated a range between 36 to 65 °C for Fontana and between 32 and 67 °C for Borelli (PAVENTA, 1873). This range is quite similar to the actual temperatures. With the exception of the springs located within the thermal spa and on the left side of the Corborant torrent, some other springs that were measured in the past are no longer there because of landslides which occurred in the past or human activities, which changed the local landscape and hydrological

setting. An example is the water intake that was built on the right side of the Corborant torrent around some hot springs, which, instead of increasing the production of thermal waters, caused the inflow of the Corborant torrent. However this loss was compensated by the wells that were drilled in the 1980's and more recently in 2001, which show an artesian flow and hot water exploited in the baths.

| | |
|--|---|
| 1. Sorgente del fango antico — da 30 a 31 gradi R. | 1. Sorgente della Cappella 36 gradi R. |
| 2. Sorgente della Maddalena — , 35 a 36 , | 2. Sorgente della stufia, che va in cucina 30 , |
| 3. Sorgente dei Nobili — , 32 a 33 , | 3. Sorgente della stufia del Quartiere 34 , |
| 4. Sorgente del Paesano — , 46 a 47 , | 4. Sorgente laterale della ròcca da 25 a 26 , |
| 5. Sorgente del Comune — , 51 a 52 , | 5. Sorgente superiore della ròcca 48 , |
| 6. Sorgente del Temperato — , 29 a 30 , | 6. Sorgente del fango 30 , |
| 7. Sorgente del Militare — , 45 a 46 , | 7. Sorgente inferiore della ròcca 46 , |
| 8. Sorgente del fango nuovo — , 45 a 46 , | 8. Sorgente della Maddalena 38 , |

Figure 1-3 Recorded temperatures by Fontana in 1878 (left) and Borelli in the 1850's (right) (mod. from Paventa, 1873)

1.4. Generalities about the geothermal resource at Terme di Valdieri

The thermal springs of Terme di Valdieri are located at 1370 m a.s.l. at the intersection of the river Gesso valley with the Valletta and Valasco valleys, in the core of the Parco Nazionale delle Alpi Marittime (Figure 1-4).

At Terme di Valdieri the thermal springs are mainly located in a cave of about 100 m². On the contrary of those of Bagni di Vinadio, the salinity of the thermal waters, is very low (300 mg/Kg) and doesn't show any significant variation among the springs. The temperature ranges between 28 and 65°C within few meters of distance. Most of the hot springs are located in a cave on the left slope of the Gesso River, few meters above the spa and the waters are only in part exploited for algae growing. Another small cave hosting a thermal spring that is not exploited is located some meters below the first cave. Another spring is located in a second cave within the building and the discharging waters are directly used for sauna bathing. Two other springs are located along the riverbed of the Gesso River and were sampled only during the winter campaign as the river hid them during the summer. A last hot spring is located on the right side of the river, close to the Hotel, shows a very small flow rate and is not exploited.

In this work samples from nine hot springs, two sub-thermal springs, two cold springs as well as the samples of the Gesso River were collected in summer and winter 2009. Two wells were recently drilled and are briefly described in Chapter 4, but are not exploited. On the base of a technical report¹, it was possible to get information about the geological formations crossed during the drilling phase and the presence of hot water at shallow depth.

¹ Report by Società Geologica Sondaggi (2002) kindly provided by Dr. Bonetto, the owner of the spa

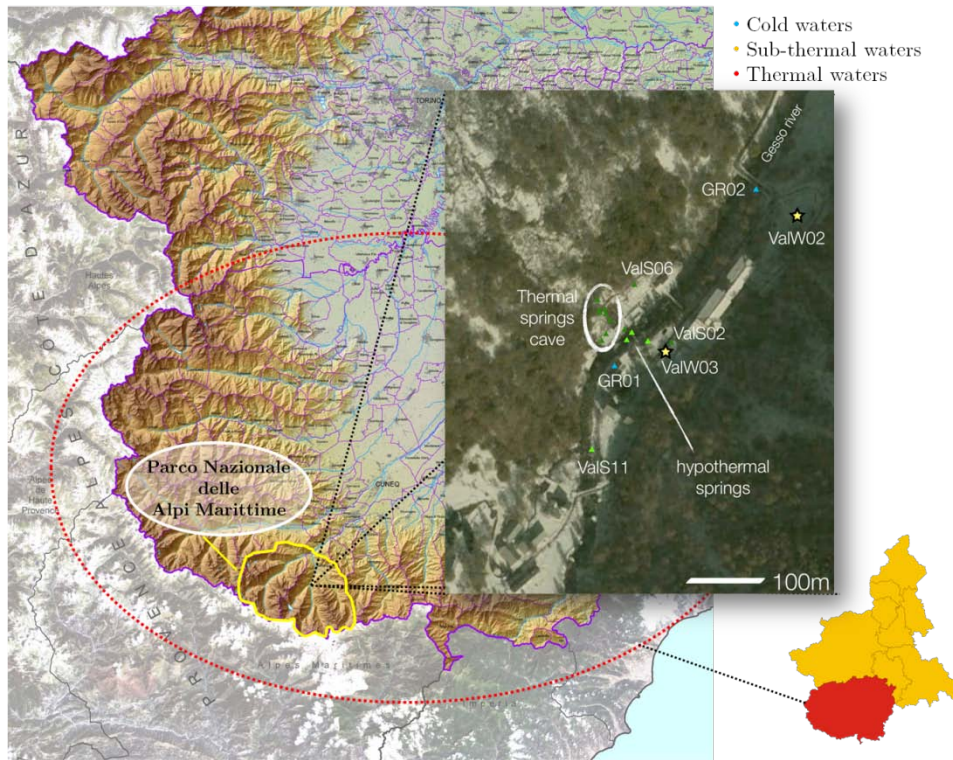


Figure 1-4 Detailed map of the location of the sampled waters at Terme di Valdieri

The hot springs have a history that dates back to 1588 when the first building for bathing usages was built in the proximity of the springs. Since then, these thermal waters have always been exploited for their "healing" properties. In 1755 Carlo Emanuele III, the King of the Reign of Sardinia, decided to improve the development of the thermal baths, followed by his successors Carlo Alberto and Vittorio Emanuele II who in 1833 and 1855, decided to spend their holidays there. Also the Count of Cavour, one of the leading figures in the movement toward Italian unification, in 1855 encouraged the construction of a real thermal spa considering this area as *"unique for the curative properties of its waters with no equals in the Reign of Sardinia and probably in Europe"*. Vittorio Emanuele II was, actually, an assiduous hunter and this area has always been popular for its wide variety of wildlife. At present day it is part of the Parco Nazionale delle Alpi Marittime that is one of the biggest national parks in Italy. In 1857 he decided to build his own holiday residence, which is today the Hotel Royal of Terme di Valdieri (Figure 1-5).



Figure 1-5 Thermal spa at Terme di Valdieri in the late 1800's and today

2

GEOHERMAL SYSTEMS IN ALPINE REGIONS

2.1. General introduction to geothermal energy systems and utilizations

Geothermal resources have been classified according to its enthalpy, which can be expressed as the amount of energy that a thermodynamic system can exchange with the surrounding environment. In the case of geothermal resources this energy is represented by the heat (thermal energy) and can therefore be linked to the temperature and vapour content of a geothermal system. There is not a general consensus about the classification of geothermal resources based on temperature (°C). Table 2-1 resumes the classification proposed by several authors. A first distinction can be based on *water dominated* or *vapour bearing to dry steam* geothermal systems. These latter two are typical of high enthalpy geothermal fields, which are nowadays exploited for power production. Another classification takes into account the circulation of the reservoir fluid and the mechanisms of heat transfer (NICHOLSON, 1993). In *dynamic* systems, which include both low and high enthalpy systems, the reservoir is continuously recharged from infiltrating water through the host rock fractures; heat is transferred by convection and circulation of the fluids is controlled by permeability heterogeneities of the subsurface. In the *static* systems, found in low enthalpy fields and in sedimentary basins, recharge is very limited and heat is mainly transferred by conduction.

Table 2-1 Classification of geothermal systems based on enthalpy of geothermal fluids. Temperatures are expressed in °C

| | Muffler & Cataldi (1978) | Hochstein (1990) | Benderitter & Cormy (1990) | Nicholson (1993) | Axellson & Gunnlaugsson (2000) |
|-----------------|--------------------------|------------------|----------------------------|------------------|--------------------------------|
| Low Enthalpy | <90 | <125 | <100 | <150 | <190 |
| Medium Enthalpy | 90-150 | 125-225 | 100-200 | - | - |
| High Enthalpy | >150 | >225 | >200 | >150 | >190 |

Power generation from geothermal fluids is nowadays mainly limited to areas with geothermal anomalies manifestations in volcanic and extension controlled regions, including high enthalpy fields, such as those at Lardarello (Italy). Figure 2-1 shows the size of the countries in relation to geothermal to the power production. Geothermal power production concentrates in few countries such as U.S.A., Philippines, Indonesia, Mexico and Italy.

Figure 2-2 shows the usages of the geothermal resource from power generation, for high temperature fluids, to the non-electric applications with low enthalpy waters. The 2010 worldwide geothermal installed capacity exceeds 10 GW with a produced energy higher than 67 GW_H (BERTANI, 2010). The most developing geothermal sector is the low temperature geothermal energy thanks to its broad application possibilities which not only include heat production but also power generation by means of binary power plants.

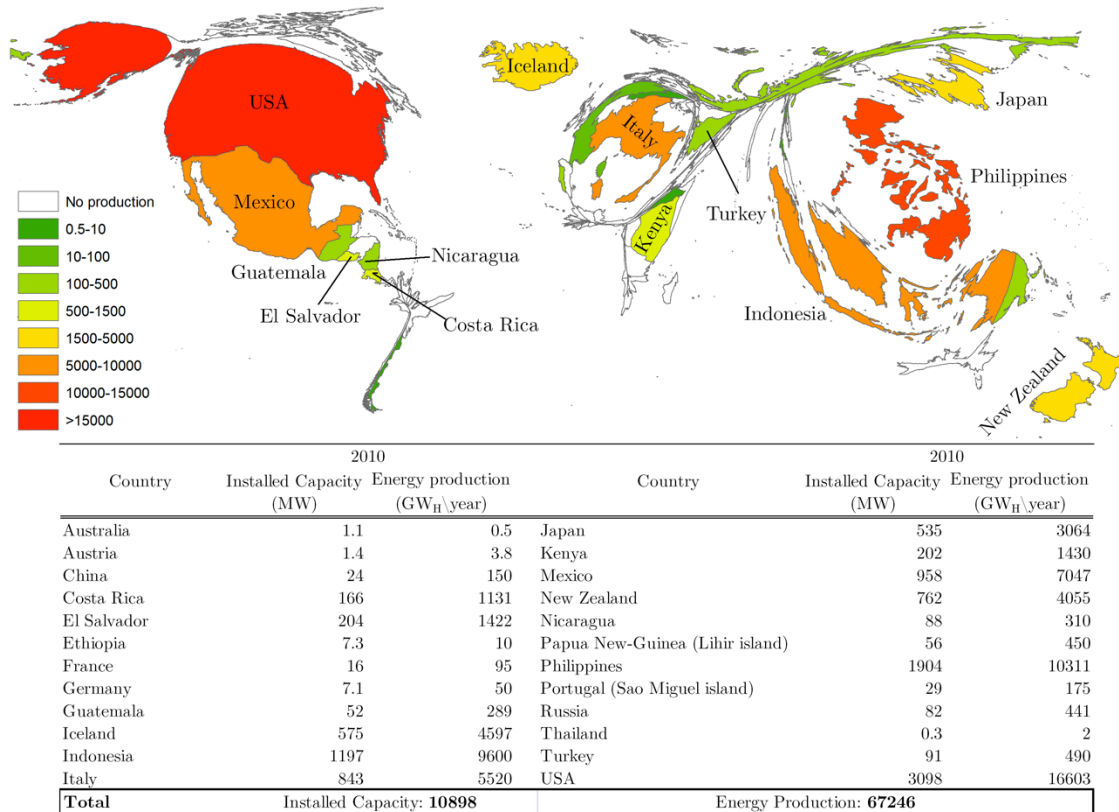


Figure 2-1 Cartogram of the 2010 worldwide electricity production from geothermal resource (data from Bertani, 2010)

Binary plant employs heat exchangers to transfer heat from the geothermal fluid, which is pumped to the surface from deep boreholes, to a secondary working fluid, having a lower boiling point and high vapour pressure at low temperature conditions. These power plants operate through a Rankine or Kalina Cycle and allow for efficient electricity production in the temperature range from 73-150 °C as further discussed in paragraph 2.2. An example is the case of Chena Hot Springs in Alaska, where geothermal waters with temperature up to 73 °C are exploited to produce electricity by means of Organic Rankine cycle (ORC) binary plant (ANEKE et al., 2011; ERKAN et al., 2008).

Non-electric uses of geothermal fluids are the most common form of utilization of geothermal energy. Direct uses typically cover the temperature range between 5 and 125° C. The main applications are space and district heating, space conditioning by means of heat pumps, agricultural application such as greenhouses or coupling soil heating and irrigation, aquaculture, spa and thermal baths or industrial applications.

District heating uses the waters at higher temperature (30-125°C) usually pumped from deep boreholes. The working temperature at the radiators is in the range of 55-80°C. Lower temperature usage for space heating is possible but requires more sophisticated methods of heat exchangers and radiant panels and building insulation. Water is usually returned into the system at 35-50°C and is reinjected in the reservoir.

Heat pumps are very often used for building heating and cooling as they allow using the heat stored in the ground at low temperature (<20°C) and shallow depth (<200m). In fact using heat pumps is possible to extract heat from the ground and make it available as

thermal energy at higher temperature. Moreover heat pumps allow extracting heat from the building during the summer season that can then be stored in the ground.

Greenhouse is another usage of geothermal waters for production of vegetables, flowers and fruits. The use of geothermal energy provides many advantages because it requires simple heating installations and it is economically competitive; greenhouses are one of the largest low-enthalpy energy consumers in agriculture.

Aquaculture or several species of marine organisms such as trout, catfish, sturgeon, frogs, oysters, mussels. Spirulina micro-algae is also an emerging usage of low temperature (15-30°C) geothermal waters.

Industrial applications can cover the entire range of temperature from low to high enthalpy fluids and include processes such evaporation, drying, distillation, sterilization, washing, paper, leather industry, CO₂ extraction, de-icing or salt extraction.

Geothermal energy also provides the possibility of an integrated exploitation of electricity and heat through a cascade approach. The cascade utilization increases the overall exploitation of geothermal energy from the same well, resulting in a better total efficiency and economical benefits. For instance, some of the most important applications of a cascade system of heat exchangers in present in today market, depending on the fluid temperature might follow the steps:

- power generation (70-170°C)
- district heating and cooling (70-40°C)
- industrial processing (70-40°C)
- spa, swimming pools (40-20°C)
- greenhouses, fish farming, de-icing (20-5°C)

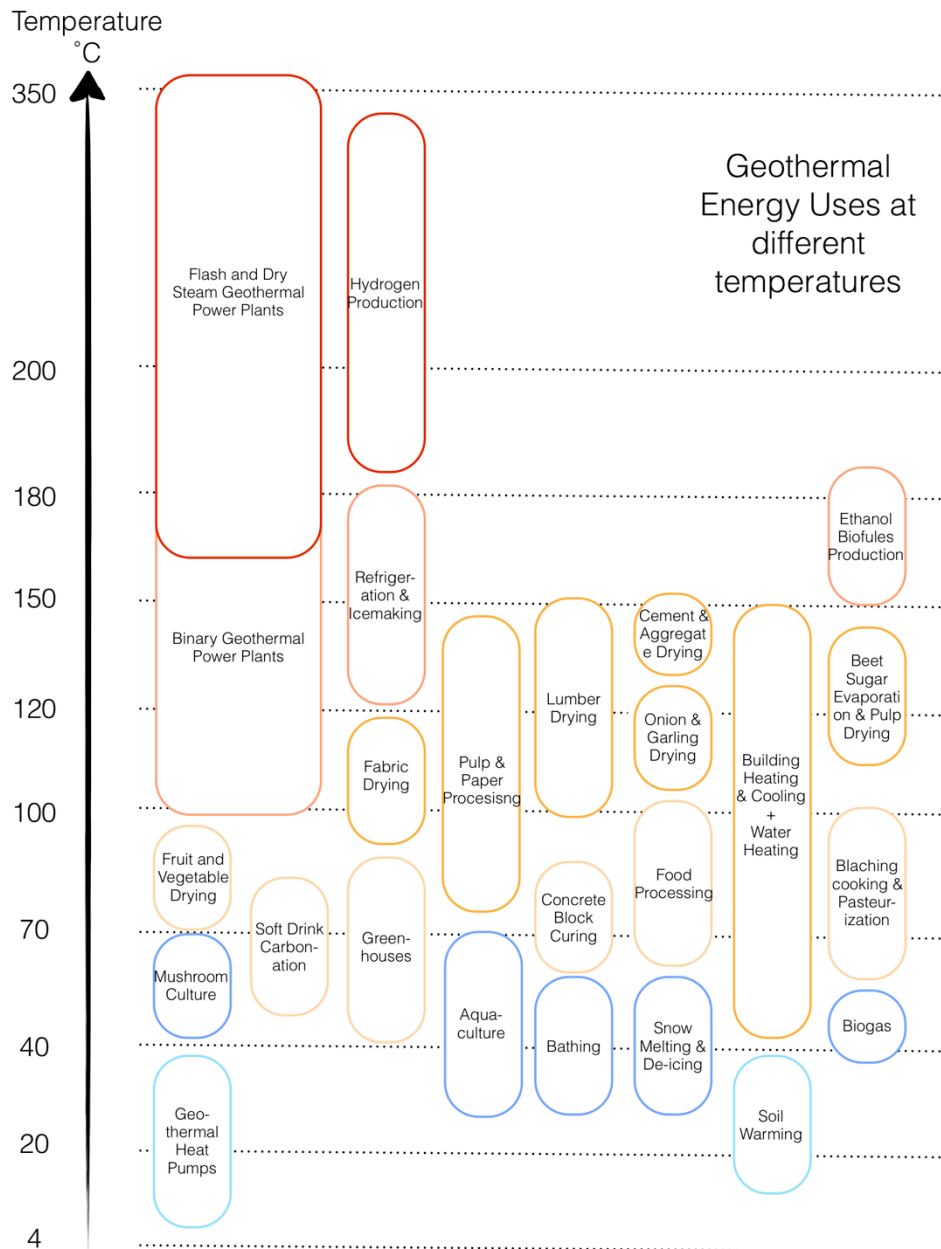


Figure 2-2 Uses of geothermal energy in function of the fluid temperature (mod. from Lindal, 1973)

Geothermal fluids are widespread at different depths in the subsurface and are exploitable for about the 70% of the total resource in high enthalpy geothermal fields (BERTANI, 2010). One of the main issues concerning the exploitation of deep geothermal fluids is the prospection of the resource, which must meet the desiderate needs and the costs *vs.* benefits ratio is favourable. It is important to distinguish between *resources* and *reserves*. If considering the total amount of a good, resources are the portion, which can be economically and technologically exploited even in the future, whilst the reserves are the portion of a resource which is exploitable with the present day technology and legal aspects, without requiring excessive costs (Figure 2-3).

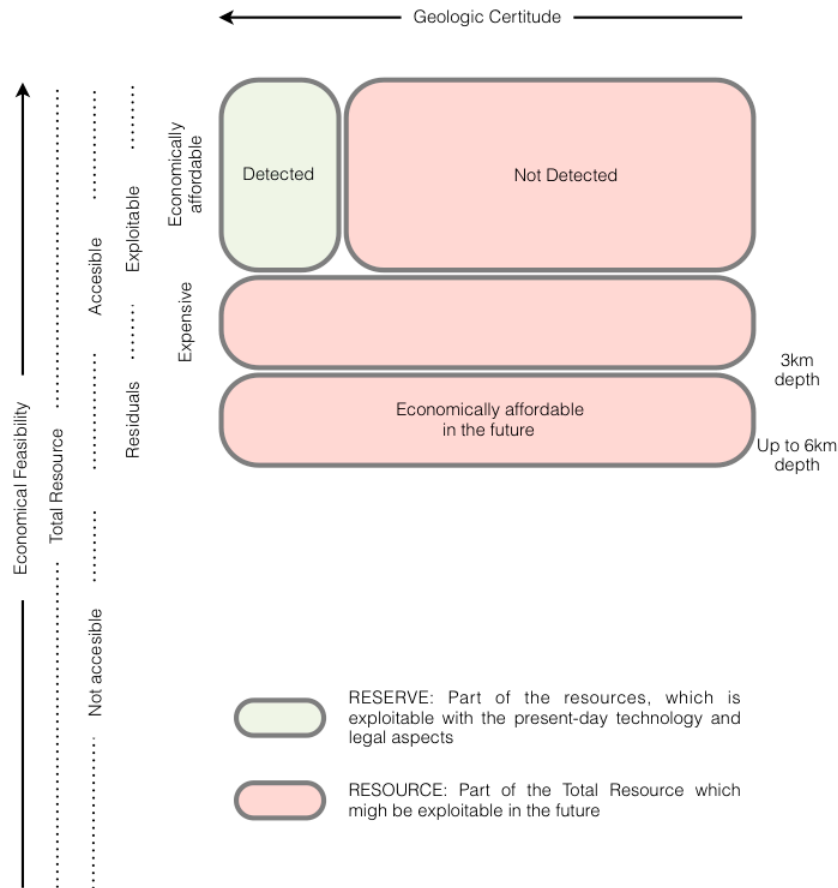


Figure 2-3 Geothermal Resources and Reserves (mod. from Muffler & Cataldi, 1978)

As shown in Figure 2-3, the two main parameters influencing the quality of a site are the economical feasibility and the geological certitude. Their evolution strongly affects the development of the renewable energy sources. For instance political, economical and social aspects related to oil & gas industry deeply influence the willingness to investing in renewable energy sources. As long as the fossil fuels will be available, at favourable technological and economical conditions any strong development in new and “green” energy sources will be carried out. This situation also reflects on a reduction of the amount of reserves resource in Figure 2-3. If considering geothermal energy, the knowledge about thermal fluids circulation and the characterization of the subsurface are of critical relevance to reduce the geological incertitude before planning the exploitation of deep resources.

2.2. Binary plants for geothermal power generation

Binary cycle geothermal plants are the most efficient way to exploit medium and low enthalpy (<150°C), water dominated geothermal systems because they show the best energy conversion method. A comparison between the amounts of geothermal fluid needed by the different types of geothermal power plants to produce 1MW_{EL} is listed in Table 2-2.

Table 2-2 Comparison between the amounts of geothermal fluids to produce 1MW_{EL} (DI PIPPO, 2008)

| Amount of geothermal fluid (t/h) | Type of Fluid | Temperature of the fluid (°C) | Type of power plant |
|----------------------------------|---------------------|-------------------------------|---------------------|
| 7-10 | Dry Steam | >250 | Traditional |
| 30-40 | Water/Steam Mixture | 200-250 | Flash Plants |
| 400-600 | Water | 73-150 | ORC Binary Plant |

Binary plants are based on a closed loop cycle in that the heat of the geothermal water is transferred to a secondary working fluid, usually an organic fluid or a mixture of ammonia and water, that has a low boiling point and high vapour pressure if compared to water at a given temperature. The working fluid, chosen for its thermodynamic properties, evaporates, expands, then is used to drive a turbine and, once condensed, it is returned to the evaporator. The cooled geothermal water is then re-injected to the ground to recharge the reservoir.

Such a geothermal plant has no emissions to the atmosphere except for water vapour from the cooling towers (only in case of wet cooling) and any losses of working fluid. Thus, environmental problems that may be associated with the exploitation of higher temperature geothermal resources, like the release of greenhouse gases (e.g. CO₂ and CH₄) and the discharge of toxic elements (e.g. Hg and As), are avoided. Another advantage of the binary technology is that the geothermal fluids (or brines), which are usually highly saline or corrosive, do not contact the moving mechanical components of the plant (e.g. the turbine), assuring a longer life for the equipment. Binary plants allow producing smaller amounts of power if compared to traditional power plants in high enthalpy fields but, have allowed the exploitation of a large number of fields that may have been very difficult (or uneconomic) using other energy conversion technologies, thereby increasing significantly the development of geothermal resources worldwide.

Today geothermal binary power plants are the most widely used type with 155 units operating worldwide producing 274 MW in 16 countries (DI PIPPO, 2008). However they only cover the 3% of the entire power generation from geothermal resource. They are usually constructed in small modular units able to produce few hundreds of kW_{EL} to few MW_{EL} and can be linked up to increase the production or pilot experimental plants or small binary units have been installed in fields where previously a flash-steam plant had been used to generate power using less than 150°C fluids, e.g. at Otake in Japan (DI PIPPO, 2004).

Geothermal binary power plants can be divided according to the installed power so that it is possible to identify two main groups according to the total power produced (LUND and BOYD, 1999). The first group includes medium and large binary power plants with output

power of at least 5 MW. The second type of geothermal binary plant is the small “stand alone” power systems with output power below 5 MW. These plants often operate through advanced thermodynamic cycles (dual pressure level Rankine cycle or Kalina cycle) and may also use different or unconventional working fluids, such as ammonia-water mixtures. They cover a wide range of geothermal fluid temperatures (74-145 °C) and the fluid flow rate lies in the range from 15 to 90 kg/s.

The most employed binary plants are the Organic Rankine Cycle (ORC) but the Kalina cycles were recently developed and few power plants have been installed in the last years, for instance Unterhaching in Germany (Table 2-3). Recent studies provided the theoretical advantages for Kalina cycle over ORC (KALINA and LIEBOWITZ, 1989; KALINA and LIEBOWITZ, 1994; KALINA et al., 1995; MLCÁK, 2002). The main difference between the Kalina Cycle system and the traditional ORC lies in the type of working fluid. In the Kalina cycle the transfer medium is a mixture of ammonia and water, while in traditional ORC it is usually pentane or isopentane. Pentane boils at constant temperature while ammonia has a boiling point of 33.7°C and mixed with water it boils at temperature related to the water/ammonia ratio, making the Kalina cycle theoretically more flexible and efficient than traditional ORC, in particular for low temperature fluids. All the running binary plants are located either in sedimentary or volcanic regions or in the planes bordering mountainous regions but none is located in alpine regions.

Table 2-3 Examples of binary power plants running worldwide

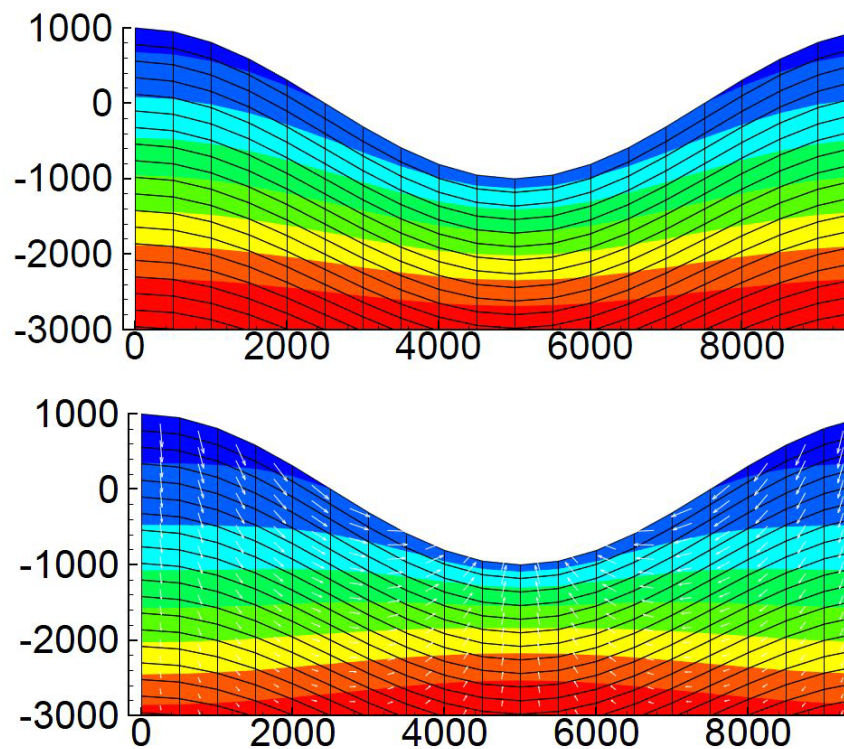
| Site | Country | WellHead Temperature (°C) | Flow rate (kg/s) | Power Production (KW _{EL}) | Power Plant Type | Source |
|-------------------|----------|---------------------------|------------------|--------------------------------------|------------------|---------------------------|
| Bad Blumau | AUT | 110 | 20-30 | 180 | ORC | Legmann, 2003 |
| Simbach & Braunau | DE & AUT | 76 | 55 | 200 | ORC | Le Bel and Chery, 2010 |
| Unterhaching | DE | 120 | 150 | 3400 | Kalina | BINE Informationsdienst |
| Altheim | AUT | 106 | 81,7 | 1000 | ORC | Pernecker and Uhlig, 2003 |
| Sulphurdale | USA | 138 | 28 | 3200 | ORC | Lund and Boyd, 1999 |
| Empire | USA | 152 | 57 | 3850 | ORC | Lund and Boyd, 1999 |
| Wabuska | USA | 104 | 60 | 1250 | ORC | Lund and Boyd, 1999 |
| Susanville | USA | 110 | 63 | 600 | ORC | Lund and Boyd, 1999 |
| Susanville | USA | 104 | 205 | 1500 | ORC | Lund and Boyd, 1999 |
| Chena Hot Springs | USA | 73 | 13 | 300 | ORC | Erkan, K. et al., 2008 |
| Fang | TH | 116 | 8,3 | 175 | ORC | Di Pippo, 2004 |
| Nagqu | Tibet | 110 | 70 | 1000 | ORC | Di Pippo, 2004 |
| Tu Chang | TWN | 130 | n.a. | 300 | OEC | Di Pippo, 2004 |
| Tarawera | NZ | 172 | 8bar | 2200 | OEC | Di Pippo, 2004 |
| Nigorikawa | JPN | 140 | 50 | 1000 | ORC | Di Pippo, 2004 |
| Tavale 21 | ITA | 115 | n.a. | 700 | ORC | Lund and Boyd, 1999 |

2.3. Geothermal resources in the Alps

In the Alpine chain several low enthalpy systems (20-70 °C) occur on relatively small surface areas of less than 500 m². They are exploited for direct uses such as spa bathing and space heating. Locally some shallow boreholes (<200m) were drilled to increase the production. Deeper wells are planned to be drilled in order to exploit the deep geothermal reservoir at Lavey-les-Bains (Table 2-4) for electricity production.

Information about geothermal fluids in the Alpine chain can be found in the BDFGeotherm database (SONNEY and VUATAZ, 2008) on geothermal fluids of Switzerland² and in the Northern Italy Geoterm database³. This second database includes all the available information about thermal springs and deep boreholes in the Italian Alps and the Po River Basin.

In Alpine regions, waters are heated due to the geothermal gradient ($\approx 25^\circ\text{C}/\text{km}$) and their circulation is described as *piston-flow* system where meteoric waters infiltrate, driven by gravity, due to the permeability of the host rock and then rapidly upflow. The upflow of the fluid occurs, usually along preferred permeable pathways such as major fault zones, due to advection which is strongly controlled by topography. Rough topography is a factor that promotes the infiltration of cold waters and the subsequent upflowing of deep hot waters at valley bottoms. Quaternary deposits often prevent part of the deep waters to reach the surface and allow mixing between these fluids and shallow cold groundwater. Figure 2-4 shows how the temperature and water flow are strongly influenced by topographic effect. The upper 2D conceptual model highlights the temperature distribution in the subsurface. In particular it is possible to observe how, even in steady-state conditions, the geothermal gradient tends to be higher along the bottom of the valley than in the surrounding regions. The lower profile shows how the water flow is driven by topography but valleys act as zone of capture where deep waters can reach the surface. In addition, in strongly tectonized regions such as in the Alps, valleys are usually associated to major fault zones. Cataclastic belts related to active faults are characterized by high permeability and the recall effect of the topographic depressions coupled to these preferential channels allow hot waters upflowing creating locally increased geothermal gradients.



² www.crege.ch

³ www.geoterm.unito.it

Figure 2-4 Topography controlled temperature distribution and water flow in steady-state conditions. Upper 2D example: temperature distribution (blue: low temperature, red: high temperature). Lower 2D example: water flow (white arrows) and its influence on temperature distribution (from Kohl, 1999)

The geothermal sites in the Western Alps have been often investigated on the geochemical structural aspects. They show a wide variety of temperatures, chemical composition and geological settings. The typical lithologies, which host the water circulation, are the porous and karstified Triassic evaporite, limestone and sediments of the allochthonous nappes, and, most of all, the fractured and tectonized gneiss and granite of the pre-Triassic basement, which also compose the External Crystalline Massifs (ECM) of the Western Alps.

The mineralogical composition of the host rock and the circulation time are only two of the parameters controlling on the chemical composition or the temperature of the thermal waters. Table 2-4 shows the chemical composition of thermal waters in the Western Alps. Ca-SO₄ waters are influenced by the dissolution of sulphate minerals (mainly gypsum and anhydrite) contained in the Triassic sediments. The Ca-SO₄ fingerprint is also easily acquired by interaction of deep waters with shallow groundwaters. Na-SO₄ and Na-HCO₃ waters (Brigerbad, Lavey-les-Bains and Saint-Gervais-les-Bains, Valdieri) mainly circulate in crystalline rocks and the sulphate content is also due to the dissolution of sulphide minerals. Sodium comes mainly from reactions with feldspars in crystalline rocks (PASTORELLI and MARINI, 2001). Some waters rather rich in calcium showing a Na-Ca-SO₄ composition (e.g. Cambioula) have an intermediate composition type between those from crystalline rocks and those in contact with Triassic gypsum and anhydrite. The Na-Cl fingerprint in thermal waters (Vinadio) is generally associated with a generally high mineralization. The origin of this fingerprint is twofold: it could be due either to the mixing of old, deep, strongly mineralized seawater and fresh water at shallow depth, or to the dissolution of halite deposits.

The sites where thermal fluids are exploited within the ECM are Brigerbad and Furka in the Aar-Gotthard Massif, Saint-Gervais-les-Bains and Lavey-les-Bains in the Aiguilles Rouges and Bagni di Vinadio, Terme di Valdieri and Berthemont-les-Bains in the Argentera Massif. The Italian side of the Argentera Massif shows the highest concentration of thermal springs with the highest temperature and flow rate of the entire Alps at Bagni di Vinadio and Terme di Valdieri where temperatures at the surface may reach 70°C and flow rate are up to 50 l/s.

In spite of the abundant and available geochemical and structural information at these sites, any study was ever aimed to investigate the subsurface for a better understanding of the geological and geothermal properties. Hence these two sites show challenging but interesting conditions to investigate the subsurface by means of geophysical methods and 3D modelling. In fact, the integration of structural geology, geochemistry, 3D models and geophysics might provide additional knowledge about the deep geological structures and the geothermal reservoir.

Table 2-4 Resuming table including thermal springs and boreholes in the External Crystalline Massifs of the Western Alps and their surroundings.

| Location | Site | Massif | Country | Sampling points | Borehole max depth (m) | Reservoir Rock | Max T (°C) | Reservoir T (°C) | Flow rate (l/s) | Geochemical Type | Water use |
|------------------|----------------------------------|------------------|----------------------------|------------------------|-----------------------------|----------------------------|-------------|------------------|--|--|------------------------|
| Western Alps | Loetschberg | Aar-Gotthard | CH | 3 springs | | Granite | 25.8 | 30 | 0.21 | Ca>Na-SO ₄ >Cl | heating & greenhouse |
| | Brigerbad | Aar-Gotthard | CH | 8 springs, 2 boreholes | 600 | Gneiss | 50.2 | 100-110 | 18* | Ca-SO ₄ >HCO ₃ | Spa |
| | Grinzel | Aar-Gotthard | CH | 2 springs | | Granite | 28 | 100 | 0.038 | Na-SO ₄ >HCO ₃ | none |
| | Funka | Aar-Gotthard | CH | 1 spring | | Gneiss | 21.7 | 50 | 0.3 | Na>Ca-SO ₄ >HCO ₃ | Spa heating |
| | Saint-Gervais-les-Bains | Aiguilles Rouges | FR | 3 springs, 2 boreholes | 198 | Micaschist | 39.6 | 60-75 | 8.4* | Na-SO ₄ >Cl | Spa |
| | Lavey-les-Bains | Aiguilles Rouges | CH | 12 boreholes, 1 spring | 517 | Gneiss | 65 | 100-110 | 28* | Na-SO ₄ >Cl | Spa |
| | Epinassey | Aiguilles Rouges | CH | 2 boreholes | 216 | Gneiss | 21.7 | 30-40 | 3.9 | Ca>Na-SO ₄ >HCO ₃ | none |
| | Bagni di Vinadio | Argentera | ITA | 6 springs, 2 boreholes | 77 | Gneiss | 70.5 | 120-130 | 20 | NaCl | Spa |
| | Terme di Valdieri | Argentera | ITA | 12 springs | 81 | Granite | 62.5 | 100-110 | 5.0 | NaSO ₄ | Spa |
| | Saint-Berthelemy-les-Bains | Argentera | FR | 2 springs | | Gneiss | 29 | 75-85 | 2.3 | HCO ₃ -SO ₄ -Cl+Na | Spa |
| | Mt. Blanc | Mt. Blanc | FR | 3 springs | | Granite | 34 | 35 | 4.8 | Ca-SO ₄ >HCO ₃ | none |
| | Bovernier | Mt. Blanc | CH | 1 spring | | Gneiss | 21.1 | 30-40 | 3.3 | Ca>Na-HCO ₃ >SO ₄ | none |
| | Saxon | Mt. Blanc | CH | 1 spring, 1 borehole | 7 | Gneiss and Trias limestone | 27 | 40-50 | 54* | Ca-SO ₄ >HCO ₃ | none |
| | Vals | Adula nappe | CH | 5 boreholes | 147 | Trias evaporite | 31 | 35-40 | 30* | Ca-SO ₄ >HCO ₃ | Spa and drinking water |
| Simplon | Antigorio Nappe | CH | 6 springs, 2 boreholes | 91 | Gneiss and Trias evaporite | 45.5 | 25-30/65-95 | 7 | Ca-SO ₄ | none | |
| Piedilago/Premia | Antigorio Nappe | ITA | 1 borehole | 248 | Gneiss | 42.7 | 45-55 | 5 | Ca>Na-SO ₄ | Spa | |
| Masino | Bergell Massif | ITA | 1 spring | | Granite | 38.1 | 60-70 | 0.6 | Na-SO ₄ | Spa | |
| Val-d'Illeaz | Dent du Midi Massif | CH | 2 springs, 1 borehole | 120 | Trias evaporite | 30.1 | 30-40 | 40* | Ca-SO ₄ | Spa | |
| Wellenberg | Drusberg nappe | CH | 6 boreholes | 1870.4 | Cretaceous limestones | 53.2 | 53 | - | Na-HCO ₃ >Cl | none | |
| Saillon | Morcles Nappe | CH | 4 boreholes | 929 | Triassic-Jurassic limestone | 32 | 40-50 | 26.6* | Ca-SO ₄ >HCO ₃ >Cl | Spa | |
| Leytron | Morcles Nappe | CH | 1 spring | | Trias evaporite | 25.1 | 25-35 | 2.1* | Ca-SO ₄ >HCO ₃ | Spa | |
| Bornio | Ortler Zone | ITA | 2 springs | | Trias evaporite | 42 | 50 | 1.2 | Ca-SO ₄ >HCO ₃ | Spa | |
| Craveggia | Piodel di Craana Zone | ITA | 1 spring | | Gneiss | 29 | 40-50 | 0.13 | Na-SO ₄ >HCO ₃ | none | |
| Saint-Moritz | Plattia Nappe | CH | 1 borehole | 1600 | Granite | 50 | 50 | 1.3 | Na-HCO ₃ >SO ₄ | none | |
| Combiotta | Pontis and Sivie-Mishabel nappes | CH | 3 springs, 3 boreholes | 438 | Trias evaporite | 31 | 40-50 | 68 | Ca>Na-SO ₄ >C | none | |
| Acquarossa | Simiano Nappe | CH | 3 springs | | Trias evaporite | 25.2 | 60-65 | 3.5 | Ca-SO ₄ >HCO ₃ | none | |
| Pre-Saint Didier | Sion-Courmayeur zone | ITA | 2 springs | | Trias evaporite | 35.9 | 45-55 | 2.3 | Ca-HCO ₃ >SO ₄ | Spa | |
| Leukerbad | Torrenthorn Massif | CH | 7 springs | | Trias evaporite | 51 | 55-65 | 32.5 | Ca-SO ₄ | Spa | |
| Rawyl | Wildhorn nappe | CH | 3 springs, 1 water channel | | Jurassic limestone | 29.7 | 40 | 38 | Na-HCO ₃ | none | |

*pumped flow rate

2.4. Geothermal exploration methods applied in Alpine context

In low-enthalpy geothermal fields in sedimentary environments, exploration is carried out using seismic surveys or exploration deep boreholes. However, in Alpine regions, carrying out a seismic survey or drilling exploration boreholes is technically difficult and cost effective. For instance seismic methods show limited capability in detecting and imaging steep structures in a rather homogeneous basement from the point of view of velocity contrasts between unaltered regions and highly fractured fault zones. Therefore geothermal exploration in the Alps has always been focussed to geological mapping and geochemical investigations, sometimes jointly interpreted to provide a hydrological conceptual model of the circulation system. However, these two methods can't provide detailed information about the three dimensional distribution of the relevant geological structures and physical properties at depth. Hence geophysical techniques capable to investigate some kilometres deep (up to 5-10 km) at reduced costs such as self-potential methods, might be combined and integrated to 3D geological models to find out the most favourable area for further investigations.

The main parameters which are important on the geothermal point of view are the characterization of natural fracture networks, hydraulic conductivity and temperature distribution at depth. The understanding of the stress field allows characterizing which structures are controlled by the present day stress distribution and therefore can show favourable geomechanic conditions (e.g. aperture, connectivity, fracture density) for thermal fluids circulation. As a consequence enhanced fracture density might reflect on higher porosity of the rock formation, hence higher hydraulic conductivity. Temperature is crucial to figure out the geothermal potential of a region and locate the most suitable areas for exploitation of the reservoir.

2.4.1. Structural geology

Fracture systems play an important role in providing a pathway to fluids in the Earth's crust. In particular in Alpine regions where thermal fluid circulation is mainly controlled by fault networks and shear zones, the description of the detailed local geological and structural setting of a study area is crucial for geothermal exploration. The main aspect is the role of faults in controlling the localization, patterns and rates of the hydrothermal flows. Highly fractured zones and fault intersections might reflect on relief depression where flow might accumulate because of increased rock fracturing (FLORINSKY, 2000). Moreover these studies can possibly help estimating the permeability and porosity of the fault zones and of the geological formations involved in fluid circulation (EVANS et al., 1997). Geothermal relevant permeability depends on fracture density, orientation, connectivity of subsidiary structures and on hydraulic conductivity of the different fractures and fault planes. The internal structure of fractures and rock-water interactions play an important role to determine zones related to past and present-day thermal fluids circulation.

Standard field observations and conventional rock mass tool (e.g. Rock Mass Rating RMR) are aimed at recognizing and comprehending the main characteristics of fault and they associated bracciated and mylonitic corridors. These characters include extension, thickness,

geometrical properties, spatial distribution of structural features, etc. Moreover the the recognition and classification of various fault rock assemblages and meso-scale kinematic data collection are crucial steps for the understanding of the kinematic evolution and the stress conditionsevolution of a study site.

These observations can benefit (e.g. where the availability of measurable outcrops is limited) from the recent advances in the use of imaging techniques like photogrammetry and laser scanner based on digital imaging. In fact this technique provides opportunities to collect high-definition digital images of outcrops (using high-resolution cameras), to produce 3D digital surfaces and renderings and to analyze them to characterize the rock mass in terms, for instance, of fracture density, dip directions, joint spacing.

Another technique recently being developed and applied to tectonic activity is the Synthetic Aperture Radars SAR interferometer technique PS-InSAR proposed by Ferretti (2001), which allows detecting small movements of ground surface. The Permanent Scatters PS are stable points on the ground (buildings, rocks, etc.), which can be used to estimate the sub-vertical motion of the ground, within the range of millimetre motions/year (fraction of the 5.6 cm-wavelength). PS velocity values are relative to a chosen reference point that is assumed to be stable. This technique has been employed in the Argentera Massif to detect the occurrence of subsidence or upflow due to the active tectonic features in the areas such as thrust and strike-slip faults as shown in Figure 2-5 (MORELLI et al., 2008). The PS data revealed differential upflow or subsidence of large areas, probably controlled by km-scale gentle flexures, precisely located individual faults.

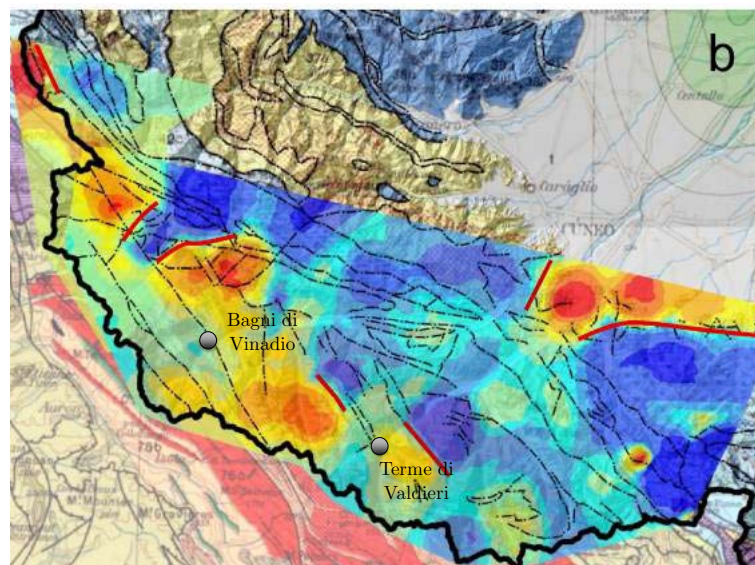


Figure 2-5 Red and blue areas represent respectively high and low velocity PS value. Red lines are the boundaries between domains showing homogeneous kinematic behaviours, dashed lines represent tectonic lineaments and know structures (mod. from Morelli et al, 2008)

In particular the Argentera Massif can be divided into three main domains: the western sector is characterized by high velocity movement that are probably controlled by the known active tectonic faults (Chapter 3). The second domain is the central sector of the massif characterized by low velocity, which can represent a transition zone towards the third domain, in the eastern sector where the high velocities might be associated to buried active faults.

In the External Crystalline Massifs few studies were carried out to investigate the relationship between fault network and thermal springs. Perello et al. (2001) and Baietto et al. (2008; 2009) provided an exhaustive overview of the structural conditions controlling thermal fluid circulation in the Argentera Massif. Perello focussed on the Bagni di Vinadio and Terme di Valdieri sites highlighting the relation between faults zones and topographic conditions while Baietto pointed out the differences between the structural settings, fault networks at the three thermal sites in the AM. The observations carried out in the framework of this study were focussed on the identification of those fracture associated to thermal springs, hence related to the final upflow of hot waters. These aspects will be further discussed in Chapter 3.

2.4.2. Exploration wells and alpine tunnels

Deep boreholes are the most useful tools to investigate the subsurface. In fact thanks to the analyses of logs and core samples it is possible to understand stratigraphy, fracture networks and stress conditions, presence of fluids and temperature distribution at the subsurface. Moreover, measures of density, electrical and thermal conductivity of the sampled lithology during logging can be carried out in the lab.

Fractures and faults provide permeable pathways for fluid circulation at several scales from deep crustal structures to fractured aquifers, hydrothermal and geothermal reservoirs. Permeability of fault zones depends on density and orientation of fractures and, more important, on hydraulic conductivity of fault planes and fractures (FRY, 1989). An exhaustive overview of several deep boreholes drilled for geothermal projects is given by Stober & Bucher (2007). They analysed hydraulic properties of several deep geothermal wells samples collected in crystalline basements. The observations carried out by these authors pointed out zones with enhanced hydraulic conductivity K , result from brittle deformation mechanisms, which represent the dominant flow porosity. Moreover K strongly depends on lithology and granite, in particular fine-grained granite, tends to be more pervious than gneiss and amphibolite by a factor of 100 or 2 orders of magnitude.

One of the goals of deep boreholes in geothermal exploration in crystalline regions is to investigate the inside of the host-rocks to finally locate the most fractured and permeable zones, which might be suitable for exploitation if thermal and flow rate conditions are favourable. Moreover deep wells allow measuring the temperature distribution at the subsurface and can be exploited as production wells whereas the conditions are favourable in terms of temperature and flow rate.

In the Western Alps very few are the cases where boreholes were drilled and exploited for geothermal purposes. Some examples are the four boreholes drilled at Brigerbad (CH) where the deeper one, 480 m deep, was converted to a production well for the swimming pool and the thermal baths (DEBELMAS and KERCKHOVE, 1980a). Two wells producing thermal waters up to 65°C at Lavey-les-Bains are exploited to heat the buildings and then to supply the swimming pools. In the Argentera Massif some shallow wells were drilled at Vinadio, Valdieri but just one at Vinadio is exploited for the swimming pool (Chapter 4). At Berthemont-les-Bains 3 wells were drilled but only the deeper one (450m) was suitable for exploitation.

Moreover, in the Argentera Massif the St. Anna borehole was drilled in 1996 as exploration well for the Mercantour Tunnel, which was supposed to connect Italy and France by a 17.4 km-long railway tunnel, but the project was abandoned after the borehole drilling. The St. Anna borehole is located at 1895 m a.s.l. in the proximities of the St. Anna Sanctuary. It is 1150 m-deep, dipping 60° north-eastward and its core mainly consists of glacial tills (0-7.1 m), migmatitic gneisses (7.15-35.2 m), granites (35.2-141.9 m), migmatitic gneisses (141.9-845.5 m) and granites (845.5-1150 m). These lithologies are involved at different levels of fracturing, therefore it is possible to distinguish between: undeformed rocks, mylonitic fabrics, fractured to intensely fractured/breccia zones, cataclastic zones and clay-rich gouge zones. This information has been employed in the framework of this study during the 3D modelling of the Argentera Massif and the Valdieri area (Chapter 6). Additionally the St. Anna borehole shows that waters flowing within the fault zones have a temperature of 24 °c at depths of 1150 m, indicating a low geothermal gradient of about 15 °C, if considering the average air temperature of 8°C (BAIETTO, 2006a; DARCY, 1997)

Alpine tunnels are a precious source of information. In fact tunnels can be considered as “horizontal boreholes” where, in addition to the boreholes, it is also possible to carry out detailed mapping of the outcropping formations, of the fracture conditions and of the geomechanic properties of the rock. Moreover one of the most challenging aspects in the preliminary phases in tunnels project is the prediction of temperature in the subsurface, as it affects the working conditions of personnel and machines.

In the Western Alps the main examples of tunnels are the Gotthard, Simplon, Lötschberg, Mont Blanc, Frejus, Maurienne-Ambin tunnels (Lyon-Turin TGV, high speed train, railway). If looking at the water circulation and thermal conditions in these tunnels, thermal distribution in alpine regions is strongly affected by circulating waters. Large inflows of cold meteoric waters along highly permeable zones induce low geothermal gradient. On the contrary, local higher geothermal gradients are related to the presence of ascending thermal waters.

Most of the water inflows are related to descending circuits in low permeable systems. The infiltration is usually slow because of the overall low permeability. This condition allows waters extracting heat from the host rock until the thermal equilibrium is reached at depth. These kinds of circuits are present in the Simplon tunnel (1000 kg/s) and in the Gotthard exploration tunnel where permeability is mainly controlled by dissolution of the Mesozoic carbonate rocks. However large inflow are possible along highly fractured fault zones, causing low temperature anomalies and an increased local cooling rate of the rock. For example, in the Mont Blanc tunnel where water infiltrates along cataclastic zones in gneissic rocks at a flow rate of 800 kg/s, a negative thermal anomaly was recorded (MARÉCHAL and PERROCHET, 1999).

Thermal springs and warm inflows in deep tunnels derive from ascending waters from relatively deep aquifers, which represent potential "geothermal reservoirs". Discharge temperatures depend on the flow rates and on the velocities of the uprising waters. Uprising warm waters with relatively high flow rates can heat the surrounding rocks and consequently induce unusual high geothermal gradients. Some examples of water inflows temperature recorded in the above mentioned tunnels are listed in Table 2-5:

Table 2-5 Temperature measured in some alpine tunnels (mod. from Goy et al, 1996)

| Tunnel | Maximum cover overburden (m) | Maximum Temperature (° C) | Rock Type |
|------------|------------------------------|----------------------------|----------------|
| Mont-Blanc | 2500 | 40 | Granite |
| Simplon | 2100 | 55.4 | Gneiss |
| Gotthard | 1750 | 30.7 | Granite |
| Lotschberg | 1630 | 34 | Granite/Gneiss |
| Frejus | 1610 | 29.5 | Schists |

The geothermal gradient can also be estimated considering the temperature of the water inflows, the average air temperature at the surface and the depth of the tunnel. For instance, in the Gotthard railway tunnel, a regional geothermal gradient of 22 C/km was estimated even though the thermal distribution along transect is affected by several parameters such as topography, exhumation rate, advective heat transfer (GLOTZBACH et al., 2009). Thermal modelling was carried out, for example, for the Maurienne-Ambin tunnel, taking into account the thermal conductivity anisotropy, the orientation of the different rock layers, topography ground surface temperatures, the geothermal flow (GOY et al., 1996) and the temperature prediction was 48° C, which is in the temperature range listed above. Kohl et al. (2001) proposed 3D thermal investigation for the Gotthard tunnel employing a transient finite element (FE) model, accounting for fluid and mass advection, climatic changes. structural effects like topography and anisotropy.

In the Argentera Massif, the exploration Ciriegia tunnel was drilled in 1966-1967 in the framework of a project aimed to connect Italy and France by means of a 12.38 km-long tunnel. The Ciriegia tunnel is located about 1km from the Terme di Valdieri site, is 600 m below the surface and is 2925 m-long. As shown in Figure 2-6, the tunnel cuts the gneiss in the first 500m, then the alternation of gneiss and amphibolites which also crop out in the proximities of the thermal site and it is very important to highlight the presence of a granitic body starting from 1060 m. This body extends along the remaining portion of the tunnel covering a distance of about 2 km. Water flow rate and temperature were measured in correspondence of the Lorusa fault zone. The reported inflow was 20 l/s and the temperature was 20°C, indicating an estimated geothermal gradient of 21°C/km.

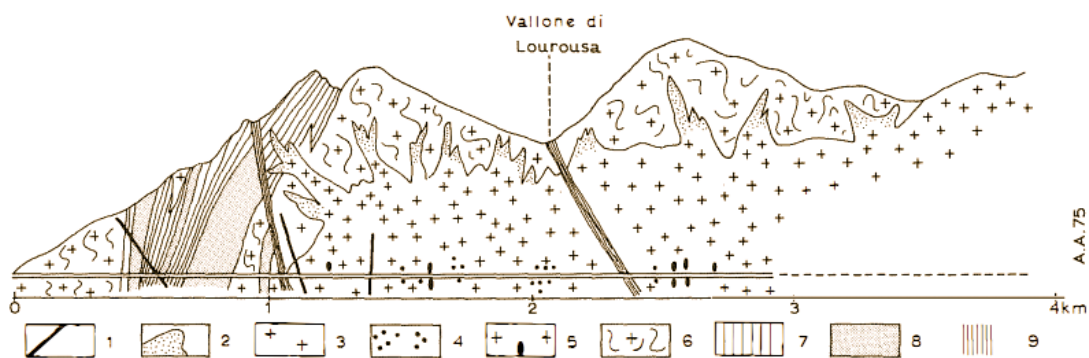


Figure 2-6 Geological profile of the Ciriegia tunnel. 1. Aplitic Dykes. 2. Fine-grained Granite. 3. Medium-grained Granite. 4. Granite with k-feldspar phenocrysts. 5. Granite with biotitic inclusions. 6. Gneiss 7. Layered Gneiss. 8. Amphibolite. 9. Mylonitic belts (mod. from Bortolami and Grasso, 1969)

2.4.3. Geochemistry of the fluids

The application of geochemical techniques is part of the early stages of geothermal exploration. Analyses of hydro-chemical composition of thermal fluids can provide information not obtainable by geological and geophysical investigations. After all, the collected thermal fluids at the surface “have been there” and therefore they carry imprints of their deeper history. The results of the chemical and isotopic analyses highlight the characteristics of the deep flow system such as the occurrence of water-rock interaction (acid-base reactions, dissolution of the host rocks, ionic exchange with clays, secondary mineral precipitation, redox reactions, bacterial decomposition), mixing processes, mean elevation of the recharge zone, reservoir temperature, groundwater residence time, etc. This information, coupled with geological and geophysical data allows the development of conceptual models for the regional deep flow patterns, which take into account the infiltration basin, the geological formations and structures controlling the circulation of the hot fluids from the reservoir towards the surface.

The studied geothermal fluids in the framework of the Thesis will be divided as follows (VUATAZ, 1982):

- cold: $T < 12^\circ \text{C}$
- sub-thermal: $12 < T < 20^\circ \text{C}$
- thermal: $T > 20^\circ \text{C}$

Two sampling campaigns took place in July and December 2009 and 30 samples including cold, sub-thermal and thermal waters were collected from springs, rivers and wells. Major and trace elements, waters stable isotopes, Tritium were analysed and interpreted. The results were compared to those of previous authors such as Fancelli (1978), Bortolami (1984), Michard (1989a), Perello (2001) and Baietto (2006b). These authors agreed on the following aspects:

- meteoric origin of the thermal waters
- absence of boiling at depth
- different composition of the thermal waters at Vinadio (NaCl) and at Valdieri (NaSO_4)
- occurrence of mixing processes between a deep thermal endmember and shallow cold groundwater
- reservoir temperature to be in the range $100\text{-}150^\circ\text{C}$
- lack of accurate information regarding the residence time

However the most debated topic about the thermal waters in the Argentera Massif is the origin of the high salinity at Bagni di Vinadio, which is clearly anomalous if assuming that this water circulate only within the crystalline host rocks (ARTHAUD and DAZY, 1989; MICHARD, 1990a; PASTORELLI and MARINI, 2001; PFEIFER and SANCHEZ, 1992; ZUPPI et al., 2004). Several hypotheses were proposed in the previous studies (cfr. Chapter 5) and the Cl/Br molar ratio method (ALCALA and CUSTODIO, 2008) was employed in this study to better decipher the origin of the high Chloride concentration.

2.4.4. 3D geological modelling

Three dimensional geological models have become, in the last years, a useful tool to better understand geology, to share and communicate geological interpretations. The increase of the demand of 3D geological models is reflecting on the need of producing models, which are more geologically reliable and realistic, geometrically correct, consistent and respectful of the relations between the geological bodies. Moreover a consistent 3D geological model is the key for computations of Earth processes (e.g. geothermic, hydrogeology, structural geology, geodynamics, geothechnic, mining and oil exploration) that need accurate representation of the geometry and the physical properties of geological bodies. In fact full 3D geological models allow for discretisation and thus numerical modelling on the basis of a realistic geology.

A 3D geological model is considered as a set of formations represented as volumes bounded by interfaces and sometimes cut by faults projected as surfaces (LAJAUNIE et al., 1997). Most of the software for 3D geological modelling was developed by oil companies, which mainly deal with seismic data and borehole stratigraphy and are usually optimized for basin environments. Moreover one of the main issues that each geologist has to face is the impossibility of collecting continuous field data and subsurface information is usually related to occasional access to drillcores or shallow depth geophysical surveys. Therefore a geologist has to merge and interpret these few data to come out with maps and cross sections. Building a 3D model helps to reduce the uncertainty of these interpretations by the integrated computation of data collected on the field, acquired from maps, cross sections, boreholes, geophysics.

The choice of a 3D software should be based on the aim of the final model. Is it a mere visualization or it would be employed for scientific vulgarization, regional tectonic studies or reservoir modelling? For example GIS environment, e.g. ArcGis[®] and Surfer[®] are useful for 2.5D visualization but don't allow any direct manipulation of the model. CAD based 3D software, AutoCad[®], cinema4D[®] rely on explicit modelling (cfr. Chapter 6) like 3D geological modelling software such as gOcad[®] and Petrel[®].

In the framework of this Thesis the software 3D-Geomodeller[®] by Intrepid Geophysics was employed as its usefulness has been well established in several studies on orogenic, basins and mining domains (FITZGERALD, 2003; MARTELET, 2004; MAXELON and MANCKTELOW, 2005; MCINERNEY, 2005). It provides all the needed tools to integrate data from different sources create *a-priori* geological models from maps, cross sections and boreholes and then validate it by means of forward modelling from geophysical data and gravity and magnetic inversion.

Some example of 3D geological modelling in the Alps are provided by Zanchi et al. (2009) who coupled GIS techniques and gOcad to reconstruct klippe, folds and thrust structures in the central Alps. ArcGis and gOcad have been employed by Bistacchi et al (1986) to model faults and folds in the framework of a project for a tunnel between Fortezza and Innsbruck. Maxelon and Mancktelow (2005) proposed three-dimensional models of the Penninic zone in the Central Alps based on geostatistical assessment of the regional foliation field and structural data using 3D Geomodeller. Finally, granitic bodies have been modelled in 3D by Strzeczynski et al. (2005) using 3D Geomodeller, which was employed as well by Schreiber et

al. (2010) to model Alpine Mohos in the south-western Alps integrating geological and geophysical data.

2.4.5. Geophysical exploration

Geophysical investigations are a major part of geothermal exploration. In fact coupled with borehole data, geophysical surveys allow detecting the underground distribution of the geological bodies and structures by means of active or passive methods. A geophysical survey is aimed to identify a geothermal reservoir, usually represented by a permeable volume of rock containing circulating hot fluids (water or vapour) that can be extracted by means of deep wells. Therefore high temperature and high permeability cause local anomalies in the petro-physical properties of the rock, which can be inferred from the surface, making the geothermal reservoir a target for geophysical techniques.

The most useful techniques applied in geothermal exploration are:

- heat flux measurements
- temperature gradient surveys
- electrical resistivity surveys
- seismic methods, both active and passive
- gravity surveys

The physical properties revealing anomalies in a geothermal context include:

- temperature
- electrical conductivity and resistivity (e.g. presence of hydrothermal alteration minerals, brine)
- elastic properties affecting the propagation of elastic waves e.g. presence of shear zones where water might circulate)
- local gravitations acceleration related to density variations in the subsurface (e.g. enhanced porosity in the reservoir)
- magnetic susceptibility (e.g. hydrothermal alteration of magnetic minerals)

Therefore gravity, magnetic, seismic and electromagnetic surveys are employed to provide information about the shape, size and depth of the geological bodies and structures causing the anomalies. All geophysical methods can provide remarkable results, especially if combined together and integrated with other exploration techniques as geological mapping, geochemistry and 3D modelling (e.g. Soultz-sous-Forets).

If Alpine regions, unfortunately, not all the methods can be employed or can provide satisfying results. In fact one of the major problems, which might affect geophysical surveys, is the strong topography. In the first place it radically reduces the areas where measurements can be carried out, preventing from collecting data with a regular spatial distribution and from reaching the desired investigation depth. Moreover it can disturb the signal being measured. For instance topography can influence electrical or magnetic surveys. In fact current flow lines tend to follow the ground surface and the equipotential surfaces are thus distorted, resulting in anomalous readings. In ground magnetic surveys, topographic effect can be strong but is not completely predictable as it depends upon the magnetic properties of the topographic features (KEAREY et al., 2009). In addition, carrying out a geophysical

survey, e.g. a large scale seismic exploration campaign, in a roughed area might reflect in a prohibitive increase of costs, thus choosing the more suitable techniques is a crucial phase in any exploration campaign.

In the framework of the Thesis two passive methods, gravity and magnetotelluric (MT), were employed. For the first time in an Alpine region, they were used to investigate the subsurface for geothermal resource exploration. Passive geophysical surveys are ones that incorporate measurements of naturally occurring fields or properties of the earth. Gravity and MT are usually employed, in mountainous regions, either to determine the thickness of the Quaternary filling of the valley or the deep crustal and mantle structures. The basic hypothesis for the application of these two methods for geothermal exploration is that rock fractures and hydrothermal alteration or fluid circulation lead to a decrease in both density and resistivity as e.g. observed in the crystalline basement of the EGS site as Soultz-sous-Forêts (ÁRNASON and EYSTEINSSON, 2010; MUÑOZ et al., 2010; SCHILL et al., 2010; VOLPI et al., 2003) and the southern Black Forest. Hence, coupling these two methods may help detecting the most fractured geological bodies, where thermal waters might circulate. Gravimetry is a quite handy method as it doesn't need a massive amount of instrument; however a high precision gravimeter and GPS are required to measure the gravity field and the position of each observation to then elaborate the data with high accuracy. The results in terms of density distribution can be integrated to 3D a-priori geological models, e.g. using 3D-Geomodeller, to carry out forward modelling and inversion processing. Magnetotelluric requires more instruments, space and observations may undergo to a significant influence from anthropogenic electromagnetic sources. The main advantage of coupling these two methods is that gravity provides a high resolution on the horizontal plane and is sensitive to lateral variations of density; however it lacks of vertical accuracy. This gap might be filled by MT soundings which usually assures a high penetration depth and is responsive of vertical variations of resistivity (BIANCHI et al., 2010; VOLPI et al., 2003). Therefore combining these two methods to three-dimensional geology may provide a reliable description of the subsurface.

3

GEOLOGICAL SETTING AND STRUCTURAL GEOLOGY

3.1. The External Crystalline Massifs of the Western Alps

The Western Alps are the curved sector of the Alpine chain running from southern Switzerland to the ligurian coastline in Italy. Moreover the term “Western” is used to denote the north-south striking westernmost part of the Alps (SCHMID et al., 2004). They can be subdivided into External Arc and Internal Arc, which are separated by the Penninic Frontal Thrust, a ductile deformation zone reactivated by brittle shearing during late Neogene. Moreover the Internal Arc is bounded eastwards by a subvertical strike-slip system corresponding to the Insubric Line and separating the Internal Alpine Arc from the Adriatic continental margin (Southern Alps).

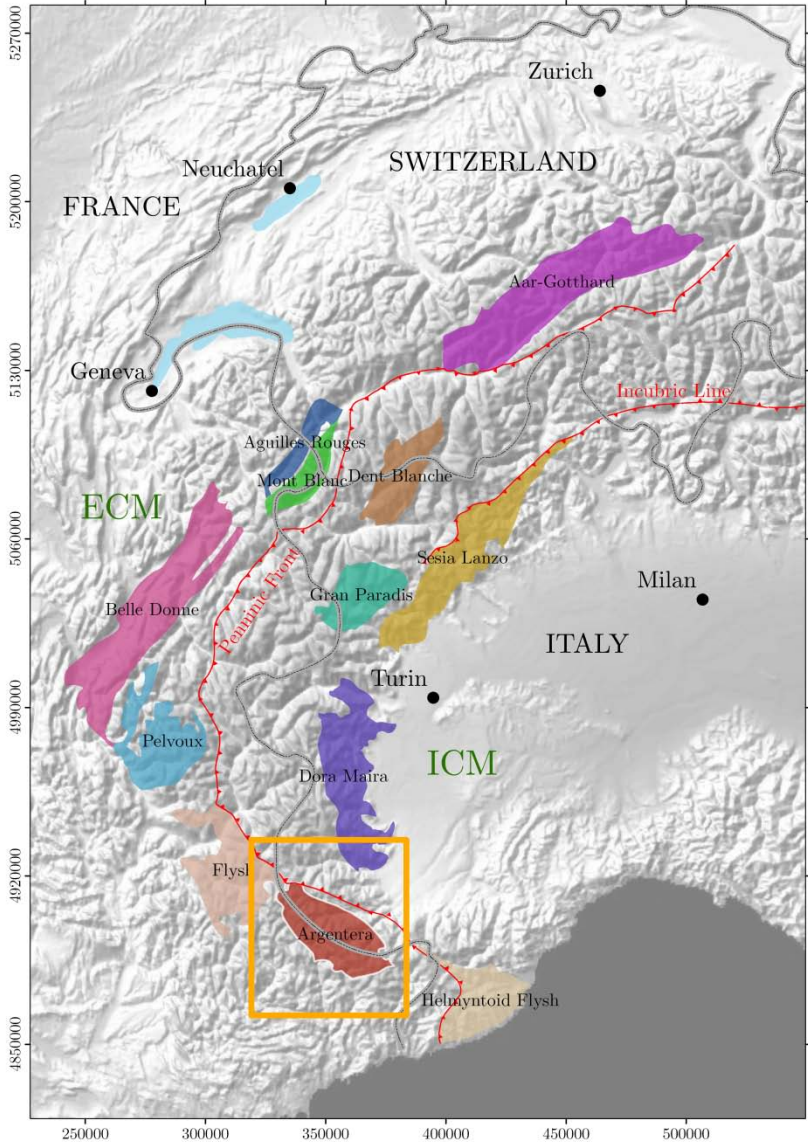


Figure 3-1 Sketch of the Crystalline Massifs of the Western Alps. ECM: External Crystalline Massifs; ICM: Internal Crystalline Massifs

The External Crystalline Massifs ECM (Figure 3-1) are a series of large crustal bodies aligned on the external part of the western and central Alpine chain. These basement units belong to the polymetamorphic European upper crust overlying the south-eastward plunging European lower crust. They are generally composed of a complex Variscan basement intruded by Permian granitoids.

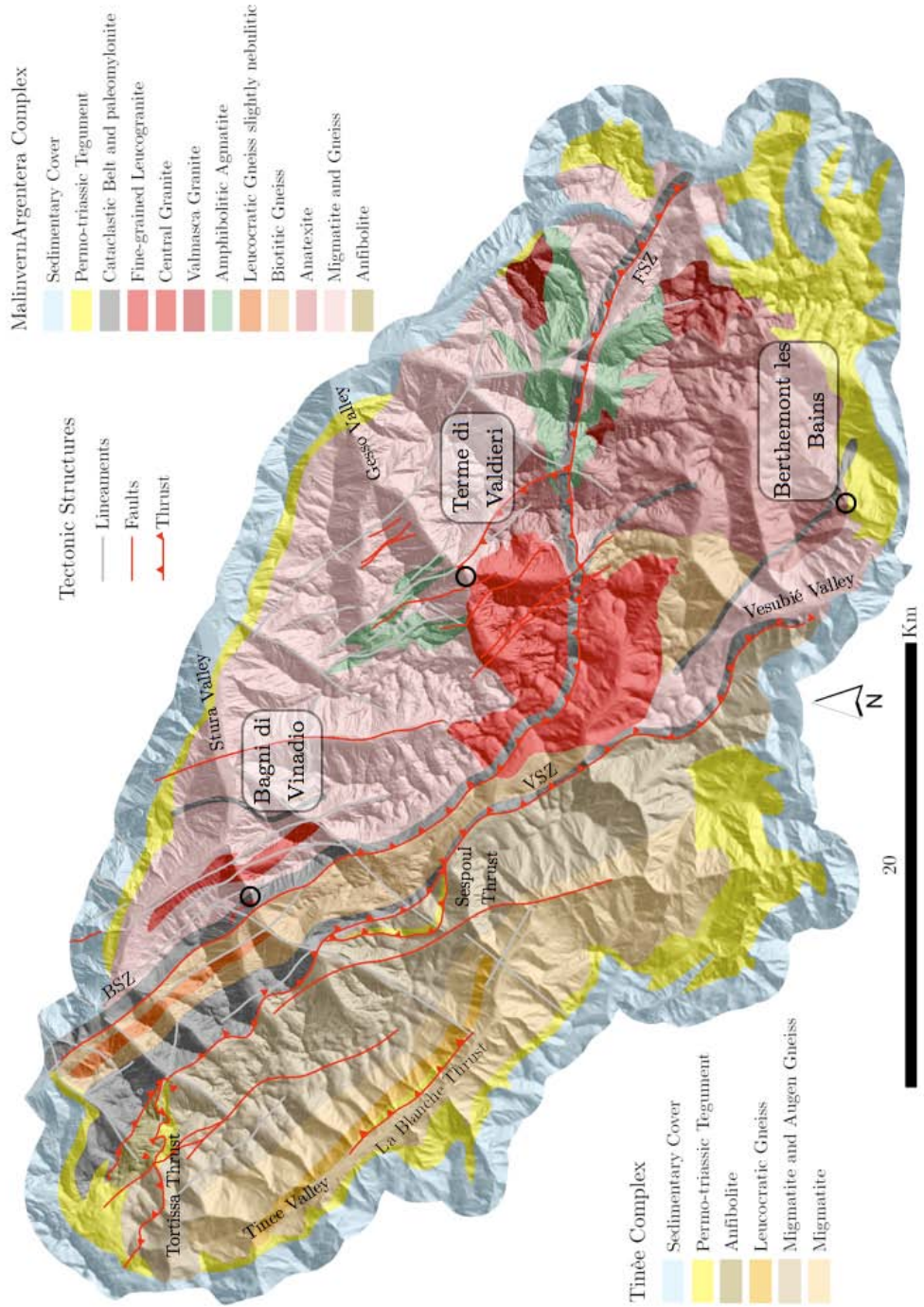
The geodynamic evolution of the ECM is still active as inferred from the recent observed upflow, estimated to be at 1 mm/y at the Aar et Pelvoux Massifs and 1.1-1.4 mm/y in the Argentera Massif (BIGOT-CORMIER et al., 2005). The exhumation of the External Crystalline Massifs started in the Miocene, at the end of the Alpine orogeny. The burial depth was higher for the northern massifs where temperature reached 350°C for the Mont Blanc and Aar massifs, whereas temperature remained in the 250°C range in the Argentera and Pelvoux massif (CORSINI and ROLLAND, 2009). As Bogdanoff (1991) proposed, this could be related to a change of the load related to the Penninic front that was minimal in the southern massifs and higher in the Mont Blanc and Aar massifs bringing to a lower burial in the southern sector up to 12-16 km in the northern ECM. A common feature among the ECM is the denudation process that started during the Oligocene even though the upflow rate had to be higher in the northern ECM (0.6 mm/y) than in the southern ones (0.3mm/y) with a strong increase at 3-4 Ma up to 1.2 mm/y, denudation rate that is comparable with the present upflow rate (VERNON et al., 2008).

3.2. The Argentera Massif

The Argentera Massif AM is the southernmost of the ECM and it is located at the border between Italy and France in the south-western Alps. It covers an area of about 1000 km² and has an NW-SE oriented elliptical shape, 25 km wide and 60 km long. The main fluvial systems of the Massif are the Gesso and Stura valleys in Italy and the Tinée and Vesubié valleys in France. In this Massif, the maximum elevations exceed 3000m a.s.l. and the landscape is the product of glacial, periglacial, hillslope and fluvial processes (MUSUMECI et al., 2003). The valleys were deeply shaped by Quaternary glaciers that abandoned large frontal and lateral moraines from 700 to 2600m a.s.l. (FEDERICI and PAPPALARDO, 1991).

The Argentera Massif (Figure 3-2) is interpreted as a pop-up structure of the pre-Triassic thickened crust, cropping out from the sedimentary cover at the footwall of the Penninic Front Thrust. It is mainly composed by high-grade metamorphic rocks (schist, migmatitic paragneiss, amphibolites, diatexite and anatectic granitoid), locally intruded by post metamorphic granitic bodies (BOGDANOFF et al., 1991; FRY, 1989). The crystalline rocks are unconformably overlaid by Triassic to Early Cretaceous carbonates that are mostly detached above the Late Triassic evaporite (FAURE-MURET, 1955; MALARODA, 1970).

Figure 3-2 Geological map of the Argentera Massif. BSZ: Bersezio Shear Zone; VSZ: Valletta Shear Zone; FSZ: Fremamorta Shear Zone; (mod. from Malaroda, 1970, Bogdanoff 1986, Musumeci 2003, Corsini 2004, Ribilini 2008 and Baietto 2009)



The AM is one of the zones of the Western Alps with the highest concentration of thermal activity related to the occurrence of fault systems. The spring sites are Bagni di Vinadio, Terme di Valdieri, on the Italian side, in the core of the massif, and Berthemont-Les-Bains in France at the south-west contact between the basement and the Dauphiné-Helvetic cover. All the three groups of thermal springs discharge at the intersection of the margin of NW-trending strike-slip fault zones and the bottom of the valley.

3.2.1. The Sedimentary Cover of the Argentera Massif

The sedimentary cover of the Argentera Massif can be subdivided into an autochthonous succession of Carboniferous–Triassic age and a detached succession of post-Late Triassic age (Figure 3-3). The Paleozoic-Cenozoic sediments of continental derivation, developed above the eroded basement, as for the other External Crystalline Massifs. Early Triassic rocks are frequently attached to the basement and form a thin cover that overlies the massif either around or within it (e.g. La Blanche, Sespoul, Tortissa Synclines). These formations are composed by quartzite, conglomerate, sandstone and siltite which locally crop out in the Italian side whereas they form a 3000-4000 m thick deposit on the French side (FAURE-MURET, 1955; MALARODA, 1970; STURANI, 1962). The Mesozoic succession starts with a 40m thick layer of green quartzite followed by two evaporitic events (Lower Cargneules and Upper Cargneules) separated by a thin layer of calcareous-dolomitic rocks. The late Triassic evaporite represent a detachment layer often involved in tectonic movement with its underlying and overlying layers. The latter ones are composed by the Jurassic limestone and dark slates (Terre Nere) that mainly crop out in the northern part of the AM in association with the dark limestones of the Barre Tithonique. In the southern part of the massif the Jurassic deposits are represented by bituminous dolostones and reef facies (MALARODA, 1970). The Early Cretaceous thin layers (0-50 m) of dark micritic limestones and calcareous sequence up to 600m thick is followed by the Upper Cretaceous detritic sequences, that reached a thickness of ca. 3000 m on the south-western and eastern border of the massif (MALARODA, 1999). The remaining Tertiary deposits, forming the Brianzonese sequence, comprehend the remnants of the foreland basins that formed during Tertiary collision between the Apulian plate with the European passive margin. The sequence starts with the deposition of limestones, calcareous slates, layers of conglomerates and sandstones with lacustrine facies and ends with the Helminthoid Flysch, an internally-derived unit overthrust on the foreland sequences starting from the Early Oligocene (CAMPREDON and GIANNERINI, 1982; FORD et al., 1999; KERCKHOVE, 1969) and presently exposed between the Pelvoux and the Argentera Massifs and south-east of the latter.

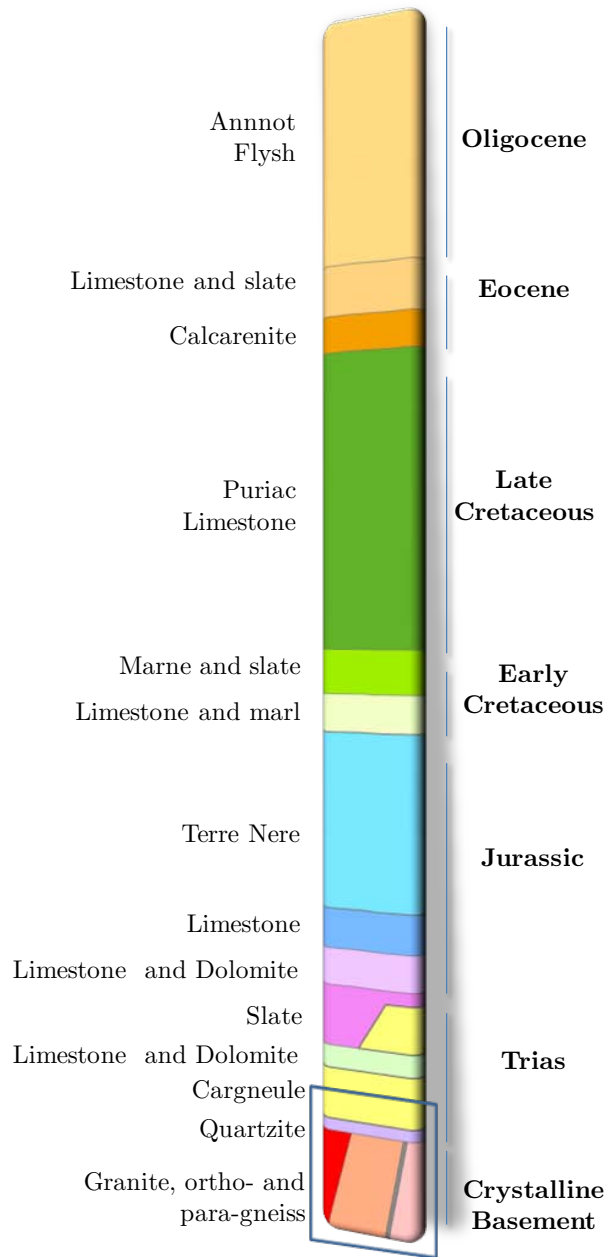


Figure 3-3 Schematic stratigraphic pile of the sedimentary cover surrounding the Argentera Massif.
 Blue square: formations accounted for the present study (mod. from Malaroda, 1979)

3.2.2. The Crystalline Basement and its Structures

The Argentera Massif comprises generally vertical metamorphic units trending N120-140°E composed of migmatite, ortho- and paragneiss, amphibolites and granites which can be divided into two main complexes classified on the basis of the different lithological associations (FAURE-MURET, 1955): the Tinée complex (TC) on the western side of the massif and the Malinvern-Argentera complex (MAC) at East. The two complexes differ by a HT-LP metamorphic event, which has been recorded only in the Malinvern Complex. The Tinée complex is constituted of anatectic gneisses derived partly from sedimentary and from intrusive protoliths (BOGDANOFF, 1986) with amphibolite, marble, quartzite, some horizons of graphite schist and metadiorite. The Malinvern-Argentera complex is mainly composed of migmatitic gneisses related to pre-Alpine, high-grade metamorphism of both para- and ortho-derivatives and composed of quartz, K-feldspar, plagioclase, biotite and minor muscovite and sillimanite (MALARODA, 1970; MALARODA, 1999) which are locally intruded by syn-anatectic, leucocratic, granites (West of Bagni di Vinadio) and tardive calc-alkaline granites (East of the Terme di Valdieri springs), where the Central Granite formation widely outcrops cutting across the foliation).

The Alpine structures cross-cutting the AM are represented mainly by ductile shear zones, strike-slip and reverse faults, often reactivating pre-Alpine and early-Alpine structures (BOGDANOFF et al., 1991). This behaviour is also the main feature of other external crystalline massifs e.g. the Gotthard (MARQUER, 1990), the Mont Blanc (GOURLAY, 1986) and the Pelvoux (FORD, 1996). In particular, three are the main structures that cross the AM: the Valletta Shear Zone (VSZ) and the Bersezio Shear Zone (BSZ) which crosscut the entire Massif north-west to south-east, with a dextral sense of shear and the Fremamorta Shear Zone (FSZ) which crosses the massif East-West (Figure 3-4).

The NW-SE trending VSZ, also known as the Ferriere-Mollières Line, crosses the entire massif and separates the two complexes. It is constituted by up to 1 km-thick mylonitic rocks that formed during a pre-Alpine stage (MUSUMECI and COLOMBO, 2002) and were partly derived by ductile shearing of high-grade metamorphic rocks of both the TC and MAC (BOGDANOFF, 1986). The VSZ splits into several E-W minor shear zones as the Tortissa Shear Zone (TSZ), at the northern border of the Massif which presents a 50° north dipping with a southward thrusting component.

The second main NW-SE structure is the BSZ, which runs parallel to the VSZ with a N150-N160 trend. The NW sector of the shear zone is characterized by a dense set of faults that strike NW-SE and are related to the BSZ. A right lateral component is described for the faults associated with the BSZ system (HORRENBERGER et al., 1978). In both shear zones, the mylonitic foliation, striking NW-SE, steeply dipping toward SW and NE, bears a gently dipping lineation and indicates transcurrent movements with a dextral sense of shear.

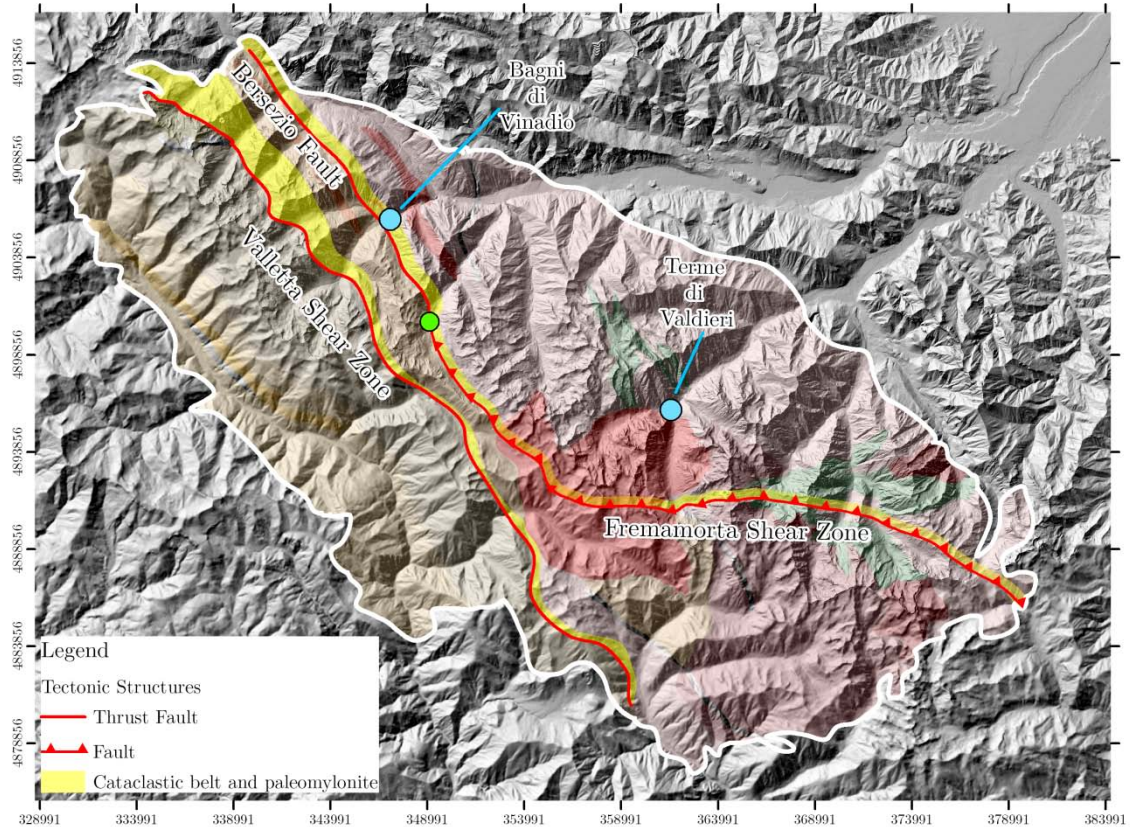


Figure 3-4 Main cataclastic belts associated to the most active strike slip faults and thrusts crosscutting the Argentera massif

Moreover both are interpreted as high angle shear zones, along which micaschists and mylonitic rocks crop out. The ensemble of the VSZ and BSZ was interpreted by Baietto (2006a) as a unique 3 km-wide zone of fracturing and pervasive cataclasis, named Bersezio Fault Zone (BFZ), bounded to the North-East by the Bersezio Fault and on the South-West by the Ferriere-Mollières Line FML. Baietto proposed this interpretation because on one hand the BSZ and the VSZ make part of a complex system of anastomosing faults cutting the crystalline rocks and lens-shaped tectonic slices, on the other hand is homogeneously made-up by Upper Carboniferous, Permian and Triassic rocks which compose the common protoliths of this sector of the massif.

In the southern part of the massif, south of the Terme di Valdieri site, the E-W oriented Fremamorta Shear Zone (FSZ), crosscuts the Central Granite formation and connects to the BSZ. The FMZ is mainly composed by mylonitic and ultramylonitic rocks that crystallized in green schist metamorphic conditions. The main tectonic elements of the SE sector show a WNW–ESE orientation connected to the FSZ. Along the FSZ the mylonitic foliation progressively dips to the north (30-50°) as it bends, while the lineation keeps consistently a north-south trend. All the shear criteria indicate a oblique-inverse sense of shear (BAIETTO et al., 2009). In the SE sector a reverse mechanism dominates the FSZ structures (MUSUMECI et al., 2003).

The rock assemblages associated to these shear zones can be divided into: mylonitic rocks, quartz and chlorite fibres and aggregates coating slickensides and filling veins, fault breccia and zones of intense fracturing and layers of cataclasites and gouges (BAIETTO et al., 2009).

These fault rocks formed in different stages and T-P conditions and can be associated to the their development following the criteria of Schmidt & Handy (2003):

- viscous regime: mylonites. They developed under green schist condition during an Alpine deformation phase (CORSINI et al., 2004):
- frictional-to-viscous transition regime: quartz–chlorite slickensides and veins. They formed syn-kinematically to the faults. Their composition indicates a lower green-schist facies and the quartz–feldspathic mylonitic foliation of some mylonites is locally plastically dragged. These are typical condition of the transition between viscous to frictional regime.
- frictional regime: cataclasites, gouges, fault breccia, fractured protolith rocks. The cataclasites and gouges occur in networks of multiple and interconnected layers, the fault breccia and fractured protoliths occur both in thick zones located on the external borders of the fault cores and in lens-shaped blocks enveloped by cataclastic-gouge layers (BAIETTO, 2006b)

3.2.3. Geodynamic Evolution and Exhumation of the Argentera Massif

The structural features of the Argentera Massif result from the superimposition of two main deformative events that occurred during the Alpine tectonic evolution of this sector of the Alps (BOGDANOFF, 1986). During the first phase (Oligocene) folding and thrusting occurred, the latter being responsible for the cover detachment at the level of the Triassic evaporites. Thrusting occurred along the FSZ and was cinematically linked to dextral strike-slip trend along the BSZ, which acted as a steep lateral ramp (transpressive transcurrent fault). During the second phase (Upper Miocene–Pliocene), some slices of basement were thrust over the overlying cover along structures corresponding to the Tortisse, Sespoul, and Colle del Sabbione thrust zones. Coeval reverse and strike-slip fault systems (e.g. Bersezio Fault; Labaume et al., 1989), reactivated the older Variscan tectonic lines with the development of cataclastic rocks along narrow bands nearly parallel to the late Variscan mylonites. Most of these structures were activated at different times along the same tectonic lines with SW vergent and right lateral compressive movements (BOGDANOFF, 1986; LABAUME et al., 1989).

The recent upflow and exhumation of the Argentera (DEBELMAS and KERCKHOVE, 1980b); (BIGOT-CORMIER et al., 2000) is due to both active tectonics and isostatic release. Even though an glacier-induced isostatic rebound cannot be neglected, the most part of the process occurred along thrust systems and oblique strike-slip faults in response to NE–SW Late Alpine transpressive tectonics (BOGDANOFF et al., 2000; FRY, 1989; TRICART, 2004). Seismic and GPS data document that the area is tectonically active, with crustal shortening of 2–4 mm/yr induced by N–S to NE–SW compression (CALAIS et al., 2000; FRECHET and PAVONI, 1979; MADEDDU et al., 1996). Crustal shortening started in the south-western Alps from around 15 Ma and is usually assumed to be still active. This has resulted in the upflow of parts of the Variscan basement (Argentera massif emplacement) and has triggered the southward thrusting of the southern subalpine belts (BOGDANOFF et al., 1991; TRICART, 2004). Exhumation is characterized by mean denudation rates of 0.25mm/yr in the late

Miocene–Pliocene (8–3 Ma) and underwent an increase at 3.5 Ma to rates of 0.8–1 mm/yr (BIGOT-CORMIER et al., 2000; BOGDANOFF et al., 2000). Apatite fission track analysis shows variable denudation rates that have been interpreted in terms of differential vertical upflow of crustal blocks. This spatial variation in denudation and upflow is also shown by the overall morphology of the Massif (cfr. 3.3), e.g in the central part, which shows a higher degree of upflow with respect to the other portions of the massif. This is in good agreement with the recognized differential vertical motions of blocks within the Argentera Massif occurred as a consequence of different cooling histories highlighted by zircon and apatite fission track analysis (BIGOT-CORMIER et al., 2000). Moreover, Pliocene to recent denudation rate of 1.1–1.4 mm/yr for the central Argentera (BOGDANOFF et al., 2000), matches with the suggested tectonic upflow of this area as consequence of south-westward thrusting along Orgials and Valetta Faults which acted as a south-west-directed thrust that yielding a vertical offset of 500 m between the NE and SW part of the AM.

3.3. Relationships between Geomorphology and Structures

In tectonically active mountain regions, such as the Argentera Massif, the recent tectonic evolution reflect on morphological features such as slopes and drainage networks. In fact deformation and upflow variations affecting the bedrock may cause perturbations in the fluvial network. In the Argentera Massif, where the maximum elevations exceed 3000 m a.s.l., morphology results from glacial, periglacial, hillslope and fluvial processes affecting the Variscan basement. Musumeci et al. (2003) pointed out the differences in landscape between the Italian and the French side of the massif. The former shows deeply incised and steep slopes, the latter is characterised by wider and smoother landscape. These differences, even though a contribution from glacier-induced isostatic rebound might not be neglected, are interpreted as the result of spatial variations occurred during the late Miocene exhumation process, which brought to differential vertical motions of the crystalline blocks within the Massif. In particular, the central part of the massif, between the Orgials Valley, Lombarda Pass and Valetta Valley, shows anomalous orographic and drainage characteristics. As climate and lithology conditions can be considered uniform, this anomaly can be explained with a maximum tectonic upflow related to a differentiated exhumation process, which affected this sector of the massif with respect to the other regions. The Orgials and Valetta Valleys, located at the intersection between the Bersezio-Colle della Lombarda and the Fremamorta-Colle del Sabbione faults, can be interpreted as the hanging wall of a thrust zone developed in transpressive regime consistent with the post-Pliocene tectonic evolution of the southern Western Alps. Moreover Ribolini et al. (2008), highlighted the strong relationship between drainage networks and tectonic lineaments (Figure 3-5). In particular a clear relationship is shown in the NW sector of the Massif, where the relief is lower (the highest elevation merely exceeds 2800 m a.s.l.) than the south-eastern sector of the massif because it is tectonically controlled by the strike-slip faults related to the Bersezio Fault, which didn't strongly affected the vertical upflow of the area. The lower relief results in higher sensitivity of drainage network to fracture and fault systems. Hence, close to the Bagni di Vinadio area the drainage pattern is the same as the lineaments and, in correspondence of the Tinée valley the most frequent drainage network is dominated by low

order channels running perpendicular to the main valleys and lineaments. In the south eastern sector of the massif, between the Orgials Valley and the Gesso River basin, most of the faults are related to the Framamorta-Colle del Sabbione thrust system and show a vertical direction related to the highest maximum upflow rate of the entire massif. As a consequence, the high relief, rather than fault and fracture systems, is the most important factor controlling the drainage network. As a result, the drainage network shows a dendritic pattern, as in the Terme di Valdieri area, and the main rivers run transversally to the Massif (RIBOLINI and SPAGNOLO, 2008).

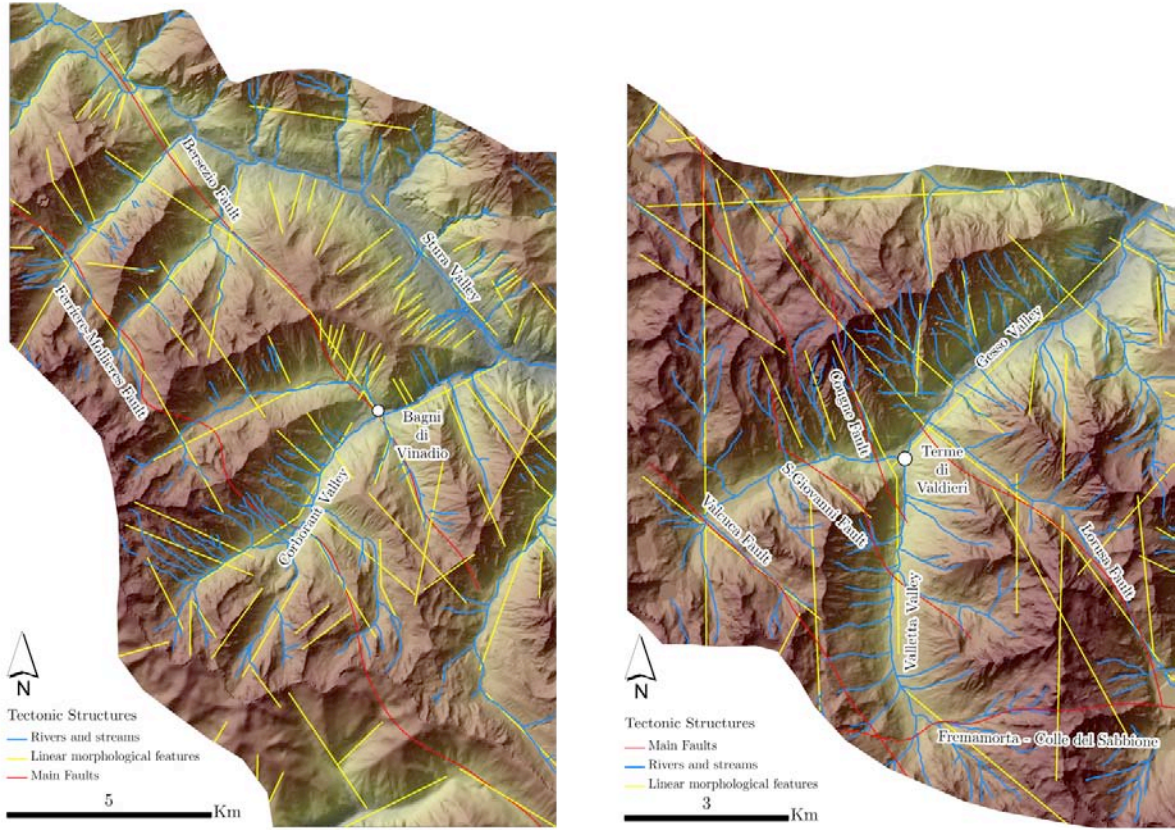


Figure 3-5 Relation between linear morphological fractures, drainage network and major faults in the Bagni di Vinadio and Terme di Valdieri regions

3.4. Seismicity of the Western Alps and the Argentera Massif

The South-Western Alps are one of the most seismically active areas among the western European countries. Several hundred events of small to medium magnitude (up to $M=6$ as the one in 1989) have been recorded ever since (Figure 3-6a). Earthquakes are not uniformly distributed within the areas of interest (Béthoux et al., 1988). Most of the seismicity is concentrated along the northern margin of the Ligurian basin and the north-eastern side of the Argentera massif following the Penninic front.

The interpretation of the focal mechanism of the swarms of microseisms helps to identify active faults and gather information about the stress state in the crust. For most events, the depth is well constrained in a range between 5 and 12 km. Recent geodetic investigations

show a significant strain rate during the last 50 years in the area between the Argentera Massif and the Mediterranean coastline (LARROQUE et al., 2001).

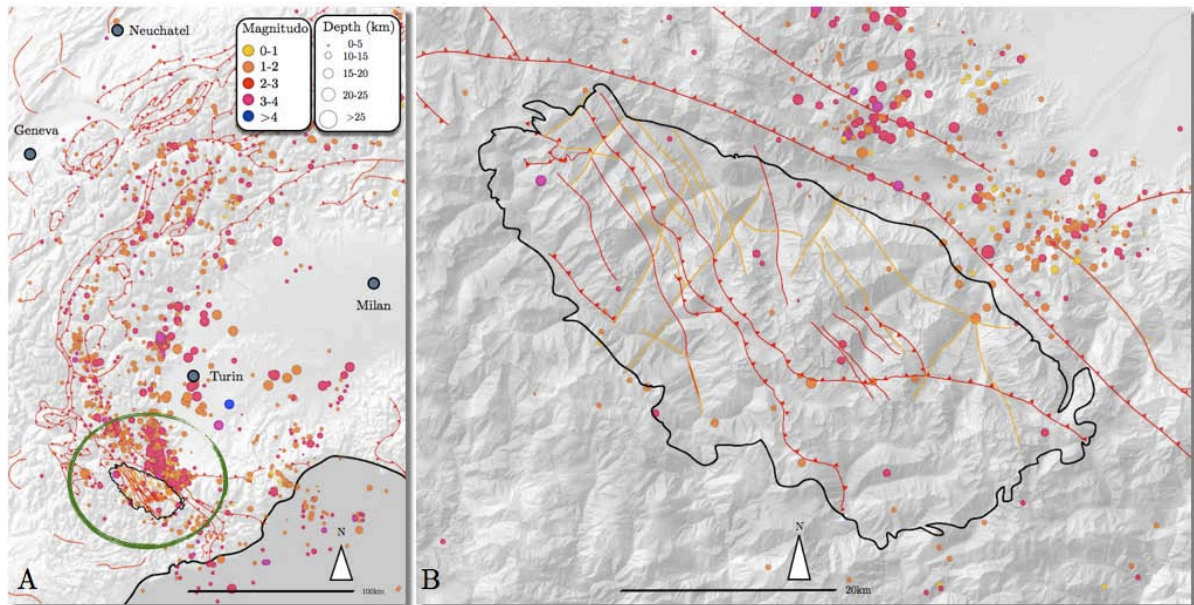


Figure 3-6 Seismicity recorded in the last 6 years. A: Overview of the western Alps; B: Detail of the Argentera Massif showing the main geological structure

In the Argentera Massif one of the most interesting zones is the central part where the Bersezio Shear Zone connects to the Fremamorta-Colle del Sabbione Line (Figure 3-6b). The Bersezio Fault is the southern prolongation of the Sérenne fault, one of the most active seismic lineaments of the Southern Alps. In this area, epicentre trends underline the Bersezio dextral strike-slip fault, striking N145E. Moreover it displays field evidence for recent reverse dextral movement (RITZ, 1992) such as offsets of moraine crest lines and tectonic scarps, that affect their dating from the last glacial maximum (SAURET and TERRIER, 1987). The study of focal mechanism reveals that this area is characterized by an extensional stress field. Furthermore, geochemical analyses and detected helium and radon anomalies straight above the trace of the fault suggest a current tectonic activity (BAUBRON J.C., 1987).

Seismic data also bring important information about the Moho depth that is an important parameter for the interpretation of the gravity data. Below the Argentera Massif, the Moho is located at a depth of 40–45 km, even though just north of the massif it reaches 51km depth (THOUVENOT et al., 2007) and becomes shallower toward the south to reach a depth around 27 km under the coast (MASSON et al., 1999). However a strong reflector is located around 25 km depth (LARROQUE et al., 2001; LARROQUE et al., 2009). Several authors have proposed the existence of a crustal blind thrust fault, connected to the South with the detachment layer in the Triassic evaporite underlying the Castellane and Nice arcs. This crustal ramp could be associated with the recent basement upflow of the Argentera massif. But no superficial E-W structure related to this deep-seated shortening has been reported in the field, for instance

4

GEOLOGICAL FRAMEWORK OF THE INVESTIGATION SITES

4.1. Geology and boreholes at Bagni di Vinadio

4.1.1. Geological observations

At Bagni di Vinadio thermal springs discharge through intensely fractured leucogranites and migmatitic gneiss, at the intersection between the Ischiator, Corborant and Insciauda valleys. The hot springs are located at the step-over zone between two brittle shear zones with dextral sense of shear in correspondence of the Bersezio Fault on the East and the Picial Fault, few hundred meters west of the springs. In particular, the Bersezio Fault is represented by a 200m wide mylonitic belt involving biotitic and mylonitic gneiss of the Argentera Massif Complex and, in correspondence of the thermal springs a small outcrop of micro-fined leucogranite probably connected, in the subsurface, to the micro-fined granite intruding the gneiss east of the thermal area (Figure 4-1).

The western sector of the Vinadio is cut by the Valletta Shear Zone VSZ, which consists of low-grade mylonitic rocks composed by mylonites and micaschist. In the study area the VSZ is up to 500 m thick and shows a dextral strike slip trend, which is compatible with the general extensional tectonic regime occurred during Carboniferous in the entire Western Alps. The mylonitic foliation strikes NW-SE and steeply dips towards NE in the northern part of the area and towards SW in the south (MUSUMECI and COLOMBO, 2002). The southern part of the VSZ runs parallel the Sespoul Thrust which outcrops immediately westward the VSZ. Along this thrust basement rocks are thrust onto the Triassic sedimentary cover, which locally crops out pinched between the footwall and the hanging wall of the reverse fault (BOGDANOFF et al., 2000).

The area bounded to the NE by the Bersezio Fault and the Valletta Fault to the SW is a 3 km-wide belt composed by high angle strike slip faults that develop two conjugate systems: a main right-lateral NW-SE to NNW-SSE system and a secondary left-lateral NE-SW to ENE-WSW system. This area was considered as a unique structure by Baietto (2009), named Bersezio Fault Zone because on one hand the BSZ and the VSZ make part of a complex system of anastomosing faults cutting the crystalline rocks and lens-shaped tectonic slices, on the other hand is homogeneously made-up by Upper Carboniferous, Permian and Triassic rocks which compose the common protoliths of this sector of the massif. The regional strain domains can be divided into 2 main groups: wrench-contraction and wrench-extension even though an isolated zone located in the western margin of the fault zone shows pure wrench kinematic. The compressional strain is located at the margins of the BFZ and reveals interlinked systems of strike-slips faults and reverse faults. On the contrary the core of the BFZ is characterized by a wrench-extensional component and is dominated by sets of E-W, NE-SW and N-S striking normal faults mutually cross-cutting with NW-SE and NE-SW strike-slip faults (Figure 4-2). In particular the hot springs are located in an extensional zone adjacent to two compressional domains (BAIETTO et al., 2009).

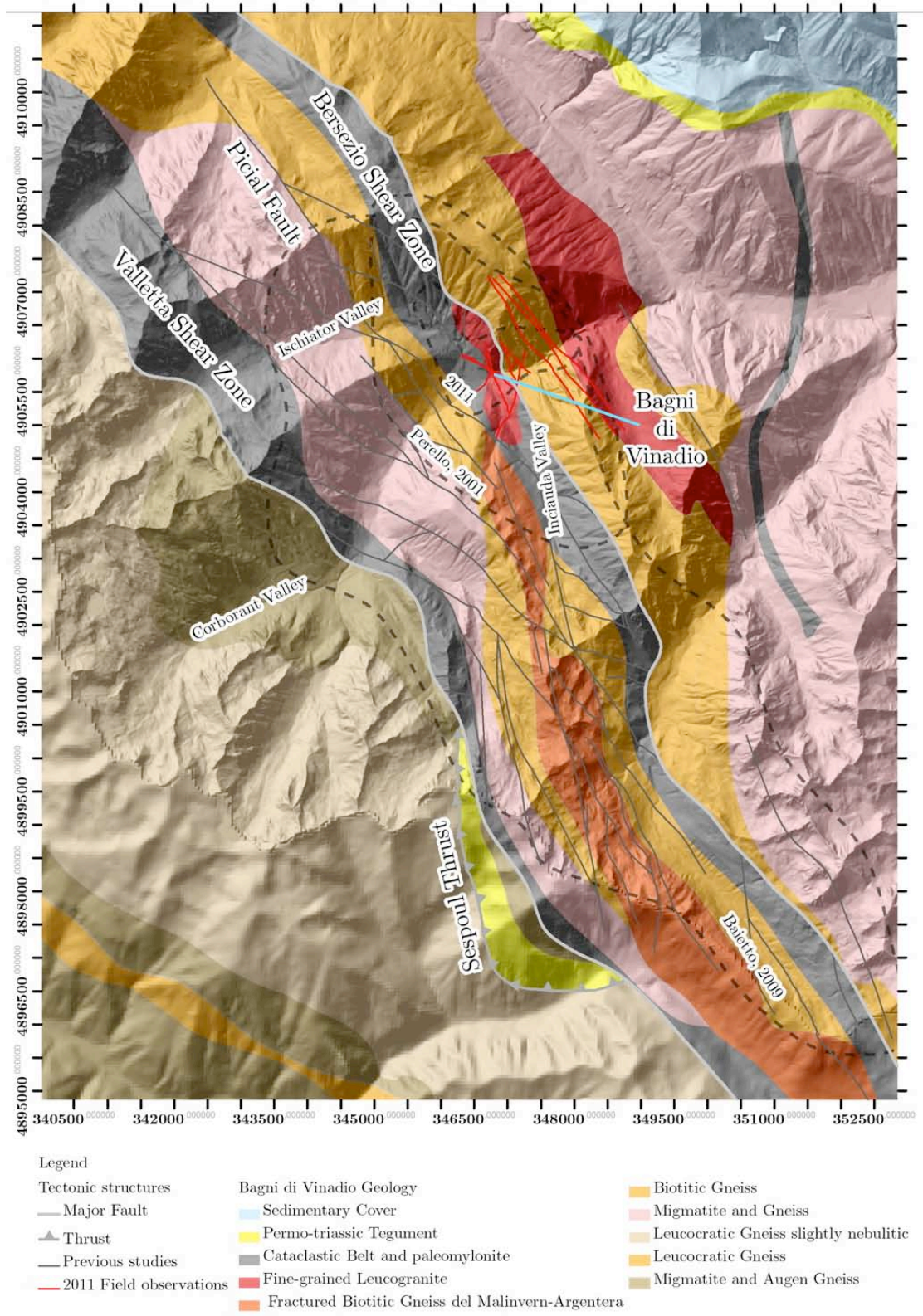


Figure 4-1 Geology and observed structures in the Bagni di Vinadio area

The foliation of the cataclastic rocks of the BFZ shows two main dipping directions towards NE and SW, indicating an overall flower structure. In this sector, migmatitic gneisses, fine-grained aplitic granites and minor slices of sedimentary rocks (yellow cavernous Triassic limestone, dolostone and strongly tectonized cagneule along the Sespoul Thrust) crop out. Small dykes of aplitic granites cutting the migmatitic foliation are widespread around Vinadio.

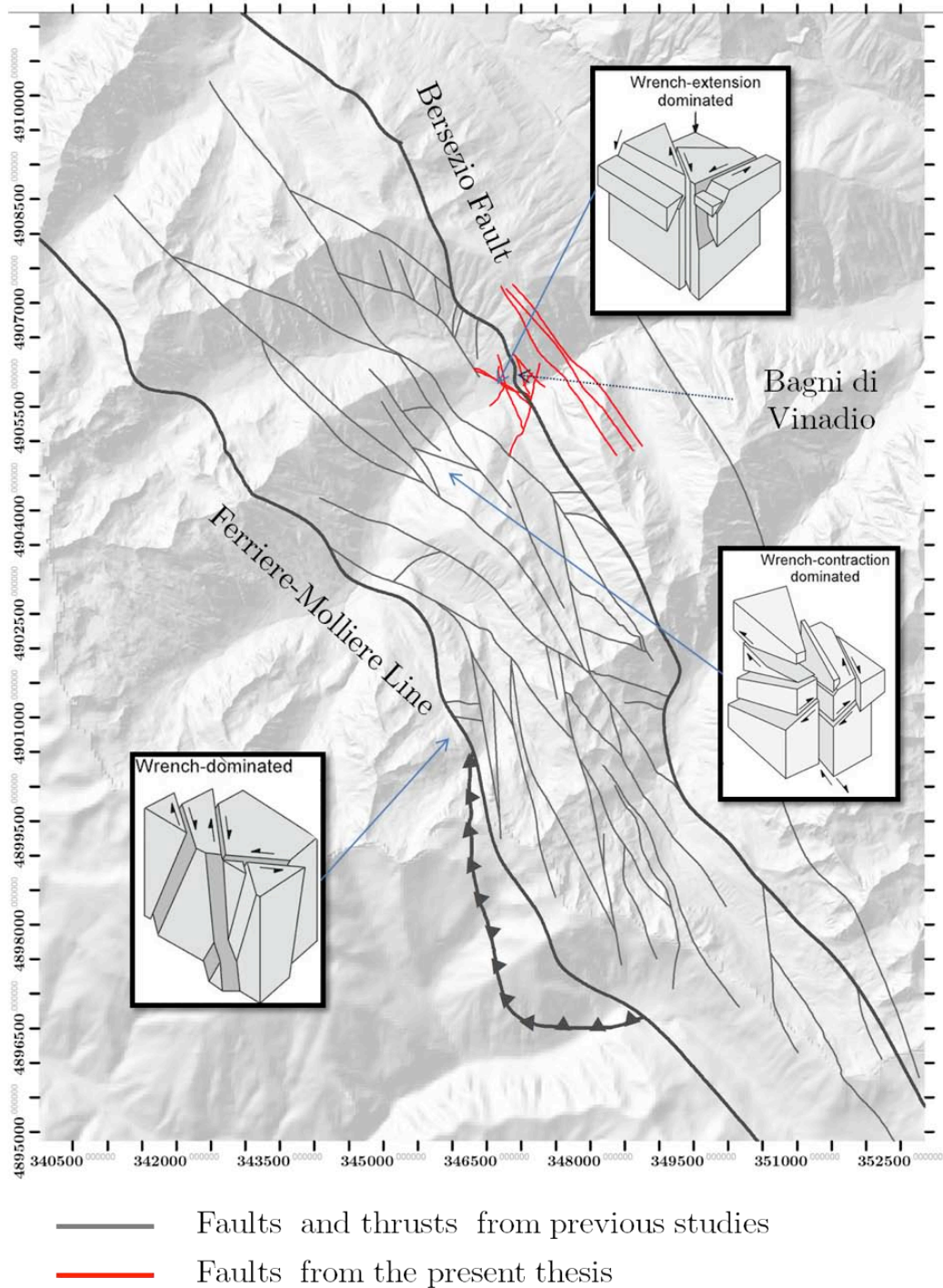


Figure 4-2 Deformational domains at Bagni di Vinadio (mod. from Baietto et al., 2009)

In the framework of this Thesis a detailed study of the fracture condition was carried out in a small area in the proximities and inside the thermal springs' caves. The study area covered about 1500 m² on the two sides of the Bersezio shear zone (Figure 4-3). A total of 20 sites were considered, with particular focus on the thermal springs' area where the entire set of fractures related to the thermal water upflow crops out, therefore it has been possible to estimate fracture density variation with respect to the surrounding zones.

North of the thermal site, highly tectonized and mylonitized potassic migmatitic gneiss of the Bersezio shear zone crops out. In the proximities of the thermal springs leucogranites, and two main sets of fractures were observed. The main system is dominated by the alpine structures of the Bersezio and Pical faults trending NW-SE (F1 system), and is associated to a pattern of perpendicular and strike-slip subvertical conjugate faults. (F2 system).

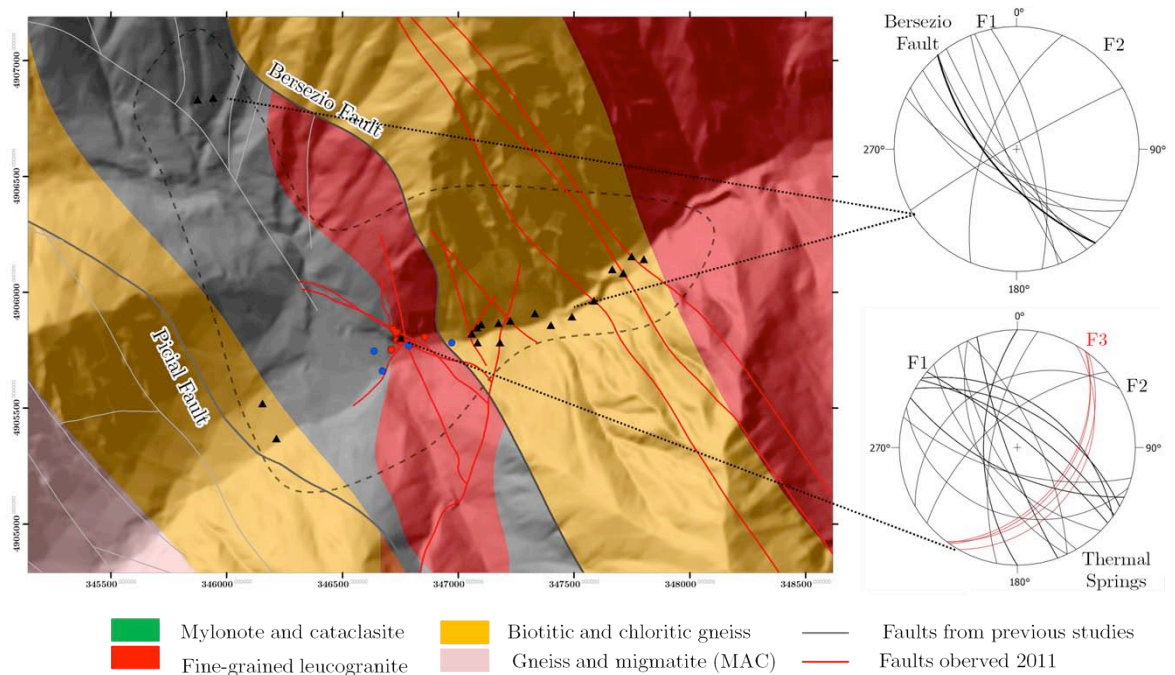


Figure 4-3 Fracture networks in the Bagni di Vinadio area with the location of the observations (black triangle) and the water sampling points (blue circles: cold water; red circles: thermal water)

East of the thermal area the same systems were observed, but an increase in fracture density was observed approaching to the fine-grained granitic body which crops out in the external sector of this study area. The increase in fracture pattern in granites with respect to the gneiss is described by Stober & Bucher (2007). They correlated the hydraulic properties of several crystalline samples collected in deep geothermal boreholes. They observed that zones with enhanced hydraulic conductivity strongly depend on the presence of fine-grained granite, which tends to be more pervious than gneiss and amphibolite by a factor of 100 or 2 orders of magnitude.

More detailed observations were carried out in the thermal springs' area (Figure 4-4), in particular in the vicinities of the garage where two shallow wells, described in the followings, were drilled in the past. In this sector the observations pointed out an outcrop of highly fractured fine-grained granite in the proximities of the thermal spa. Moreover, in correspondence of the leucogranites, a low angle NE-SW system of fractures develops coupled

to the two main systems (F3 system). As shown in Figure 4-4, all thermal springs seem to be aligned along this latter system, which might extend up to 750-1 km in the subsurface, according to the 3D modelling simulations (Chapter 6), where it connects to the main structures of the Bersezio fault hence might control the final upflow of the thermal waters along the Bersezio shear zone.

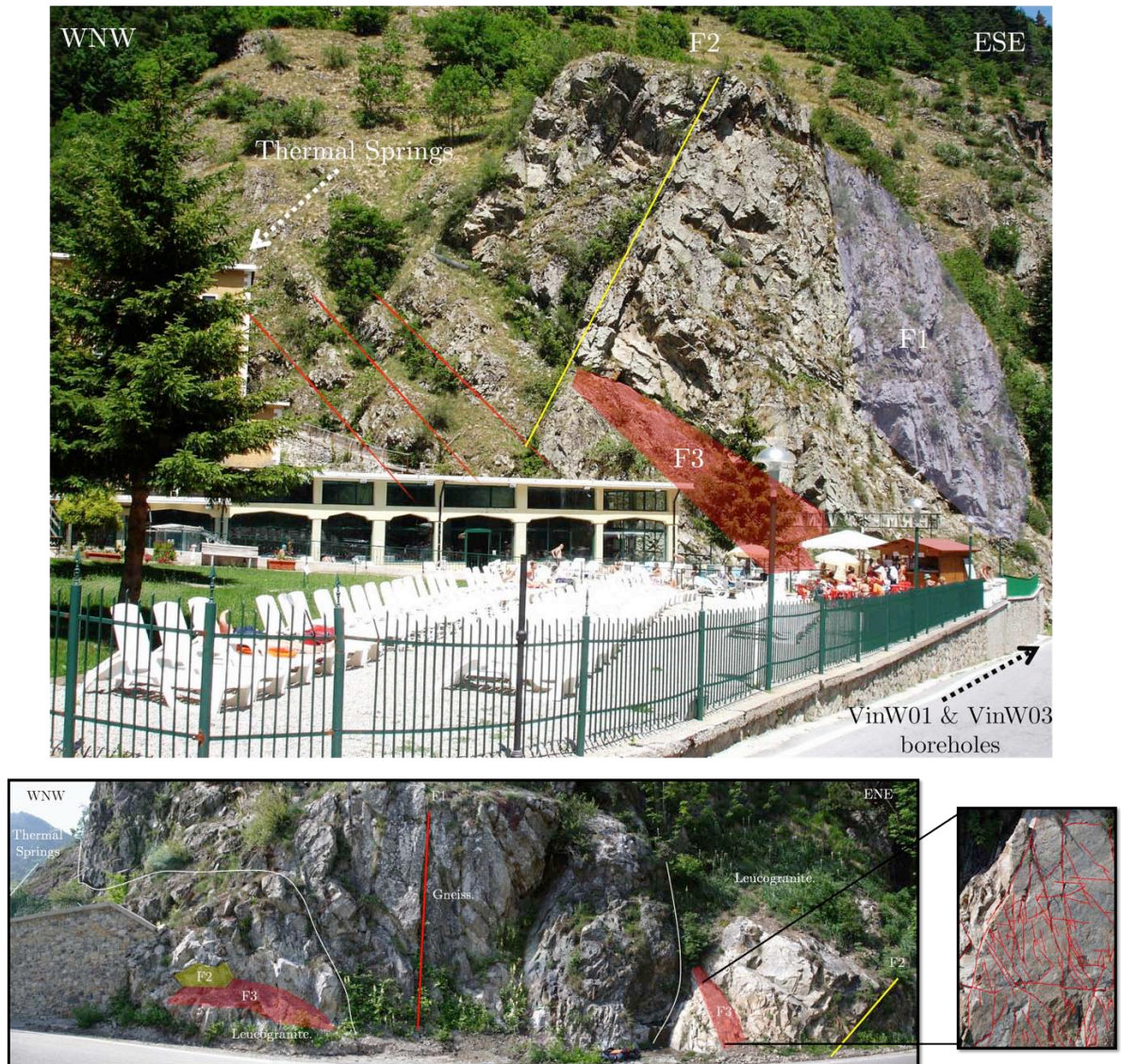


Figure 4-4 Fault planes and fracture network in the spring area and fracture network of the leucogranite cropping out within the biotitic gneiss paleomylonites of the BSZ

4.2. Boreholes

In the thermal spa, three boreholes⁴ were drilled in the past and, in this paragraph, they will be referred as VinW01, VinW02 and VinW03. The VinW03 was drilled in the 1980's but no documentation is available. The information about these wells are very scarce but according to the owner of the spa it has an artesian flow rate of 5 l/s, a diameter of 60 cm and is 80 m depth. The VinW01 and VinW02 were drilled in October-December 2001. The former is located in the parking lot at the entrance of the spa, the latter few meters from VinW03 and reaches a depth of 77 m.

Figure 4-5 shows the sketches of the lithologies crossed during the drilling of the VinW01 and VinW02 wells. VinW01 crosses unconsolidated rock for the entire length of the well up to 117 m depth. This lithology can be interpreted as glacial till, but because the well is perfectly located in the core of the Bersezio Shear Zone, the unconsolidated rock can be considered as cataclasites, totally similar to those observed north of the thermal springs, where the BSZ clearly crops out. This second interpretation can be also supported by the fact that the crystalline bedrock crops out around the thermal springs and along the river bed, only 10 meters below them. A pumping test was carried out in 2001 and temperature showed a drop down from 78 to 65°C and conductivity decreased from 3200 µS/cm to 2600 µS/cm. This was interpreted as mixing, probably due to excessive pumping, between deep and shallow cold waters, either located in the first 60m of detritic cover or in the river bed. A maximal flow rate of 15 l/s was therefore suggested for its exploitation to avoid the capture of shallow cold waters. The stratigraphy of VinW02 indicates that the crystalline bedrock is located below 18 m of detritic cover. A 2001 pumping state showed a flow rate of 8 l/s. Hot waters were found during drilling at 43 m (referred as "*hot water*") and showed an increasing temperature towards the bottom of the well (reported as "*hot water with steam*"⁵). Nowadays just the waters of well VinW02 are partially exploited for the swimming pool after being cooled down with cold waters and for heating during winter.

4 Information regarding the wells is taken from a technical report compiled by Dr. Geol. Sassone and kindly provided by Mr. Calabrese, the owner of the thermal baths.

5 According to geochemical observations, no steam phase is present for the thermal waters circulating within the Argentera Massif, therefore this information has to be interpreted just as an increase of temperature.

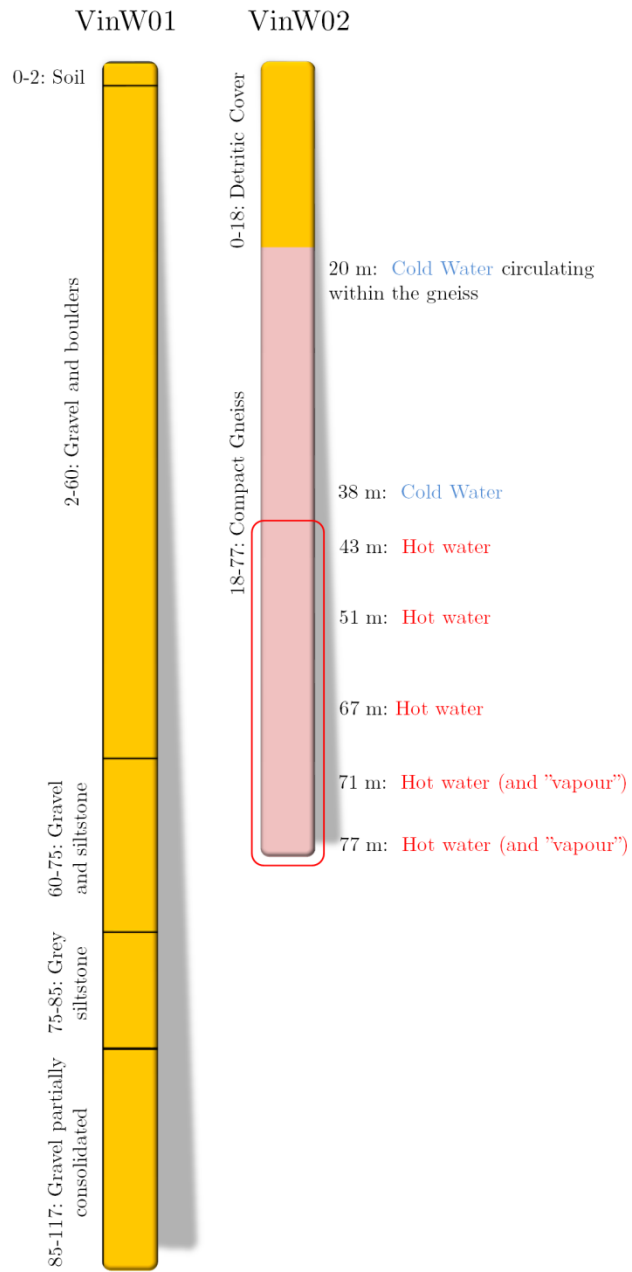


Figure 4-5 Sketches of the well ValW01 and ValW02 indicating the depth where hot water was found (mod from Dr. Geol. Sassone technical report, 2001)

4.3. Geological Setting of the Terme di Valdieri Area

4.3.1. Geological observations

The thermal springs of Terme di Valdieri are located in correspondence of the intersection between the northern termination of the 200m-wide cataclastic shear zone of the Lorusa Fault and the Gesso River. The Lorusa Fault represents the south-eastern border of a zone of intense fracturing limited to the NW by the Cougne Fault, a strike slip fault with dextral sense of shear that crosses both the migmatites and the granite (Figure 4-7).

The interpretation of slickensides by Baietto (2009), suggests that the zone between these two faults was deformed in a wrench, slightly transtensive, tectonic regime (Figure 4-6). Both faults dip south-westward while two other main strike slip faults, the S. Giovanni and the Valcuca faults in the SW part of the area, show a progressive north-eastward rotation of the dip direction.

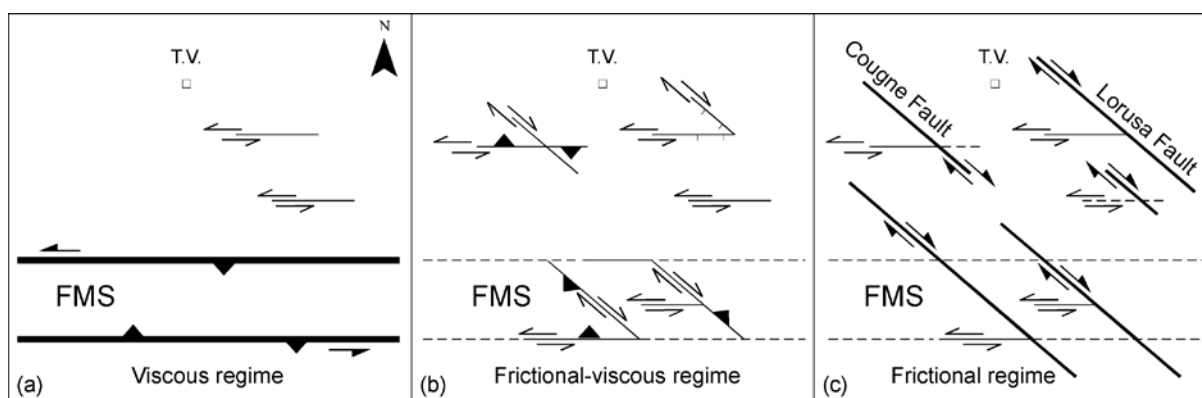
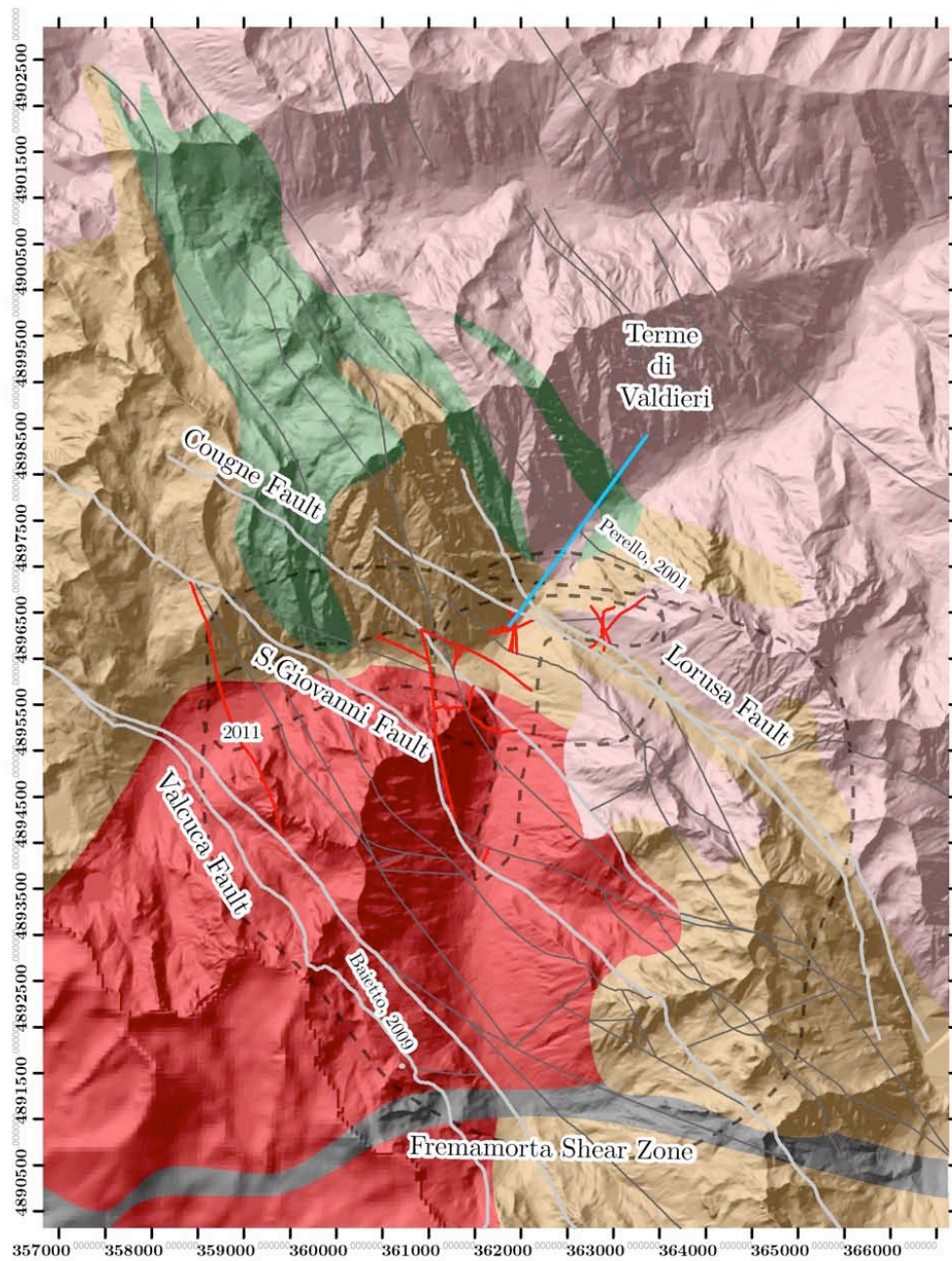


Figure 4-6 Structural evolution of the Terme di Valdieri Area (after Baietto, 2006)

These four faults form a regional flower structure, similar to the structure of the BFZ. As like as at Vinadio, the springs discharge in correspondence of high fractured aplitic dykes. The main outcropping lithologies around the thermal springs are migmatitic gneisses (biotite-rich embrechites and by leucocratic anatexites) and, to the south, the medium grained granite of the Central Granite formation which locally grades to fine grained leucogranites, in particular in correspondence of the thermal springs. The granite was also observed in the Ciriegia Tunnel which was drilled few kilometres East of Terme di Valdieri and where a large granitic body was crossed after 1km from the entrance of the tunnel and cropped out over a distance of two kilometres (BORTOLAMI and GRASSO, 1969).



Legend

| | | |
|---------------------|--------------------------------------|---|
| Tectonic structures | Terme di Valdieri Geology | Migmatite and Gneiss |
| — Main Fault | — Cataclastic Belt and paleomylonite | — Leucocratic Gneiss slightly nebulitic |
| — Previous studies | — Central Granite | — Biotitic Gneiss |
| — 2011 Observations | — Amphibolitic Agmatite | — Biotitic and Muscovite Embrichites |

Figure 4-7 Geology and observed structures in the Terme di Valdieri area

The structural setting of Terme di Valdieri is controlled by pervasive en-echelon NW–SE to NNW–SSE directed faults showing evidences of right-lateral displacement and cutting the migmatites and the granitic body with persistence up to 10 km. These main faults are locally coupled to ENE–WSW and NE–SW faults characterized by left-lateral movements. The strike slip faults architecture is characterized by an internal gouge zone intermediate cataclastic domain and an outer brecciated and highly fractured zone. The fracture spacing ranges from a few centimetres to a meter and the opening is usually of a few millimetres. The thickness of these zones varies whether the fault crosses the mylonites or the granites. In fact Baietto observed that within the mylonites the gouge, the cataclastic and the breccia zones have thickness ranging, respectively, between 0.1 to 2, 0.5 to 5 and 1 to 50 metres, while within the granites the cataclastic and gouge zones are less abundant and the breccia zones are much wider (hundreds of metres thick).

As for the Vinadio area, some fracturing observations were carried out in the thermal spring area along the Valasco, Valletta and Lorusa valleys and inside the springs' caves (Figure 4-8).

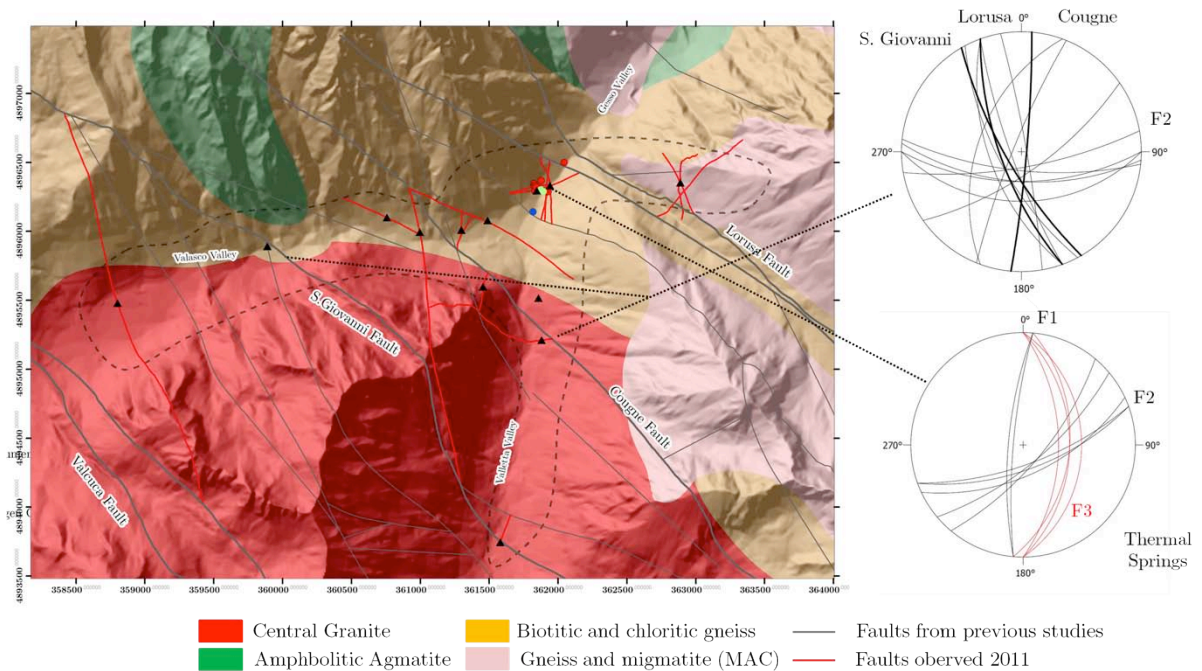


Figure 4-8 Fracture Networks in the Terme di Valdieri area with the location of the observations (black triangle) and the water sampling points (blue circles: cold water; red circles: thermal water)

Along the Valasco valley it was possible to follow the contact between the biotitic gneiss of the Malinvern Argentera Complex and the medium grained granites of the Central Granite formation, which is the most prevalent lithology in the area. Moreover it was possible to perceive the Cougne Fault, few hundreds of meters Eastwards the thermal springs and S.Giovanni fault (Figure 4-9), visible from the Casa di Caccia, which are the two major strike slip faults (F1 system) in this sector and crosscut the Granito Centrale formation to then reach the Valletta valley towards SE. These two faults are associated with a conjugated system dipping 60-70 ° towards SSE.

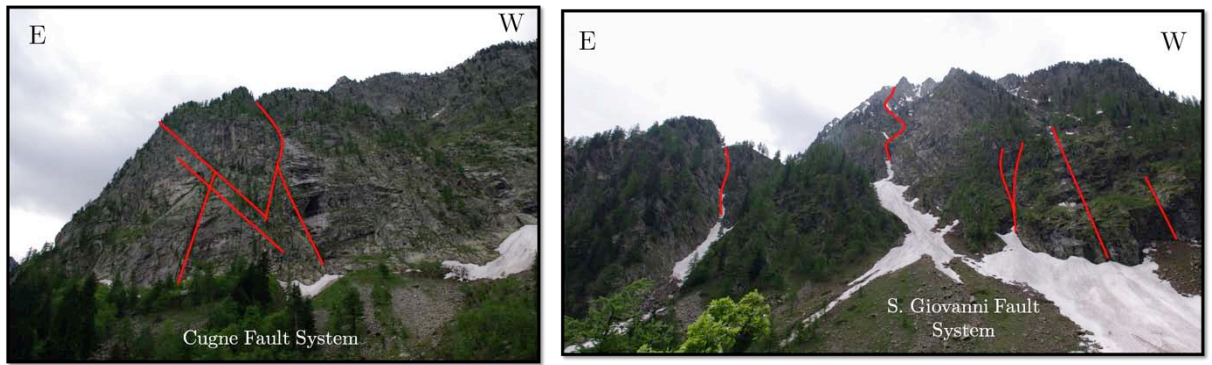


Figure 4-9 Cugne and S.Giovanni faults systems from the Valasco Valley

The road which brings to Piano Casa del Re along the Valletta valley crosses the Central Granite, hence a better overview of the fracturing conditions of the granite is possible. In fact as shown in Figure 4-10, the medium granite is highly fractured compared to the gneiss outcropping North of the thermal area. Moreover in this sector the E-W fracture system (F2) is clearly visible.

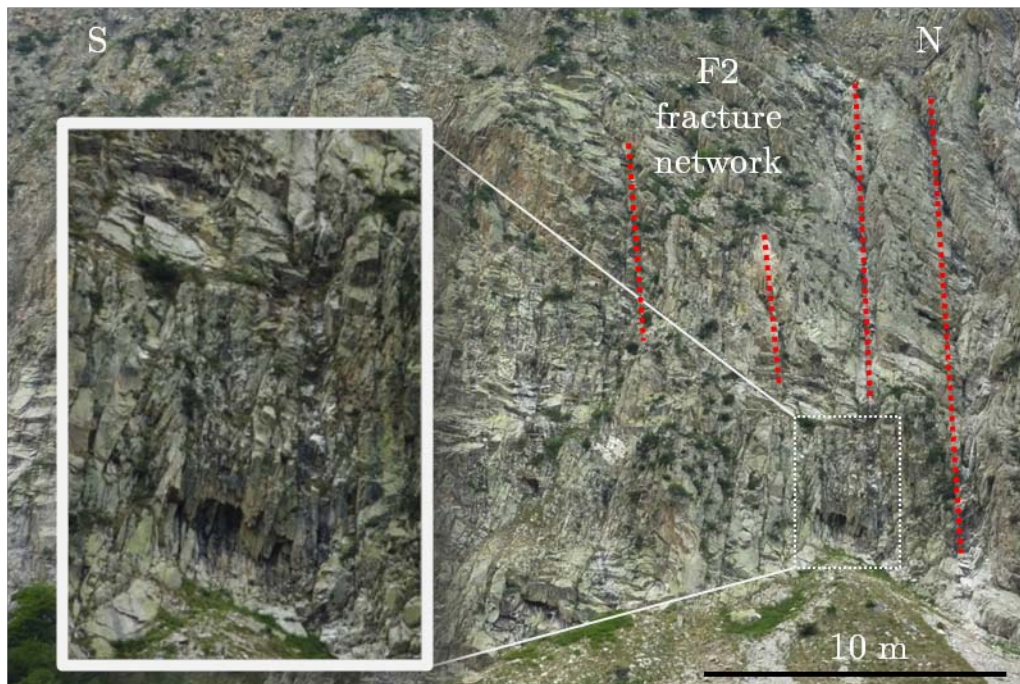


Figure 4-10 Details of the fracturing condition of the Central Granite as observed along the Valletta Valley

Along the Lorusa valley the same intense fractured biotitic gneiss and amphibolic gneiss outcrop and are crossed by the Lorusa Fault and the same sets of main fractures as those along the Valasco Valley, were observed.

In the caves of the thermal springs it was possible to get a three dimensional overview of the fracture systems and of the outcropping rocks. Three caves were analyzed. The upper cave shows the highest concentration of hot springs which discharge through leucogranite and mylonite at the intersection of the three systems of fractures respectively oriented 130/70°,

275°/75° and 90/35°. The same systems were observed in the wellness cave where the low angle seems to be more pervasive.



Figure 4-11 Detail of one of the thermal springs' cave where the low angle F3 set of fractures cuts the fine grained granite in correspondence of the thermal springs

Finally, at the lower cave shows how two main hot springs. When entering the cave the mylonitic gneiss crops out on the floor whilst the wall is composed by leucogranite, intensely fractured. The fracture spacing within the granite was here estimated to be 5-10 cm. Thermal springs discharge in correspondence of a cataclastic outcrop, which follows the low angle F3 set of fractures, in the upper right corner of the cave.

4.4. Boreholes

Two wells, ValW02 and ValW03, were recently drilled and are here briefly described. These wells are not exploited; therefore it was not possible to collect samples. In addition historical data were neither available. As for Vinadio the available data are poor, however on the basis of a technical report⁶, it was possible to get information about the stratigraphy and the presence of hot water at shallow depth. The well ValW03 is located next to the spring ValS01, near the Hotel building and the well ValW02 is located close to the entrance of the Hotel.

The wells were drilled in 2003 in the framework of a private research project aimed to implement the exploitation of geothermal resource. The well ValW02 is 51m deep and the

⁶ Report by Società Geologica Sondaggi (2002) kindly provided by Dr. Bonetto, the owner of the spa

well ValW03 reaches a depth of 81 m. The stratigraphy of the two wells is summarized in Figure 4-12.

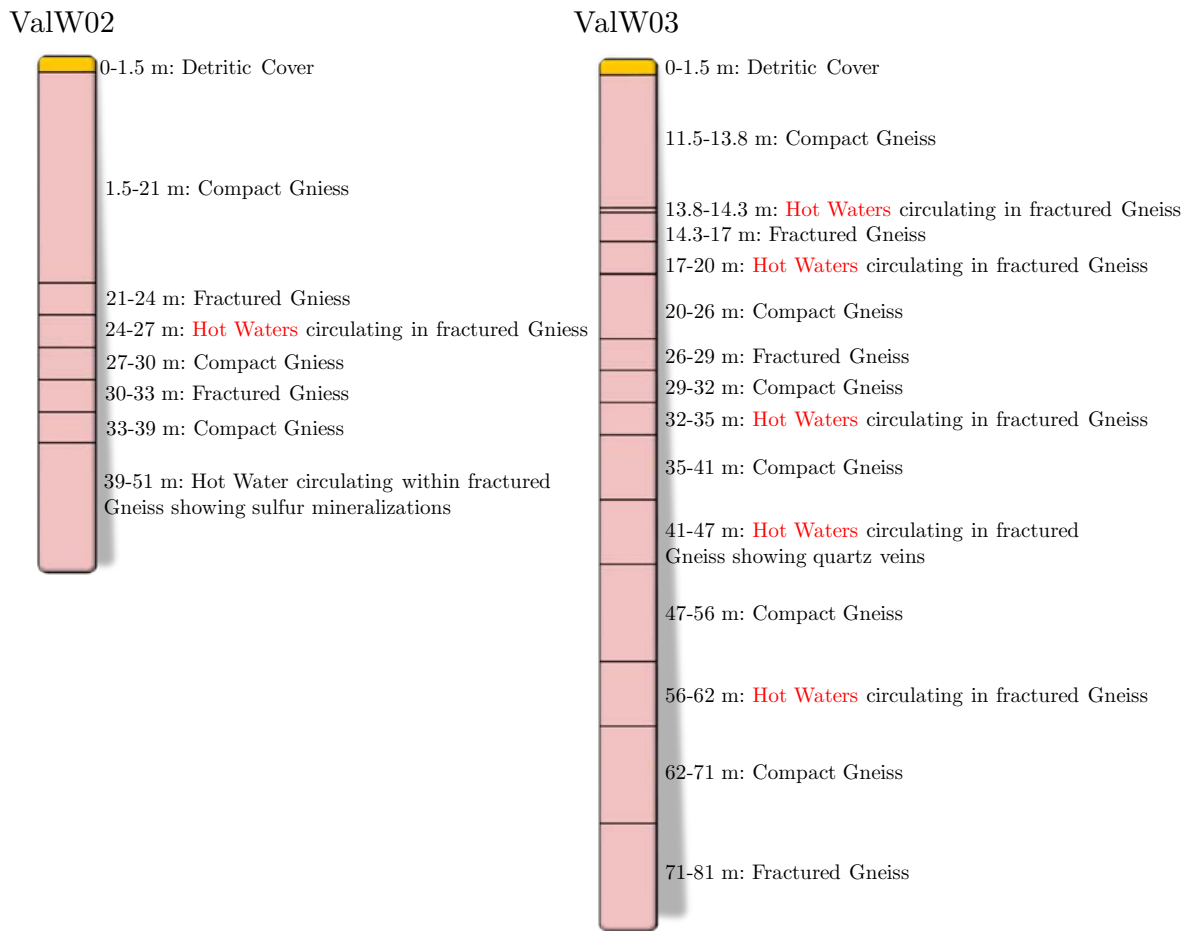


Figure 4-12 Sketch of the wells ValW02 and ValW03 indicating the depth where hot water was found during drilling (mod from Società Geologica Sondaggi technical report, 2002)

Hot water was found at different depth along the two wells and it circulates within sets of fractures that separate the more compact sectors of the crystalline host rock, represented at surface by the anatexites and gneisses of the Malinvern Argentera Complex and by the Central Granite at shallow depth. Any chemical and physical data are available for these two wells as no sampling was carried out during drilling.

5

GEOCHEMICAL INVESTIGATIONS

5.1. Geochemical investigations

5.1.1. On site measurements

Two sampling campaigns were carried out in summer and winter 2009 and a total of 30 samples were collected. During sampling, in-situ measurements were carried out for the physic and chemical parameters. Temperature, conductivity, pH and dissolved oxygen were measured using a Hach Lange HQ40d with a probe CD401 for temperature and electrical conductivity, a probe pH301 for pH, and finally a probe LDO101 for dissolved oxygen. Flow rate was estimated using graduated containers and chronometers. pH and electrical conductivity were also measured in laboratory of the Dipartimento di Scienze della Terra of the University of Turin, using Hanna Instruments HI4211 for pH and Hanna Instruments HI8820N for electrical conductivity.

Collected samples were filtered with a manual vacuum pump (0.45 μm) to remove particles. This is imperative for analyses of major ions, trace elements and water stable isotopes. In addition to the filtration, acidification of samples for cationic and trace elements analyses was undertaken directly in the field to avoid precipitation of carbonates as well as iron and manganese hydroxides. Samples were then stored in a closed container at ambient temperature to avoid abrupt changes in temperature especially for thermal waters and to protect from light.

5.1.2. Chemical analysis

The major ions (Li, Na, Mg, K, Ca, F, Cl, Br, Sr, SO_4) were analyzed by ion chromatography in the Laboratory of the Dipartimento di Scienze della Terra of the University of Turin by means of a Metrohm Metrostep C4 150 for cations and Metrostep A Supp4 for anions. Cation and anions were not analyzed at the same time. The instruments require the sample to have conductivity lower than 100 $\mu\text{S}/\text{cm}$; therefore samples with higher conductivity were diluted with pure water ($\text{Cond} < 20 \mu\text{S}/\text{cm}$). The dilution factor depends on the concentration of the sample and the process was carried out using a graduate micro-pipette. The ionic balance was calculated for each sample, and if it exceeded $\pm 5\%$ the analysis was repeated. Alkalinity was determined by titration with HCl 0.1N using methylorange as indicator.

Trace elements (Al, Cd, Co, Cr, Cu, Fe, Mn, Ni, Pb, Zn) and Si were analyzed by means of Inductive Coupled Argon Plasma spectrometry (ICAP) at the Laboratory of the Dipartimento di Scienze Mineralogiche e Petrologiche of Turin University. The data for trace elements are not interpreted in the framework of this work because they are not one of the main objectives of this study. However the Si concentration was used to estimate the Silica (SiO_2) content in the waters and the obtained concentrations show a good fit with those of the previous studies.

Water stable isotopes (D/H and $^{18}\text{O}/^{16}\text{O}$) of water samples were determined in the ISO4 Laboratory of the Dipartimento di Scienze della Terra of the University of Turin by means of a Finningan 250 spectrometer, following the procedures by (FRIEDMAN, 1953) and (EPSTEIN,

1953), respectively. Calibration was carried out by using an internal standard, which is calibrated against the V-SMOW reference materials.

Tritium (^3H) was analysed by Hydroisotop GmbH in Schweitenkirchen, Germany.

5.1.3. Water chemistry

The constituents of geothermal fluids can be divided into two main groups (GIGGENBACH, 1991):

- *tracers* are non-reactive elements, which, once added to the fluid phase should remain unchanged providing a direction to track back to their source components. Example are the noble gasses and elements such as Cl, B, Li, Rb and N_2
- *geoinicators* are those reactive species that respond to changes in their host environment. Na, K, Mg, Ca, SiO_2 take part to temperature-dependent reactions with the alumino-silicates rock usually forming the geothermal reservoir.

Moreover elements like H_2 , H_2S , CH_4 and CO_2 are usually involved in temperature and pressure-dependent redox reactions between each other's or with redox systems of the rock phase.

The studied waters are represented in the triangular Piper plot which aims to identify the geochemical water types, whereas the Schoeller plot helps to highlight the differences between waters having the same geochemical type but different salinity.

5.1.4. Mixing processes

The deep hot waters circulating in the Alps usually mix with shallow cold groundwaters during the upflow before discharging at the springs. Cold waters are usually less mineralized than the deep hot fluids therefore the mixing between this two types of waters affects the composition of the fluids discharging from thermal springs. The comparison between the geochemical signature of samples collected from springs or shallow wells, discharging different types of waters in response to different degree of mixing, helps to decipher the chemical composition of the pure deep thermal endmember. Mixing models using binary plots of chemical and isotopic data usually illustrate the mixing processes. In this work correlation between temperature and the major ions were employed as well as the comparison between Tritium and Chloride, as more recent waters (low Tritium content) are usually the less mineralized.

Using mass balance equations of the conservative and major elements (chloride, lithium, Sulphate in particular) was also possible to infer the % of mixing between the different water types

$$[\text{X}_{\text{mix}}] = [\text{X}_a] \cdot x + [\text{X}_b] \cdot (1 - x)$$

where the concentrations are expressed in mmol/l, A and B are the two endmembers which are involved in the mixing process.

Two assumptions have to be taken into account:

- the concentration of the selected element X is directly connected to temperature;

- the chemical concentration of the elementX within the reservoir is attained at the temperature calculated by means of geothermometers and saturation indexes

According to these assumptions and taking into account the regression curve of the elementX vs. T °C plot it was possible to estimate its concentration in the reservoir.

5.1.5. Water-rock interactions

The chemical reactions occurring between the circulating thermal water and host-rock are controlled by several parameters such as the mineralogical assemblage of the rock, temperature, dissolved CO₂, pH, time. Therefore the most mineralized thermal waters are usually those who reached the highest temperature and often the longest residence time. On the contrary the chemical composition of cold groundwater, in particular those rapidly circulating at the surface of the crystalline bodies are almost exclusively controlled by the alteration of the mineral composing these rocks.

Every mineral has a maximal solubility, which can be compared to the effective concentration in the analyzed samples to evaluate the degree of saturation of the water in respect to the considered mineral. Saturation Indexes (SI) are a measure of the ratio of the ion activity IAP and the solubility product K_{SO}:

$$SI = \log\left(\frac{IAP}{K_{SO}}\right)$$

Where

$$IAP = \{Na\} \cdot \{Cl\}$$

in terms of actual activities in water sample and

$$K_{SO} = \{Na\} \cdot \{Cl\}$$

in terms of activities at the equilibrium.

For SI = 0, the solution is at equilibrium; SI < 0 indicates under-saturation and SI > 0 over-saturation. Fluid-mineral equilibria were computed with PHREEQC (PARKHURST, 1999) code choosing the most representative samples in terms of temperature and mineralization.

5.1.6. Flow Systems

The origin of thermal waters and elevation of the recharge zone in morphologically complex regions can be estimated by means of the stable isotopes of hydrogen and oxygen. The content of δ²H and δ¹⁸O are given relative to the Standard Mean Oceanic Water (SMOW). The differences are generally caused by isotope fractionation during phase transformation therefore, for geothermal fluids, it is possible to understand if boiling occurred at depth. The temperature dependency is also essential. With increasing elevation the content of heavy isotopes decreases. The reason is especially the lower temperature but it is also influenced by other parameters such as latitude, seasonal period, origin and intensity of precipitation, location of precipitation and distance to ocean. The results of the analysed

samples can be compared to the world meteoric water composition or to a local meteoric water composition using a $\delta^2\text{H}$ vs. $\delta^{18}\text{O}$ plot.

The employed meteoric lines in this thesis are:

- World Meteoric Water Line (GAT and GOFIANTINI, 1981):

$$\delta^2\text{H}(\%) = 8.2 \cdot \delta^{18}\text{O} + 10.8$$

- Mediterranean Meteoric Water Line (BORTOLAMI et al., 1979)

$$\delta^2\text{H}(\%) = 8 \cdot \delta^{18}\text{O} + 22$$

To relate the elevation of the recharge zone with the stable isotopes of hydrogen and oxygen, the employed correlation equation are those for the Maritime Alps (BORTOLAMI et al., 1979) and for the Mt. Blanc (JAMIER and OLIVE, 1977):

$$\delta^{18}\text{O}(\%) = -0.00312 \cdot h + 8.03$$

$$\delta^2\text{H} = -0.0249 \cdot h - 51.1$$

$$\delta^{18}\text{O}(\%) = -0.0243 \cdot h + 51.1$$

5.1.7. Reservoir Temperature

In the framework of this study choosing the geothermometers which better suited the geological setting (crystalline rocks) and the thermal ($T^{\circ}\text{max} < 150^{\circ}\text{C}$) and hydrodynamic (ascent rate) conditions become crucial.

Geothermometers and saturation indexes (SI) can be employed to estimate temperature at which water and rock may have equilibrated at depth and therefore the reservoir temperature. Many chemical and isotopic reactions might be used as chemical thermometers (FOURNIER, 1991; FOURNIER et al., 1981; GIGGENBACH, 1988; GIGGENBACH, 1991). Most geothermometers were developed between the 1960's and the 1980's and those employed for this thesis are listed in

Table 5-1.

5.1.7.1. The Giggenbach Plots.

The SiO_2 vs. $\log(\text{K}^2/\text{Mg})$ (GIGGENBACH et al., 1994) plot and the Na-K-Mg ternary plot (GIGGENBACH, 1988), are a useful tool for both estimating the reservoir temperature and to recognize which waters have attained the equilibrium with the reservoir lithologies. The former diagram considers global equilibrium condition between the aqueous solution, chalcedony, chlorite, illite and K-feldspar comparing between the K-Mg geothermometric function and the solubility of the chalcedony or quartz. The latter is a useful tool to estimate reservoir temperature and to recognize groundwaters, which have attained equilibrium with the host lithology, and therefore to figure out which cation geothermometers can be employed. In constructing this plot Giggenbach adopted the Na/K and $\text{K} / \sqrt{\text{Mg}}$ geothermometers formulas. The upper part of the plot corresponds the conditions in which Na/K values are controlled according to the Giggenbach et al. (1983) geothermometer. The

lower part, most Mg-rich corresponds to the condition in which Na/K values are controlled by the Truesdell Na/K geothermometer (1976). Therefore using this plot is possible to infer thermodynamic and kinetic correlations between geothermal fluid and host rock and to delineate mixing processes trends between the different endmembers. As Fournier (1991) pointed out, it also allows recognizing which waters are more suited for geothermometers, eliminating those which are closer to the immature line because of dilution/mixing with shallow groundwaters or near-surface water-rock interactions. Also cold water samples were plotted because their disposition can help to identify trends related to mixing processes involving the thermal waters.

Solute geothermometers are based on temperature-dependent mineral-fluid equilibria and their successful application relies on five basic assumptions (NICHOLSON, 1993):

- the concentration of the elements or species to be used in the geothermometers is controlled only by a temperature-dependent mineral-fluid reaction.
- there is an abundance of the minerals and/or dissolved species in the rock-fluid system for the reaction to occur readily.
- the reaction attains equilibrium in the reservoir or aquifer.
- there is a fast flow towards the surface with no re-equilibration after the fluid leaves the reservoir, no near-surface reactions occur.
- there is no mixing or dilution of the deep fluid.

However in the case of the studied waters in this Thesis mixing occurs, close to the surface, between deep hot waters and shallow cold groundwaters. Therefore this assumption was circumvented estimating the extent of dilution/mixing by means of mass balance equations.

5.1.7.2. Silica geothermometers

Silica geothermometer of chalcedony and quartz were employed as they fit the expected reservoir temperature conditions of 120-160°C for the study region. Chalcedony has a higher solubility than quartz and controls the silica concentration in solution at temperatures lower than 110°C temperatures, whereas quartz controls it at temperature above 110°C (ARNORSSON, 1975; NICHOLSON, 1993). However there is some uncertainty in the interpretation of dissolved silica concentration in geothermal fluids. The silica concentration is strongly affected by mixing processes with low-silica cold waters and by precipitation of SiO₂ during the ascent. Therefore, calculated silica content of the discharged mixed water is usually below the reservoir concentration and as a consequence silica temperatures are often underestimated.

5.1.7.3. Cation geothermometers

The alkaline geothermometers of Na-K and Na-K-Ca with Mg correction were employed and compared to the others equations as it is demonstrated that the Na-K geothermometer, developed by Fournier (1979) and Giggenbach highly overestimates the temperature for low enthalpy fluids (SONNEY and VUATAZ, 2010). In fact at temperatures below 120°C the sodium and potassium concentration are controlled by minerals such as clays and not only by the feldspar ion-exchange reactions which occur at higher temperatures. (NICHOLSON, 1993).

To overcome this the Na-K-Ca geothermometer was developed by Fournier and Truesdell (1976) and later corrected by (PACES, 1975) to permit this equation to be reliably applied for temperature below 75 ° C and to dilute-chloride fluids as those of Vinadio.

The K²-Mg (FOURNIER et al., 1981; GIGGENBACH et al., 1983) and Li-Mg equations (KHARAKA, 1989) are based on the ion-exchange reactions between feldspars and can be applied in crystalline settings for low enthalpy reservoir fluids which have not attained the full equilibrium with mineral assemblage of the host-rock in particular with alkali feldspars (NICHOLSON, 1993). In fact the studied waters are partially equilibrated or mixed waters.

Some geothermal fluids have high Na/Li ratios because are enriched in sodium by the dissolution of halite or the leaching of trapped seawater. The Na/Li geothermometer (FOUILLAC, 1979) appears to be sensitive to the total dissolved solids of the water at depth, locally controlled by contributions of Na-Cl, and the rock type (e.g. the thermal waters of Vinadio could undergo the influence of halite dissolution). This equation was applied as it seems to be effective for low enthalpy fluids, in particular where the ascent occurs rapidly and the lateral contribution of cold waters is limited.

5.1.7.4. Saturation indexes

Another way to estimate the reservoir temperature is by means of saturation indexes. The behaviour of SI of major minerals was simulated using the PHREEQC code. On selected samples (the hottest and/or the most mineralized ones) a simulation of the saturation indexes is carried out with increasing temperature from emergence temperature to a selected temperature higher than the supposed reservoir temperature, calculated by the geothermometers. The reservoir temperature can be estimated observing at which temperature the SI lines are close to the value equal to zero.

| Author | Type | Equation |
|-----------------------------|------------------------|---|
| Fournier (1977) | Chalcedony | $T_{SiO_2} = \frac{1032}{4.69 - \log(SiO_2)} - 273.15$ |
| Arnórsson et al. (1983) | Chalcedony | $T_{SiO_2} = \frac{1112}{4.91 - \log(SiO_2)} - 273.15$ |
| Fournier (1973) | Quartz (no steam loss) | $T_{SiO_2} = \frac{1309}{5.19 - \log(SiO_2)} - 273.15$ |
| Truesdell (1975) | Na-K | $T_{Na-K} = \frac{854}{0.857 + \log(Na / K)} - 273.15$ |
| Fournier (1979) | Na-K | $T_{Na-K} = \frac{1217}{1.483 + \log(Na / K)} - 273.15$ |
| Giggenbach (1980) | Na-K | $T_{Na-K} = \frac{1390}{1.750 + \log(Na / K)} - 273.15$ |
| Arnórsson et al. (1983) | Na-K | $T_{Na-K} = \frac{933}{0.993 + \log(Na / K)} - 273.15$ |
| Fournier & Truesdell (1973) | Na-K-Ca | $T_{Na-K-Ca} = \frac{1647}{\log(Na / K) + \beta \log(\sqrt{Ca} / Na) + 2.24} - 273.15$ <p>$\beta=4/3$ for $T < 100^\circ C$ and $\sqrt{Ca/Na} > 1$ (Valdieri) $\beta=1/3$ for $T > 100^\circ C$ and $\sqrt{Ca/Na} > 1$ (Vinadio)</p> $R = \frac{Mg}{Mg + 0.61Ca + 0.31K} \cdot 100$ <p>Mg corrections: if $R=5-50$</p> $\Delta t_{Mg} = 10.664 - 4.7415 \log R + 325.87(\log R)^2 - \frac{1.032 \cdot 10^5 (\log R)^2}{T_{Na-K-Ca}} - \frac{1.968 \cdot 10^7 (\log R)^2}{T_{Na-K-Ca}^2} + \frac{1.605 \cdot 10^7 (\log R)^3}{T_{Na-K-Ca}^2}$ <p>if $R > 50$</p> $\Delta t_{Mg} = -1.03 + 59.97 \log R + 145.05(\log R)^2 - \frac{35711 \cdot 10^5 (\log R)^2}{T_{Na-K-Ca}} - \frac{1.67 \cdot 10^7 \log R}{T_{Na-K-Ca}^2}$ |
| Giggenbach (1988) | K ² -Mg | $T_{K^2-Mg} = \frac{4410}{13.95 - \log(K^2 / Mg)} - 273.15$ |
| Fournier (1991) | K ² -Mg | $T_{K^2-Mg} = 1000 / (3.66 - 0.542 \cdot \log(K^2 / Mg) + 0.05751 \cdot \log(K^2 / Mg)^2 - 0.0027484 \cdot \log(K^2 / Mg)^3) - 273.15$ |
| Kharaka & Mariner (1988) | Li-Mg | $T_{Na-Li} = \frac{2200}{5.47 - \log Li(\sqrt{Mg})} - 273.15$ |
| Fouillac & Michard (1981) | Na/Li, Cl<0.3m | $T_{Na-Li} = \frac{1000}{0.389 - \log(Na / Li)} - 273.15$ |

Table 5-1 Selection of geothermometers to calculate the reservoir temperature for Alpine deep flow systems. Other geothermometers and their use are also given in Arnórsson 2000. All concentrations are in mg/kg. Note that not all the geothermometers have been employed in the present study

5.1.8. Residence Time

Groundwater residence time can be approached by means of Tritium values and Carbon-14 analyses. Tritium (^3H , T) is a radiogenic and radioactive isotope of hydrogen with a half-life of 12.43 years (GAT and GOFIANTINI, 1981), which decays to ^3He . It is a natural tracer for determining time scales for the mixing and flow of waters, and is suited for studying processes that occur on a time-scale of less than 100 years. Tritium content is expressed in tritium units (TU) where 1 TU equals 1 ^3H in 10^{18} atoms of hydrogen. Prior to the advent of atmospheric testing of thermonuclear devices in 1953, the tritium content of precipitation was in the range of 2-8 TU (L L THATCHER, 1977); this background concentration is produced by cosmic ray spallation. Since 1952, tritium produced by thermonuclear testing ("bomb tritium") has been the dominant source of tritium in precipitation. A peak concentration of several thousand TU was recorded in precipitation in the northern hemisphere in 1963. After 1963, the tritium levels in precipitation began to decline because of radioactive decay, mixing into the ocean, and the cessation of atmospheric testing. Present day Tritium content in precipitations in the Mediterranean area varies between 4 and 10 TU (IAEA, 2007). Modern waters with higher tritium content are the results of either recent meteoric waters infiltrated after 1953 or mixing of old water with a fraction of young fluids. Thus, tritium concentration can be a useful marker for recharge since the advent of nuclear testing.

5.2. The Bagni di Vinadio Thermal Site

5.2.1. Water Chemistry

Thermal springs at Bagni di Vinadio discharge waters with temperature ranging from 26.6 to 54.3 °C whereas the wells show a higher temperature in the range 51 to 70.2 °C. The pH is between 7.1 and 9.1 at the springs and between 7.8 and 8.8 at the wells. The TDS stretches between 513 mg/kg and 1469 mg/kg for the springs and 374 mg/kg to 2736 mg/kg for the wells (Table 5-2).

Shallow waters were sampled from a cold spring and the Corborant and Ischiator torrents. In particular the Corborant torrent was sampled upstream and downstream the thermal area during the winter campaign when the flow rate of the torrent is low. The cold waters show an average temperature of 6 °C, a pH of 7.8 and TDS around 45mg/Kg. Moreover the temperature recorded for the Corborant torrent shows an increase of 1 °C downstream the thermal spa (from 4 to 5 °C), which can be related to the contribution of the thermal waters discharging from the spa, as could be confirmed by a significant increase the Sodium (from 1.7 to 5.4 mg/kg) and chloride (0.3 to 3.6 mg/kg) contents which are the main component of the thermal waters. Their chemical composition is controlled by Ca, HCO₃ and SO₄, which account for more than the 80% of the total ionic salinity. These waters have the highest Mg/TDS ratio, which is a sensitive indicator of shallow, cold waters (MICHARD, 1990b).

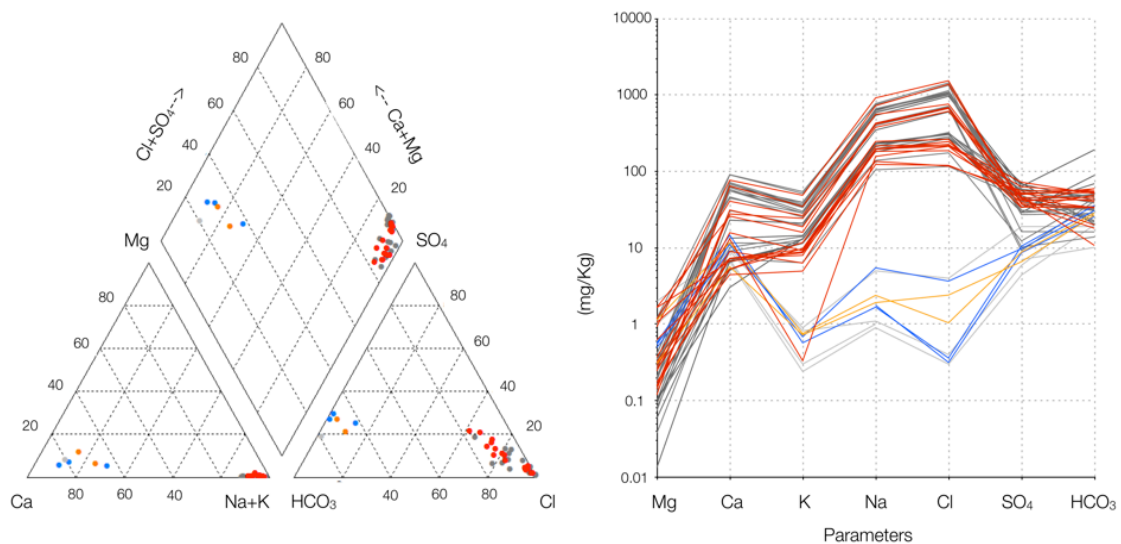


Figure 5-1 Piper and Schoeller Plot of the Bagni di Vinadio area.

As shown in Figure 5-1 The main elements composing the thermal waters are Na, Cl, HCO₃ and SO₄, which hold more that the 90% of the TDS, which shows a direct relation with temperature. Sulphate and alkalinity play an important role as well as they are good markers of mixing processes. In fact the concentrations of SO₄ and HCO₃+CO₃ decrease with increasing temperature, e.g. as shown in the well VinW03 which discharges the hottest and more saline waters of all the sampled waters. Moreover spring VinS04, which is located along

the Corborant Torrent, also shows the highest chloride concentration among all springs. This spring is located at an elevation 20 m lower than the well VinW03, which roughly corresponds to the depth at which, the reported “*hot water*” was found during the drilling.

5.2.2. Mixing Processes

As mentioned before, the observed increase of temperature corresponds to an increase of TDS which in this case is strictly controlled by the two major ions Na and Cl and secondary by the sulphates and the alkalinity. Moreover higher Cl correspond to lower HCO_3 , SO_4 , F and SiO_2 , compensated by an increase in Na, K, Ca, Li.

The thermal waters of Vinadio waters can be subdivided into three main groups:

- spring VinS01 group includes springs showing a Na-Cl composition but are highly diluted with the Na- SO_4 endmember, which is a more common water type of thermal waters circulating within the crystalline basements (VUATAZ, 1982). In fact they show the lowest chloride ($\text{Cl} < 300$ mg/kg), highest HCO_3 (avg. 50 mg/kg) and SO_4 (avg. 50 mg/Kg) among all the thermal waters. This group includes the majority of the hot springs, which discharge the waters with the highest % of mixing. The behaviour of the alkalinity, which increases with decreasing temperature help to describe the occurring mixing. Moreover the recorded variations of temperature are strictly controlled by the different degree of mixing with Ca- HCO_3 cold and shallow groundwaters, which, on one hand contribute to the dilution of the deep endmember and on the other controls the alkalinity concentration of the thermal mixture discharging from the hot springs.
- spring VinS04 group also includes the well VinW02. This group shows an intermediate composition with an increase of the contribution of the Na-Cl endmember. In fact these two waters show a chloride concentration of about 700 mg/l, which is three times higher than the average chloride content in the other springs.
- well VinW03 group, which discharge the hottest and most saline waters of the entire Argentera Massif showing a Na-Cl composition. In VinW03 water, Na and Cl dominate more than the 90% of the salinity. Moreover this sample shows the highest Cl/SO_4 and Cl/HCO_3 ratios with respect to the other thermal waters indicating that mixing impacts less on the composition of the thermal water. This waters, which can be considered as the closest to the reservoir fluid, represent an anomaly for thermal waters circulating within the crystalline basement, as this composition is typical of waters deriving from deep brines or circulating within carbonate and evaporitic formations.

Using mass balance equations it was possible to estimate the % of mixing between the Na-Cl and Na- SO_4 endmembers and also between cold and hot fluids.

The Chloride concentration at reservoir temperature was estimated to be 2300 mg/kg (=64.87 mmol/kg). The contribution of the two endmembers for all the sampling points:

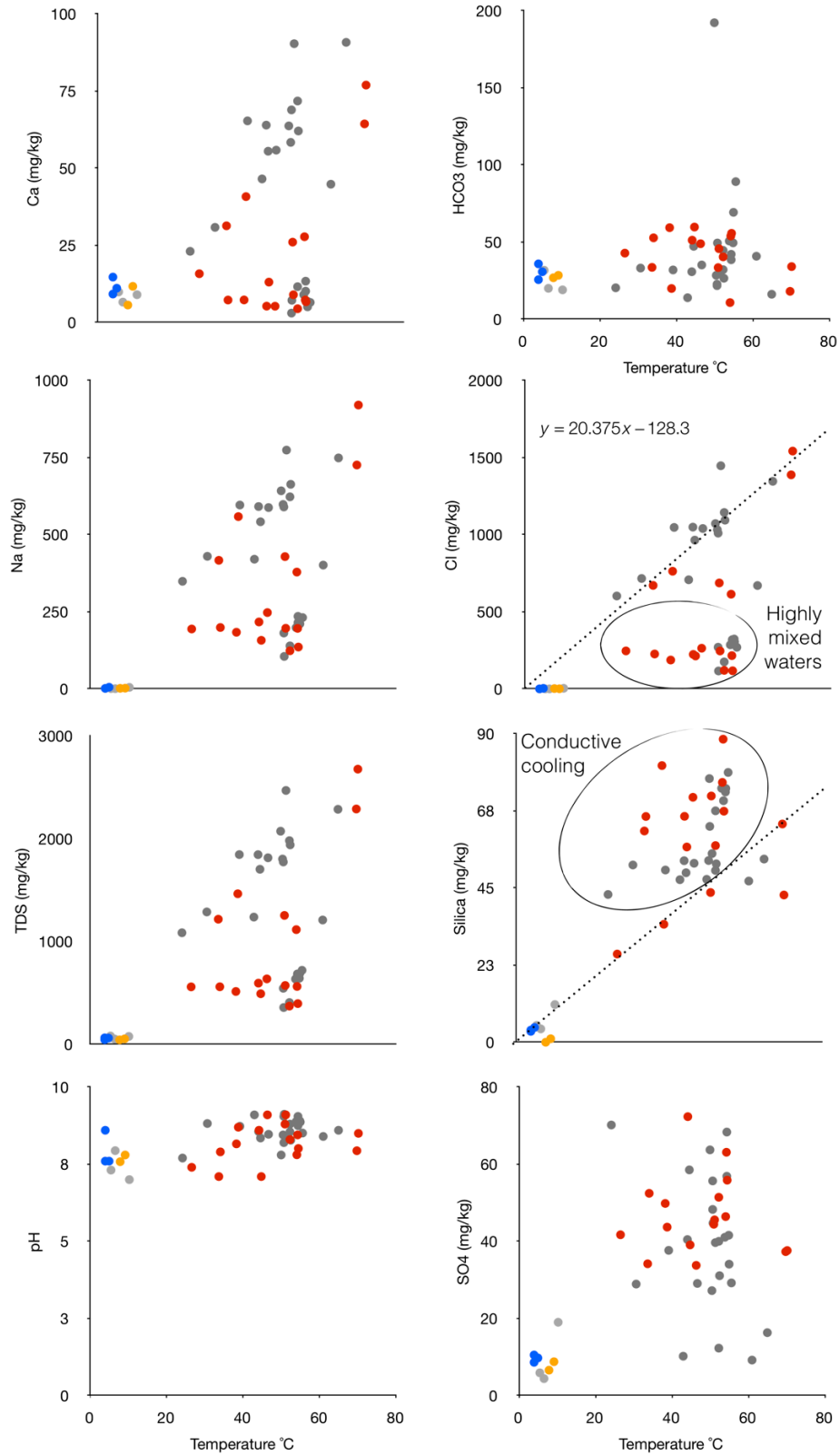
- VinS01 group: 15% deep, 85% shallow
- VinS04 group: 35% deep, 65% shallow
- VinW03 group: 65% deep, 35% shallow

Table 5-2a Resuming table reporting the chemical and isotopic compositions of the sampled waters in the Bagni di Vinadio Area (results from samples collected during the present thesis)

| Author | Code | Date | T° CQ | (l/min) | pHCond | µS/cm | TDS | Type | Na ⁺ | K ⁺ | Ca ²⁺ | Mg ²⁺ | Li ⁺ | Si ²⁺ | Cl ⁻ | F ⁻ | Br ⁻ | HCO ₃ ⁻ | CO ₃ ²⁻ | SO ₄ ²⁻ | SiO ₂ | δD | δ ¹⁸ O | U.T. |
|--------------|---------|----------|-------|---------|--------|----------|---|---------|-----------------|----------------|------------------|------------------|-----------------|------------------|-----------------|----------------|-----------------|-------------------------------|-------------------------------|-------------------------------|------------------|--------|-------------------|------|
| Guglielmetti | Vms_01 | 25.11.09 | 46.4 | 9.1 | 988 | 637.619 | Na-Cl | 247.500 | 11.780 | 5.266 | 0.175 | 0.538 | 263.800 | 15.330 | 48.920 | 10.540 | 33.770 | 71.470 | 1.0 | | | | | |
| Guglielmetti | Vms_01 | 16.07.09 | 51.2 | 9.0 | 992 | 573.329 | Na-Cl | 196.600 | 6.325 | 8.983 | 0.320 | 0.353 | 0.313 | 246.100 | 14.520 | 0.226 | 45.700 | 8.319 | 45.570 | 71.850 | -92.15 | -12.77 | | |
| Guglielmetti | Vms_02 | 25.11.09 | 34.1 | 7.9 | 852 | 560.890 | Na-Cl | 199.100 | 7.990 | 7.274 | 0.287 | 0.450 | 226.500 | 13.960 | 0.139 | 52.740 | | 52.450 | 65.870 | -91.98 | -12.73 | | | |
| Guglielmetti | Vms_02 | 16.07.09 | 38.3 | 8.2 | 908 | 514.981 | Na-Cl | 183.700 | 8.870 | 7.304 | 0.155 | 0.467 | 0.283 | 187.400 | 12.670 | 0.141 | 59.330 | 4.831 | 49.830 | 80.720 | | | | |
| Guglielmetti | Vms_03 | 25.11.09 | 44.2 | 8.6 | 947 | 596.112 | Na-Cl | 217.100 | 9.795 | 5.292 | 0.624 | 0.463 | 223.700 | 15.450 | 0.128 | 51.220 | | 72.340 | 65.910 | | | | | |
| Guglielmetti | Vms_03 | 16.07.09 | 54.3 | 8.5 | 907 | 564.049 | Na-Cl | 196.200 | 9.628 | 7.289 | 1.058 | 0.483 | 0.208 | 215.900 | 14.580 | 0.223 | 53.920 | 1.460 | 63.100 | 88.420 | | | | |
| Guglielmetti | Vms_04 | 25.11.09 | 38.8 | 3.0 | 2320 | 1465.237 | Na-Cl | 558.600 | 26.450 | 40.800 | 1.176 | 1.451 | 763.000 | 10.180 | 19.890 | | 43.690 | 34.420 | -93.20 | -12.64 | | | | |
| Guglielmetti | Vms_04 | 16.07.09 | 33.7 | 7.1 | 1980 | 1217.933 | Na-Cl | 416.900 | 18.860 | 31.330 | 0.142 | 1.188 | 1.236 | 671.100 | 9.032 | 0.375 | 33.590 | 34.180 | 61.640 | | | | | |
| Guglielmetti | VmsW_01 | 25.11.09 | 52.3 | 8.3 | 624 | 372.966 | Na-Cl | 123.700 | 4.964 | 4.452 | 0.265 | 0.285 | 120.400 | 13.740 | 0.070 | 40.410 | 13.250 | 51.430 | 57.380 | -90.57 | -12.43 | | | |
| Guglielmetti | VmsW_01 | 16.07.09 | 54.5 | 8.0 | 689 | 397.138 | Na-Cl | 135.700 | 8.620 | 6.712 | 1.652 | 0.361 | 0.191 | 117.700 | 12.970 | 0.181 | 55.670 | 1.521 | 55.860 | 67.410 | | | | |
| Guglielmetti | VmsW_02 | 25.11.09 | 51.0 | 8.8 | 1612 | 1254.712 | Na-Cl | 428.900 | 15.980 | 26.040 | 1.666 | 0.725 | 687.100 | 10.670 | 0.289 | 33.450 | 5.461 | 44.430 | 43.690 | | | | | |
| Guglielmetti | VmsW_02 | 16.07.09 | 54.1 | 7.8 | 1630 | 1116.547 | Na-Cl | 378.800 | 24.350 | 27.790 | 0.158 | 1.068 | 1.047 | 614.200 | 11.550 | 0.404 | 10.760 | 0.000 | 46.420 | 75.810 | | | | |
| Guglielmetti | VmsW_03 | 25.11.09 | 70.2 | 8.5 | 4160 | 2677.354 | Na-Cl | 920.200 | 48.770 | 76.950 | 0.926 | 2.201 | 1542.000 | 13.830 | 0.767 | 34.100 | | 37.610 | 42.960 | -92.53 | -12.53 | 0.6 | | |
| Guglielmetti | VmsW_03 | 16.07.09 | 69.8 | 10.0 | 4290 | 2289.895 | Na-Cl | 725.900 | 34.830 | 64.370 | 0.118 | 2.112 | 2.228 | 1388.000 | 14.150 | 1.155 | 18.050 | 1.652 | 37.330 | 63.680 | | | | |
| Guglielmetti | Vms_TOT | 25.11.09 | 26.6 | 7.4 | 940 | 560.121 | Na-Cl | 194.300 | 9.176 | 15.800 | 0.244 | 0.469 | 246.500 | 8.943 | 0.148 | 42.830 | | 41.710 | 25.730 | | | | | |
| Guglielmetti | Vms_TOT | 16.07.09 | 44.8 | > 60 | 989 | 502.248 | Na-Cl | 157.600 | 9.464 | 13.080 | 0.372 | 0.415 | 0.419 | 213.600 | 8.489 | | 59.730 | 39.080 | 56.970 | | | | | |
| Guglielmetti | Vms_05 | 25.11.09 | 9.2 | 16.0 | 75 | 54.306 | Ca-HCO ₃ -SO ₄ | 2.390 | 0.753 | 11.710 | 1.134 | | 1.044 | 0.050 | | | 28.440 | 8.785 | 1.026 | -85.60 | -11.87 | 6.3 | | |
| Guglielmetti | Vms_05 | 16.07.09 | 7.9 | 7.6 | 176 | 44.576 | Ca-HCO ₃ -SO ₄ | 1.921 | 0.723 | 5.651 | 0.306 | 0.033 | 2.410 | 0.090 | | | 26.850 | 6.591 | 0.000 | | | | | |
| Guglielmetti | CT_01 | 25.11.09 | 4.0 | 7.6 | 62 | 46.089 | Ca-HCO ₃ -SO ₄ | 1.773 | | 9.219 | 0.493 | | 0.316 | 0.040 | | | 25.620 | 8.628 | 3.175 | | | | | |
| Guglielmetti | CT_02 | 25.11.09 | 5.0 | 7.6 | 80 | 62.190 | Ca-Na-HCO ₃ -SO ₄ | 5.471 | 0.684 | 11.100 | 0.543 | | 3.670 | 0.214 | | | 30.750 | 9.758 | 4.319 | | | | | |
| Guglielmetti | IC | 25.11.09 | 4.0 | 8.6 | 73 | 64.314 | Ca-HCO ₃ -SO ₄ | 1.675 | 0.571 | 14.710 | 0.571 | | 0.361 | 0.026 | | | 35.870 | 10.530 | 3.538 | | | | | |

Table 5-3b Resuming table reporting the chemical and isotopic compositions of the sampled waters in the Bagni di Vinadio Area (data from previous studies)

| Author | Code | Date | T° CQ (l/min) | pH | Cond $\mu\text{S/cm}$ | TDS | Type | Na ⁺ | K ⁺ | Ca ²⁺ | Mg ²⁺ | Li ⁺ | Si ²⁺ | Cl ⁻ | F ⁻ | Br ⁻ | HCO ³⁻ | CO ³⁻ | SO ²⁻ | SiO ₂ | δD | $\delta^{18}\text{O}$ | U.T. | |
|------------------|-------------|----------|---------------|------|-----------------------|----------|--------------------------------------|-----------------|----------------|------------------|------------------|-----------------|------------------|-----------------|----------------|-----------------|-------------------|------------------|------------------|------------------|------------------|-----------------------|--------|--|
| Baetto | Vi_1 | 27.06.05 | 52.3 | 8.8 | 1076 | 407.419 | Na-Cl | 139.500 | 11.410 | 11.600 | 0.201 | 0.446 | 0.426 | 175.300 | 7.496 | 44.600 | 4.141 | 12.300 | 67.520 | -89.12 | -12.40 | | | |
| Baetto | Vi_2 | 27.06.05 | 65.0 | 8.6 | 3400 | 2286.821 | Na-Cl | 748.800 | 54.460 | 90.800 | 1.201 | 1.895 | 3.291 | 1346.000 | 4.584 | 16.170 | 3.300 | 16.320 | 53.450 | -90.18 | -12.50 | | | |
| Baetto | Vi_3 | 27.06.05 | 43.0 | 9.1 | 2640 | 1238.595 | Na-Cl | 420.500 | 25.320 | 46.530 | 1.100 | 1.009 | 1.634 | 707.600 | 7.061 | 13.910 | 3.721 | 10.210 | 47.430 | -90.00 | -12.53 | | | |
| Baetto | Vi_4 | 27.06.05 | 61.0 | 8.4 | 2520 | 1210.260 | Na-Cl | 401.400 | 28.620 | 44.820 | 1.100 | 1.048 | 1.465 | 670.300 | 7.221 | 40.820 | 4.261 | 9.205 | 47.030 | -90.00 | -12.41 | | | |
| Perello | V1 | 04.06.96 | 54.4 | 9.1 | 672.938 | | Na-Cl | 215.000 | 14.090 | 10.140 | 0.038 | 0.811 | | 319.400 | 13.790 | 38.530 | 4.259 | 56.880 | 70.470 | | | | | |
| Perello | V2 | 05.06.96 | 44.1 | 8.6 | 1845.723 | | Na-Cl | 591.200 | 34.810 | 63.970 | 0.202 | 2.321 | | 1049.000 | 12.210 | 30.770 | 20.780 | 40.460 | 52.970 | | | | | |
| Perello | V3 | 05.06.96 | 52.3 | 8.6 | 1981.724 | | Na-Cl | 622.700 | 37.160 | 71.790 | 0.263 | 2.531 | | 1144.000 | 10.830 | 32.100 | 20.350 | 40.000 | 50.120 | | | | | |
| Perello | V4 | 05.06.96 | 39.2 | 8.7 | 1846.338 | | Na-Cl | 596.100 | 33.630 | 65.350 | 0.252 | 2.306 | | 1047.000 | 11.980 | 31.920 | 20.140 | 37.660 | 50.250 | | | | | |
| Perello | V5 | 05.06.96 | 50.8 | 9.1 | 359.082 | | Na-Cl | 105.300 | 6.378 | 7.188 | 0.132 | 0.385 | | 116.400 | 12.650 | 49.400 | 16.500 | 44.750 | 62.970 | | | | | |
| Perello | V6 | 05.06.96 | 53.9 | 8.9 | 635.963 | | Na-Cl | 198.700 | 12.870 | 9.022 | 0.081 | 0.740 | | 285.900 | 14.290 | 50.690 | 22.610 | 41.060 | 74.100 | | | | | |
| Perello | V7 | 05.06.96 | 51.4 | 8.3 | 2470.123 | | Na-Cl | 774.200 | 51.410 | 90.370 | 0.405 | 3.208 | | 1447.000 | 10.020 | 30.870 | 22.970 | 39.670 | 55.050 | | | | | |
| Michael et al. | 1a | 01.01.89 | 46.7 | 2.0 | 1817.350 | | Na-Cl | 587.900 | 28.690 | 55.860 | 0.192 | 1.980 | 1.928 | 1040.000 | 10.300 | 35.150 | 26.260 | 29.090 | 52.220 | | | -13.10 | | |
| Michael et al. | 1c | 01.01.89 | 30.7 | 1.0 | 1288.656 | | Na-Cl | 429.800 | 19.780 | 30.830 | 0.073 | 1.376 | 1.227 | 716.000 | 10.740 | 33.140 | 16.770 | 28.920 | 51.720 | | | -13.00 | | |
| Michael et al. | 1d | 01.01.89 | 50.5 | 3.0 | 1804.934 | | Na-Cl | 598.000 | 28.330 | 58.380 | 0.182 | 2.034 | 1.928 | 1032.000 | 10.320 | 28.430 | 18.110 | 27.220 | 53.020 | -88.00 | -12.80 | 0.0 | | |
| Michael et al. | 1e | 01.01.89 | 52.5 | 8.3 | 1940.812 | | Na-Cl | 663.300 | 30.080 | 62.070 | 0.192 | 2.177 | 2.103 | 1094.000 | 10.330 | 26.530 | 18.940 | 31.090 | 52.050 | | | | | |
| Michael et al. | 2a | 01.01.89 | 55.0 | 30.0 | 689.262 | | Na-Cl | 229.200 | 11.660 | 6.795 | 0.013 | 0.700 | 0.394 | 305.300 | 14.000 | 69.270 | 17.850 | 34.080 | 74.040 | -91.70 | -12.80 | 0.8 | | |
| Michael et al. | 2b | 01.01.89 | 55.6 | 42.0 | 721.212 | | Na-Cl | 231.300 | 11.460 | 6.493 | 0.059 | 0.680 | 0.350 | 269.900 | 14.810 | 89.170 | 67.770 | 29.220 | 78.720 | -89.00 | -12.90 | | | |
| Bortolami | 1d | 01.01.84 | 50.7 | 8.2 | 2800 | 1774.684 | Na-Cl | 589.900 | 35.520 | 68.910 | 0.334 | | | 1010.000 | | 21.750 | | 48.270 | | | | | 0.2 | |
| Bortolami | 2a | 01.01.84 | 54.4 | 8.8 | 1100 | 686.591 | Na-Cl | 235.200 | 14.500 | 13.380 | 0.091 | 0.700 | | 312.300 | | 42.080 | | 68.340 | | | | | 0.0 | |
| Fancelli & Nutti | 1a | 01.01.78 | 44.6 | 8.4 | 1735 | 1703.593 | Na-Cl | 541.900 | 35.320 | 55.510 | 0.303 | | | 964.800 | | 47.230 | | 58.530 | 49.450 | | | -13.10 | 1.5 | |
| Fancelli & Nutti | 1b | 01.01.78 | 50.0 | 7.8 | 2000 | 1881.485 | Na-Cl | 642.200 | 39.440 | 63.720 | 0.405 | | | 1072.000 | | | | 63.720 | 47.530 | | | -13.30 | 1.2 | |
| Fancelli & Nutti | 1c | 01.01.78 | 24.2 | 7.7 | 1125 | 1086.130 | Na-Cl | 348.900 | 21.050 | 23.060 | 0.100 | | | 602.500 | | 20.350 | | 70.170 | 43.110 | | | -13.00 | | |
| Fancelli & Nutti | 2a | 01.01.78 | 54.9 | 8.9 | 706 | 643.922 | Na-Cl | 211.000 | 13.180 | 5.071 | 0.101 | | | 323.500 | | 49.490 | | 41.580 | 73.020 | | | -13.00 | 1.5 | |
| Fancelli & Nutti | 2b | 01.01.78 | 50.7 | 9.1 | 615 | 546.138 | Na-Cl | 181.200 | 13.160 | 3.037 | 0.101 | | | 270.300 | | 22.670 | | 55.670 | 76.930 | | | -13.30 | 1.2 | |
| Perello | V8 | 05.06.96 | 5.5 | 7.3 | 82.120 | | Ca-CO ₃ -HCO ₃ | 1.100 | 0.820 | 9.900 | 0.600 | | | 0.400 | | 31.700 | 31.700 | 5.900 | 4.900 | | | | | |
| Perello | CO | 05.06.96 | 6.6 | 7.9 | 52.790 | | Ca-HCO ₃ | 0.900 | 0.240 | 6.600 | 0.350 | | | 0.300 | | 20.000 | 20.000 | 4.400 | 3.900 | | | | | |
| Fancelli & Nutti | AF | 01.01.78 | | 8.2 | 36.609 | | Ca-HCO ₃ -SO ₄ | 1.003 | 0.301 | 7.021 | 1.003 | | | | | 10.130 | 10.130 | 7.021 | 20.060 | | | | -13.00 | |
| Fancelli & Nutti | Combal Jors | 01.01.78 | 10.3 | 7.0 | 77.937 | | Ca-HCO ₃ -SO ₄ | 5.002 | 0.900 | 9.003 | 2.001 | | | 4.001 | | 19.010 | 19.010 | 19.010 | 11.000 | | | | -12.90 | |



- Thermal waters (Guglielmetti, 2009) ● Cold springs (Guglielmetti, 2009) ● Rivers (Guglielmetti, 2009)
- Thermal waters (previous works) ● Cold waters (previous works)

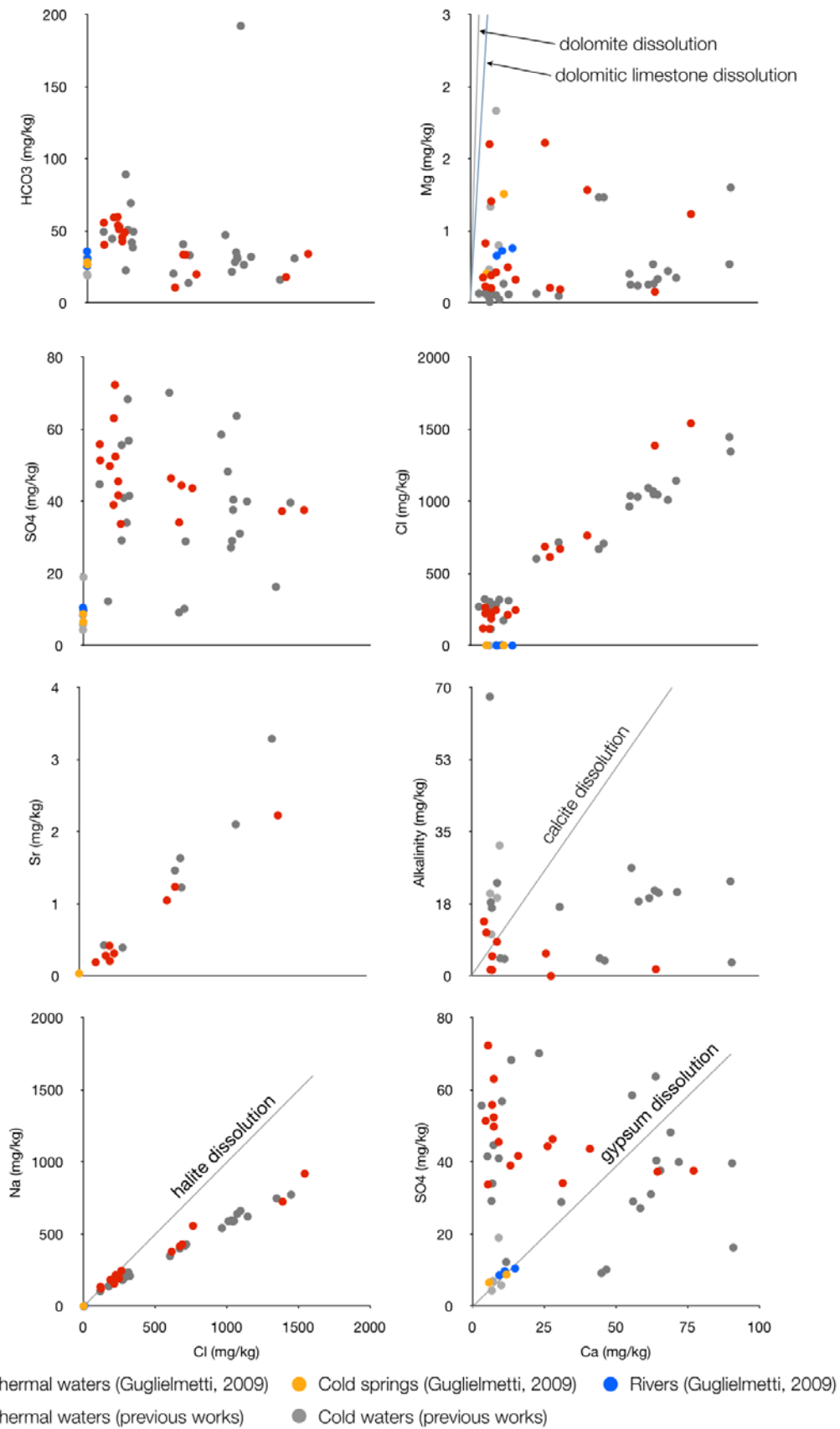


Figure 5-2 Correlation between the physico-chemical parameters at Bagni di Vinadio for all existing data

Also the plot of Tritium vs. Cl (Figure 5-3) indicates the occurrence of mixing processes. Tritium contents in thermal waters are often higher than 0.5 TU, the average value for thermal waters having long residence times (SONNEY, 2010a). In the case of the waters at Bagni di Vinadio the well VinW03 shows the lowest content with 0.6 T.U., whereas thermal springs have slightly higher content with 1-2 T.U. and shallow cold waters show 6 T.U. which is the average value for modern meteoric waters. Therefore this variation might confirm the presence of a young type of water within this hydrothermal system.

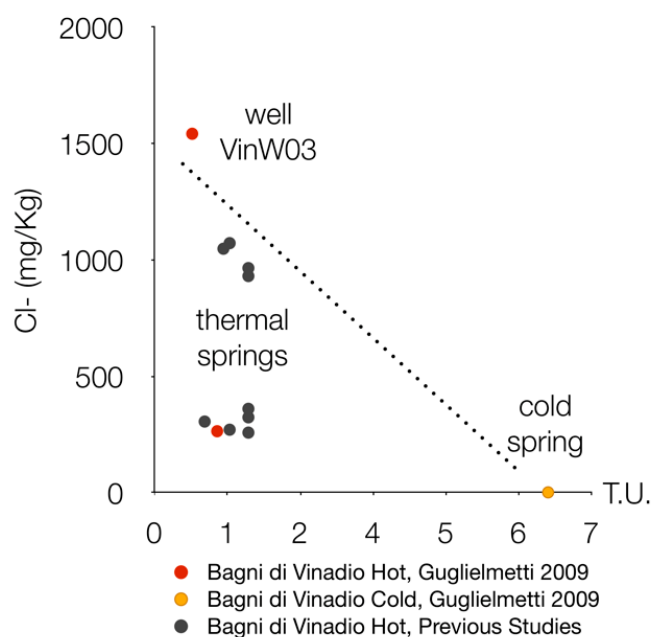


Figure 5-3 Tritium vs Chloride plot. It is possible to locate the three main groups of waters and the difference between Tritium content for the thermal waters measured in the past (values between 0.8 and 1.5 T.U.) an measured in this Thesis (<1 T.U.).

5.2.3. Water-Rock Interactions

Fluid-mineral equilibria were computed with PHREEQ code choosing, from the current and the previous studies, the most representative samples in terms of temperature and mineralization. Three main types of water can be identified in the Vinadio area:

5.2.3.1. Ca-HCO₃-SO₄ waters

In the case of the shallow waters of Bagni di Vinadio, the Ca-HCO₃ composition of the superficial waters might be related to the alteration of the minerals composing the gneiss which represent the majority of the outcropping lithologies in the Vinadio area.

5.2.3.2. Na-SO₄ waters

Thermal waters circulate within the widespread zones of intense fracture conditions and pervasive cataclasis, such as the Bersezio Shear Zone, the Valletta Shear zone and the associated mylonitic and cataclastic belts, embodied in the Bersezio Fault Zone. The BFZ, which is considered the main corridor for thermal waters circulation for this area (BAIETTO

et al., 2009; MARINI et al., 2001) is constituted mainly by gneisses and micro-grained granites containing quartz, k-feldspar, plagioclase, biotite, and chlorite. The Na-SO₄ waters are related to the dissolution of sulphide minerals under oxidizing conditions, which brings to production of H₂SO₄, and subsequent neutralization of H₂SO₄ by reaction with silicates, mainly feldspars. In this type of water, Na usually derives from the alteration of the sodium feldspars (albite, oligoclase), whereas sulphate originates through leaching of the sulphide minerals (pyrite) forming the crystalline rocks. This water-type is probably related to fluids circulating within the lithologies not involved in the shear zones and where the lithology is more similar, in terms of fracture density and mineralogical assemblage, to that of Valdieri where the thermal waters show a Na-SO₄ composition.

5.2.3.3. Na-Cl waters

This type of water is anomalous if just considering fluids circulating within crystalline rocks but not rare. Brines appear to fill the largest faults and the main tectonic contact and are squeezed by tectonic activity and mobilised at depth by freshwater from the surface. Several water inflow showing a Na-Cl composition were found in many alpine tunnels (BIANCHETTI, 1993; MARÉCHAL and PERROCHET, 1999; MARÉCHAL, 1998a; MARÉCHAL, 1998b; MARÉCHAL and ETCHEVERRY, 2003).

The presence of high concentration of Na in this water is just in part related to dissolution of silicates and sodium feldspar that form the mineralogical matrix of the geological system. However it is more likely related to the deep Na-Cl endmember which strongly controls the Sodium content in these waters. Moreover the most debated point about the thermal waters at Bagni di Vinadio is the origin of Chloride. The salinity of the fluids circulating within the crystalline rocks can derive from external, non-crystalline sources (halocinèse theory, (DEBELMAS and KERCKHOVE, 1980b)) or from water-rock interaction occurring within the crystalline basement. Three main hypotheses were proposed by Bortolami (1984), Michard (1989) and Perello (2001). The first two authors supported the halocinèse theory, the third proposed an interpretation supporting the internal origin. Bortolami proposed that the Na-Cl endmember is very similar to that at Acqui Terme (another thermal area located in the Po River Basin, 120km NW of Bagni di Vinadio), therefore deep connate brines from the Po Plane might flow towards Vinadio following the main tectonic lineaments. Michard (1989) proposed, on the basis on the Cl/Br ratio, that descending waters dissolve the evaporitic formations of the sedimentary cover, and then mix with low-Chloride waters, during the upflow, resulting in the variable Cl concentration in the different springs. Perello (2001) however proposed that the main sources of Chloride are phyllosilicates and fluid inclusions. Chloride could replace the OH⁻ group in the phyllosilicates and associated with Sodium represent the major solute of fluid inclusions which are abundant in particular in the cataclastic belts surrounding the Vinadio Area (FACELLO, 2011). Among these three hypotheses, only that of Bortolami might be rejected. In fact, as Perello pointed out on the structural point of view, the migration direction of the waters from the Po Valley towards the Argentera Massif is perpendicular to the main cataclastic zones, NW-SE oriented. Moreover the permeability of these zones (BAIETTO et al., 2008) is too low to allow the infiltration and the circulation of the waters.

The Na-Cl correlation plot of indicates that all samples show an enrichment of Cl⁻ with respect to the halite dissolution line. This is probably related to a deep origin of Chloride as a consequence of long circulation time (5000-12000 years) (ZUPPI et al., 2004).

Cl/Br ratio observations were also carried out in this study, as it is an effective method to decipher the origin of the salinity in the deep endmember of Vinadio. In fact values above 655 indicate halite dissolution, close to 655 is the value typical of seawaters, below 655 indicate that brines contribute to the Chloride content (ALCALA and CUSTODIO, 2008; SONNEY, 2010b). In the waters of Vinadio the Cl/Br molar ratio is above 700 for all the samples. This supports the idea that Cl derives from the dissolution of halite as proposed by Michard. However, on the basis of these results and previous interpretations it is not possible to completely reject neither the hypothesis of Michard neither that of Perello. The contribution of the dissolution of fluid inclusions to the salinity of this water cannot be neglected. However high Cl concentrations such as those at Vinadio (up to 1500 mg/kg) are very anomalous for waters circulation in a crystalline massif and are hardly explained just by considering the contribution of fluid inclusions and mineral dissolution. Therefore a second source of Cl has to be involved. The Triassic formations surrounding the Argentera Massif, rich in sulphate rocks which could be associated to halite deposits, are also locally pinched within some of the thrusts and fault zones (e.g. Sespoul Thrust, Tortissa Thrust) associated to the Bersezio Fault Zone. Therefore halite deposits, even if not clearly outcropping as it has a very high solubility, could lie within these structures and might be leached by circulating thermal fluids, which then flow within the Bersezio Fault Zone and finally upflow.

5.2.4. Origin and Elevation of the Recharge Zone

Isotopic analyses were carried out on selected water samples chosen from both thermal and cold waters. $\delta^2\text{H}$ and $\delta^{18}\text{O}$ content were evaluated to understand the origin of the waters and the occurrence of phase changes at depth (Figure 5-4). Both thermal springs and cold waters plot close the meteoric water line and fall into the range between -13 and -12 ‰ for the isotope $\delta^{18}\text{O}$ and within -93 and -85 ‰ for the $\delta^2\text{H}$ isotope. Thermal waters do not exhibit positive $\delta^{18}\text{O}$ -shift, typical of high-temperature geothermal systems (>150 °C) with long water residence time. The position of the $\delta^2\text{H}$ - $\delta^{18}\text{O}$ samples along and between the meteoric water lines indicates that the reservoir temperature is probably lower than 150 °C, that there is not apparent effect of boiling in the reservoir and that the geothermal fluid circulates in dynamic and fluid- dominated systems.

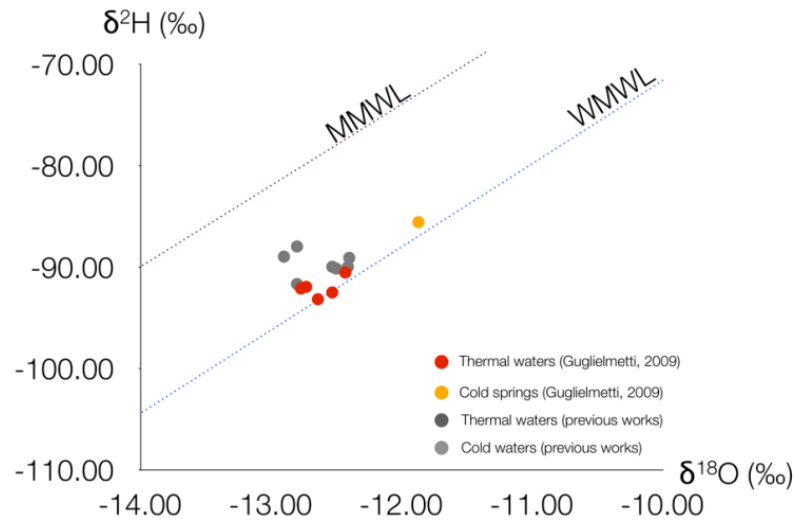


Figure 5-4 Plot showing the distribution of the stable isotopes of hydrogen and oxygen for the thermal waters of Vinadio. WMWL: World Meteoric Water Line; MMWL: Mediterranean Meteoric Water Line

The average elevation of the recharge basin of the Vinadio thermal system can also be inferred from these isotopic data. In fact it is possible to correlate the elevation with the isotopic signature as elevation is one of the factors, which control the isotopic composition in terms of stable isotopes of hydrogen and oxygen in the waters. This relation varies according to the different geographical regions and, for the study area those of Bortolami (1978) referring to the Maritime Alps were initially employed. The calculation results show that the average elevation quote is 1500 m a.s.l., which seems to be underestimated as the average elevation of the hydrographic basins in the Vinadio areas is around 1800 m a.s.l. Therefore the relation proposed for the Mt. Blanc by Jamier & Olive (1977) was also employed and, showed a more fitting elevation range between 1800 and 2200 m a.s.l. (Table 5-4 and Figure 5-5).

Table 5-4 Available data for the stable isotopes of hydrogen and oxygen and their correlation with the calculated elevation of the recharge basin for the Vinadio area

| Author | Code | T° C | $\delta^{18}\text{O}$ | δD | Elevation $\delta^{18}\text{O}$ | Elevation δD | AVG | Elevation $\delta^{18}\text{O}$ |
|-----------------|-------------|------|-----------------------|------------------|---------------------------------|----------------------------|---------------------------|---------------------------------|
| | | | | | Bortolami (1978) | Bortolami (1978) | Jamier & Oliver (1977) | |
| Guglielmetti | VinS_01 | 51,2 | -12,77 | -92,15 | 1519 | 1649 | 1584 | 1947 |
| Guglielmetti | VinS_02 | 34,1 | -12,73 | -91,98 | 1506 | 1642 | 1574 | 1930 |
| Guglielmetti | VinW_01 | 52,3 | -12,43 | -90,57 | 1410 | 1585 | 1498 | 1807 |
| Guglielmetti | VinW_03 | 70,2 | -12,53 | -92,53 | 1442 | 1664 | 1553 | 1848 |
| Guglielmetti | VinS_04 | 38,8 | -12,64 | -93,20 | 1478 | 1691 | 1584 | 1893 |
| Baietto | Vi_1 | 52,3 | -12,40 | -89,12 | 1401 | 1527 | 1464 | 1794 |
| Baietto | Vi_2 | 65,0 | -12,50 | -90,18 | 1433 | 1569 | 1501 | 1835 |
| Baietto | Vi_3 | 43,0 | -12,53 | -90,00 | 1442 | 1562 | 1502 | 1848 |
| Baietto | Vi_4 | 61,0 | -12,41 | -90,00 | 1404 | 1562 | 1483 | 1798 |
| Michard et al. | 1a | 46,7 | -13,10 | | 1625 | | 1625 | 2082 |
| Michard et al. | 1c | 30,7 | -13,00 | | 1593 | | 1593 | 2041 |
| Michard et al. | 1d | 50,5 | -12,80 | -88,00 | 1529 | 1482 | 1505 | 1959 |
| Michard et al. | 2a | 55,0 | -12,80 | -91,70 | 1529 | 1631 | 1580 | 1959 |
| Michard et al. | 2b | 55,6 | -12,90 | -89,00 | 1561 | 1522 | 1541 | 2000 |
| Fancelli & Nuti | 1a | 44,6 | -13,10 | | 1625 | | 1625 | 2082 |
| Fancelli & Nuti | 1b | 50,0 | -13,30 | | 1689 | | 1689 | 2165 |
| Fancelli & Nuti | 1c | 24,2 | -13,00 | | 1593 | | 1593 | 2041 |
| Fancelli & Nuti | 2a | 54,9 | -13,00 | | 1593 | | 1593 | 2041 |
| Fancelli & Nuti | 2b | 50,7 | -13,30 | | 1689 | | 1689 | 2165 |
| Guglielmetti | VinS_05 | 9,2 | -11,87 | -85,60 | 1231 | 1386 | 1308 | 1576 |
| Fancelli & Nuti | AF | | -13,00 | | 1593 | | 1593 | 2041 |
| Fancelli & Nuti | Combal Jors | 10,3 | -12,90 | | 1561 | | 1561 | 2000 |



Figure 5-5 Map of the calculated elevation of the recharge basins (white dotted line). The yellow line represents the 1800 m a.s.l. contour

5.2.5. Reservoir Temperature

5.2.5.1. The Giggenbach Plots

The Silica vs. $\log(K^2/Mg)$ plot and the ternary plot of Giggenbach (Figure 5-6) were employed to infer thermodynamic and kinetic correlations between geothermal fluid and host rock and define which waters were the best suited for temperature calculations. Cold-water samples were also plotted because their disposition can help to identify trends related to mixing processes. It is possible to observe a sampling point plotting on the right side of the plot. This is water derives from the mix of all the thermal springs and the cold shallow water used in the spa to cool the thermal waters down before flowing into the swimming pool. This sample will not be considered for geothermometers. The samples plotting in the immature water field will neither be considered as they correspond to the sources VinS01 and VinS03 sampled in summer 2009 which chemical composition is related to a strong dilution with shallow cold waters. Other samples plot in the field of the partially equilibrated waters and their disposition is strictly controlled by the degree of mixing. In fact the waters of the well VinW03, the less diluted, plot close to the fully equilibrated curve.

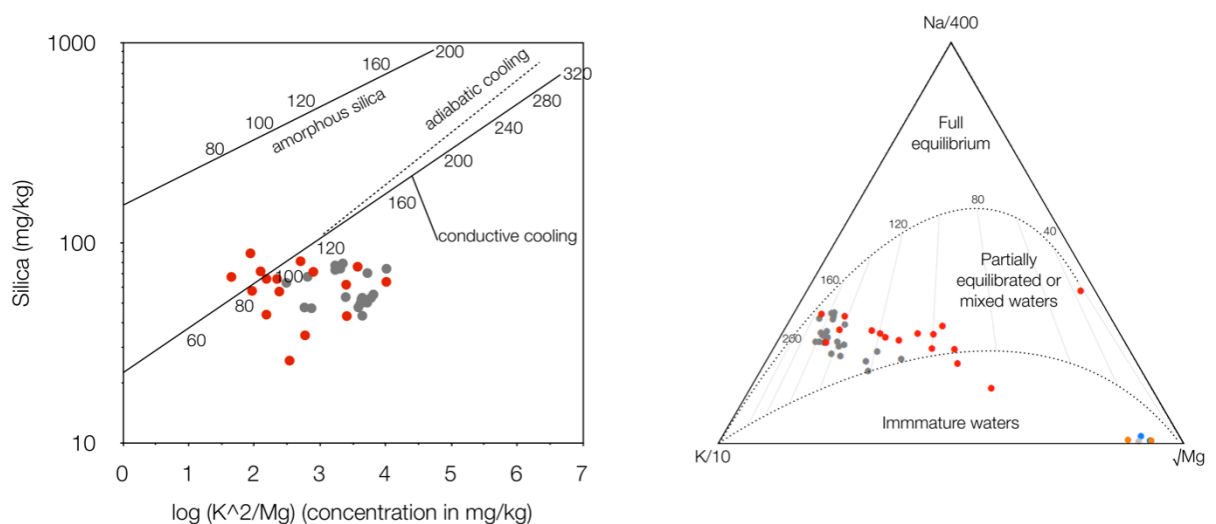


Figure 5-6 Silica vs. $\log(K^2/Mg)$ and Giggenbach triangular plot showing the distribution of the thermal waters of Vinadio with respect to the theoretical line of the fully equilibrated waters at increasing temperatures

5.2.5.2. Solute Geothermometers

Solute geothermometers of Chalcedony, Quartz, Na-K-Ca, Na-K, K^2 -Mg, Li-Mg and Na-Li were calculated and compared to test their applicability (Table 5-5).

The silica geothermometers work for reservoir lower than 120-160°C, as those expected for the studied region. As expected the calculate temperature with the Chalcedony equation is the lowest, showing an average value of 80°C. The quartz geothermometers indicates an higher temperature of about 110°C which suits better the range from the saturation indexes and from the Silica vs. $\log(K^2/Mg)$ plot.

As shown in Table 5-5, the Na-K equations of Fournier and Giggenbach show high temperatures, 173 and 191 °C respectively, than those around 140 °C shown by the other Na-

K equations (ARNORSSON et al., 1983; TRUESDELL, 1976). Therefore it can be considered strongly overestimated also if compared to the Na-K-Ca equation that averages 150° C. The K²-Mg and Li-Mg equations were applied, as the thermal waters of Vinadio are understaturated with respect to K-feldspar and a useful tool to better constrain the temperature range estimated by the Na-K and Na-K-Ca geothermometers. In fact they show an average temperature of 140 °C, which is probably slightly overestimated with respect to the expected temperature range (5.2.5.3). Finally the Na-Li (FOUILLAC, 1981) equation was applied as it seems to be effective for low enthalpy fluids, in particular where the ascent occurs rapidly and the lateral contribution of cold waters is limited. Therefore this equation was employed for the less diluted samples indicating a temperature of about 145 °C.

Table 5-5 Calculated reservoir temperature by means of selected geothermometers for the thermal waters of Bagni di Vinadio. Temperature values are expressed in °C

| Sample ID | Chalcedony | | Quartz (no steam loss) | K ² /Mg | K ² /Mg | Na-K-Ca $\beta=1/3$ Mg corrected | | Na-K | Na-K | Li-Mg | Na/Li, Cl<0.3m |
|--------------|--------------------|---------------------|------------------------------|--------------------|-----------------------|--|-------------------------------|---------------------|--------------------------------|---------------------------------|-------------------|
| | Fournier (1977) | Arnorsson (1983) | Fournier (1973) | Fournier (1991) | Giggenbac h (1988) | Fournier & Truesdell (1973) | Arnorsson et al. (1983) | Truesdell (1975) | Kharaka & Mariner (1988) | Fouillac & Michard (1981) | |
| VinS_01 | 91 | 91 | 119 | 108 | 112 | 147 | 116 | 105 | 133 | 116 | |
| VinS_02 | 92 | 92 | 120 | 109 | 113 | 150 | 124 | 113 | 129 | 117 | |
| VinS_03 | 95 | 94 | 123 | 89 | 98 | 123 | 129 | 119 | 151 | 129 | |
| VinS_04 | 83 | 83 | 99 | 134 | 133 | 149 | 128 | 117 | 108 | 127 | |
| VinW_01 | 83 | 84 | 112 | 78 | 90 | 113 | 135 | 125 | 162 | 126 | |
| VinW_02 | 80 | 80 | 109 | 125 | 127 | 148 | 133 | 123 | 124 | 132 | |
| VinW_03 | 74 | 76 | 104 | 161 | 158 | 141 | 134 | 124 | 91 | 138 | |
| VinS_TOT | 79 | 79 | 91 | 107 | 111 | 152 | 139 | 129 | 136 | 133 | |
| Vi_1 | 88 | 88 | 116 | 122 | 123 | 174 | 175 | 167 | 129 | 150 | |
| Vi_2 | 75 | 76 | 105 | 148 | 145 | 179 | 165 | 156 | 112 | 132 | |
| Vi_3 | 69 | 71 | 99 | 120 | 121 | 163 | 148 | 139 | 130 | 129 | |
| Vi_4 | 69 | 70 | 99 | 125 | 125 | 170 | 163 | 154 | 129 | 135 | |
| V1 | 90 | 90 | 119 | 162 | 158 | 145 | 156 | 146 | 88 | 163 | |
| V2 | 75 | 76 | 105 | 165 | 160 | 145 | 147 | 137 | 83 | 166 | |
| V3 | 72 | 73 | 102 | 162 | 158 | 151 | 148 | 138 | 84 | 169 | |
| V4 | 72 | 73 | 102 | 159 | 155 | 149 | 143 | 133 | 86 | 165 | |
| V5 | 84 | 84 | 113 | 108 | 112 | 160 | 149 | 139 | 127 | 160 | |
| V6 | 93 | 93 | 121 | 144 | 141 | 166 | 155 | 145 | 101 | 162 | |
| V7 | 77 | 78 | 106 | 166 | 162 | 164 | 157 | 147 | 83 | 171 | |
| 1a | 74 | 75 | 104 | 158 | 154 | 139 | 132 | 121 | 86 | 154 | |
| 1c | 74 | 75 | 103 | 162 | 158 | 120 | 127 | 117 | 83 | 150 | |
| 1d | 75 | 76 | 105 | 159 | 155 | 135 | 129 | 119 | 85 | 155 | |
| 1e | 74 | 75 | 104 | 160 | 156 | 133 | 126 | 116 | 84 | 152 | |
| 2a | 93 | 93 | 121 | 175 | 171 | 103 | 135 | 125 | 79 | 146 | |
| 2b | 96 | 96 | 124 | 146 | 143 | 156 | 133 | 123 | 99 | 143 | |
| 1d | | | | 156 | 152 | 158 | 148 | 139 | | | |
| 2a | | | | 146 | 143 | 160 | 150 | 141 | | | |
| 1a | 71 | 73 | 101 | 157 | 154 | 164 | 155 | 146 | | | |
| 1b | 69 | 71 | 99 | 156 | 152 | 166 | 150 | 140 | | | |
| 1c | 65 | 66 | 95 | 159 | 155 | 152 | 149 | 139 | | | |
| 2a | 92 | 92 | 120 | 141 | 138 | 175 | 151 | 142 | | | |
| 2b | 95 | 95 | 123 | 141 | 138 | 184 | 164 | 155 | | | |
| AVG | 81 | 81 | 109 | 141 | 140 | 151 | 144 | 134 | 108 | 145 | |
| TOTAL AVG | | | | | | | | | | 123 | |

5.2.5.3. Saturation Indexes

The variations of SI with increasing temperature were simulated using PHREEQC code, and temperature increments were set from the emergence temperature up to 150 °C which is a suitable temperature for the reservoir conditions. S.I. vs. temperature plots were created (Figure 5-7) to visualize the temperature at which the main minerals attain conditions close equilibrium (S.I.=0). The three selected samples show with consistency a temperature range of 110-140 °C. The lower temperatures are shown on the sample VinW01 which is also the most diluted sample whereas sample VinW03, the hottest and most representative of the deep endmember, shows a range of 120-140 °C.

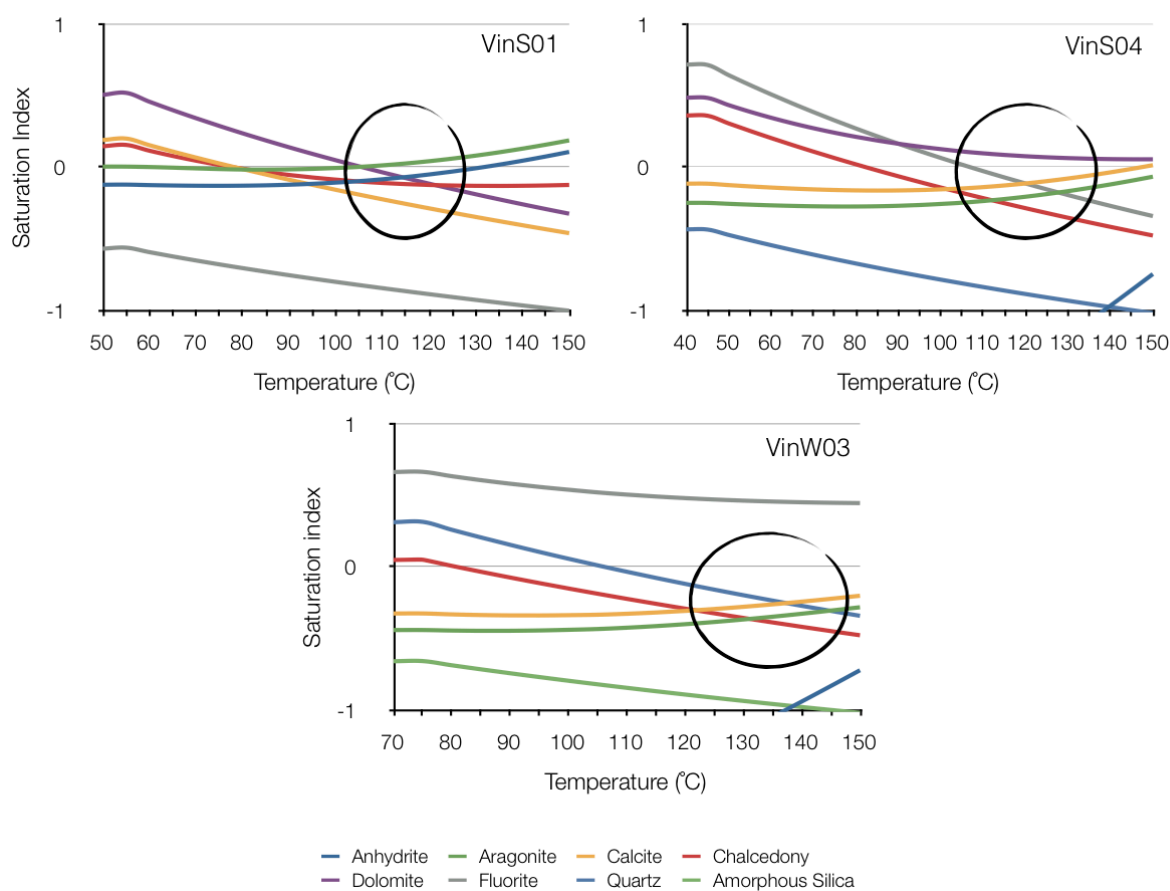


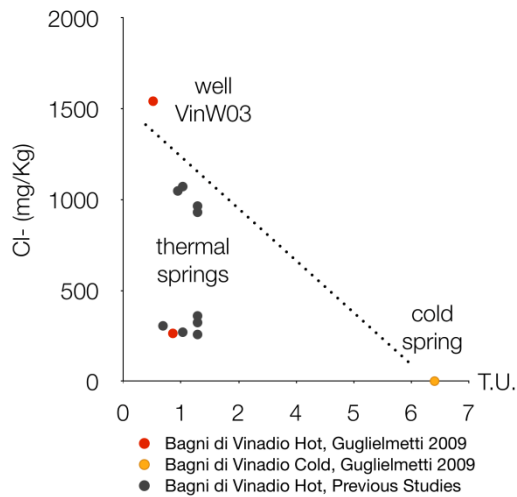
Figure 5-7 Saturation index vs. temperature plots for selected samples from the Vinadio Area. The circles indicate the temperature range at which the main minerals are close to saturation

On the basis of the observation made by means of saturation indexes, SiO_2 vs. $\log(K^2/\text{Mg})$, ternary plot of Giggenbach and calculation of the geothermometers equation it is possible to constrain the temperature of the reservoir of the Bagni di Vinadio Area. The saturation indexes indicate a range of 115-135 °C, the SiO_2 vs. $\log(K^2/\text{Mg})$ shows a range between 90 and 120C while the triangular plot of Giggenbach show an overestimated temperature of about 160C which are in agreement with the Na/K geothermometers. Average temperature from geothermometers indicates a temperature of 120 °C. Finally the temperature of the reservoir for the Bagni di Vinadio area can be constrained to the range between 110 and 130 °C.

5.2.6. Groundwater Residence Time

Residence time for geothermal fluids was evaluated by means of Tritium (Table 5-6).

The plot of Tritium vs. Chloride (Figure 5-8) shows that the samples with higher chloride content (1500 mg/l), therefore the hottest and the most representative of the deep endmember, have the lowest T.U. content (0.6 T.U.). The highest content (6.3 T.U.) in the sampled waters, also compared to previous works (MICHARD 1989, FANCELLI 1978, REGIONE PIEMONTE 1976), corresponds to low temperature samples, poor in Chloride (2.5 mg/l).



| Author | Code | T° C | Sampling Date | U.T. |
|------------------|---------|------|---------------|------|
| Guglielmetti | VinS_01 | 46,4 | 2009 | 1,0 |
| Guglielmetti | VinW_03 | 70,2 | 2009 | 0,6 |
| Guglielmetti | VinS_05 | 9,2 | 2009 | 6,3 |
| Michard et al. | 2a | 55,0 | 1989 | 0,8 |
| Fancelli & Nuti | 1a | 44,6 | 1989 | 1,5 |
| Fancelli & Nuti | 1b | 50,0 | 1978 | 1,2 |
| Fancelli & Nuti | 2a | 54,9 | 1978 | 1,5 |
| Fancelli & Nuti | 2b | 50,7 | 1978 | 1,2 |
| Regione Piemonte | I-1a | 42,3 | 1976 | 1,5 |
| Regione Piemonte | I-1b | 52,2 | 1976 | 1,1 |
| Regione Piemonte | i-2a | 55,2 | 1976 | 1,5 |
| Regione Piemonte | i-2b | 48,0 | 1976 | 1,5 |
| Regione Piemonte | I-1c | 18,6 | 1976 | 1,5 |

Figure 5-8 Tritium vs Chloride plot for the Vinadio waters

Table 5-6 Resuming Table of the Tritium content in sampled waters from 1976 to the present work.

On the basis of this data it is possible to infer that the cold waters are recent as the actual Tritium content in today meteoric water in the Mediterranean area is around 6-8 T.U. Deep waters residence time however cannot be evaluated because of the extremely low Tritium content as in most of the deep waters circulating in the Alps and also in sedimentary basins. It was proven that thermal waters in the Alps have very long residence time (e.g. more than 8000 years at Lavey les Bains, Sonney 2010) and a period larger than several thousands of years was proposed by Perello (2001) for the thermal waters at Vinadio. In this case, on the base of the T.U. it is just possible to state that these waters infiltrate before the period of the nuclear atmospheric tests in the '60s but it is impossible to date with more accuracy.

5.3. The Terme di Valdieri Thermal Site

5.3.1. Water Chemistry

Thermal waters show a wide range of temperature from 32.5 °C to 65 °C, pH is between 7.6 and 9.8 and the TDS is about 220 mg/kg. Two hypothermal springs located on the riverbed have a temperature of 17 °C, pH of 7.6 and TDS around 80 mg/kg. Shallow waters were also sampled from two cold springs and the Gesso River, upstream and downstream the thermal area. Temperature reaches 11.2 °C for both cold springs, pH around 8 and TDS 75 mg/Kg. The water from the river shows a temperature of 3.8 °C upstream the springs and 20.5 °C, downstream the thermal area. As a consequence the pH also increases from 7.6 to 8.1 and the salinity from 26 to 159 mg/kg. Cold springs show a Na>Ca-HCO₃>SO₄ composition, the Gesso River a Ca-HCO₃ water type upstream the springs, which become more Na-SO₄-HCO₃ downstream. The thermal waters are representative of a Na-SO₄ type, which is typical of waters circulation in the Alpine crystalline massifs (Figure 5-9).

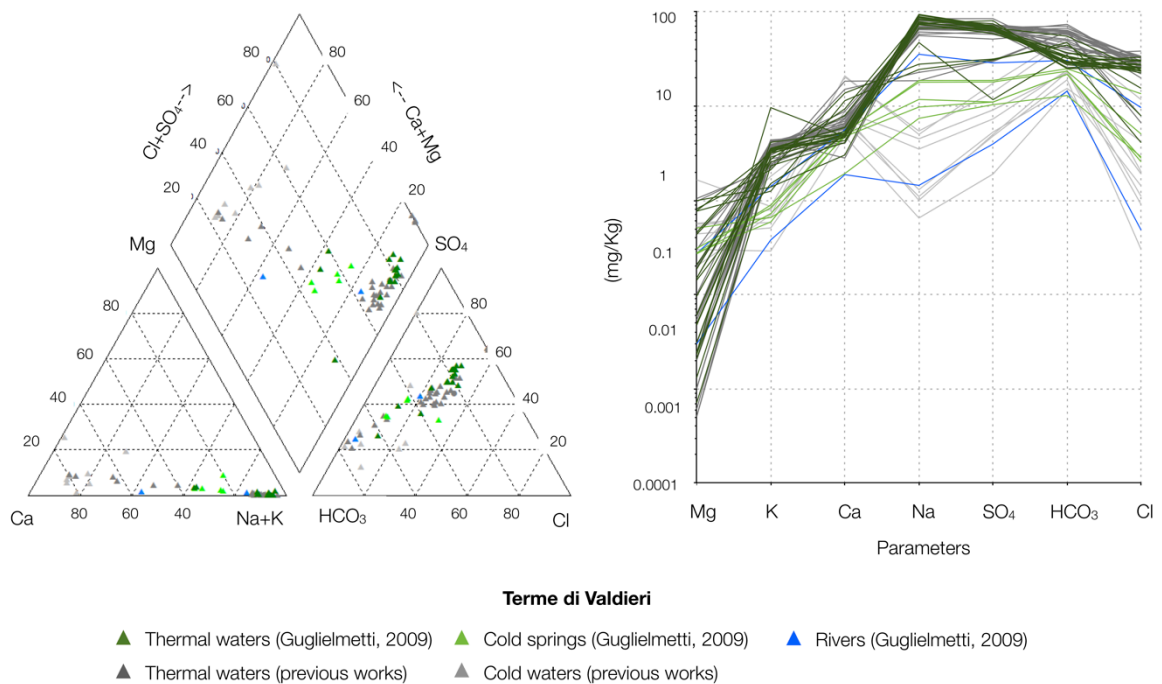


Figure 5-9 Piper and Schoeller plots of the Terme di Valdieri waters

It is possible to divide the waters at Valdieri into four groups which can be easily correlated with a straight line:

- cold waters showing low TDS, Low T °C and Na-HCO₃-SO₄ composition;
- sub-thermal waters with temperatures of 17 °C and slightly more mineralized but still showing a Na-Ca-HCO₃-SO₄ composition;
- waters of the Gesso river, mixed with the discharged thermal springs, are hotter and clearly show a Na-SO₄-HCO₃ composition;
 - hot NaSO₄ springs with higher TDS and decreasing alkalinity with respect to increasing temperature and sulphate concentration.

Table 5-7a Resuming table reporting the chemical and isotopic compositions of the sampled waters in the Terme di Valdieri Area (results from samples collected during the present thesis).

| Author | Code | Date | T° C | Q (l/min) | pH | Cond $\mu\text{S/cm}$ | TDS | Type | Na ⁺ | K ⁺ | Ca ²⁺ | Mg ²⁺ | Li ⁺ | Sr ²⁺ | Cl ⁻ | F ⁻ | Br ⁻ | HCO ₃ ⁻ | CO ₃ ²⁻ | SO ₄ ²⁻ | SiO ₂ | δD | $\delta^{18}\text{O}$ | U.T. |
|--------------|-------------|----------|------|-----------|-----|-----------------------|---------|---|-----------------|----------------|------------------|------------------|-----------------|------------------|-----------------|----------------|-----------------|-------------------------------|-------------------------------|-------------------------------|------------------|------------------|-----------------------|------|
| Guglielmetti | Vals_01 | 25.11.09 | 32.5 | | 9.4 | 355 | 244.617 | Na-SO ₄ | 92.640 | 1.383 | 3.028 | 0.994 | 0.172 | 0.188 | 27.250 | 10.040 | 29.670 | 10.430 | 69.010 | 37.920 | -88.59 | -12.13 | | |
| Guglielmetti | Vals_01 | 17.07.09 | 34.3 | 2.0 | 9.4 | 359 | 249.066 | Na-SO ₄ | 83.240 | 3.181 | 5.039 | 0.435 | 0.188 | 0.077 | 27.950 | 11.640 | 0.155 | 29.450 | 12.850 | 74.860 | 103.800 | | | |
| Guglielmetti | Vals_03 | 25.11.09 | 62.5 | 0.5 | 9.5 | 349 | 234.529 | Na-SO ₄ -Cl | 86.760 | 3.356 | 4.632 | 0.021 | | | 22.510 | 10.030 | | 32.340 | 10.640 | 64.240 | 55.130 | -87.59 | -12.19 | 1.8 |
| Guglielmetti | Vals_03 | 17.07.09 | 62.0 | 0.5 | 9.5 | 387 | 242.115 | Na-SO ₄ -Cl | 78.540 | 9.631 | 4.762 | 0.024 | 0.165 | 0.077 | 30.890 | 11.290 | 0.236 | 32.150 | 11.320 | 63.030 | 77.690 | | | |
| Guglielmetti | Vals_04 | 25.11.09 | 34.4 | 6.0 | 9.5 | 204 | 132.429 | Na-Ca-HCO ₃ -SO ₄ -Cl | 24.480 | 1.251 | 11.420 | 0.768 | | | 7.870 | 3.638 | 0.054 | 47.120 | 4.947 | 30.880 | 25.050 | -84.17 | -11.59 | |
| Guglielmetti | Vals_04 | 17.07.09 | 33.0 | 6.0 | 8.9 | 205 | 145.095 | Na-Ca-HCO ₃ -SO ₄ | 27.840 | 2.111 | 13.750 | 0.813 | 0.058 | 0.062 | 15.440 | 5.394 | 0.108 | 44.400 | 3.558 | 31.560 | 31.810 | | | |
| Guglielmetti | Vals_05 | 25.11.09 | 55.1 | 3.0 | 9.8 | 323 | 242.324 | Na-SO ₄ | 82.410 | 2.726 | 9.349 | 0.208 | 0.148 | | 25.330 | 11.790 | 0.193 | 25.000 | 13.570 | 71.600 | 59.420 | | | |
| Guglielmetti | Vals_05 | 17.07.09 | 54.1 | 3.0 | 9.5 | 350 | 236.801 | Na-SO ₄ | 75.310 | 3.181 | 7.942 | 0.775 | 0.157 | 0.077 | 25.030 | 11.530 | 0.200 | 29.440 | 12.960 | 70.200 | 76.510 | | | |
| Guglielmetti | Vals_06 | 25.11.09 | 52.0 | 9.0 | 9.0 | 331 | 252.090 | Na-SO ₄ -Cl | 75.490 | 3.407 | 4.801 | 0.458 | 0.113 | | 30.600 | 13.000 | 0.180 | 25.210 | 18.170 | 80.660 | 69.180 | -89.48 | -12.21 | |
| Guglielmetti | Vals_06 | 17.07.09 | 53.0 | 9.0 | 9.7 | 410 | 261.863 | Na-SO ₄ -Cl | 89.210 | 3.503 | 4.292 | 0.013 | 0.202 | | 29.870 | 12.660 | 0.213 | 36.840 | 16.720 | 68.340 | 83.400 | | | |
| Guglielmetti | Vals_07 | 25.11.09 | 46.7 | 3.0 | 9.4 | 355 | 245.146 | Na-SO ₄ | 88.890 | 3.296 | 5.424 | 0.049 | 0.170 | | 23.370 | 10.530 | 0.217 | 34.030 | 13.520 | 65.650 | 54.650 | | | |
| Guglielmetti | Vals_07 | 17.07.09 | 46.4 | 4.0 | 9.7 | 366 | 223.621 | Na-SO ₄ | 74.220 | 3.156 | 4.992 | 0.047 | 0.157 | 0.079 | 23.800 | 10.290 | 0.180 | 33.530 | 14.360 | 58.810 | 75.380 | | | |
| Guglielmetti | Vals_08 | 25.11.09 | 54.2 | | 9.4 | 331 | 260.777 | Na-SO ₄ | 92.570 | 4.130 | 5.189 | 0.031 | 0.172 | | 33.180 | 10.970 | 0.185 | 29.070 | 15.450 | 69.830 | 57.010 | -87.93 | -12.16 | |
| Guglielmetti | Vals_08 | 17.07.09 | 56.9 | 4.0 | 9.6 | 351 | 238.662 | Na-SO ₄ -Cl | 78.060 | 2.879 | 5.018 | 0.023 | 0.169 | 0.075 | 25.370 | 11.620 | 0.208 | 36.910 | 15.160 | 63.170 | 77.700 | | | |
| Guglielmetti | Vals_09 | 17.07.09 | 57.2 | 6.0 | 9.7 | 365 | 224.950 | Na-SO ₄ | 73.090 | 2.328 | 4.098 | 0.007 | 0.142 | 0.075 | 25.180 | 11.650 | 0.200 | 29.860 | 15.710 | 62.610 | 77.710 | | | |
| Guglielmetti | Vals_09 | 25.11.09 | 56.6 | | 9.7 | 354 | 255.921 | Na-SO ₄ | 94.000 | 3.494 | 5.190 | 0.187 | 0.173 | | 25.590 | 11.800 | 0.168 | 28.730 | 15.830 | 70.760 | 57.180 | | | |
| Guglielmetti | Vals_10 | 25.11.09 | 49.5 | 20.0 | 9.7 | 294 | 256.584 | Na-SO ₄ -HCO ₃ | 88.510 | 3.510 | 5.954 | 0.061 | 0.163 | | 24.000 | 11.050 | 0.166 | 55.180 | 67.990 | 59.590 | -87.46 | -12.03 | | |
| Guglielmetti | Vals_TOT_01 | 17.07.09 | 58.1 | 30.0 | 9.7 | 358 | 121.522 | Na-HCO ₃ -CO ₃ | 47.260 | 1.503 | 4.886 | 0.142 | 0.102 | 0.075 | 4.096 | 1.998 | | 34.950 | 14.810 | 11.700 | 77.970 | | | |
| Guglielmetti | Vals_TOT_02 | 17.07.09 | 49.8 | 20.0 | 9.5 | 356 | 215.805 | Na-SO ₄ | 67.110 | 2.550 | 4.667 | 0.096 | 0.134 | 0.074 | 23.780 | 10.570 | 0.174 | 28.390 | 10.930 | 67.330 | 73.120 | | | |
| Guglielmetti | Vals_TOT_02 | 25.11.09 | 44.7 | 20.0 | 9.7 | 296 | 240.980 | Na-SO ₄ -Cl | 88.200 | 3.564 | 5.936 | 0.149 | 0.168 | | 23.920 | 10.480 | 0.133 | 27.470 | 13.870 | 67.090 | 52.020 | | | |
| Guglielmetti | Vals_11 | 25.11.09 | 17.0 | 15.0 | 7.5 | 89 | 85.341 | Na-Ca-HCO ₃ -SO ₄ -Cl | 18.710 | 0.894 | 5.269 | 0.276 | 0.028 | | 13.520 | 2.935 | 0.049 | 24.920 | 18.740 | 14.610 | | | | |
| Guglielmetti | Vals_12 | 25.11.09 | 17.1 | 12.0 | 7.6 | 72 | 73.776 | Na-Ca-HCO ₃ -SO ₄ | 17.920 | 0.835 | 5.341 | 0.309 | 0.025 | | 5.049 | 2.768 | 0.039 | 23.450 | 18.040 | 17.790 | | | | |
| Guglielmetti | Vals_02 | 25.11.09 | 11.2 | | 8.5 | 27 | 36.974 | Na-Ca-HCO ₃ -SO ₄ | 7.414 | 0.657 | 1.925 | 0.508 | | | 2.892 | 0.215 | 0.034 | 12.970 | 10.360 | 4.675 | -86.15 | -11.97 | 6.0 | |
| Guglielmetti | Vals_02 | 17.07.09 | 13.0 | 200.0 | 8.0 | 83 | 52.799 | Na-SO ₄ -HCO ₃ | 9.768 | 0.723 | 4.756 | 0.270 | 0.011 | 0.021 | 2.801 | 1.642 | 0.026 | 21.730 | 11.050 | 5.498 | | | | |
| Guglielmetti | Vals_13 | 25.11.09 | 11.2 | | 7.6 | 74 | 54.716 | Na-Ca-HCO ₃ -SO ₄ | 11.770 | 0.590 | 4.973 | 0.278 | 0.012 | | 2.559 | 1.734 | 0.020 | 21.730 | 11.050 | 9.956 | | | | |
| Guglielmetti | GR_01 | 25.11.09 | 3.8 | | 7.6 | 21 | 33.691 | Ca-CO ₃ -HCO ₃ | 1.442 | 0.380 | 1.874 | 0.030 | 0.029 | | 0.483 | 0.293 | | 14.400 | 10.800 | 3.960 | 3.325 | | | |
| Guglielmetti | GR_02 | 25.11.09 | 20.5 | | 8.1 | 159 | 118.409 | Na-SO ₄ -HCO ₃ | 35.500 | 1.405 | 5.607 | 0.274 | 0.066 | | 9.633 | 4.505 | 0.085 | 30.560 | 2.044 | 28.730 | 27.840 | | | |

Table 5-8b Resuming table reporting the chemical and isotopic compositions of the sampled waters in the Terme di Valdieri Area (data from previous studies)

| Author | Code | Date | T° C | Q (l/min) | pH | Cond $\mu\text{S/cm}$ | TDS | Type | Na ⁺ | K ⁺ | Ca ²⁺ | Mg ²⁺ | Li ⁺ | Si ²⁺ | F ⁻ | Br ⁻² | HCO ³⁻ | CO ²⁻ | SO ²⁻ | SiO ₂ | δD | $\delta^{18}\text{O}$ | U.T. |
|-----------------|-------------|----------|------|-----------|-------|-----------------------|---------|--|-----------------|----------------|------------------|------------------|-----------------|------------------|----------------|------------------|-------------------|------------------|------------------|------------------|------------------|-----------------------|--------|
| Baietto | Va_1 | 27.06.05 | 58.9 | | 9.0 | 396 | 211.197 | Na-SO ₄ -Cl | 66.810 | 4.200 | 6.402 | 0.200 | 0.142 | 0.091 | 26.010 | 10.670 | 28.250 | 4.021 | 64.400 | 62.410 | -85.09 | -11.50 | |
| Baietto | Va_2 | 27.06.05 | 63.7 | | 9.0 | 390 | 208.577 | Na-SO ₄ -Cl | 67.720 | 4.100 | 6.902 | 0.200 | 0.132 | 0.092 | 26.410 | 10.490 | 25.750 | 4.081 | 62.700 | 63.010 | -85.74 | -11.90 | |
| Baietto | Va_3 | 27.06.05 | 53.2 | | 8.9 | 360 | 207.601 | Na-SO ₄ -Cl | 61.210 | 3.801 | 7.801 | 0.300 | 0.122 | 0.081 | 23.500 | 8.615 | 39.720 | 4.741 | 57.710 | 58.820 | -84.50 | -11.65 | |
| Perello | S1 | 04.04.96 | 30.1 | | 9.0 | | 192.433 | Na-Ca-CO ₃ -HCO ₃ -SO ₄ | 22.800 | 2.210 | 15.070 | 1.045 | 0.060 | | 7.834 | 3.214 | 61.260 | 49.210 | 29.730 | 38.270 | | | |
| Perello | S1 | 30.10.95 | 31.7 | | 8.7 | | 196.983 | Ca-Na-CO ₃ -HCO ₃ -SO ₄ | 18.590 | 2.311 | 18.390 | 0.975 | 0.060 | | 6.632 | 3.215 | 61.300 | 54.960 | 30.550 | 28.540 | -81.40 | -11.00 | |
| Perello | S2 | 04.04.96 | 56.5 | | 9.3 | | 280.795 | Na-SO ₄ -HCO ₃ | 75.930 | 3.654 | 6.598 | 0.030 | 0.203 | | 26.490 | 12.180 | 73.690 | 20.000 | 62.020 | 71.660 | | | |
| Perello | S2 | 30.10.95 | 57.0 | | 8.6 | | 258.127 | Na-SO ₄ -HCO ₃ | 64.570 | 3.757 | 5.686 | 0.010 | 0.234 | | 25.890 | 11.980 | 61.930 | 20.710 | 63.360 | 73.610 | | | |
| Perello | S3 | 04.04.96 | 58.5 | | 9.2 | | 287.500 | Na-SO ₄ -HCO ₃ -Cl | 76.510 | 3.861 | 6.198 | 0.048 | 0.203 | | 26.820 | 11.790 | 70.620 | 23.170 | 68.280 | 68.790 | | | |
| Perello | S3 | 30.10.95 | 60.0 | | 9.3 | | 240.315 | Na-SO ₄ -HCO ₃ | 65.990 | 3.762 | 5.999 | 0.010 | 0.234 | | 26.230 | 11.900 | 46.570 | 13.630 | 65.990 | 75.240 | -12.30 | | |
| Perello | S4 | 04.04.96 | 32.8 | | 9.6 | | 280.582 | Na-SO ₄ -HCO ₃ -Cl | 80.210 | 3.920 | 5.830 | 0.101 | 0.231 | | 30.150 | 12.160 | 61.310 | 14.470 | 72.170 | 66.540 | | | |
| Perello | S4 | 30.10.95 | 33.6 | | 9.5 | | 260.574 | Na-SO ₄ -HCO ₃ -Cl | 70.380 | 3.921 | 5.832 | 0.010 | 0.251 | | 29.260 | 12.170 | 57.310 | 11.060 | 70.380 | 77.620 | -85.50 | -12.30 | |
| Perello | S5 | 30.10.95 | 21.2 | | 8.1 | | 260.833 | Na-CO ₃ -SO ₄ -HCO ₃ | 57.710 | 3.006 | 8.016 | 0.150 | 0.170 | | 21.940 | 10.220 | 49.500 | 48.800 | 61.320 | 42.980 | | | |
| Perello | S5 | 04.04.96 | 19.0 | | 8.2 | | 264.379 | Na-CO ₃ -SO ₄ -HCO ₃ | 55.980 | 2.504 | 7.311 | 0.441 | 0.140 | | 19.830 | 8.313 | 59.790 | 58.690 | 51.380 | 46.170 | | | |
| Perello | S6 | 31.10.95 | 43.6 | | 9.2 | | 288.674 | Na-SO ₄ -CO ₃ -HCO ₃ | 69.940 | 3.936 | 6.156 | 0.020 | 0.222 | | 26.640 | 11.910 | 63.380 | 33.300 | 73.170 | 55.910 | | | |
| Perello | S7 | 04.04.96 | 49.5 | | 9.4 | | 271.106 | Na-SO ₄ -HCO ₃ | 74.570 | 3.743 | 7.487 | 0.054 | 0.202 | | 26.310 | 11.840 | 62.930 | 14.770 | 69.200 | 67.690 | | | |
| Perello | S7 | 31.10.95 | 51.0 | | 9.1 | | 270.923 | Na-SO ₄ -HCO ₃ | 68.340 | 3.746 | 8.808 | 0.006 | 0.203 | | 25.610 | 11.740 | 60.540 | 20.960 | 70.970 | 78.260 | | | |
| Michard et al. | 2 | 01.01.89 | 60.5 | | 84.0 | | 258.123 | Na-SO ₄ -HCO ₃ -Cl | 73.430 | 4.272 | 4.984 | 0.024 | 0.173 | | 33.870 | 12.100 | 58.990 | 7.750 | 62.550 | 68.450 | -84.90 | -12.40 | 4.3 |
| Michard et al. | 3 | 01.01.89 | 60.3 | | 210.0 | | 253.571 | Na-SO ₄ -HCO ₃ -Cl | 77.190 | 4.373 | 4.983 | 0.062 | 0.183 | | 28.880 | 12.510 | 60.200 | 6.610 | 58.580 | 70.880 | -85.40 | -12.20 | |
| Michard et al. | 4 | 01.01.89 | 56.1 | | 30.0 | | 278.267 | Na-SO ₄ -HCO ₃ -Cl | 83.730 | 3.755 | 4.059 | 0.005 | 0.223 | | 32.370 | 13.500 | 66.880 | 10.350 | 63.330 | 75.000 | -86.70 | -12.40 | 1.0 |
| Michard et al. | 5c | 01.01.89 | 31.6 | | 12.0 | | 277.077 | Na-SO ₄ -HCO ₃ -Cl | 82.490 | 3.919 | 4.019 | 0.058 | 0.221 | | 32.050 | 13.360 | 63.800 | 11.550 | 65.610 | 73.650 | -88.00 | -12.30 | |
| Bortolami | 4 | 01.01.84 | 55.5 | | 9.1 | | 250.623 | Na-SO ₄ -Cl | 84.020 | 4.393 | 2.810 | 0.020 | | | 38.350 | | 35.710 | | 84.720 | | 4.0 | | |
| Bortolami | 3b | 01.01.84 | 57.0 | | 9.3 | | 205.826 | Na-SO ₄ -Cl | 65.690 | 3.676 | 5.077 | 0.193 | | | 29.550 | | 32.190 | | 69.450 | | 4.1 | | |
| Fancelli & Nuti | 2 | 01.01.78 | 59.9 | | 8.0 | | 220.131 | Na-SO ₄ -Cl-HCO ₃ | 73.720 | 2.542 | 4.982 | 0.024 | 0.173 | | 33.860 | | 41.380 | | 63.450 | 62.530 | | | |
| Fancelli & Nuti | 3b | 01.01.78 | 48.3 | | 8.3 | | 214.926 | Na-SO ₄ -Cl-HCO ₃ | 76.750 | 2.427 | 4.955 | 0.062 | 0.182 | | 28.720 | | 42.170 | | 59.660 | 58.250 | -12.50 | | |
| Fancelli & Nuti | 3d | 01.01.78 | 60.2 | | 9.5 | | 231.893 | Na-SO ₄ -Cl-HCO ₃ | 83.900 | 2.746 | 4.068 | 0.005 | 0.224 | | 32.440 | | 42.410 | | 66.100 | 63.460 | -12.40 | 4.0 | |
| Fancelli & Nuti | 4 | 01.01.78 | 55.6 | | 9.6 | | 238.624 | Na-SO ₄ -Cl-HCO ₃ | 83.300 | 3.653 | 4.059 | 0.059 | 0.223 | | 32.370 | | 51.040 | | 63.920 | 66.260 | -12.30 | 6.0 | |
| Perello | S8 | 04.06.96 | 5.5 | | 8.1 | | 51.750 | Ca-CO ₃ -HCO ₃ | 1.100 | 0.510 | 6.600 | 0.440 | | | 0.300 | | 19.000 | | 19.000 | 4.800 | 5.200 | | |
| Perello | S8 | 31.10.95 | 9.1 | | 6.8 | | 61.823 | Ca-CO ₃ -HCO ₃ | 1.000 | 0.580 | 8.102 | 0.560 | 0.010 | | 0.900 | 0.070 | 22.800 | | 22.800 | 5.001 | 6.001 | -77.10 | -11.10 |
| Perello | S9 | 04.06.96 | 8.5 | | 6.6 | | 69.023 | Ca-CO ₃ -HCO ₃ | 3.501 | 0.660 | 7.401 | 0.570 | 0.010 | | 1.100 | 0.480 | 24.000 | | 24.000 | 7.301 | 7.701 | | |
| Perello | S9 | 31.10.95 | 12.4 | | 6.9 | | 71.784 | Ca-CO ₃ -HCO ₃ | 4.502 | 0.800 | 8.705 | 0.520 | | | 1.901 | 0.630 | 22.810 | | 22.810 | 9.105 | 10.310 | | |
| Perello | S9 | 31.10.95 | 12.4 | | 6.9 | | 71.784 | Ca-CO ₃ -HCO ₃ | 4.502 | 0.800 | 8.705 | 0.520 | | | 1.901 | 0.630 | 22.810 | | 22.810 | 9.105 | 10.310 | | |
| Bortolami | R.Remondino | 01.01.84 | 6.2 | | 6.5 | | 23.930 | Ca-HCO ₃ | 0.650 | 0.290 | 4.770 | 0.300 | | | 1.420 | | 14.600 | | 1.900 | | | | |
| Bortolami | Chirugia | 01.01.84 | 14.8 | | 4.7 | | 102.836 | Ca-HCO ₃ -Cl-SO ₄ | 5.444 | 0.861 | 20.320 | 1.651 | | | 11.710 | | 48.840 | | 14.010 | | | | |
| Fancelli & Nuti | Tunipi | 01.01.78 | 8.6 | | 6.9 | | 50.903 | Ca-CO ₃ -HCO ₃ | 1.300 | 1.800 | 7.201 | 0.300 | | | 4.201 | | 15.400 | | 15.400 | 5.301 | 4.001 | | |
| Fancelli & Nuti | Chirugia | 01.01.78 | 15.0 | | 7.2 | | 154.437 | Ca-CO ₃ -HCO ₃ | 5.004 | 0.701 | 20.920 | 0.200 | | | 2.002 | | 54.050 | | 54.050 | 17.510 | 9.008 | | |

5.3.2. Mixing Processes

The interpretation of correlations plots between (Figure 5-10) physic-chemical parameters reveals that one hand the behaviour sodium, chloride and sulphate displays a straight relation with TDS and T ° C, on the other calcium and alkalinity show an opposite trend.

Four main groups of waters can be identified:

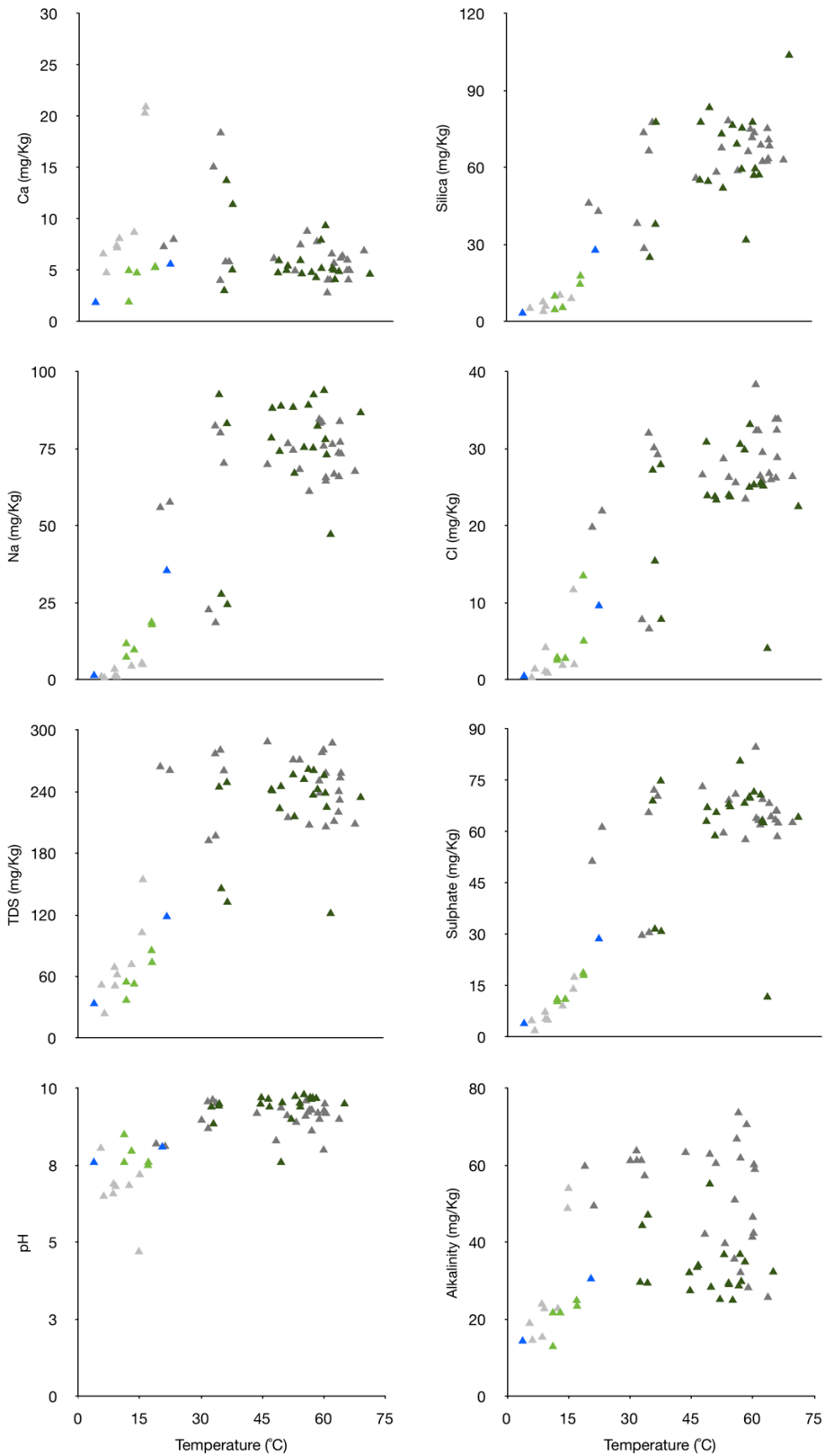
- spring ValS02 spring group comprehends the cold waters showing low mineralization and a Na-Ca-HCO₃-SO₄ composition;
- spring ValS12 group, which includes the hypothermal waters with temperatures of 17 ° C. These waters show an increase of sulphate content, indicating the influence of the deep endmember;
- GR02 group is represented by the waters of the Gesso river downstream the spa and by spring ValS10 which is located along the Gesso River and shows a temperature of 49.5 ° C. These Na-SO₄-HCO₃ waters show the clear signature of mixing between the deep Na-SO₄ endmember discharged thermal springs, and the Ca-HCO₃ superficial water of the Gesso River;
- spring ValS01 group shows the Na-SO₄ composition of the thermal springs. This springs are the hottest and less diluted waters

As for Vinadio, the Tritium vs Chloride (Figure 5-15) plot highlights the occurrence of mixing process. The hottest spring (ValS03) shows a content of 1.8 T.U., which is in slightly higher than the range (0.5-1 T.U.) present in thermal waters of Vinadio. This difference could indicate on one hand that the waters have a shortest residence time, on the other, that probably also have a higher degree of mixing with the shallow cold groundwaters. Tritium content of cold spring ValS02 shows a concentration of 6 T.U., which confirms the value of the cold and recent waters circulating at Vinadio as well.

Using simple mass balance equation the contribution of the two endmembers (deep Na-SO₄ and shallow Ca-CO₃) was estimated thermal water, assuming that the concentration in major ions follows a direct relation with temperature and that the reservoir temperature was at 100 ° C.

Here it follows the quantitative estimation of the presence of the two endmember within the waters of the spring ValS01 and ValS03:

- ValS03: 80% deep, 20% shallow
- ValS01: 30% deep, 70% shallow



▲ Thermal waters (Guglielmetti, 2009) ▲ Cold springs (Guglielmetti, 2009) ▲ Rivers (Guglielmetti, 2009)
 ▲ Thermal waters (previous works) ▲ Cold waters (previous works)

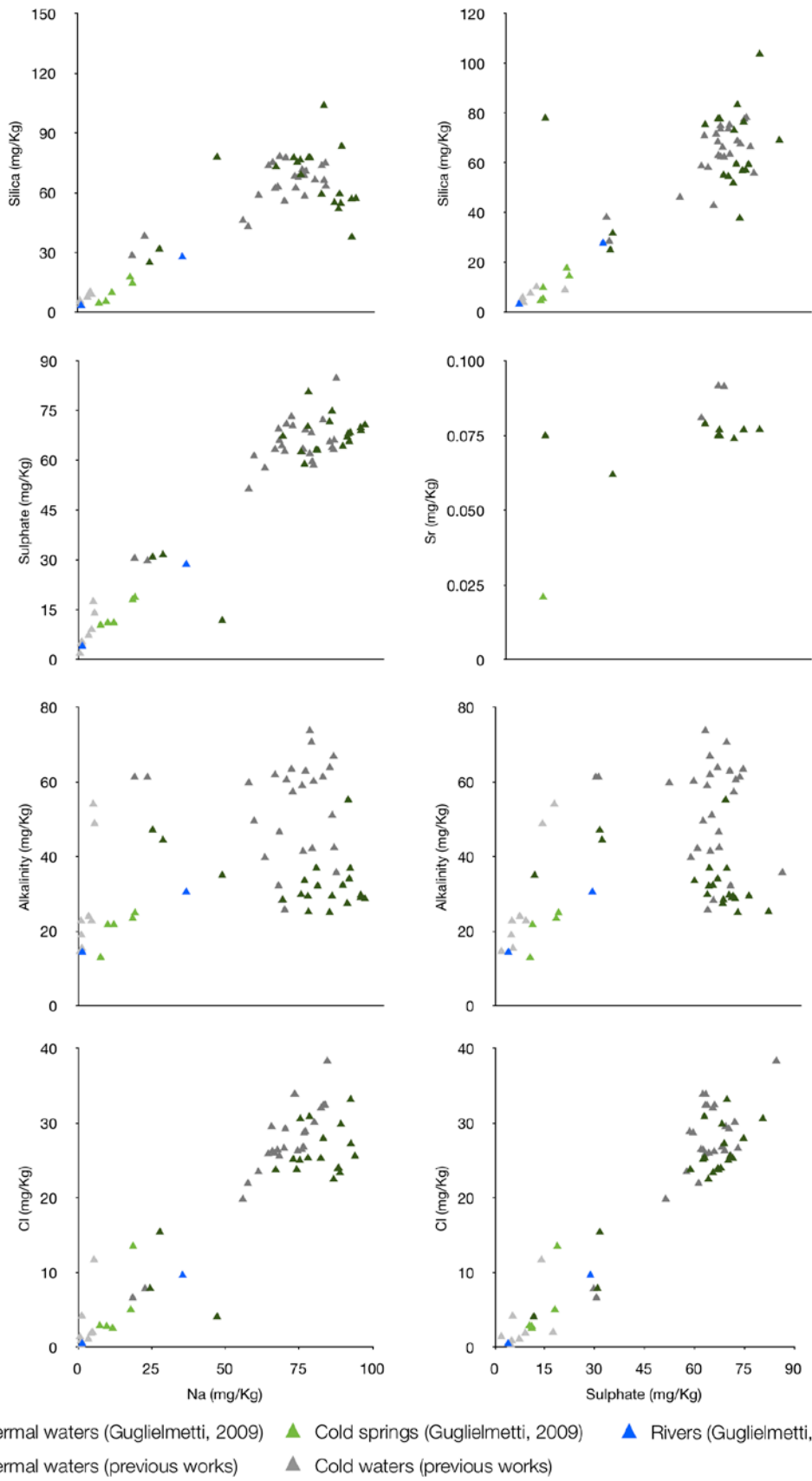


Figure 5-10 Correlation between the physico-chemical parameters at Terme di Valdieri for all existing data

5.3.3. Water-Rock Interactions

The interactions between infiltrating waters and the host rock are controlled by the Central Granite formation which is the dominant lithology at depth and which also controls the infiltration of rain waters on the western sector of the Valdieri area. In this area thermal waters do not circulate within wide zones of pervasive cataclasis, such as the Bersezio Fault Zone at Vinadio, but react with the entire intense fracture networks of granitic body and find their path towards the surface thanks the localized faults such as the Lorusa Fault. Therefore the water rock interactions seem to be less intense than those at Vinadio. This behaviour might be mainly related to lower temperatures at reservoir conditions, which, coupled to a shorter residence time might reflect to a sensibly lower mineralization.

5.3.3.1. Ca-HCO₃ waters

The Ca and HCO₃ concentrations of the cold waters originate from the dissolution and alteration of the minerals composing the outcropping gneiss and granites similarly to Vinadio.

5.3.3.2. Na-SO₄ waters

The origin of the Na-SO₄ type hot water is strictly related to the circulation within the crystalline rocks of the Malinvern Argentera Complex. The origin of sodium could be related to rock-fluid interactions in particular to the dissolution of the plagioclase contained in the granite. The dissolved sulphate required a more detailed investigation. In fact in Alpine thermal waters it can derive from the dissolution of the Triassic cover, oxidation of sulphides contained in crystalline rocks, leaching of residual seawater brines trapped within the structures or from variable contribution of all these sources (VUATAZ, 1982). In geothermal systems of low temperature, where circulating waters interact exclusively within the crystalline rocks (gneiss and granites) without contact with primary or secondary evaporite (Triassic layers or fracture filling), the coexistence of sulphates and sulphides in the aqueous solution can be mainly related bacterial reduction of SO₄ to H₂S or HS or S²⁻ (depending on pH), accompanied by oxidation of organic matters (LI, 2006; OHMOTO, 1997). Baietto (2006b) analyzed sulphur isotopes pointing out that in the waters circulating in the Argentera Massif the $\delta^{34}\text{S}$ of SO₄²⁻ in the range +19.22 to +19.34 ‰ and $\delta^{34}\text{S}$ of S²⁻ in the interval -2.4 to +2.1 ‰. Moreover the ³⁴S/³²S isotope ratios of sulphates resulted to be in the range of +15 to +25‰. On the basis of his investigations Baietto stated that the SO₄ contribution from evaporites is subordinated (5%) with respect to the SO₄ derived from the oxidation of sulphide minerals (95%).

5.3.4. Origin and Elevation of the Recharge Zone

Analyses of the stable isotopes $\delta^2\text{H}$ and $\delta^{18}\text{O}$ were carried out on selected water samples chosen from both thermal and cold waters. Available data from previous works were also considered and plotted on the $\delta^2\text{H}$ vs $\delta^{18}\text{O}$ to better constrain the trend. Both thermal springs and cold waters plot close the meteoric water line and fall into the range between -12.2 and -11.6 (‰) for the isotope $\delta^{18}\text{O}$ and within -89.4 and -84.1 (‰) for the $\delta^2\text{H}$ isotope. Thermal waters of Valdieri, as those from Vinadio, do not exhibit positive $\delta^{18}\text{O}$ -shift, indicating that

no boiling occurs at reservoir conditions and that also this geothermal system is dynamic and fluid-dominated.

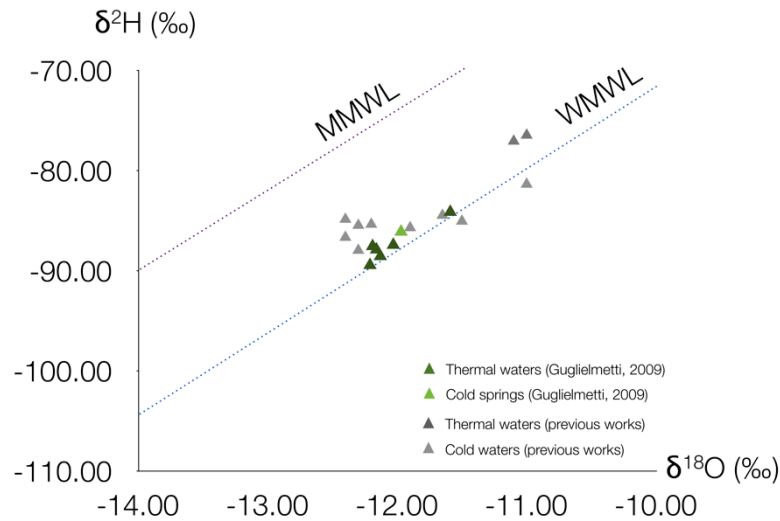


Figure 5-11 Plot showing the distribution of the stable isotopes of hydrogen and oxygen for the thermal waters of Vinadio. WMWL: World Meteoric Water Line; MMWL: Mediterranean Meteoric Water Line

The stable isotopes of hydrogen and oxygen also allow estimating the average elevation of the recharge zone. The equation of Bortolami (1979) was at first employed for the Valdieri area and the calculation resulted in an altitude range between 1350 and 1450 m a.s.l.

These values seem to be underestimated as the average elevation of the topography in the Valdieri areas is above 1900 m a.s.l. Moreover, accepting this elevation would imply to assume a steam separation during the upflow of the thermal waters, which is demonstrated does not occur. Therefore the relation proposed for the Mt. Blanc (JAMIER and OLIVE, 1977) was employed and showed a more fitting average elevation of 1900 m a.s.l (Table 5-9 and Figure 5-12).

Table 5-9 Available data for the stable isotopes of hydrogen and oxygen and their correlation with the calculated elevation of the recharge basin for the Vinadio area

| Author | Code | T° C | $\delta^{18}\text{O}$ | δD | Elevation $\delta^{18}\text{O}$ | Elevation δD | AVG | Elevation $\delta^{18}\text{O}$ |
|-----------------|----------|------|-----------------------|------------------|---------------------------------|----------------------------|---------------------------|---------------------------------|
| | | | | | Bortolami (1978) | Bortolami (1978) | Jamier & Oliver (1977) | |
| Guglielmetti | ValS_01 | 32.5 | -12.13 | -88.59 | 1314 | 1506 | 1410 | 1683 |
| Guglielmetti | ValS_03 | 65.0 | -12.19 | -87.59 | 1333 | 1465 | 1399 | 1708 |
| Guglielmetti | ValsS_04 | 34.4 | -11.59 | -84.17 | 1141 | 1328 | 1235 | 1461 |
| Guglielmetti | ValS_06 | 52.0 | -12.21 | -89.48 | 1340 | 1541 | 1441 | 1716 |
| Guglielmetti | ValS_08 | 54.2 | -12.16 | -87.93 | 1324 | 1479 | 1401 | 1695 |
| Guglielmetti | ValS_12 | 49.5 | -12.03 | -87.46 | 1282 | 1460 | 1371 | 1642 |
| Perello 10 | S1 | 31.7 | -11.00 | -81.40 | 952 | 1217 | 1084 | 1218 |
| Perello 16 | S4 | 33.6 | -12.30 | -85.50 | 1369 | 1382 | 1375 | 1753 |
| Perello 14 | S3 | 60.0 | -12.30 | | 1369 | | 1369 | 1753 |
| Baietto 1 | Va_1 | 58.9 | -11.50 | -85.09 | 1112 | 1365 | 1239 | 1424 |
| Baietto 2 | Va_2 | 63.7 | -11.90 | -85.74 | 1240 | 1391 | 1316 | 1588 |
| Baietto 3 | Va_3 | 53.2 | -11.65 | -84.50 | 1160 | 1341 | 1251 | 1486 |
| Michard et al. | 2 | 60.5 | -12.40 | -84.90 | 1401 | 1357 | 1379 | 1794 |
| Michard et al. | 3 | 60.3 | -12.20 | -85.40 | 1337 | 1378 | 1357 | 1712 |
| Michard et al. | 4 | 56.1 | -12.40 | -86.70 | 1401 | 1430 | 1415 | 1794 |
| Michard et al. | 5c | 31.6 | -12.30 | -88.00 | 1369 | 1482 | 1425 | 1753 |
| Fancelli & Nuti | 3b | 48.3 | -12.50 | | 1433 | | 1433 | 1835 |
| Fancelli & Nuti | 3d | 60.2 | -12.40 | | 1401 | | 1401 | 1794 |
| Fancelli & Nuti | 4 | 55.6 | -12.30 | | 1369 | | 1369 | 1753 |
| Guglielmetti | ValS_02 | 11.2 | -11.97 | -86.15 | 1263 | 1408 | 1335 | 1617 |
| Perello 24 | S8 | 9.1 | -11.10 | -77.10 | 984 | 1044 | 1014 | 1259 |
| Perello 28 | GE | 5.9 | -11.00 | -76.50 | 952 | 1020 | 986 | 1218 |
| Perello 25 | S9 | 12.4 | -12.00 | | 1272 | | 1272 | 1630 |
| Fancelli & Nuti | Tumpi | 8.6 | -12.20 | | 1337 | | 1337 | 1712 |

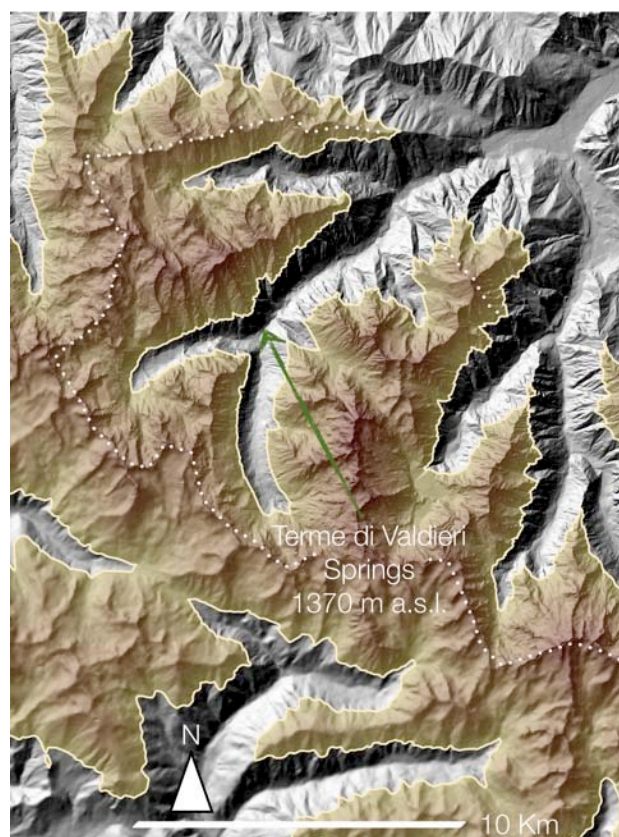


Figure 5-12 Map of the calculated elevation of the recharge basins (white dotted line). The yellow line represents the 1800 m a.s.l. contour

5.3.5. Reservoir Temperature

5.3.5.1. The Giggenbach Plots

The SiO_2 vs. $\log(\text{K}^2/\text{Mg})$ (GIGGENBACH et al., 1994) plot and the ternary plot of Giggenbach were employed as for Valdieri and they proven their efficacy to estimate the reservoir temperatures (Figure 5-13). The former plot shows that the hot waters plots between 80 and 120° C and the Giggenbach plot shows that all samples plot below the full equilibrium curve in the partially equilibrated and the immature waters fields. The hottest thermal waters are closer to the equilibrium curve while the colder thermal waters are closer to the points related to cold freshwaters at the $\sqrt{\text{Mg}}$ corner of the triangular plot, indicating a water-rock interactions at low temperature or more likely a mixing process with shallow, Mg rich, cold waters. In particular the hottest samples plot close to an estimated temperature of 150° C which is in agreement with the Giggenbach Na/K geothermometer that, for low temperature fluids, tends to overestimates temperature.

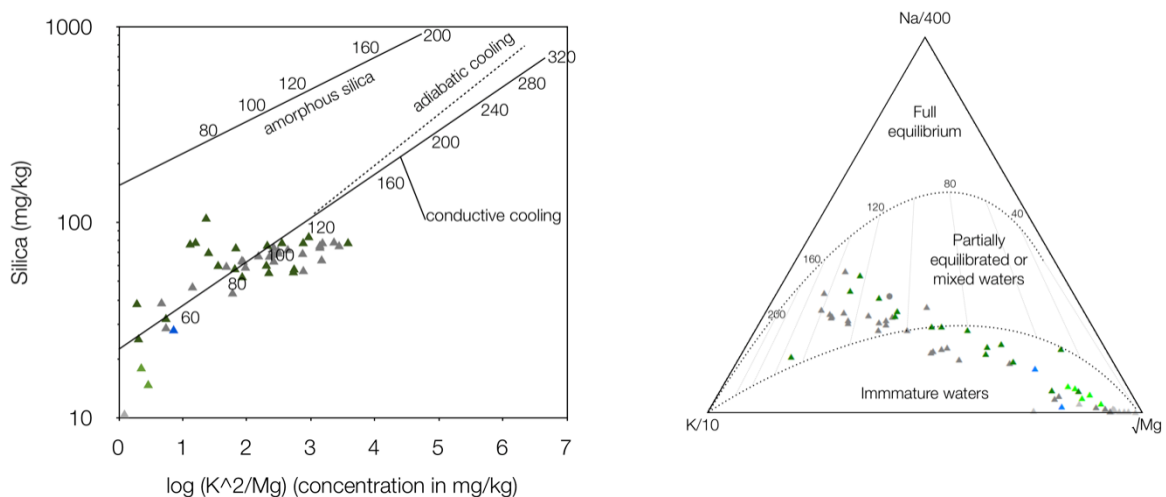


Figure 5-13 Giggenbach triangular plot showing the distribution of the thermal waters of Valdieri with respect to the theoretical line of the fully equilibrated waters at increasing temperatures

5.3.5.2. Solute Geothermometers

Solute geothermometers of Chalcedony, Na-K-Ca, Na-K, K^2 -Mg, Li-Mg and Na-Li were calculated and compared to test their applicability (Table 5-10). In the case of the waters of Valdieri Chalcedony controls the solubility of Silica, therefore has to be considered as the suitable equation and shows a temperature of 89 °C. The Na-K-Ca geothermometer fits within the same temperature while the K^2/Mg geothermometer shows slightly higher values of 97°C. Also the Na-K, Li-Mg and Na-Li were applied they highly overestimated temperatures, therefore are not considered for. Moreover excluding this equations suggests that thermal waters of Valdieri might entirely circulate within the crystalline rocks, without having any interaction with the Triassic cover successions.

Table 5-10 Calculated reservoir temperature by means of selected geothermometers for the thermal waters of Terme di Valdieri. Temperature values are expressed in °C

| Sample ID | Chalcedony | | Quartz (no steam loss) | K ² /Mg | K ² /Mg | Na-K-Ca $\beta=4/3$ Mg corrected |
|--------------|--------------------|---------------------|------------------------------|--------------------|----------------------|--|
| | Fournier (1977) | Arnorsson (1983) | Fournier (1973) | Fournier (1991) | Giggenbach (1988) | Fournier & Truesdell (1973) |
| ValS_01 | 113 | 35 | 114 | 35 | 77 | 82 |
| ValS_03 | 86 | 86 | 115 | 137 | 136 | 92 |
| ValS_04 | 46 | 48 | 77 | 22 | 55 | 40 |
| ValS_05 | 88 | 88 | 116 | 57 | 77 | 74 |
| ValS_06 | 94 | 94 | 122 | 94 | 103 | 77 |
| ValS_07 | 85 | 85 | 114 | 101 | 106 | 89 |
| ValS_08 | 87 | 87 | 116 | 115 | 117 | 79 |
| ValS_10 | 96 | 95 | 124 | 51 | 73 | 60 |
| ValS_09 | 96 | 95 | 108 | 51 | 73 | 60 |
| ValS_12 | 81 | 82 | 110 | 100 | 106 | 90 |
| ValS_TOT_01 | 96 | 95 | 124 | 51 | 73 | 103 |
| ValS_TOT_02 | 88 | 88 | 112 | 75 | 89 | 75 |
| Va_1 | 83 | 84 | 112 | 84 | 94 | 91 |
| Va_2 | 84 | 84 | 113 | 83 | 94 | 89 |
| Va_3 | 80 | 81 | 110 | 72 | 86 | 82 |
| S1 | 52 | 55 | 90 | 29 | 60 | 41 |
| S2 | 92 | 92 | 77 | 126 | 126 | 70 |
| S3 | 91 | 91 | 119 | 122 | 123 | 90 |
| S4 | 91 | 91 | 121 | 116 | 119 | 93 |
| S5 | 66 | 68 | 117 | 62 | 80 | 71 |
| S7 | 88 | 88 | | 105 | 109 | 83 |
| S6 | 78 | 78 | 116 | 125 | 125 | 58 |
| S7 | 92 | 92 | 124 | 126 | 126 | 83 |
| 2 | 88 | 89 | 95 | 125 | 125 | 81 |
| 3 | 90 | 90 | 98 | 108 | 112 | 109 |
| 4 | 93 | 93 | 107 | 150 | 147 | 16 |
| 5c | 92 | 92 | 117 | 105 | 109 | 102 |
| 4 | 92 | 92 | 124 | 130 | 129 | 106 |
| 3b | 92 | 92 | 117 | 79 | 91 | 92 |
| 2 | 83 | 84 | 119 | 105 | 109 | 66 |
| 3b | 80 | 80 | 122 | 85 | 95 | 80 |
| 3d | 84 | 85 | 121 | 138 | 136 | 6 |
| 4 | 87 | 87 | 112 | 102 | 107 | 100 |
| AVG | 89 | 88 | 112 | 97 | 96 | 87 |
| TOTAL AVG | | | | | | 95 |

5.3.5.3. Saturation Indexes

Saturation indexes of the main minerals and solute geothermometers were employed to estimate the reservoir temperature.

The evolution of saturation indexes was computed with PHREEQ code choosing ValS03, S3 from Perello (2001) and 2 from Michard (1989b) as the most representative samples in terms of temperature and mineralization. SI vs. temperature plots indicate that equilibrium temperature ranges between for 95 and 120 °C for the selected samples (Figure 5-14).

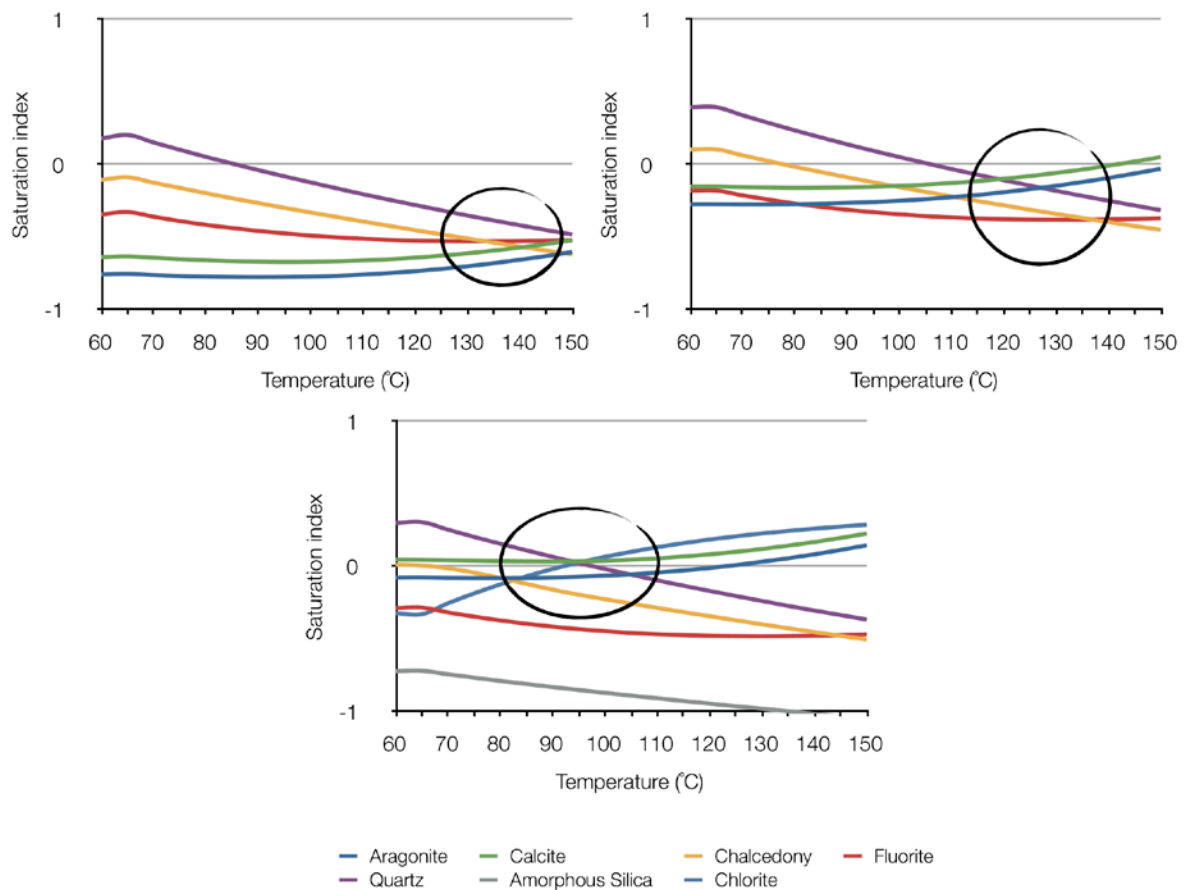


Figure 5-14 Saturation index vs. temperature plots for selected samples from the Vinadio Area. The circles indicate the temperature range at which the main minerals are close to saturation

On the basis of the observation made by means of saturation indexes, SiO_2 vs. $\log(\text{K}^2/\text{Mg})$, ternary plot of Giggenbach and calculation of the geothermometers equation it is possible to constrain the temperature of the reservoir of the Terme di Valdieri Area. The saturation indexes indicate a range of 95-120 °C, the SiO_2 vs. $\log(\text{K}^2/\text{Mg})$ shows a range between 80 and 120° C while the triangular plot of Giggenbach show higher temperature of about 160 C which is in agreement with the Na/K geothermometer which highly overestimates the temperatures as the Na/Li and Mg/Li equations. Finally the temperature of the reservoir for the Terme di Valdieri area can be constrained, considering also the Chalcedony, Na-K-Ca, K^2/Mg geothermometers equations, to the range between 90 and 100 °C.

Therefore it is possible to constrain the chemical equilibrium conditions, which are reached at an average temperature of 95-105°C.

5.3.6. Groundwater Residence Time

Residence time for geothermal fluids was evaluated by means of Tritium. The plot of Tritium vs. Time (Figure 5-15) indicates a trend from the younger and colder waters to the thermal waters which, on the contrary, show low T.U. values. Moreover it was possible to

compare the behaviour of the spring 4 with time from literature data. It must be considered that this spring is also one of the hottest of the area:

- 1978 (Fancelli & Nuti): 6 T.U.
- 1984 (Bortolami): 4 T.U.
- 1989 (Michard): 1 T.U.

This behaviour shows a decreasing trend, which is logical considering the Tritium half-life time (12.3 years). It probably also suggests that the thermal waters at Valdieri have a shorter residence time than those at Vinadio which, on the contrary, don't show any variation in time. Moreover it is possible to infer that very little mixing occurs for this sample as cold water sampled from the Ciriegia tunnel (BORTOLAMI and GRASSO, 1969) indicates a high Tritium content of 54 T.U which corresponds.

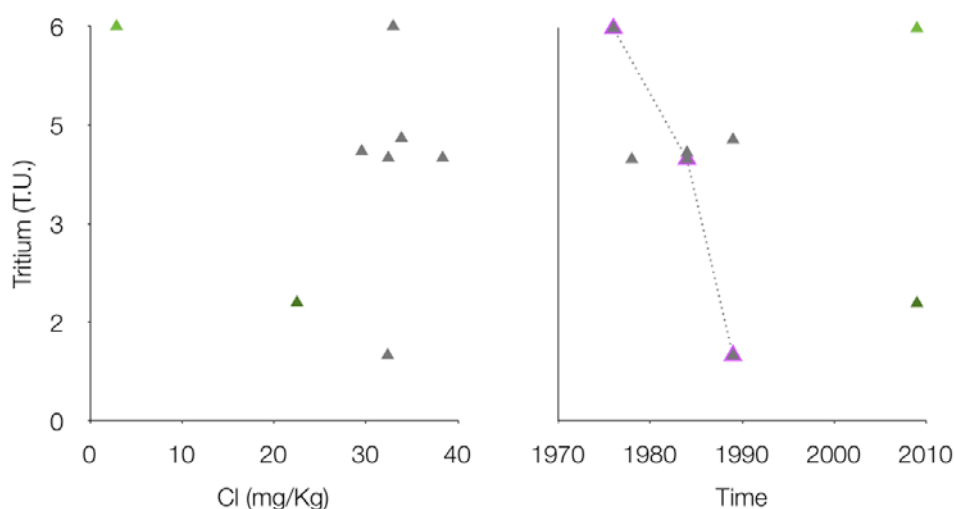


Figure 5-15 Tritium vs time and Tritium vs chloride plots (bored triangles - purple - correspond to spring 4)

Bortolami (1984) proposed a turnover time (defined by this authors as the total renovation time) of 100 years and a circulation time of 30 years. This seems quite unrealistic, as deep water must have time to reach the equilibrium with the host rock. On the opposite the range of a thousand to several thousands of years proposed by Perello (2001), on the basis of the two theoretical models of piston flow and perfect mixing (PEARSON, 1978), might be the most suitable.

Table 5-11 Tritium content in sampled waters from 1976 to present work.

| Author | Code | T° C | Sampling Date | U.T. |
|------------------|----------|------|---------------|------|
| Guglielmetti | ValS_03 | 65 | 2009 | 1.8 |
| Guglielmetti | ValS_02 | 11 | 2009 | 6.0 |
| Michard et al. | 2 | 61 | 1989 | 4.3 |
| Michard et al. | 4 | 56 | 1989 | 1.0 |
| Bortolami | 4 | 56 | 1984 | 4.0 |
| Bortolami | 3b | 57 | 1984 | 4.1 |
| Fancelli & Nuti | 3d | 60 | 1978 | 4.0 |
| Regione Piemonte | 4 | 55 | 1976 | 6.0 |
| Bortolami | Ciriegia | 56 | 1984 | 56.0 |

6

3D GEOLOGICAL MODELLING

6.1. Concepts and Methods

Three dimensional modelling is based on two main interpolation methods. Traditional *explicit* methods, highly time consuming in particular for complex-shaped geological bodies, rely on manual definition of the 3D geological boundaries digitising the points which lie on the surface. The solids are defined by surface elements, such as triangles, which coordinates are known and the surface or volume shape can be then rendered. For example in the case of borehole data, the geological contacts are manually interpolated by the geologist and the final result will be a “rigid” unique geological model which will require a lot of manipulation and time if new data will become available as explicit surfaces cannot be automatically updated.

Alternatively, new 3D interpolations methods allow building 3D models without explicitly digitising and defining the surface contained in a 3D volume but a solid is given by a function defined throughout space. Therefore the volume function is modelled by interpolating e.g. sampled borehole data and the existence of the surface in the volume function is implicit, thus these processes are called *implicit modelling*. This method allows describing shapes of any geometry such as overturned folds. Implicit 3D potential functions are able to interpolate each component of a geological body and automatically compute the intersections between the different components of a geological model. One of the main advantages of the implicit method lies in its ability to build a model with scarce data such as dip and lithological contacts mapped on the surface. The model can be rapidly be improved by adding wells and geophysical data and cross-sections if available. 3DGeomodeller was developed with the goal to infer 3D geological models taking into account the usually scarce and scattered field data measured on outcrops or borehole and integrate them with data from other sources to test the interpretative hypothesis.

The software employed in the thesis, 3D-Geomodeller[®] by INTREPID Geophysics, was developed with the goal to infer 3D geological models taking into account the usually scarce and scattered field data, which are usually available to geologists. Observations on outcrops or borehole can be combined to come out with some interpretative *a-priori* 3D model, which can be then calibrated and modified according to data from geophysical surveys such as gravity, magnetic and seismic methods.

The basic concepts that must be considered are (CALCAGNO et al., 2008):

- geological interface delimits two geological formations
- some orientation data sampled within geological formations are relevant to model the interfaces separating the formations
- interfaces to be modelled may be regarded as belonging to an infinite set of surfaces aligned with the orientation field.

And two assumptions have to be taken into account:

- contact data for each interface lie on a potential field surface (an iso-potential);
- orientation vectors are normal to a local tangential plane to the potential field and not necessarily lie on the geological interface

Three dimensional modelling of any body is never a completely exact representation of the original, but some incertitude always remain because of the scale of the model, of the computing capability of a software, because of the quality and quantity of the available data.

In particular if a 3D model is based on qualitative data, such as geological interpretative maps and cross sections, it is necessary to find a compromise between geological skills of the modeller and informatics aspects (e.g. computing performances, mathematical coding) to come out with the optimal model. Geostatistical methods have been employed (AUG, 2004) to estimate the uncertainty of 3D geological models computed by 3D-Geomodeller which are based on the potential field method. This method allow now modelling real-world situations thanks to its covariance fitting, which improves the model in comparison to a conventional model (CHILÈS et al., 2005). 3D-Geomodeller also allows computing the geophysical response of the 3D models given the formations proper geophysical properties (e.g. rock density, magnetic susceptibility, thermal conductivity and seismic velocity) by means of forward modelling. Geophysical data can be integrated to the 3D model to modify its properties and geometries using inversion processing which allows reducing the misfit between the model and the field observations. Such data integration is crucial to come out with a more realistic representation of the subsurface. and reducing the uncertainty of 3D bodies.

6.1.1. Data Type

The potential field method employed by 3D-Geomodeller is based on the following data:

- a digital terrain model (DTM) to define the topography;
- geological maps and cross sections to infer interface location and orientation data;
- borehole data;
- geophysical data.

Topography is computed as a boundary surface representing the present-day erosion and deposition surface. The user can choose whether the model is limited by the topography or compute the hypothetical simulation of the topographic surface not existing. Moreover the available maps and digital data can be imported as images (e.g. .jpeg, .bmp, .gif, .tiff, .png) and/or shapefiles on the topography as well as on vertical cross sections, and employed to define the geological limits and dips.

The basic geological unit is termed a *formation* and it is constrained by points and lines, termed *interfaces*, lying on the boundary surface. Structural orientation data, termed *foliations*, must be linked to formations but can be located anywhere in space and define the tangent plane to a surface. Foliations have a 3D location, dip angle, azimuth angle, polarity (normal or overturned).

Once interfaces and foliations are defined for a certain formation it is possible to compute its 3D geometry. The units are considered to occupy a half space on one side of the boundary surface, depending on the dip and the choice of mapping the top or bottom of an interface between formations (LANE, 2007). To compute the geometry and geology of several formations a *stratigraphic pile needs to be defined*. It represents the geological history and, as a consequence, the geometrical order. The user has then to chose between *erode* or *onlap* behaviour, which finally govern the intersections between geological bodies. The rules to compute the model are (CALCAGNO et al., 2008):

- Interfaces of geological formations having sub-parallel behaviours can be grouped together into a series, which is modelled using a single potential field. Thus formations sharing a common geological history can be considered as a unique geological series

and the software computes them as a unique body divided into formations having a common geometry. The advantage of this setting occurs if a formation lacks of data and is modelled considering the geometrical distribution of the underlying formation belonging to the same series.

- A chronology defines the time-order of series within the model. However in crystalline geological settings, as for the Argentera Massif, a chronological order is hard to define with the exception of intrusive bodies that are considered as tardive with respect to the surrounding formations. In fact lithologies are usually divided on the basis of the mineralogical assemblage, therefore, in 3D-Geomodeller a stratigraphic pile has to be employed to manage the geometrical order and hierarchy between formations.
- An erosional or depositional relationship is defined for each series to drive its (modelling) behaviour with respect to the chronologically older ones. In the case-study of the Argentera Massif, the *erode* relationship was chosen as it allows series to occur and truncate, or cut across older ones, whereas the *onlap* relation enables the series to be present only where space is available without changing the geometry of the older series.

Geological formations are impacted by faults and folds. Faults are defined by *interface* and *foliations* and interpolation is performed in the same way as geological bodies. The geometry of a fault is defined by the intersection of the iso-surface and a sphere (or an ellipsoid) of a given radius centred on the data defining the fault. Faults in 3D-Geomodeller can be *infinite* or *finite* relatively to the study area. In the latter case it is necessary to define the extent of the fault in terms of *horizontal* and *vertical radius* and the *influence radius* which represents the tip line where no more deformation occurs. Fault network are simply defined by hierarchic fault-fault relation (“FaultA terminates on FaultB”). Folds are defined by interface points and fold foliation points, which are used to define an axial surface for each fold. A fold is specified to be an anticline or a syncline. A hinge line is defined on the axial surface by interface points that are associated with a formation. These points will lie on the boundary surface calculated for this formation. The shape of the fold at the hinge line is defined by a set of points that are described by their position along the hinge line and a displacement vector away from the axial plane. The displacement vector is assumed to lie in a plane perpendicular to the axial surface. These vectors are specified by a distance away from the axial plane, an aperture angle from the axial surface, and a polarity (left or right) which identifies the relevant side of the axial surface.

6.2. Computing the 3D Models of the study sites

In this part of the chapter the employed methodologies and main issues encountered during the modelling of the three models computed for the entire Argentera Massif and the Vinadio and Valdieri sites.

The available data for computing the 3D models were:

- topographic surfaces;
- geological maps;
- cross sections;

- field data;
- a 850m deep borehole drilled in the core of the Beserzio Shear Zone.

6.2.1. Definition of the topography.

Topography behaves as the upper border of the 3D model and is also employed by the software for the forward modelling of geophysical data. Therefore it is necessary to get the most detailed topographic surface taking into account the computation limits of the software. A 30-meter NASA Shuttle Radar Topography Mission SRTM30+ DEM⁷, is available for the entire globe and can be downloaded from NASA's EOS data archive and Japan's Ground Data System⁸. This DEM was employed for the Argentera Massif model, however a 10-meter DEM (RIBOLINI and SPAGNOLO, 2008) was employed for the two smaller models of Vinadio and Valdieri. 3D-Geomodeller can support several formats of DEM files (.grd, .semi, .dxf, .ERS, .gdm, .tif). For this study the downloaded topographic grids were converted, via ESRI ArcGis[®], to ASCII files and then to .grd or .semi (3 columns XYZ) and finally imported in 3DGeomodeller.

6.2.2. Definition of the extent of the model.

For the Argentera Massif model the extent was set to be the Massif itself with a buffer of some hundreds of meters to include the Trias formation, cropping out around the crystalline basement, and the surrounding autochthon sedimentary cover and also to take into account the development of the AM in the subsurface. For the models of the two thermal areas the limits were set to the hydrological basins in the surroundings of the thermal springs. The depth for all models was set to 4500 meters below the sea level. This depth allowed computing a 5km-deep models which is the expected depth for the thermal fluids circulation, as the average elevation of the study regions is about 1300 m a.s.l.

6.2.3. Collection of the available data.

Among all the available geological maps and cross sections, those containing useful information, enough detail and accuracy were imported to constrain the geological limits, faults and dips. Unfortunately no detailed geophysical data were initially available, therefore the a-priori models were computed exclusively on the basis of the surface data and few interpretative cross-sections such as the Carta geologica del Massiccio dell'Argentera (MALARODA, 1970) and those from the studies of Bogdanoff (1986; 2000), Perello (2001), Musumeci (2002), Ribolini (2008), Corsini (2009) and Baietto (2009).

6.2.4. Modelling criteria

The study areas are mainly represented by several types of metamorphic formations locally intruded by granitic bodies and surrounded by the autochthonous Carbo-Triassic sedimentary cover and the detached carbonate Mesozoic succession. Other important

⁷ ftp://topex.ucsd.edu/pub/srtm30_plus/topo30/

geological features are the fault zones such as the Valletta, Bersezio and Fremamorta shear zones, which are representative of the reactivation of Variscan structures during the Early (22 Ma) and Middle Miocene (12 Ma). These structures are mainly composed by mylonitic rocks which thickness ranges between 100 and 2000 m and, because of their importance for the fluid circulation and the density variations, they were modelled as separate geological formations, hence defined by a volume, and not simply as faults just defined by a plane.

Geological bodies were modelled respecting the above-mentioned maps, however some simplifications were needed. In particular the selection of the lithologies was based on two main criteria: geometrical extension and geophysical importance in terms of density distribution. Therefore formations such as small dykes were not modelled on the model of the Entire Argentera Massif, but were introduced in the two smaller models of the study sites whereas they play an important role for the gravity response of the models. However formations having significant heterogeneities in terms of mineralogical composition and/or fracture network density were selected, also according to field observations, to be able comparing the geological model with the results from the geophysical surveys described in Chapter 7. Moreover the available cross-sections were not deep enough to constrain the underground development of the formations down to 5 km, therefore the geological bodies were assumed to have constant dip on the basis of those observed on cross sections and maps.

Some draft models were computed to figure out the best way to come out with a realistic model without requiring an excessive amount of contact points, dips, hence of computing time. The first approach was to strictly digitize the surface geology as it appears to be in the geological maps. A simple model including just 3 formations (Tinée, Valletta and MAC) was firstly computed to set the stratigraphic pile in terms of chronological hierarchy of the series and their relationship. It meant to define whether grouping formations together into series or considering each formation as a separate serie and which relation, either erode or onlap, better satisfied the modelling needs. Thanks to this preliminary approach it was possible to figure out that the best way to model the several formations was to consider each formation as individual, the *erode* relation was chosen and the contact points were chosen to represent the *bottom* of each formation. The entire model of the Argentera Massif was then modelled following an iterative process that allowed gradually adding the several formations, faults and shear zones and adjusting the model step by step. The final result is shown in Figure 6-1. This images also shows how the Argentera Massif had to be split into 6 main geological/geometrical “blocks” to make the modelling respectful of the geometries of the formations:

- 1 Western carbonate and evaporite cover (French side)
- 2 Tinée Complex including the Valletta Shear Zone
- 3 Malinvern Argentera Complex between the Valletta shear zone and the Bersezio shear zone (included)
- 4 Malinvern Argentera Complex between the Bersezio shear zone, the Cover and North of the Fremamorta Shear Zone
- 5 Malinvern Argentera Complex South of the Fremamorta Shear Zone (included)
- 6 Eastern carbonate and evaporitic cover (Italian side)

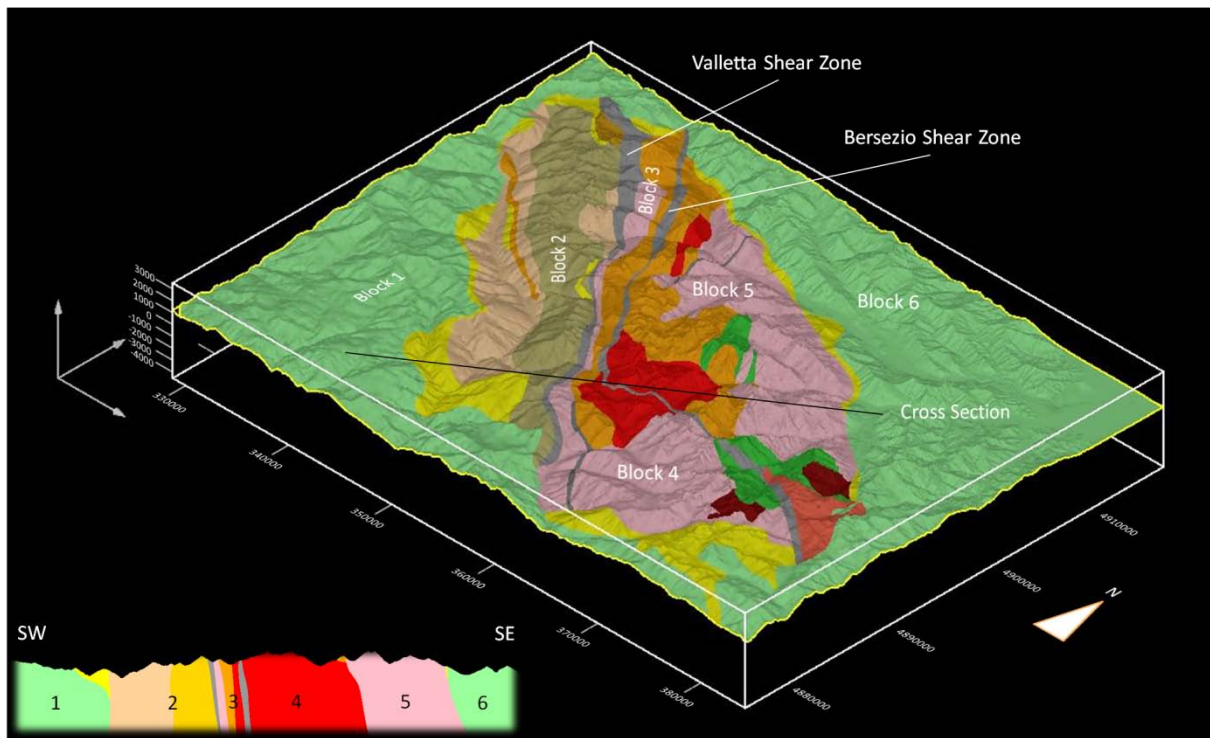


Figure 6-1 3D geological model of the Argentera Massif computed on the topography and on a cross section

Faults were modelled to represent the main features for the large scale model of the Argentera Massif and the detailed and complex fault systems for the areas of Vinadio and Valdieri (Figure 6-2). The main data sources were the studies of Perello (2001) Baietto (2009) for the detailed models of Vinadio and Valdieri but other geological maps and structural sketch were useful for large-scale information such as the extension at depth of fault zones and outcropping formations. Moreover some data collected, during this thesis, in the proximities of the thermal springs were integrated into the detailed models to better figure out which fracture systems were directly connected to the presence of the springs.

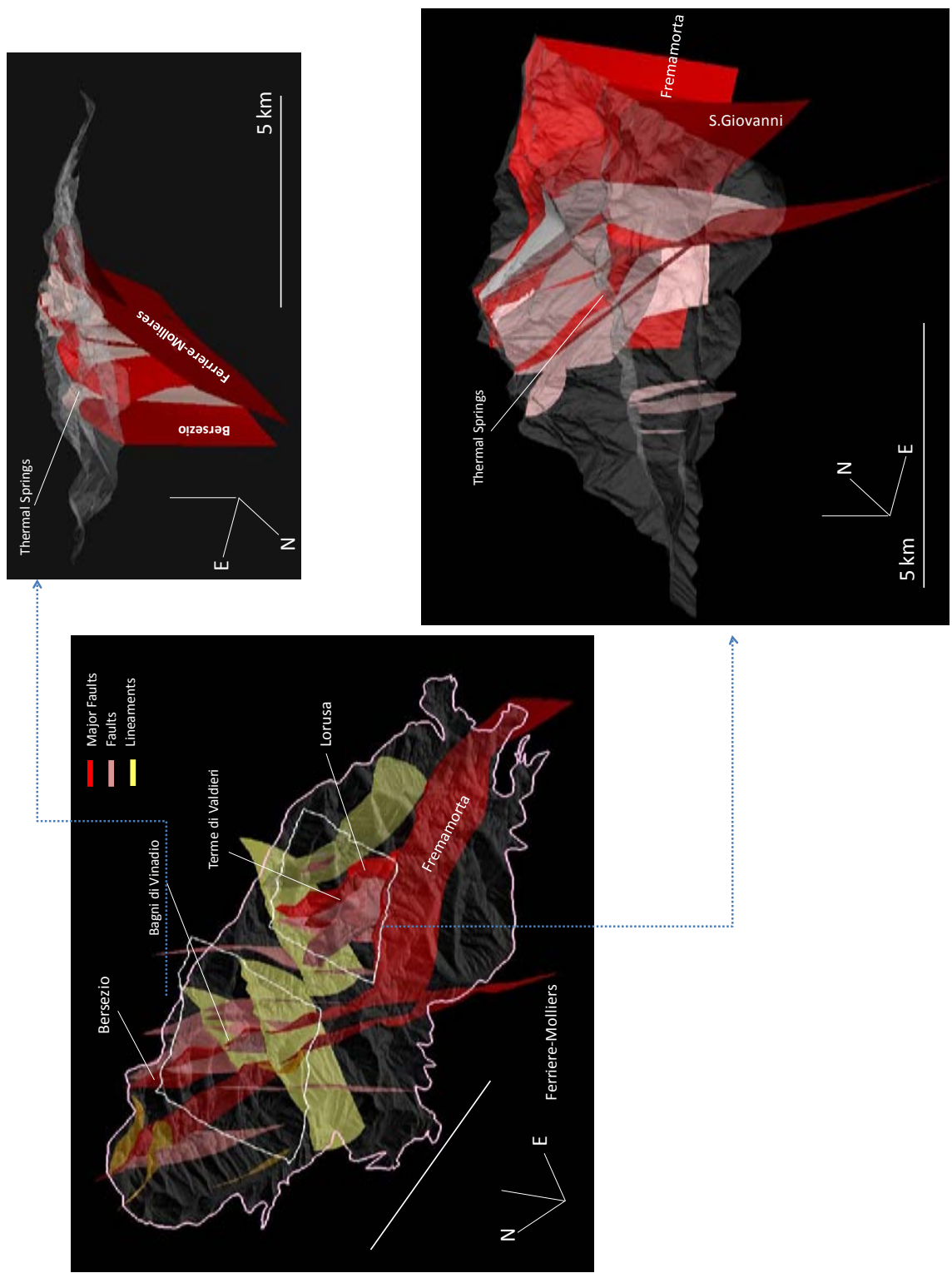


Figure 6-2 3D fault network at in the Argentera Massif and detailed structures at Bagni di Vinadio and Terme di Valdieri

6.2.5. Results

The 3D model of the Argentera Massif allows visualizing the distribution of the geological bodies in the subsurface. In particular the shear zones and the Central Granite formation were modelled with particular attention because the formers might represent the main path for thermal fluids circulation, the latter is a major infiltration zone and can be the possible geothermal reservoir for the thermal waters at Valdieri. All the formation were modelled assuming a constant dip of NE 70-80° with the exception of the granitic and agmatitic bodies which were interpreted as intrusive bodies with sub-vertical limits.

6.2.5.1. Modelling the shear zones

Fault zones were modelled as formations, which could have a significant geophysical signature in terms of density, permeability and electrical resistivity. The simplified model also helped to construct the fault zones and the cataclastic belts. The first approach was to try keeping a chronological order of the fault zones with respect to the crystalline formations. Hence the first test was to consider the cataclastic belts as erosional at the top of the stratigraphic pile. They are characterized by a strong geometrical anisotropy (e.g. the Valletta and Bersezio Shear Zones are 40 to 60 km long whereas they are just up to 1km large). In this case the software showed some computation limits. In fact, considering the available data it wasn't able to correctly model those structures in three dimensions. The main issues regarded that, even if they were correctly constrained at the surface, they were modelled just for a reduced vertical extension (just few hundred meters).

Therefore the software was forced to properly compute these formations adding more contact points and dips on the topography and on many cross sections but the 3D model showed several "holes", which were not justifiable on a geological point of view. Hence, to obtain a spatial continuity of the shear zones we had to add contact lines on horizontal cross sections at different depths. However even though on one hand the geometrical result was satisfying, this approach involved tricky geological interpretations and it also reflected on an increase of computation time and most of the time the software even crashed. Moreover this model was supposed to be employed for geophysical processing data integration, so we tried to simulate some gravity inversion processing letting the software change both the densities and the geometries but such a "rigid" model didn't provide the software enough "freedom" to eventually modify the model according to the geophysical data.

To avoid all these problems the main fault zones were considered as formations within the stratigraphic pile and not at the top of the pile. This solution reduced the computation time and, even though it is not chronologically strict, the geometries were well constrained and the results also can be quite reliable on the lithological point of view. In fact fault zones are composed by mylonites deriving from the alteration of the original gneissic and granitic formations (Figure 6-3).

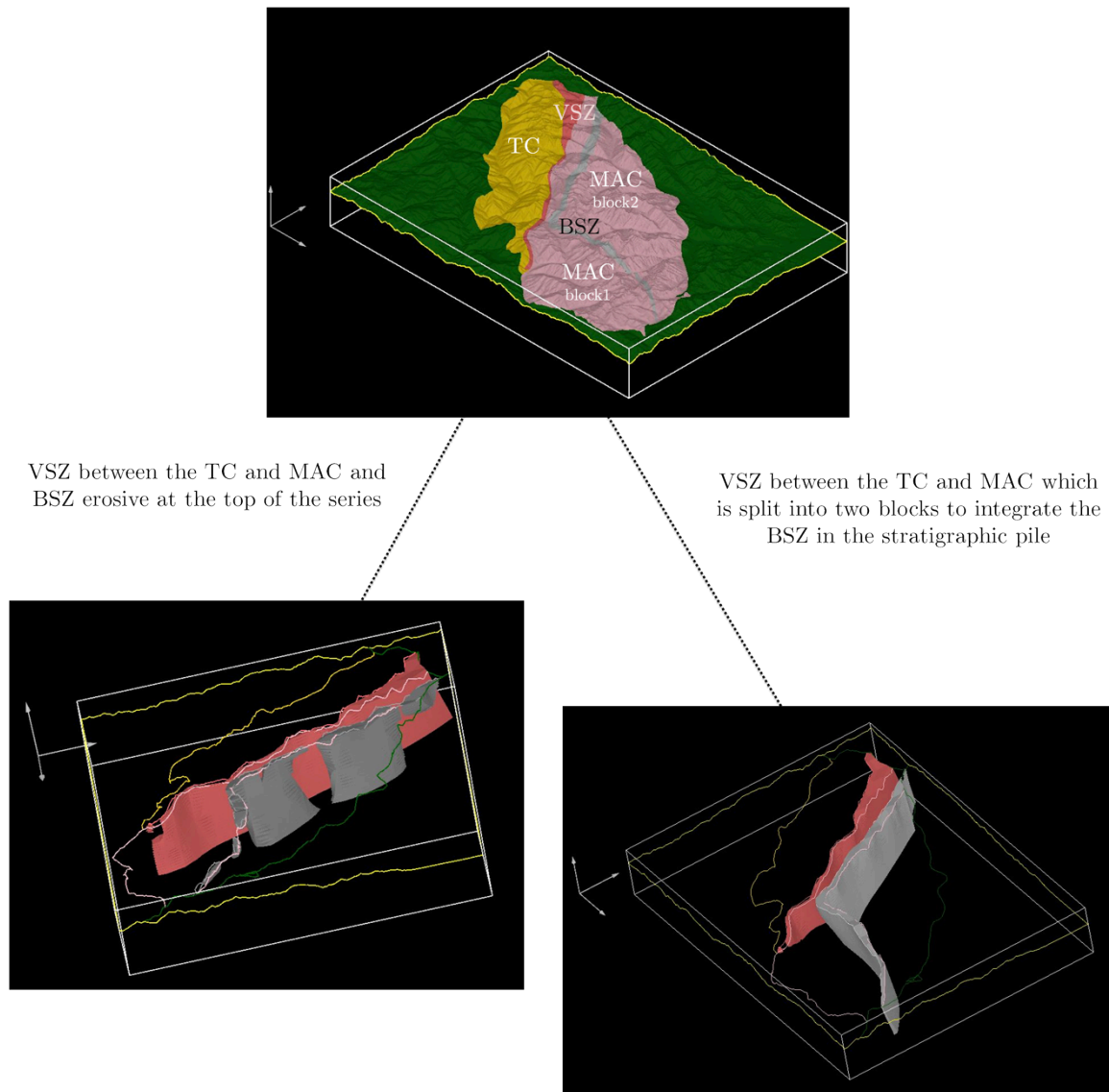


Figure 6-3 Comparison between the two approaches regarding the modelling of the shear zones. It is possible to observe the difference between a shear zone at the top of the pile (grey in the lower left image) and another integrated within the other formations (pink in the lower images). Even though the result is good on the topography, the grey formation shows a very irregular geometry if located at the top of the pile (lower left) while it is more geological reliable if integrated in the pile (lower right).

6.2.5.2. Bagni di Vinadio - Modelling the gneiss formations and the fault zones

In the Bagni di Vinadio region, metamorphic formations owing both to the Tinée and the Malinvern-Argentera Complex crop out. These formations have been involved, during the Upper Miocene-Oligocene, by the intense tectonic activity which brought to the development of thrusts faults and to the reactivation of older Variscan tectonic lines. The Bersezio and the Valletta shear zones are two mylonitic corridors related to these latter events and are mainly composed by paleo-mylonite and cataclasite.

On the geometrical point of view these formations show an average 70-80° dip towards NE and are crossed by the Varetta and Bersezio shear zones. These two mylonitic corridors appear to be slightly steeper. The Varetta zone was modelled to have a constant dip of 80°, parallel to the gneiss formations, the Bersezio mylonites were considered almost vertical having a dip of 85-90°.

The Tinée Complex was modelled considering the four main formations including the sedimentary cover, pinched in the Sepsoul Thrust, and the metamorphic basement (embranchites, leucocratic gneiss, eye-shaped gneiss), while the Malinvern-Argentera Complex is composed by five metamorphic formations (migmatitic gneiss, biotitic and chloritic gneiss, biotitic anatexites, amphibolitic agmatites, granites) locally intruded by leuco-granitic bodies in correspondence of the thermal site and East from it.

With the exception of the granitic bodies which were separately modelled as intrusive (cfr. 6.2.5.3), all the gneissic formations have been geometrically interpreted as parallel units steeply trending NE and unconformably covered by the sedimentary sediments. As 3D-Geomodeller needs a stratigraphic pile to be defined, the Tinée Complex formations were chosen to be at the bottom of the stratigraphic pile below the Malinvern Argentera Complex. The southern part of the MAC Complex, in particular the biotitic gneiss are characterized by a zone on intense fracture density between the Varetta and the Bersezio Faults (dark orange in Figure 6-4), which was modelled not modelled in the AM model, but was here introduces as a separate block to take into account for the integration with gravimetric data.

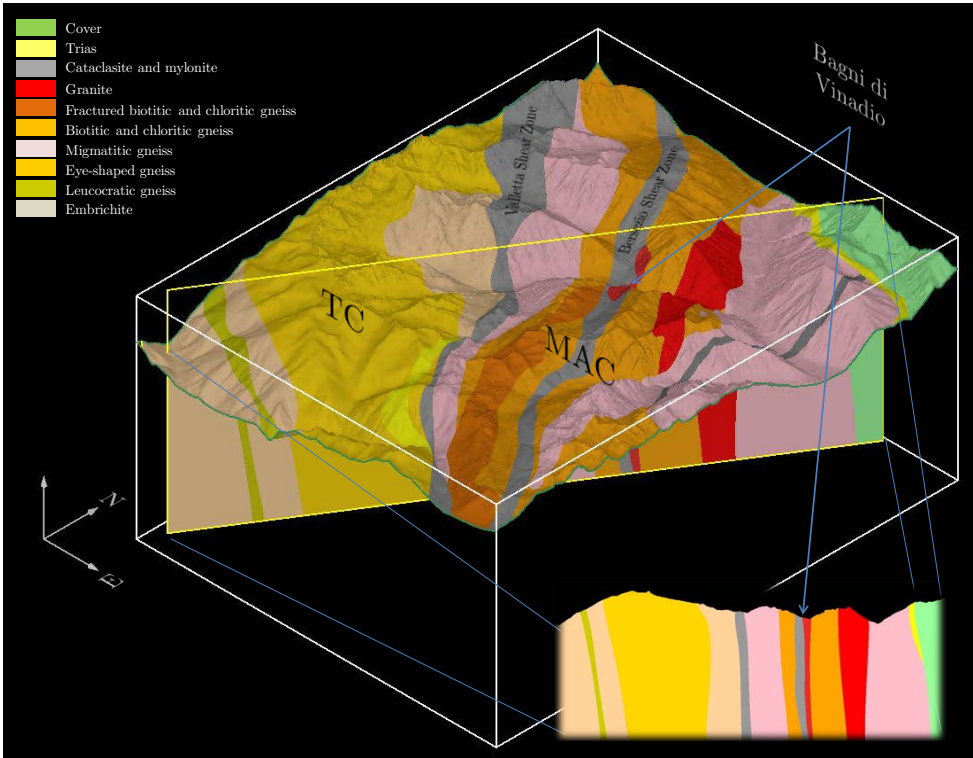


Figure 6-4 3D model of the Bagni di Vinadio area plotted on the topography and in cross-section

6.2.5.3. Terme di Valdieri - The 3D model of the Central Granite

In the Terme di Valdieri region, metamorphic formations owing to the Malinvern-Argentera Complex crop out. These formations include biotitic and chloritic gneiss, biotic anatexite, amphibolitic agmatite, which are intruded by the Central Granite formation in the south-eastern part of the model. The two main tectonic features are the Lorusa fault zone and the Fremamorta shear zone which crops out in the south-eastern part of the area (Figure 6-5).

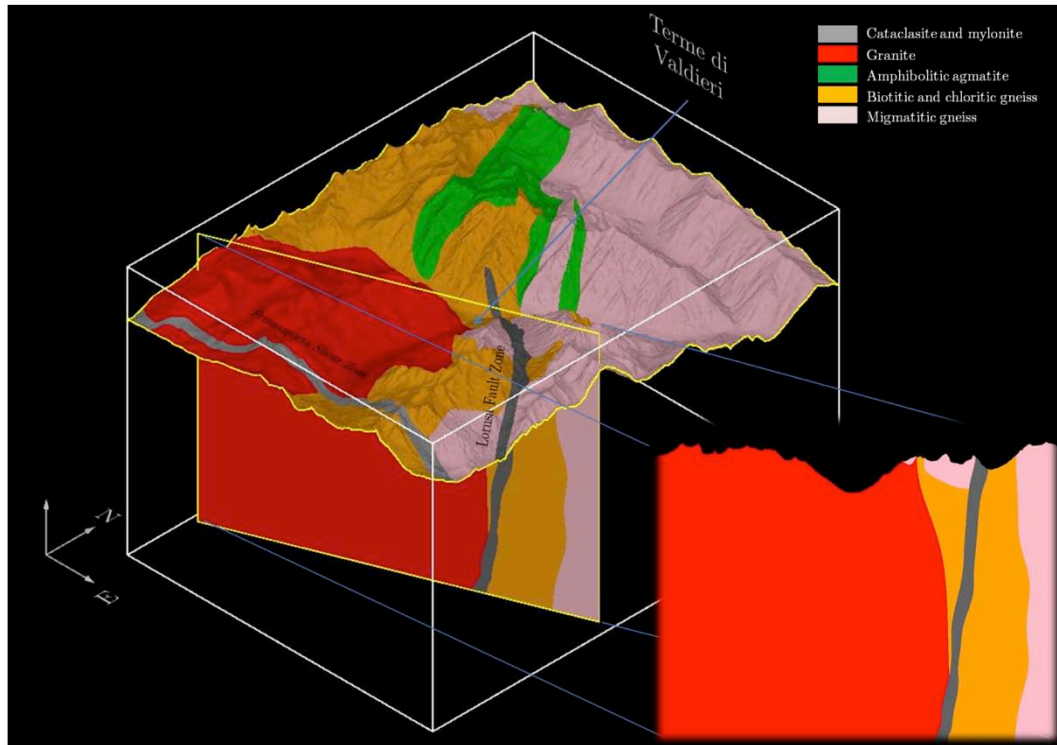


Figure 6-5 3D model of the Terme di Valdieri area plotted on the topography and in cross-section

Granitic intrusive bodies are localized in all the External Crystalline massifs but their geometrical shape of their roots is usually hard to define and model in 3D (STRZERZYNSKI et al., 2005). The Central Granite formation covers an area of about 50km² in the Valdieri area, West of the thermal springs and it is crossed, East to West, by the Fremamorta Shear Zone. It has a roughly circular shape and its emplacement post-dates the three migmatitic events (DEBON and LEMMET, 1999). Moreover its extension in the subsurface is complex and was estimated taking into account the Ciriegia Tunnel cross-section (BORTOLAMI and GRASSO, 1969) and the S.Anna Borehole (BAIETTO, 2006b).

The 3D shape of the Central Granite formation was built in four modelling steps:

- 1 the vertical foliation roughly trending NW-SE, indicated on the geological map of Malaroda (1970) and which was developed during the emplacement of the granite, was assumed to be representative and of the initial intrusive contact. This first stage brought to a constrained model of the granitic body on the basis of the geographical localization of the contact points and foliations (Step1 in Figure 6-7).

- 2 the second step was to integrate the Fremamorta Shear Zone cutting the granite. This structure is interpreted as a high angle shear zone composed by micashistes and mylonitic rocks. Because of the above mentioned software limits in modelling the shear zones, the Central Granite formation was split into two main bodies divided by the FSZ (Step2 in Figure 6-7).
- 3 the third step was to consider the subsurface granite/gneiss contact at the roof of the granite. The plunge of this contact is low towards NE and then becomes vertical in the proximities of the entrance of the Ciriegia tunnel. This contact is indicated on the Cirigia Tunnel cross section (BORTOLAMI and GRASSO, 1969). This step led to the modification of the geometry of the northern portion of the granitic body, which was extended towards NE (Step3 in Figure 6-7).
- 4 the fourth step was to integrate the S. Anna Borehole. This borehole is 1150m long, 60° deviated towards NE and reaches a depth of 850m. Its log shows two main granitic bodies. One at 35 meters in depth is 100 m thick and is described as “micro-granite”, the second at 860 m in depth is more than 400m thick and described as “fractured granite” (Step 4 in Figure 6-7). The former was interpreted as a local intrusion or dyke very similar to the outcropping granite in the proximities of the Vinadio springs, the latter as part of the Central Granite formation. However, as it is an arbitrary interpretation, we preferred not to modify the previously modelled geometry but to model this extension towards North as a separate body, split into two blocks by the Bersezio Shear Zone

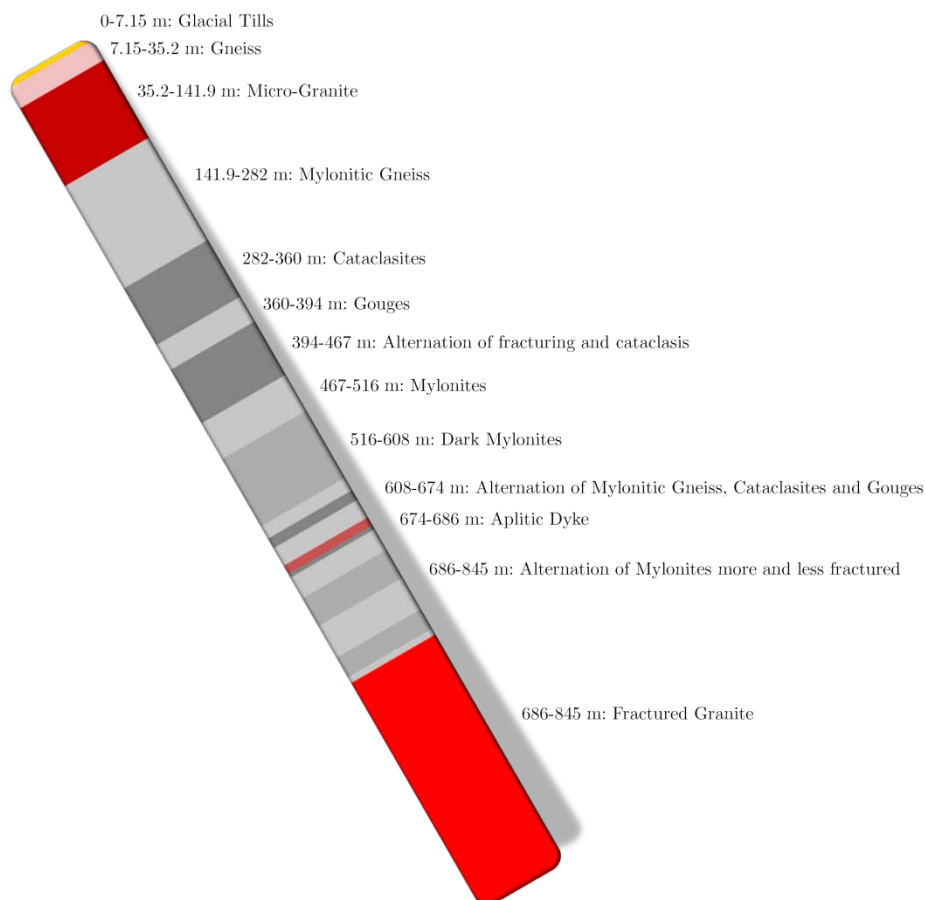


Figure 6-6 Stratigraphic log of the S. Anna Borehole (mod. from Baietto, 2006)

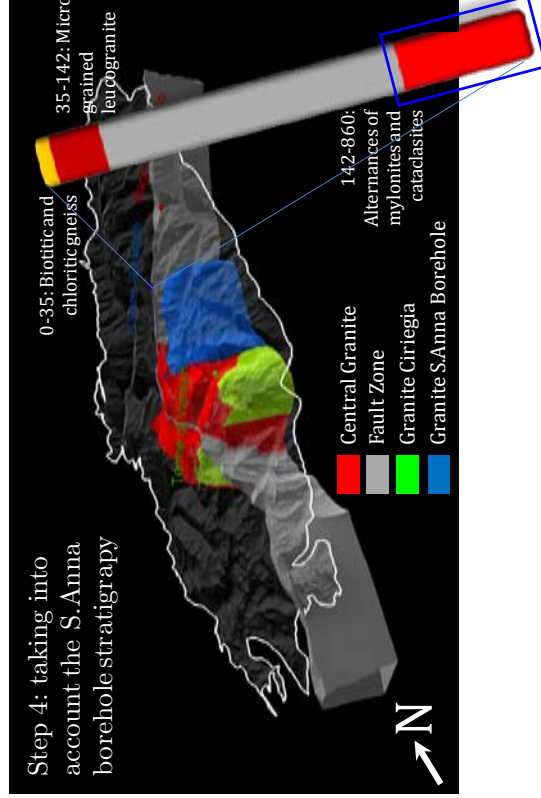
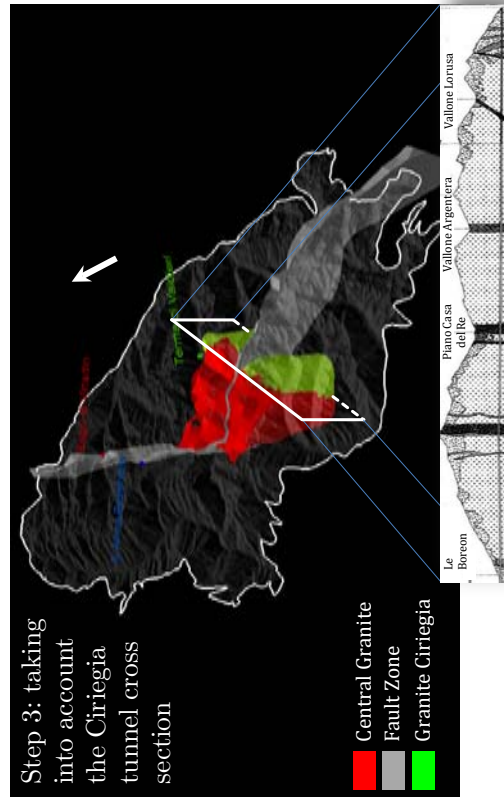
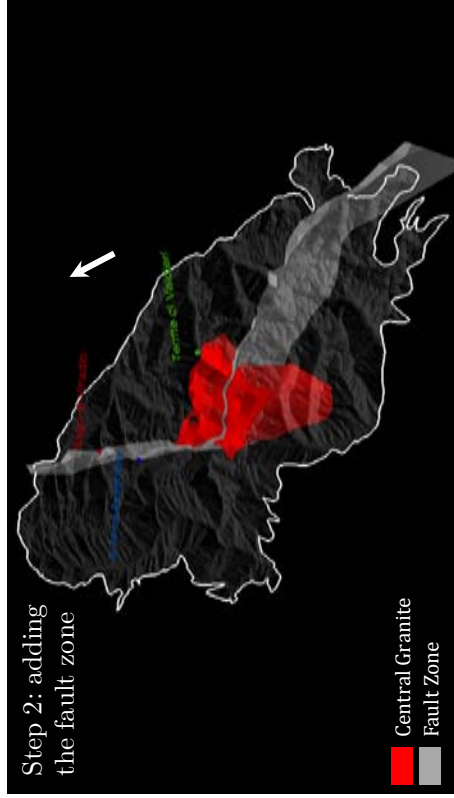
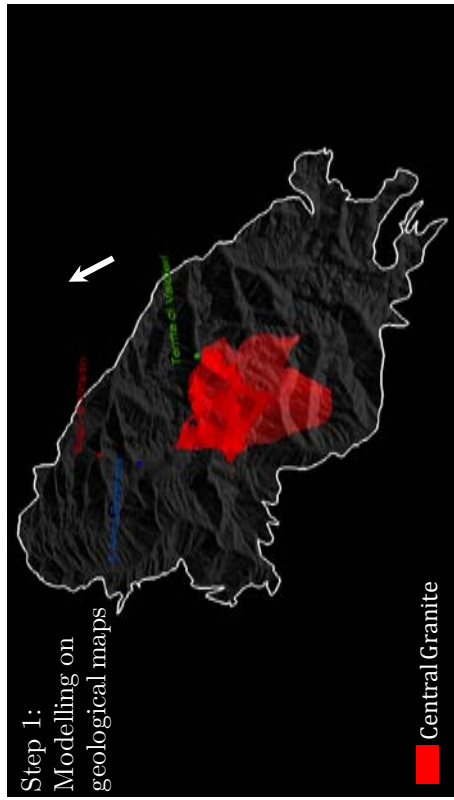


Figure 6-7 Modelling sequence for the Central Granite formation

7

GEOPHYSICAL SURVEYS IN THE ARGENTERA MASSIF

7.1. Concepts and Methods

7.1.1. The gravity method

Gravity is a natural-source method and together with the magnetic techniques composes the so-called potential methods. It is based on the measurements at the surface of the variations in the gravitational field of the Earth caused by variations of density in the subsurface. It is usually employed as method to support seismic or electromagnetic surveys and it helps detecting local density anomalies related to the presence of more or less dense bodies and structures (TELFORD et al., 1990). The gravity method has a wide variety of utilizations (e.g. oil, engineering, archaeology, glaciology, tectonics, geodynamics, hydrogeology, mining) but, in geothermics, it is usually employed to detect deep magmatic bodies, which might represent a heat source, or zones of enhanced fractures where geothermal fluids might circulate, or to monitor subsidence, which could occur if, during the exploitation of a geothermal field, the fluid extraction is not balanced by an adequate reinjection or recharge of fluids at depth.

Differences in rock density are related to several parameters, including mineralogical composition and porosity and produce small variations in Earth field, which reflect in the gravimetric response (measured in milligal⁹) of the Earth. Reynolds (1997) listed the degree to which these parameters might affect the rock density (Table 7-1):

Table 7-1 Rock density variation related to geological processes (REYNOLDS, 1997)

| Factor | Density variation (%) |
|---------------------------|-----------------------|
| Mineralogical composition | 35 |
| Cementation | 10 |
| Age and depth of burial | 25 |
| Tectonic processes | 10 |
| Porosity and pore fluids | 10 |

In sedimentary rocks the parameters controlling the density of a rock are the mineralogical composition, the degree of cementation, the depth and age of burial. Density variations among the different igneous rocks are basically related to their mineralogical composition and to their fracture density and conditions. Density increases with decreasing silica content, therefore basic igneous rock are denser than acid ones. Moreover plutonic rocks are denser than volcanic ones. Similarly in metamorphic rocks, density increases with decreasing acidity and increasing grade of metamorphism. Fracture network might affect the density of a rock, in particular if those fractures are open or filled with water. In geothermal reservoirs porosity of a deep reservoir granite is hard to define but some estimations by means of the integration of gravity and other geophysical methods, coupled to 3D modelling

⁹ 1mGal=10 g.u. ($\mu\text{m}\cdot\text{s}^{-1}$). The gravitational constant, G, has a value of $6.67 \times 10^{-11} \text{ N}\cdot\text{m}^2\cdot\text{kg}^{-2}$. Gravity fields are equivalent to accelerations, for which the SI unit is the $\text{m}\cdot\text{s}^{-2}$ (alternatively written as the $\text{N}\cdot\text{kg}^{-1}$). This is too large for geophysical works and the gravity unit (g.u. or $\mu\text{m}\cdot\text{s}^{-2}$) is generally used.

and inversion processing showed that porosity might increase up to 0.08 with respect to porosity <0.03 for the unaltered granite at the surface. The increase in porosity reflects to a reduction of density of the reservoir granite and its density can decrease of 250 kg/m^3 , according to recent numerical modelling studies (SCHILL et al., 2010).

In the Alps, gravity has mainly been used to support seismic campaigns carried out to detect deep crustal structures, e.g. within the framework of the European Geotraverse (BLUNDELL, 1993), the TRANSALP project (ZANOLLA et al., 2006), to model the Moho geometry in the south-western Alps (MASSON et al., 1999; SCHREIBER et al., 2010) or in the Mt. Blanc massif (MASSON et al., 2002): Moreover it has been used to determine the thickness of the alluvial and quaternary filling of the valleys (ROSSELLI, 2001; STEINHAUSER et al., 1990). However in mountain regions showing geothermal anomalies, any study about the usage of this method for geothermal exploration has ever been carried out.

7.1.1.1. Gravity reductions

Gravity data collected on the field need some processing before being interpreted. A standard treatment of gravity data has to take into account some reductions of the measured data before carrying out a Bouguer Anomaly map:

- Tidal Correction (TC): the gravity field varies as a consequence of the gravitational effects of the Sun and Moon associated with their orbital motions. Therefore this effect has to be removed from the recorded values. The employed instrument in the present Thesis, Stratagem[®] CG-5 Autograv, which automatically corrects the measured values.
- Latitude correction (g_φ): gravity also varies with latitude because of the increase of angular velocity at the equator and because of the non-spherical shape of the Earth. The latitude correction is obtained by differentiating the equation (TELFORD et al., 1990):

$$g_\varphi = 9780318.5 \cdot \left(1 + 0.005278895 \cdot \sin^2 \varphi + 0.000023462 \cdot \sin^4 \varphi\right)$$

where φ is the latitude.

- Instrumental drift Correction (DC): this correction is based on a looping procedure, which involves repeated readings for a gravimetric base-station at recorded times throughout the day (Figure 7-1). Moreover placing a gravity base station for the entire survey is crucial to tie together the measurements of each cycle. Readings are plotted against time and drift is assumed to be linear between consecutive base readings. The drift correction is then subtracted from the observed value.

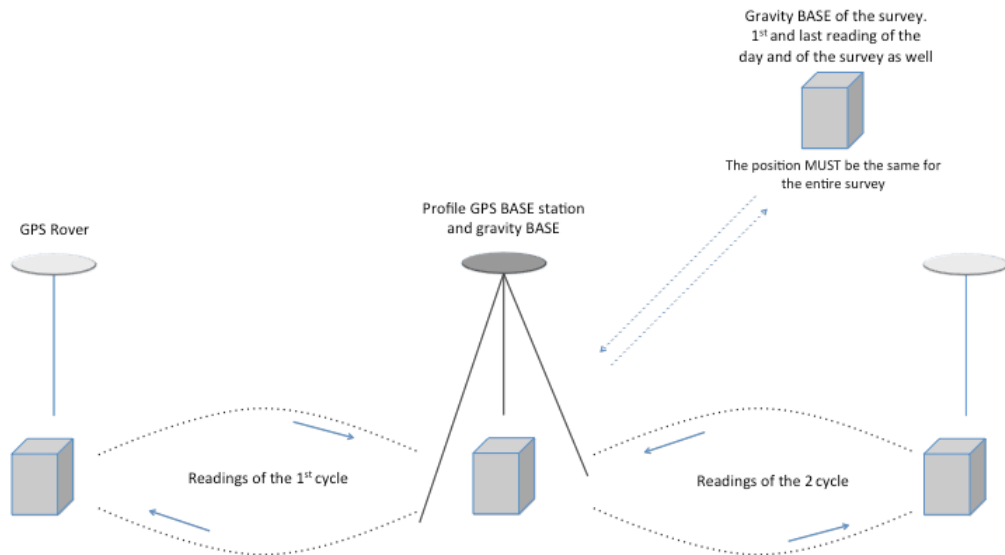


Figure 7-1 Employed setting for the gravity looping procedure

- Free Air Correction (FAC): gravity varies inversely with the square of the distance, therefore it is necessary to eliminate the elevation differences between stations to reduce the readings to a datum surface:

$$FAC=0.3086 \cdot h$$

where **h** is expressed in meters

- Bouguer Correction (BC): it removes the gravitational effect of the rock between the observation point and the datum at the surface by approximating the rock layer beneath the station to an infinite horizontal slab with a thickness equal to the elevation of the observation above datum. If ρ is the density of the rock, BC is described by the following equation:

$$BC=2\pi G\rho h=0.4191\rho h$$

where **h** is expressed in meters and ρ in kg/m^3

- Terrain Correction (TC): The Bouguer correction assumes the topography around the gravity stations to be flat. However this is rare, therefore the terrain correction is necessary to take into account the effect of the relief. The terrain correction is added to the reading and is usually calculated by means of the Hammer chart.

Finally the free air anomaly (FAA) and the Bouguer anomaly (BA) can be calculated for each station:

$$FAA=g_{\text{obs}}-DC-g_{\varphi}+FAC$$

$$BA=g_{\text{obs}}-DC-g_{\varphi}+FAC\pm BC+TC$$

For this Thesis the new GraviFor3D, which is being developed at Centre of Hydrogeology and Geothermics CHYN of the University of Neuchatel was tested and finally used (7.1.1.2). This code computes the plateau effect (BC correction) and the topography effect (TC reduction) at once directly using digital elevation models (DEM). The main interesting aspect for the employed topography correction is the obtained high accuracy results because

the earth topography is well reproduced using detailed (cellsize<10m) Digital Elevation Model (DEM) and there is not any approximation calculated on the gravity effect.

7.1.1.2. Application of the GraviFor3D code to calculate the Bouguer Anomaly of the Argentera Massif

The basic concepts of the algorithm development are briefly explained in the followings.

The terrain correction is calculated on the basis of the Hammer reticular method (HAMMER, 1936) but the new approach proposed is based on the principle of the gravity effect of a prism. Topography, represented by a DEM, is discretized into prisms and the effect of each prism on each gravity station is then computed. To carry out this computation, the area around each station is divided into four zones of increasing radius with respect to the station: 150 m, 8 km, 70 km and 167 km¹⁰. Each zone is associated to a DEM, which cell size increases with the distance from the station. It is possible to use two DEMs which are combined to avoid overlaps or empty spaces: the first zone should include the most accurate DEM (cellsize<10m), the second and the third zone a DEM up to 30 times the resolution of the first one, the fourth zone is covered by a 1km DEM, derived from resampling of the second DEM (Figure 7-2). These different radiuses also express the weight of the specific sub-area in terms of effect to the gravity station.

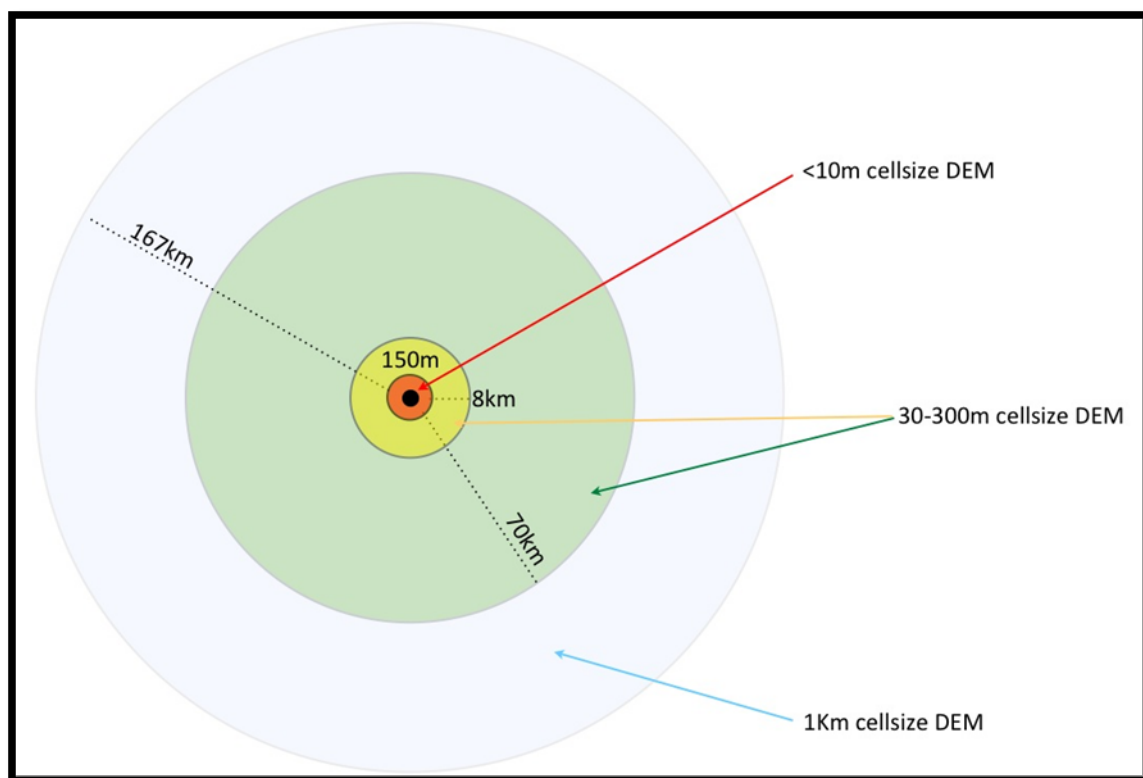


Figure 7-2 The four zones around the gravity station and the associated DEMs

The topographic effect is calculated considering the two inner zones and then the two external ones. For the inner zones the gravity effect of the prisms is calculated using the formula of the rectangular prism (BLAKELY, 1996; PARASNIS, 1999). Therefore for a specific

¹⁰ These distances were selected after sensibility studies

prism having $x_1 < x < x_2$, $y_1 < y < y_2$ and $z_1 < z < z_2$ in the x, y and z directions, the vertical gravity attraction g_{mn} for a uniform density prism δ observed at point m can be computed as follows:

$$g_{mn} = G\delta \sum_{i=1}^2 \sum_{j=1}^2 \sum_{k=1}^2 \mu_{ijk} \left[z_k \arctan \frac{x_i y_i}{z_k R_{ijk}} - x_i \log(R_{ijk} - y_i) - y_i \log(R_{ijk} - x_i) \right]$$

where:

$$R_{ijk} = \sqrt{x_i^2 + y_i^2 + z_i^2}$$

$$\mu_{ijk} = (-1)^i (-1)^j (-1)^z$$

G is the gravitational constant

Therefore to calculate the whole gravity effect g_m it is sufficient to sum the effect of each prism:

$$g_m = \sum_{n=1}^N g_{mn}$$

where m is the number of gravity stations and N is the total number of prisms

For the two outer zones, the gravity effect is calculated on the theory of the vertical gravity attraction where the gravity effect is computed at the centre of the prism:

$$g = \frac{G\delta V Z}{r^3}$$

where, being x_0 , y_0 , z_0 the coordinates of the gravity station:

$$V = (x_2 - x_1) \cdot (y_2 - y_1) \cdot (z_2 - z_1)$$

is the volume of a prism

$$r = \sqrt{(x_0 - x_1 - \Delta x)^2 + (y_0 - y_1 - \Delta y)^2 + (z_0 - z_1 - \Delta z)^2}$$

is the distance between the observation point and the centre of the prism with

$$\Delta x = \frac{x_2 - x_1}{2}, \quad \Delta y = \frac{y_2 - y_1}{2}, \quad \Delta z = \frac{z_2 - z_1}{2}$$

$Z = z_1 - z_0 + \Delta z$ is the elevation difference between the centre of the prism and the observation point located on the topography.

7.1.1.3. Inversion processing of the gravity data

One of the main problems related to gravity interpretation lies into the reconstruction of the geometry of the geological bodies at the subsurface and their density estimation. 3D-Geomodeller provides a tool to compute joint 3D inversion of gravity and magnetic data and its efficacy is well proven (GUILLEN A., 2004; LANE et al., 2007) if the amount of observations uniformly covers the study area. However, because, in the Argentera Massif, the gravity stations are concentrated along widely spaced profiles (up to 7km of distance) and any magnetic susceptibility data is available, the inversion process was focussed on the 2D

profiles were observation were collected, to keep the accuracy of the processing and to reduce the uncertainty of the interpretations.

Usually two are the classic inversion approaches: the first consists in modelling the geometry of the bodies keeping the densities fixed; the second is to fix the geometries and allow the densities of the bodies vary. The inversion process employed in this thesis is based on 2D constrained compact gravimetric inversion. As starting point an algorithm, written in Matlab[®] environment, was elaborated according to 2D compact magnetic inversion from the original approach by Last and Kubik (1983). The code has been however opportunely modified by appropriate equations to account for the gravimetric anomaly even if the code structure has been maintained. This approach has been previously applied (STOCCO et al., 2009) for simple shapes such as prisms and dykes using magnetic data and the challenge of this part of the Thesis was to prove its efficacy for gravity observations.

The principle of the compact inversion involves minimizing the area of the source body thus maximizing its compactness. The advantage of this approach is that desirable geologic characteristics are automatically incorporated into the model with a minimum of subjective judgments on the part of the interpreter.

A gravimetric body can be defined to be 2D when its strike length in the direction perpendicular to the profile is at least 10 times its width (TELFORD et al., 1990). Following Bhattacharyya (1964), the domain beneath the gravimetric profile can be split in \mathbf{M} rectangular prisms orthogonal to the profile direction, being \mathbf{d}_j the unknown relative density of the \mathbf{j}_{th} prism. Using the formula reported by Telford we are then able to calculate at each of the \mathbf{N} measuring points along the gravimetric profile the value g_i of the Bouguer anomaly due to the gravity fields of all the prisms:

$$g_i = \sum_{j=1}^M K_{i,j} d_j$$

where $K_{i,j}$ is a geometrical function relating the size and the distance of the prism \mathbf{j} from the measurement point \mathbf{i} . This equation can also be written as matrix:

$$g = K \times d$$

being \mathbf{g} a column vector with \mathbf{N} rows, \mathbf{K} a kernel matrix $\mathbf{N} \cdot \mathbf{M}$ and \mathbf{d} a column vector with \mathbf{M} rows. The matrix changes with an iterative procedure until a satisfying convergence with the original data is obtained.

The input parameters for the inversion procedure are:

- maximum number of iterations
- resolution of the matrix gridding
- gravity anomaly (Bouguer or residual) values plotted on the profile
- topography of the profile

Moreover, the algorithm allows evaluating the best subsoil gridding and determining the maximum depth to which the vertical section of the model could be extended and, at the same time, reduces the number of problems to be computed. For the profiles where the inversion was applied in this work a depth of 2000m was set.

The inversion code was validated by means of a similar procedure as that applied to validate the algorithm. The results of the forward modelling of the simple three-dimensional

model were considered as the real gravity response of the model. Then a profile was drawn to come out with its anomaly values and topography. Hence these two parameters were computed by the inversion.

The code was finally applied to each profile covering the study areas and the results of a profile are reported in Figure 7-3. Relative density values (expressed in Kg/m^3) are reported in contour maps accounting also for the topography of the profiles. As it can be observed a very good fitting with experimental data is obtained by means of the adopted procedure.

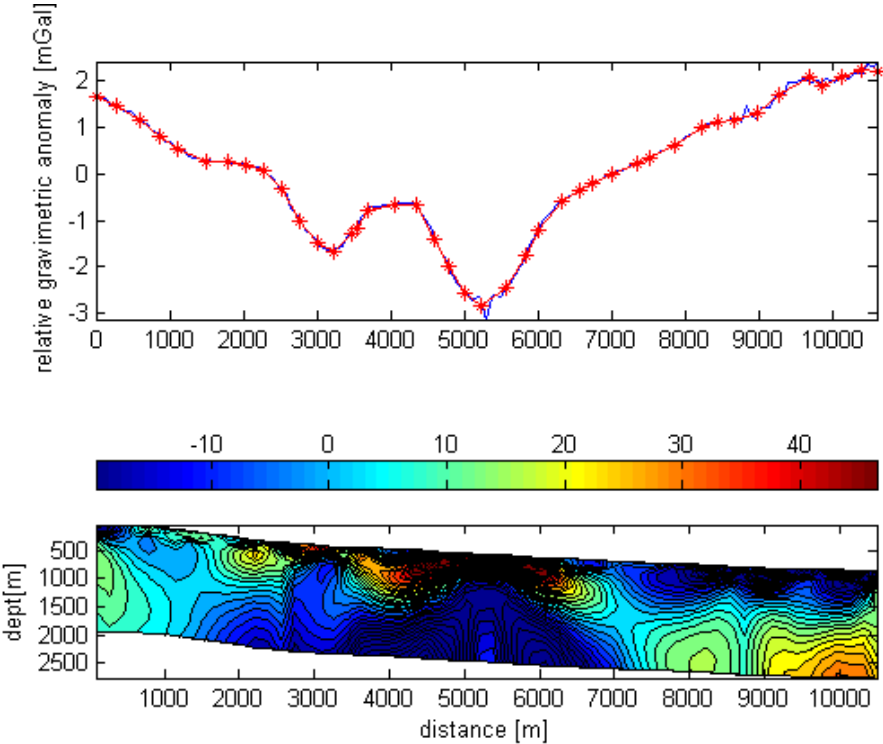


Figure 7-3 Example of the results of the inversion models for a randomly selected gravity profile in the Argentera Massif. In the upper plot the red line represents the observed anomaly and the blue one is the computed model. The density variation is expressed in kg/m^3

7.1.1.4. Laboratory density measurements

During the field campaigns several rock samples were collected along the observation profiles to then measure their density in the laboratory. A total of 35 rock samples were analyzed as representative of the outcropping rocks in the study area. Density measurements were carried out at the Centre of Hydrogeology and Geothermics CHYN, in Neuchâtel (CH).

These measurements were simply based on the Archimedes’s principle according to which, the observed weight difference of a body immersed into a liquid corresponds to its volume.



Figure 7-4 Rock sample immersed in deionized water during a density measure.

Therefore, being F_a the Archimede force:

$$P_2 = P_1 - F_a$$

according to the 2nd Newton law:

$$P_1 = m_1 \cdot g \text{ and } P_2 = m_2 \cdot g$$

where m_1 is the mass of the Becker filled with water and m_2 is the weight of total mass once the rock sample is immersed

and

$$F_A = V_s \cdot \delta_{\text{water}} \cdot g$$

hence

$$V_s = (m_1 - m_2) / \delta_{\text{water}}$$

Which is the volume of the sample.

- density measurements were carried out according to the following procedure:
- rock samples were cut in a regular shape
- samples were dried at 40°C for 12 hours
- the weight of dry samples was measured using a balance Ohalis Explorer Pro which assures an accuracy of 0.001 gr.
- rock samples were immersed in deionised water for 12 hours
- saturated samples weight was then measured to estimate the porosity of the samples by the difference between dry and saturated sample
- a Becker was filled with deionised water and put on the balance which tare was then set to zero
- water temperature was measured as well to calculate the accurate density of water
- water-saturated rock samples were immersed and their weight was observed

The results of the analysed are summarized in Table 7-2:

Table 7-2 Density values of the samples from the Argentera Massif

| Rock Type | Dry Weight [g] | Sat. Weight [g] | Wight immersed [g] | t_{water} [°C] | Volume [cm ³] | Porosity [%] | Dry Density [g/cm ³] | Sat Density [g/cm ³] | AVG Density [g/cm ³] |
|----------------------------------|----------------|-----------------|--------------------|------------------|---------------------------|--------------|----------------------------------|----------------------------------|----------------------------------|
| Amphibolite | 196,33 | 197,14 | 71,37 | 22,3 | 72 | 1 | 2,745 | 2,756 | 2,750 |
| Amphibolite | 216,14 | 216,43 | 77,40 | 22,3 | 78 | 0 | 2,786 | 2,790 | 2,788 |
| Amphibolite | 98,89 | 99,38 | 35,68 | 22,3 | 36 | 1 | 2,765 | 2,779 | 2,772 |
| Amphibolitic Agmatite | 161,42 | 162,85 | 60,98 | 22,3 | 61 | 2 | 2,641 | 2,664 | 2,653 |
| Amphibolitic Anatexite | 103,09 | 104,67 | 39,41 | 22,3 | 40 | 4 | 2,610 | 2,650 | 2,630 |
| Biotitic and Amphibolitic Gneiss | 135,65 | 135,94 | 46,71 | 22,3 | 47 | 1 | 2,897 | 2,904 | 2,901 |
| Amphibolitic Anatexite | 124,8 | 125,8 | 48,11 | 22,3 | 48 | 2 | 2,588 | 2,609 | 2,598 |
| Biotitic Anatexite | 171,84 | 173,04 | 63,44 | 22,3 | 64 | 2 | 2,702 | 2,721 | 2,712 |
| Biotitic Anatexite | 169,31 | 172,88 | 65,33 | 22,3 | 65 | 5 | 2,586 | 2,640 | 2,613 |
| Biotitic and Chloritic Gneiss | 207,78 | 209,26 | 76,57 | 22,3 | 77 | 2 | 2,707 | 2,727 | 2,717 |
| Biotitic and Chloritic Gneiss | 221,57 | 222,33 | 79,24 | 22,3 | 79 | 1 | 2,790 | 2,799 | 2,795 |
| Biotitic and Chloritic Gneiss | 147,64 | 148,18 | 53,87 | 22,3 | 54 | 1 | 2,734 | 2,744 | 2,739 |
| Biotitic and Chloritic Gneiss | 78,01 | 78,86 | 29,45 | 22,3 | 30 | 3 | 2,643 | 2,672 | 2,657 |
| Biotitic and Chloritic Gneiss | 213,1 | 214,42 | 80,33 | 22,3 | 81 | 2 | 2,647 | 2,663 | 2,655 |
| Biotitic Gneiss | 134,14 | 134,39 | 48,89 | 22,3 | 49 | 1 | 2,737 | 2,743 | 2,740 |
| Embrichite | 211,1 | 212,67 | 77,39 | 22,3 | 78 | 2 | 2,721 | 2,742 | 2,732 |
| Embrichite | 223,69 | 225,22 | 84,89 | 22,3 | 85 | 2 | 2,629 | 2,647 | 2,638 |
| Embrichite | 134,98 | 135,76 | 48,08 | 22,3 | 48 | 2 | 2,801 | 2,817 | 2,809 |
| Embrichite | 94,95 | 95,82 | 34,66 | 22,3 | 35 | 2 | 2,733 | 2,758 | 2,746 |
| Fine-Grained Granite | 105,31 | 106,28 | 40,80 | 22,3 | 41 | 2 | 2,575 | 2,599 | 2,587 |
| Fine-Grained Granite | 72,59 | 73,3 | 27,23 | 22,3 | 27 | 3 | 2,660 | 2,686 | 2,673 |
| Leuco-Granite | 95,34 | 96,51 | 37,12 | 22,3 | 37 | 3 | 2,563 | 2,594 | 2,578 |
| Granitoid Gneiss | 84,98 | 85,41 | 31,36 | 22,3 | 31 | 1 | 2,704 | 2,717 | 2,710 |
| Granitoid Gneiss | 369,32 | 371,27 | 140,71 | 22,3 | 141 | 1 | 2,619 | 2,632 | 2,626 |
| Leuco-Gneiss | 262,95 | 263,91 | 100,11 | 22,3 | 100 | 1 | 2,621 | 2,630 | 2,625 |
| Leuco-Gneiss | 30,84 | 31,58 | 11,75 | 22,3 | 12 | 6 | 2,619 | 2,691 | 2,650 |
| Leuco-Gneiss | 31,2 | 31,43 | 11,88 | 22,3 | 12 | 2 | 2,620 | 2,640 | 2,630 |
| Marble | 213,92 | 214,38 | 78,90 | 22,3 | 79 | 1 | 2,705 | 2,711 | 2,708 |
| MicaSchist | 70,53 | 70,98 | 25,27 | 22,3 | 25 | 2 | 2,785 | 2,802 | 2,794 |
| Migmatite | 267,58 | 268,79 | 98,29 | 22,3 | 99 | 1 | 2,716 | 2,728 | 2,722 |
| Migmatite | 148,6 | 149,63 | 54,83 | 22,3 | 55 | 2 | 2,704 | 2,723 | 2,713 |
| Mylonite | 155,64 | 156,63 | 59,52 | 22,3 | 60 | 2 | 2,609 | 2,626 | 2,617 |
| Mylonite | 110,85 | 111,75 | 41,50 | 22,3 | 42 | 2 | 2,665 | 2,687 | 2,676 |
| Mylonite | 106,6 | 107,47 | 40,45 | 22,3 | 41 | 2 | 2,629 | 2,651 | 2,640 |
| Quartzite | 89,03 | 89,53 | 34,01 | 22,3 | 34 | 1 | 2,612 | 2,626 | 2,619 |

7.2. The magnetotelluric method

Magnetotelluric **MT** is a natural source method, which aims at measuring the natural fluctuations of the electric **E** and magnetic **B** fields in orthogonal directions to probe the electrical resistivity distribution in the subsurface from few tens of meters up to several hundreds of kilometres. The basics of MT theory were firstly approached by Tikhonov (1950; 1986) and Cagniard (1953). Natural source of MT fields can be divided into two main groups: thunderstorms, which lightning propagate to great distances, produce fields above 1Hz and current systems in the magnetosphere set up by solar activity produce frequencies below 1 Hz (FEDERICI and PAPPALARDO, 1991).The electromagnetic fields are composed by a broad spectrum of frequencies, generated by the ionospheric currents from the interaction between the plasma emitted from the sun and the earth's magnetic field. Fluctuations having lower frequency up to 0.1 Hz, named ultra-low frequency pulsations **ULF**, propagate vertically and induce eddy currents in the earth. Their distribution is controlled by the local conductivity of the structures. Pulsations having higher frequency as high as 100 kHz, might be superimposed onto ULF and are generated by electric storms. Their signals, which propagate horizontally, are called *atmospherics* or *spherics*. Spherics can be separated into transverse electric TE, transverse magnetic TM or transverse electric and magnetic TEM waves.

Because the direction of polarisation of the incident magnetic field is variable and not known beforehand, it is common practice to measure at least two components of the electric field and three components of the magnetic field variation to obtain a fairly complete representation.

One of the main parameters of a MT sounding is the *electromagnetic skin depth* $\rho(T)$, which describes the exponential electromagnetic response decays as it propagates into a medium. The skin depth is proportional to the sounding period T (ranging from 10^{-3} to 10^5 s), to the conductivity of the penetrated medium (the average value of Earth's crust and upper mantle is $100 \text{ } \Omega\text{m}$) and its magnetic permeability μ :

$$\rho(T) = (T / \pi\mu\sigma)$$

The skin depth, in MT studies, is usually equated to the *penetration depth* of the electromagnetic field as follows:

$$\rho(T) = 500 \cdot \sqrt{T / \rho}$$

where ρ_a is the *apparent resistivity* (SIMPSON and BAHR, 2005).

Therefore the depth achieved by a MT sounding for a given sounding period, is controlled by the average conductivity of the overlying sample of earth that is penetrated.

The resistivity of the subterranean geological structures is usually related to its chemical and physical conditions such as temperature, pressure, porosity, permeability, presence and composition of fluids, mineralogical composition. For instance saline waters act as electrolytes since free ions (e.g. Na^+ , Cl^-), deriving from the dissolution and leaching of minerals, enter the solution and have an important effect on the increase of the bulk conductivity of a rock formation, hence a decrease of resistivity. Similarly, the presence of ore minerals, such as hematite, magnetite, pyrite, sulphides or graphite, which contain free electrons able transporting charges, have an important relevance on the resistivity of a formation.

Temperature of these fluids plays a major role as well (SPICHAK et al., 2007). In fact, with increasing temperature, the viscosity of a solution is decreased, promoting increased ionic mobility and therefore tending to enhance conductivity. The Dakhnov's Law gives the relation between resistivity ρ and temperature:

$$\rho_T = \frac{\rho_{18}}{1 + 0.025 \cdot (t - 18)}$$

with ρ_T for the fluid saturated rock resistivity, and ρ_{18} for the fluid resistivity at 18°C .

The Archie's law (1942) describes the relation between porosity and electric conductivity and may also lead to further indication on porosity changes in the subsurface:

$$C_T = \frac{1}{a} C_W \Phi^m S_W^n$$

where Φ denotes the porosity, C_T the electrical conductivity of the fluid saturated rock, C_W represents the electrical conductivity of the brine, S_W is the brine saturation, m is the cementation exponent of the rock (usually in the range 1.9–2.2 for crystalline rock), n is the saturation exponent (usually close to 2) and a is the tortuosity factor (sometimes used to correct for variation in compaction, pore structure and grain size)

The same equation can be transposed to resistivity:

$$\phi^m = \frac{a \cdot \rho_w}{\rho_T \cdot S_w^n}$$

with ρ_T for the fluid saturated rock resistivity, and ρ_w for the brine resistivity.

$$F = \frac{a}{\phi^m} = \frac{\rho_o}{\rho_w}$$

is also called the *formation factor*, where ρ_o is the resistivity of the rock filled with only water ($S_w=1$)

In the case of the study area, assuming that fractures at depth are only filled with water and a being 1 (straight path of the fluids) the relationship between electrical resistivity and porosity can be written as follows:

$$\phi^m = \frac{\rho_w}{\rho_T}$$

The MT method has been broadly used in geothermal exploration because of its ability to detect conductive rocks at depth because of thermal excitation and presence of geothermal fluids (ÁRNASON and EYSTEINSSON, 2010; BIANCHI et al., 2010; NEWMAN et al., 2008; SCHILL et al., 2010; THOMAS et al., 1981; VOLPI et al., 2003). In thermal areas the depth may be 10 km or less. It has also to be taken into account that geothermal reservoirs are economically exploitable up to 5-6 km in depth, otherwise the costs of drilling and production are not affordable. Therefore an MT survey must be targeted, in terms of sampling period and frequency ranges to detect geothermal anomalies above the 10 km depth.

7.3. Gravity Observations in the Argentera Massif

7.3.1. Comparison between the original data and the results of the GraviFor3D code

This phase was carried out comparing the Bouguer Anomaly **BA** of the International Gravimetric Bureau BGI¹¹ and the computed one by means of the GraviFor3D code. Free gravity data can be downloaded from the BGI website. Only five BGI stations are however available for the Italian side of the Argentera Massif but more observations cover the French side and the surrounding regions. As the BGI data include both raw and **BA** values¹², a Bouguer Anomaly map was carried out using these latter values (Figure 7-5a). Then raw values were treated using the GraviFor3D code to compute the Bouguer anomaly. The two results were then compared to show the degree of misfit (Figure 7-5b). The employed DEM was the 30m NASA Shuttle Radar Topography Mission SRTM30+ DEM, including the bathymetry as the Mediterranean Sea is less than 50km far from the study area.

A total of 842 stations were considered in this phase, a 30m DEM was used for the first zone whereas a sub-sampled 260m cell size was used for the outer zones. The Mediterranean Sea effect also had to be taken into account assuming a density of 1g/cm^3 for the sea water. The radiuses of the two zones were 20 and 167 km. The first radius was extended from 150 m to 20 km because any DEM of higher resolution was available to improve the accuracy of the result in the inner region.

The results of the comparison between the two Bouguer Anomalies showed an encouraging low misfit. In fact the gravity anomaly's regional trend, NW-SE oriented, is similar in both anomalies. The north-western negative anomaly is interpreted as a strong deepening of the Moho down to 51km, whilst the positive anomaly N-E of the Argentera Massif, highlights the Ivrea body¹³ 10-30 km deep, N-S trending and passing beneath the Dora Maira massif towards the Argentera Massif to the south with an eastward plunge (SCHREIBER et al., 2010). The main difference is in the SE sector of the map where the prolongation of the negative anomaly towards SE well defined in the BGI maps, is less constrained in the map computed by the code. A reason might be related to the different topographic effect computed using the Hammer method for the BGI anomaly and computed using the SRTM30+ DEM, which is not accurate enough to constrain the inner zone around each gravity stations.

¹¹ <http://bgi.omp.obs-mip.fr/>

¹² calculated using the classical Hammer reticular method

¹³ The Ivrea body is a slice of lower-crustal-upper-mantle material that was obducted from the southern (Adriatic) plate and thrust to a shallow level

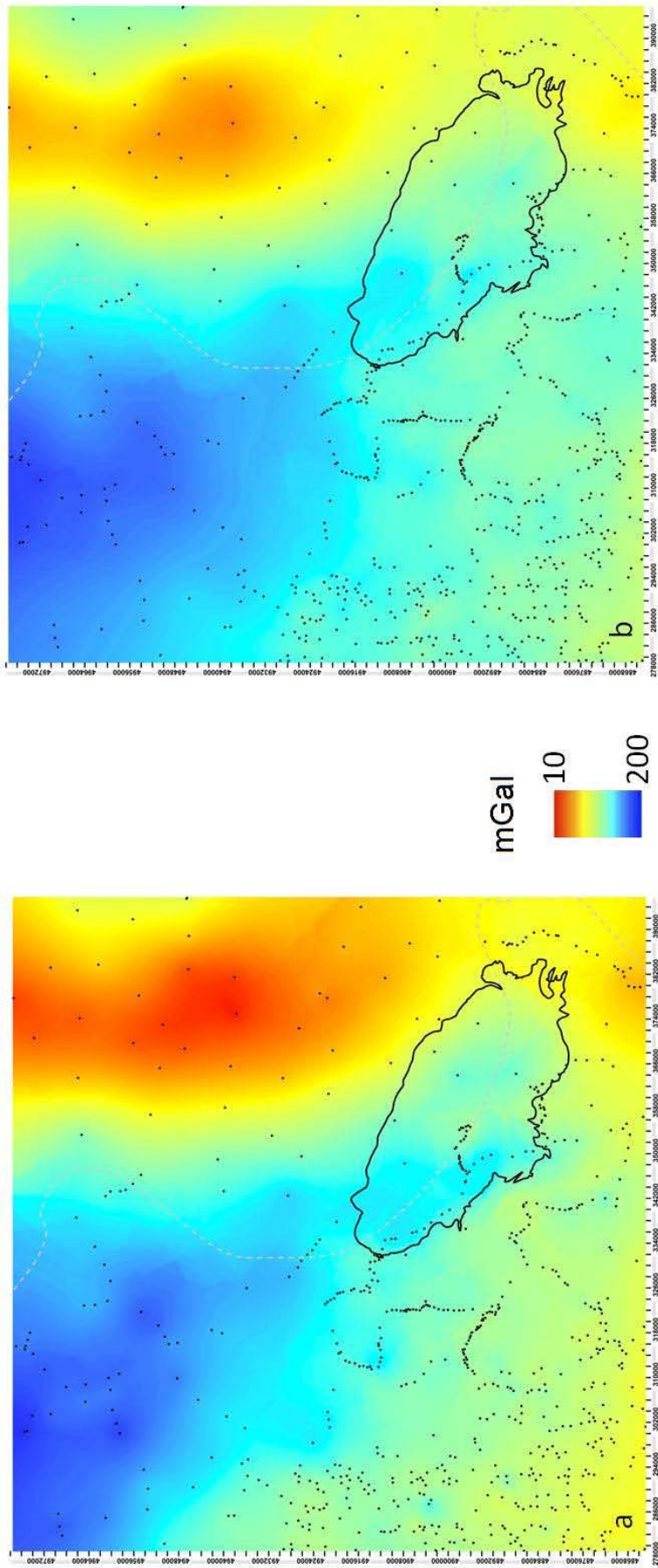


Figure 7-5 Comparison between the Bouguer Anomaly map computed on BGI data (left) and that resulting from the GraviFor3D code

7.3.2. Field data collection

Two gravity surveys were carried out in summer 2010 and spring 2011 on the entire Italian side of the Argentera Massif. The aim of the surveying was to cover as much as possible the study-area keeping a high resolution of the data. Therefore a spacing of the stations of 250 was chosen. Because of the complex topography of the region, characterized by high peaks up to 3300 m a.s.l. (Mount Argentera) and narrow valleys down to 800 m a.s.l., data was mainly collected along 14 profiles following roads and trails corresponding to axes of the main valleys which run perpendicular to the main geological structures (Figure 7-6 and Figure 7-7)

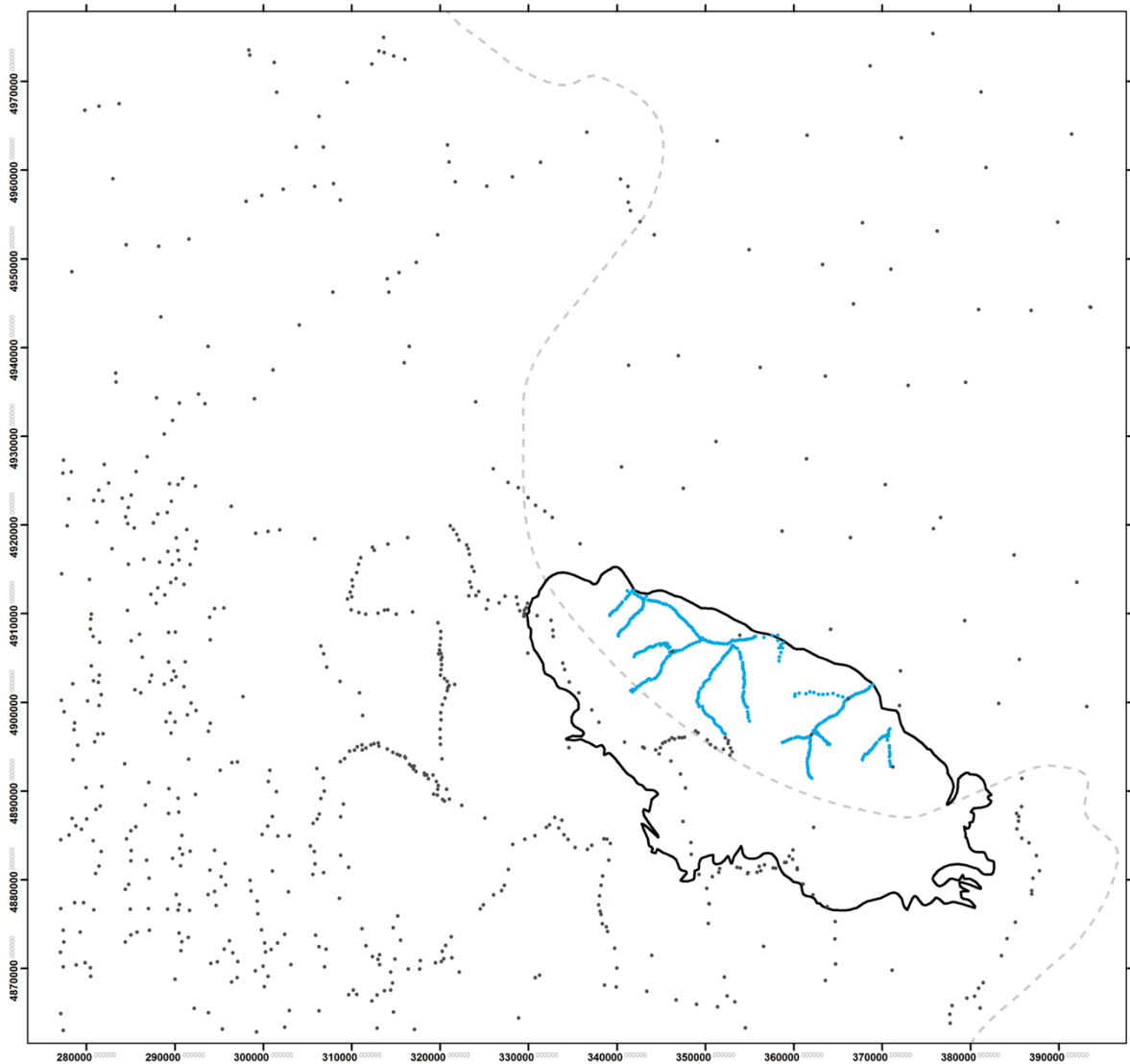


Figure 7-6 Treated gravity records. Total of 1070 points: 667 from BGI (black dots) and 403 collected during the Thesis (blue dots)

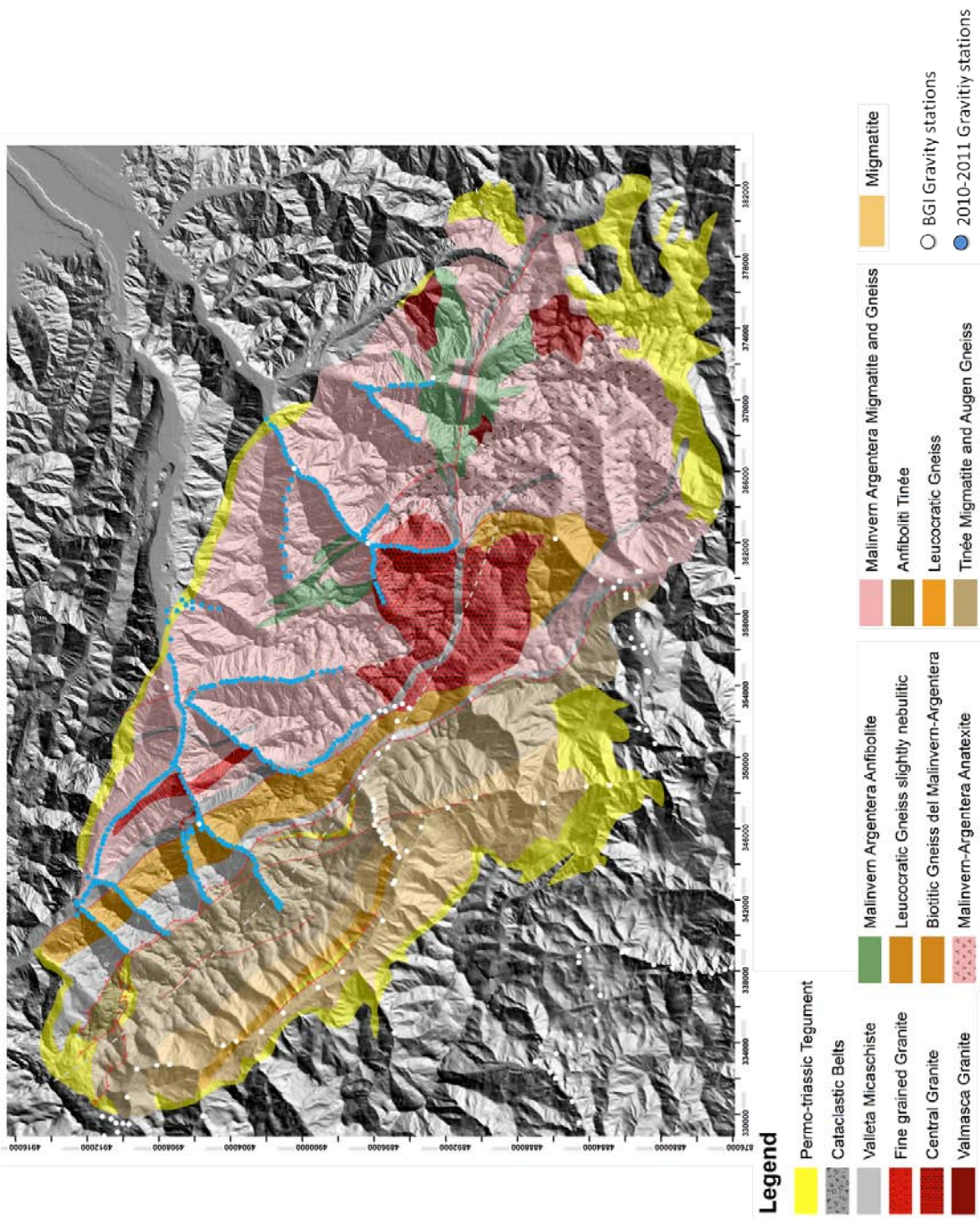


Figure 7-7 Detail of the gravity profiles plotted over the geology used for the interpretations

The BGI observations in the Italian side were used to tie together the data collected on the field to those already available online and then come out with a homogenised Bouguer Anomaly map of the region including all the available stations.

Two differential GPS (DGPS) AshTech ProMark2[®] were used to collect the accurate position of each measurement. During the survey one DGPS was placed as a *base* station usually in the middle of the profile to be covered by gravity measurements during the day, recording its position with 5 seconds intervals. The other DGPS was moved, as *rover*, to record the position of each station. The recording interval was set, in this case, to 2 seconds and the position was collected for 15 minutes. The maximal distance between the DGPS base and rover was usually less than 4km, ensuring high accuracy of the rover positions after post-processing. GPS positions were then post-processed using the GNSS permanent base stations network of the Provincia di Cuneo¹⁴. Station positions have been processed using the AshTech[®] Solutions Tools software and as a result the 97% of the GPS positions indicated a vertical accuracy below 10 centimetres.

A total of 403 measurements were collected using a Scintrex[®] CG-5 Autograv gravimeter that assures a reading resolution of 1 μ Gal. The instrument was calibrated and stabilized following standard procedures during the week before each survey. Gravity measuring adopted a looping procedure, which involves the measuring at the base stations of the survey and of each profile at recorded time intervals, usually at the beginning and at the end of each survey and cycle. This procedure aimed to construct the daily instrumental drift curve of each profile and of the whole survey. For each station, gravity values were repeatedly recorded until the variation among the last three readings was lower than 5 μ Gal, with a minimum of three readings. The 403 stations have been tied to those from BGI by measuring some of these during the survey to obtain a uniform series of data to treat.

7.3.3. Data processing and results

The new observations have been integrated to the old ones and a final version of the Bouguer anomaly was computed using a 10m Argentera Massif DEM (RIBOLINI and SPAGNOLO, 2008), which was combined to the SRTM30+ DEM to process the complete set of data.

Gravity data were reduced to complete Bouguer gravity anomalies with a reduction density of 2.67 g/cm^3 by applying the reductions and corrections to a 167 kilometres radius. The calculated Bouguer anomaly was compared to the gravity response of the 3D geological models to find the best fit and it was also plotted along the survey profiles and then inverted to estimate the distribution of the density at the subsurface, the shape and volume of the bodies along the 2D profiles. Finally all these data were integrated to the 3D models.

Moreover the Bouguer Anomaly of the Argentera Massif was filtered to come out with three residual anomalies. These *residuals* resulted from the application of a high-pass Butterworth filters at 50, 20 and 10 kilometres. The application of a high-pass filter to a Bouguer Anomaly removes the wavelengths related to regional trend and to the effect of deep and regional masses (e.g. Moho or Ivrea Body), emphasizing the effect of shallow structures

¹⁴ <http://gnss.regione.piemonte.it/frmIndex.aspx>

in the subsurface. This is a crucial step if gravity data will be integrated into a 3D geological model.

As shown in Figure 7-8, the Bouguer Anomaly of the Argentera Massif shows a NE-SE regional trend from more negative values in the NW to higher values in the SE sector, probably related to the influence of the deepening of the Moho in the NW and to Ivrea Body lying in the subsurface at north-east. However the regional trend is removed after filtering and more localized anomalies appear. In particular it is possible to constrain three main negative anomalies which are visible in the three residual anomalies. The first is along the Tinée Valley in the western part of the Argentera Massif, the second NW of the Bagni di Vinadio area, the third spreads towards south from the Valdieri site. These anomalies tend to be more constrained with low amplitude filter, indicating that their source is increasingly shallower. The 10-km filter shows how the three anomalies are restricted to the Isola2000 village area, at the bottom of the Tinée valley and in the surroundings of the thermal sites of Vinadio and Valdieri. The first anomaly is probably related to the quaternary deposits, which covers the crystalline basement in this area, explanation which could also fit the Vinadio area. In fact, according to the shallow wells drilled at the spa, the unconsolidated rock was found in the well VinW01. If interpreting that as glacial till, the cover can be thicker than 115 meters. However it is more likely, also taking into account the geological field observations and the 3D geological model that the lithology crossed by the well owns to the cataclasites of the Bersezio Shear Zone. This lithology is very weathered at the surface, intensely tectonized and fractured, hence it can behave almost as unconsolidated during drilling and during drilling can be easily misinterpreted as unconsolidated cover. The thickness of the deposits at Valdieri is about 2-5 meters. Therefore, for both sites either the quaternary deposits and the topographic influence can be excluded as sources of the negative anomalies. Hence a more geologically complex source might be the cause of the negative anomaly in this area.

Bouguer Anomaly

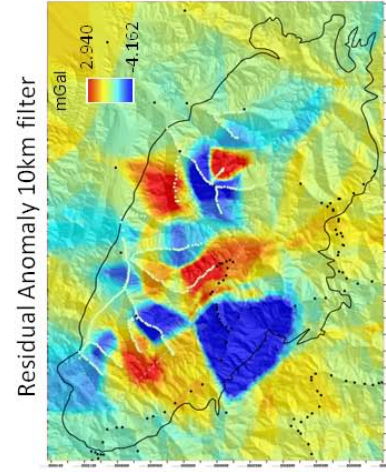
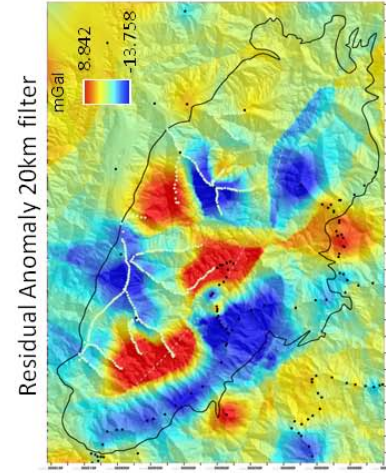
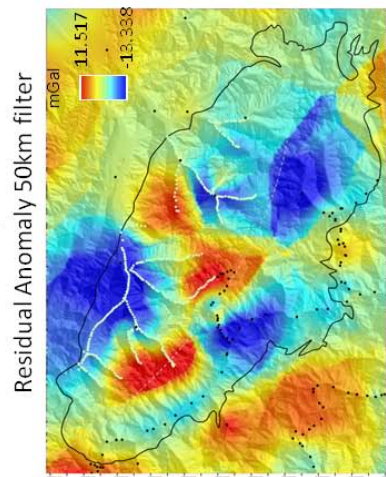
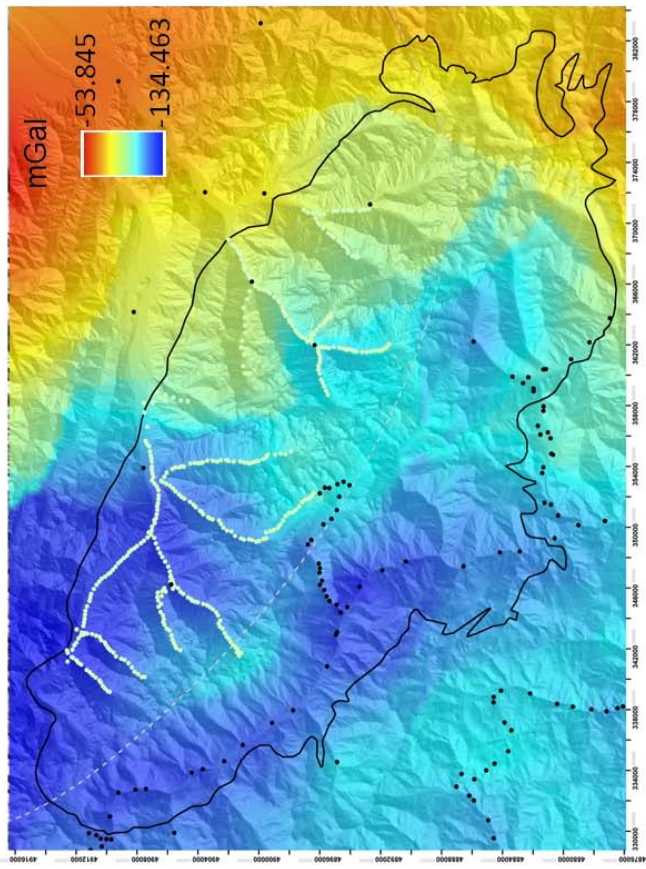


Figure 7-8 Bouguer anomaly of the Argentera Massif and residual anomalies resulting from Butterworth filtering

7.3.4. Integration of the computed models to the 3D geology

The goal of this part was to integrate gravity observations into the 3D models of the Bagni di Vinadio and Terme di Valdieri areas to eventually improve the geological models in the subsurface in terms of density distribution. The main hypothesis was to consider the starting model as any density variation occurred in response to the presence of open sets of fractures. This allowed figuring out whether the gravity survey was able to detect the influence of region of increased fracture density.

The first step was to compare the gravity response of the 3D models to the observed gravity anomaly by means of forward modelling. To compute a forward model the software needs some parameters to be set:

- density of the formations: in this phase the densities measured in the laboratory were considered.
- reference density: 2.67 g/cm^3 accordingly to the reference density employed to calculate the Bouguer Anomaly
- altitude of observations: this parameter has to be set usually for airborne surveys, which account for a constant elevation of observation. For convenience at least one voxel above the highest point of the topography has to be set even for ground observations. If comparing the response of the model to a Bouguer Anomaly, air is replaced by a material having the same density as the reference density, since the observed data no longer contain the effect of the Earth–Air boundary as shown in Figure 7-9 (MCINERNEY, 2007). The main issue adopting this method is to adapt the calculated anomalies to the gravity effect of the model. In fact one side Geomodeller needs the altitude for the observations to be the same for all stations, on the other the field observation are placed on the exact topography. To reduce this gap, an extension towards the reference altitude was set to place all the observations at required reference altitude. This resulted on one hand in a reduction of the overall values of the residual anomaly and also in a loss of accuracy, but on the other it allowed comparing with more reliability the computed effect of the model with field observations.
- reference grid: a grid representing the real Bouguer anomaly can be included to visualize the misfit between field observations and the model
 - the size of the voxel divisions of the geology model: for the study areas it was set to 250m.

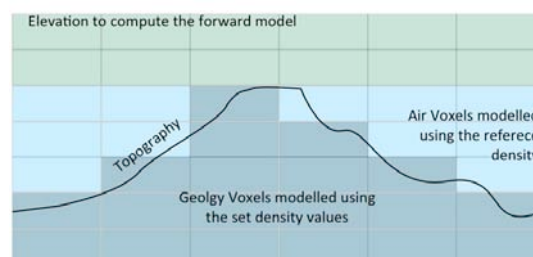


Figure 7-9 Setting for the forward modelling when using fully terrain-corrected Bouguer gravity data (mod. from McInerney, 2007)

7.3.4.1. The Bagni di Vinadio area

The Bagni di Vinadio area is characterized by lithological homogeneity if compared to the Valdieri area. In fact only orto- and paragneiss crop out with the exception of intrusive leucogranite at the eastern border of the study area. Furthermore two mylonitic belts, controlled by the Bersezio and Valletta faults and crossing the entire model from NW to SE, are two important elements in this area. In this region, observations were carried out along the axes of the Corborant, Ischiator, S. Anna and Stura valleys with an altitude range between 896 and 2357 m a.s.l.

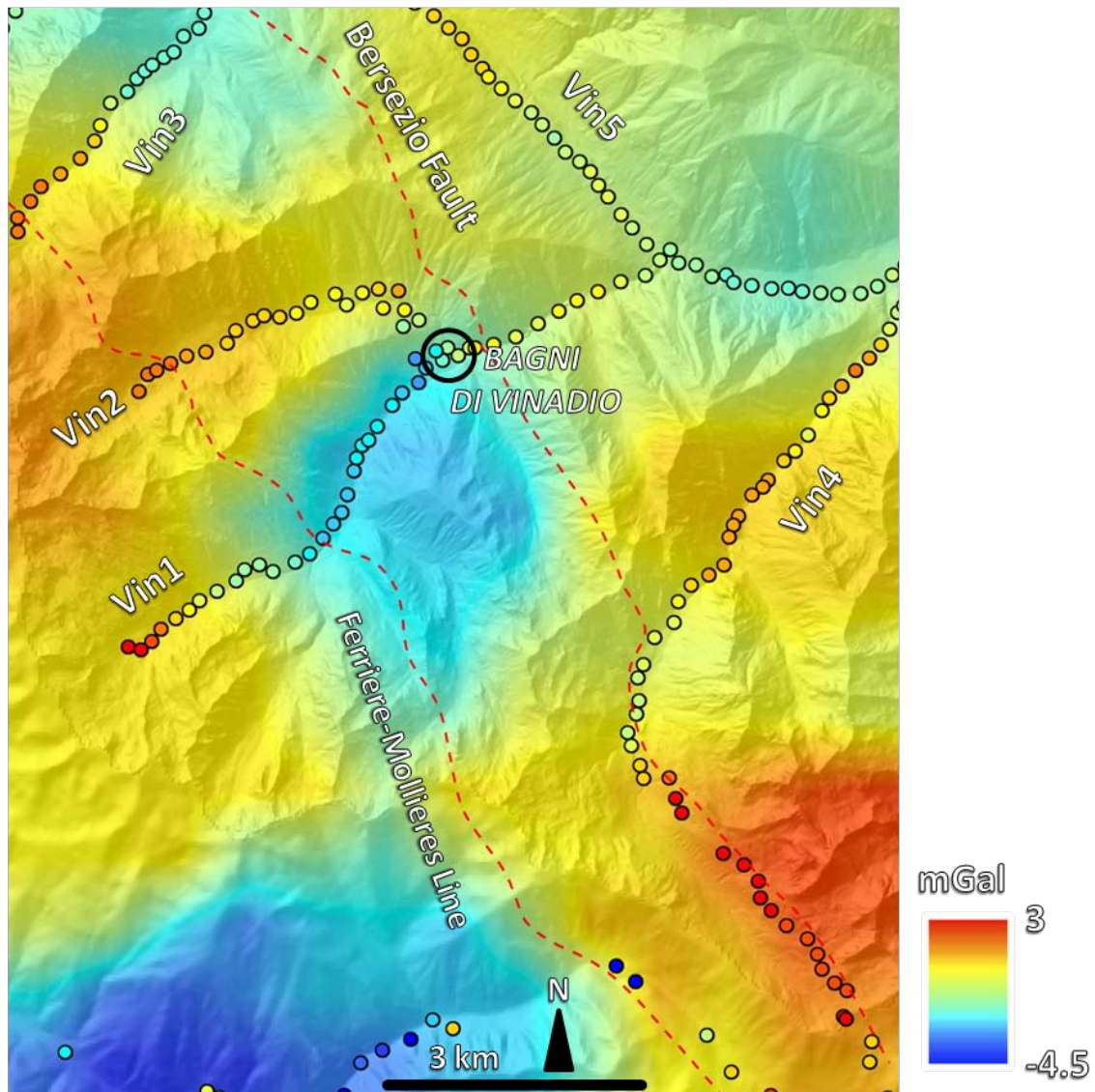


Figure 7-10 Residual gravity anomaly after a 10km filter in the Bagni di Vinadio area

As shown in Figure 7-10, a 4km-long negative anomaly is located at west of the thermal springs, along the Corborant Valley and in the south-western corner of the study area.

Several models were computed combining the different densities of the outcropping formations (Table 7-3) to figure out the right residual anomaly to use in Geomodeller. Once the simulations for each density configuration were calculated, the results were averaged and

then compared to the residual anomalies. As shown in Table 7-4, the 10km residual anomaly showed the lower misfit to the averaged gravity effects of the Vinadio model.

Table 7-3 Measured densities for the outcropping lithologies in the Vinadio region

| Rock Type | Density (g/cm ³) | | | | Porosity |
|-------------------------------|------------------------------|-------|-------|------|----------|
| | min | Max | AVG | SD | |
| Biotitic Anatexite | 2,598 | 2,712 | 2,641 | 0,07 | 0,03 |
| Biotitic and Chloritic Gneiss | 2,655 | 2,795 | 2,717 | 0,08 | 0,01 |
| Embrichite | 2,638 | 2,809 | 2,731 | 0,07 | 0,02 |
| LeucoGranite | 2,578 | 2,673 | 2,613 | 0,06 | 0,03 |
| Leucocratic Gneiss | 2,625 | 2,71 | 2,648 | 0,04 | 0,02 |
| Migmatite | 2,713 | 2,722 | 2,718 | 0,01 | 0,02 |
| Mylonite | 2,617 | 2,794 | 2,682 | 0,11 | 0,02 |
| Cover | 2,619 | 2,708 | 2,664 | 0,05 | 0,01 |

Table 7-4 Example of comparison between gravity effect of the 3D models computed according to different density ranges and the residual anomalies

| | | min | Max | Anomaly range | Anomaly range average | Misfit |
|-------------------------------|-------|---------|--------|----------------|-----------------------|--------------|
| 3D model gravity effect | dmin | -9,098 | -4,983 | -4,115 | | |
| | dMax | 13,434 | 26,768 | -13,334 | -9,155 | |
| | dAvg | 0,363 | 10,378 | -10,015 | | |
| Calculated residual anomalies | Res50 | -12,633 | 9,885 | -22,518 | | -13,363 |
| | Res20 | -5,679 | 6,799 | -12,478 | | -3,323 |
| | Res10 | 1,225 | 8,126 | -6,901 | | 2,254 |

As shown in Figure 7-11, the distribution of the anomalies in the computed models doesn't reproduce the anomalies distribution of the real observations, in particular in the north-western and central parts of the model

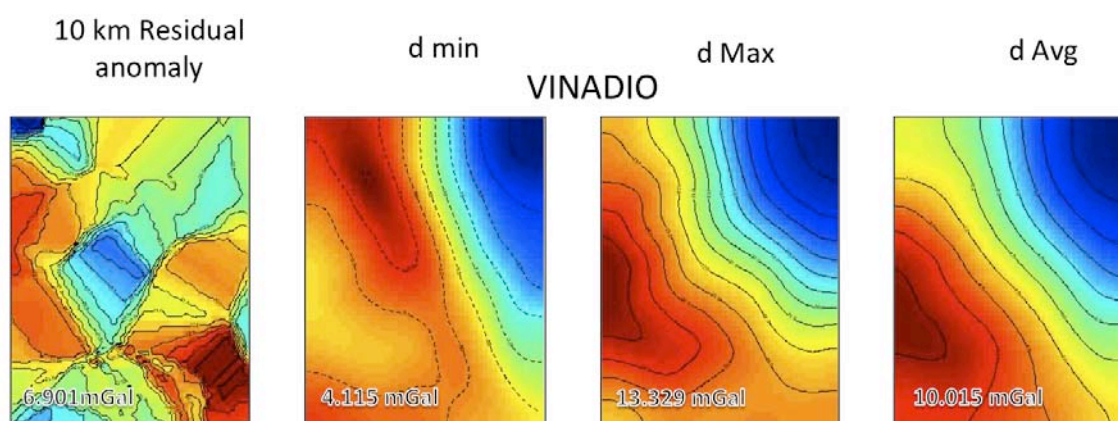


Figure 7-11 Gravity responses of the geological model with different density distributions and comparison to the 10km residual anomaly

The densities were gradually modified, by an iterative process, according to the laboratory data, to reduce the misfit of the model. As shown in Figure 7-12, these modifications brought to better constrain the positive anomalies in the western and

southeastern portions of the region and the negative anomalies in the Northern part. However a misfit still occurred in the central portion of the model and in the SW part, the latter being at the boundary of the model and covered only by very few observations.

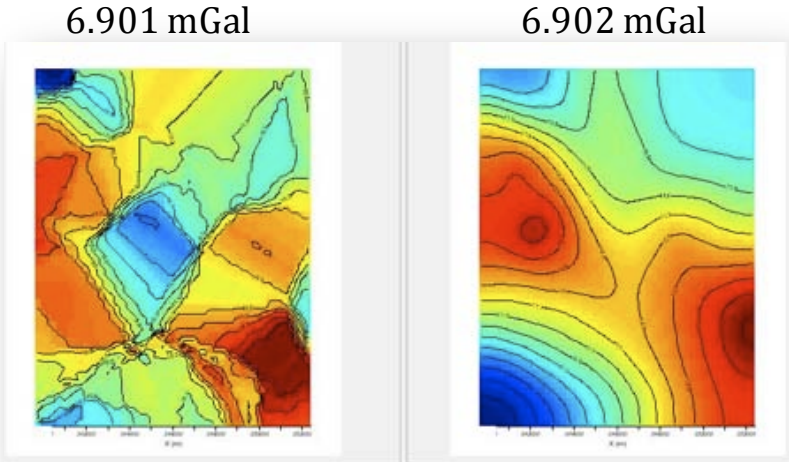


Figure 7-12 Model resulting from the modification of the densities to get better fit with the residual

The concentration was focussed on the identification of the possible sources of the negative anomaly in the springs' region. To exclude the effect of the superficial low density fillings of the main valleys, they were modelled considering a thickness of 200 m, which is quite larger than what shown on the well logs. The effect of the deposits was computed considering a density of 2 g/cm³ gradually lowered to 0.5 g/cm³ to simulate an extreme case. As shown in Figure 7-13, the obtained effect is negligible and does not reproduce the observed gravity anomaly, suggesting that the source of the gravity anomaly is located at depth more than 200 meters and its volume is bigger than the modelled quaternary deposit.

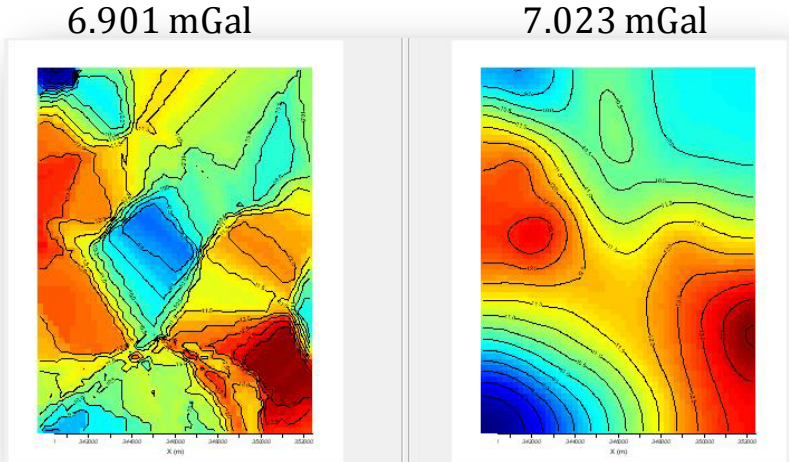


Figure 7-13 Gravity response of the 3D model which includes the Quaternary deposits in the thermal springs area having a density of 2 g/cm³

To reproduce the negative anomaly in the central region, a geological body was introduced into the model. The density initially fixed for this formation was set to 2.42 g/cm³, which represents a density variation of about 250 kg/m³ lower than the average density (2.67 g/cm³) of the formations outcropping in this area. The new formation was

modelled starting from the bottom of the model at a depth of 6000 below topography and then was gradually extended towards the surface until a good fit the negative anomaly values was reached. The results of the proposed model are shown in Figure 7-14, where the anomaly range and the anomalies distribution fits fine the field observations. However, to reach this result the density of the cover formation located in the NE sector of the study area had to be increased up to 2.73 g/cm^3 , which is a higher than the laboratory records.

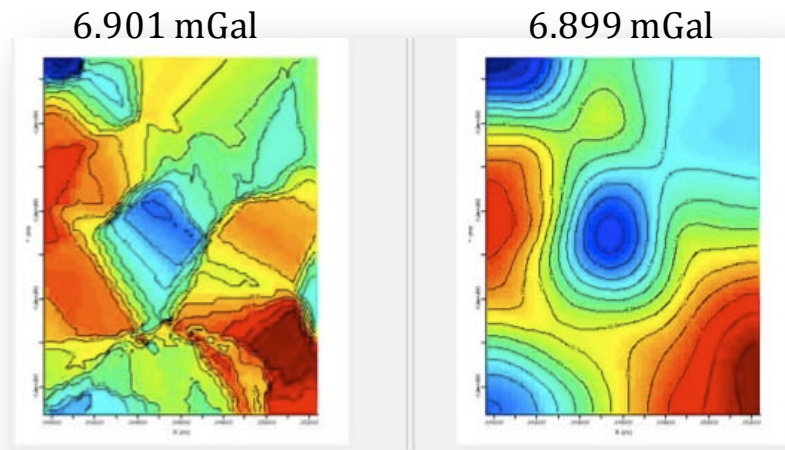


Figure 7-14 Resulting model after introducing a geological body into the model representing a fractured and water saturated formation

As a consequence the lower density body was modified according to the 2D inversions models calculated on selected profiles covering the gravity anomaly. As shown in Figure 7-15, the new geological body was modified and limited by the Valletta shear zone on the West and the Bersezio Fault on the East. A density of 2370 kg/m^3 was finally determined for the body, about 300 kg/m^3 less than the average density of the metamorphic formations. This density variation can be interpreted in several ways. On one hand it can be related to a porosity of 20% of the new modelled geological body, assuming a saturation of 100% with a brine of density 1000 kg/m^3 . However this interpretation seems quite unrealistic both in terms of porosity and presence of fluids in that region. However is assuming the role played only by the fractures, without taking into account the presence of water, hence a saturation of 0%, the porosity decreases to 12%, which is still high but more realistic. Moreover it has to be considered that the negative anomaly is bounded by the Valletta and Bersezio faults. Hence it is located in the step over area between these two strike slip faults, suggesting that these structures might be combined in a unique Fault Zone as proposed by Baietto (2009). The gravity anomaly might reflect the effect of the associated fracture systems, almost perpendicular to the main faults, which are visible north of the springs. The negative anomaly is not totally clear in the Vin2 profile, indicating that the fracture conditions are probably more pervasive along the Vin1 profile, which might justify the presence of the thermal springs at the border of the anomaly in correspondance of the Bersezio Fault, where the fluid circulation might concentrate, supporting the geological observations.

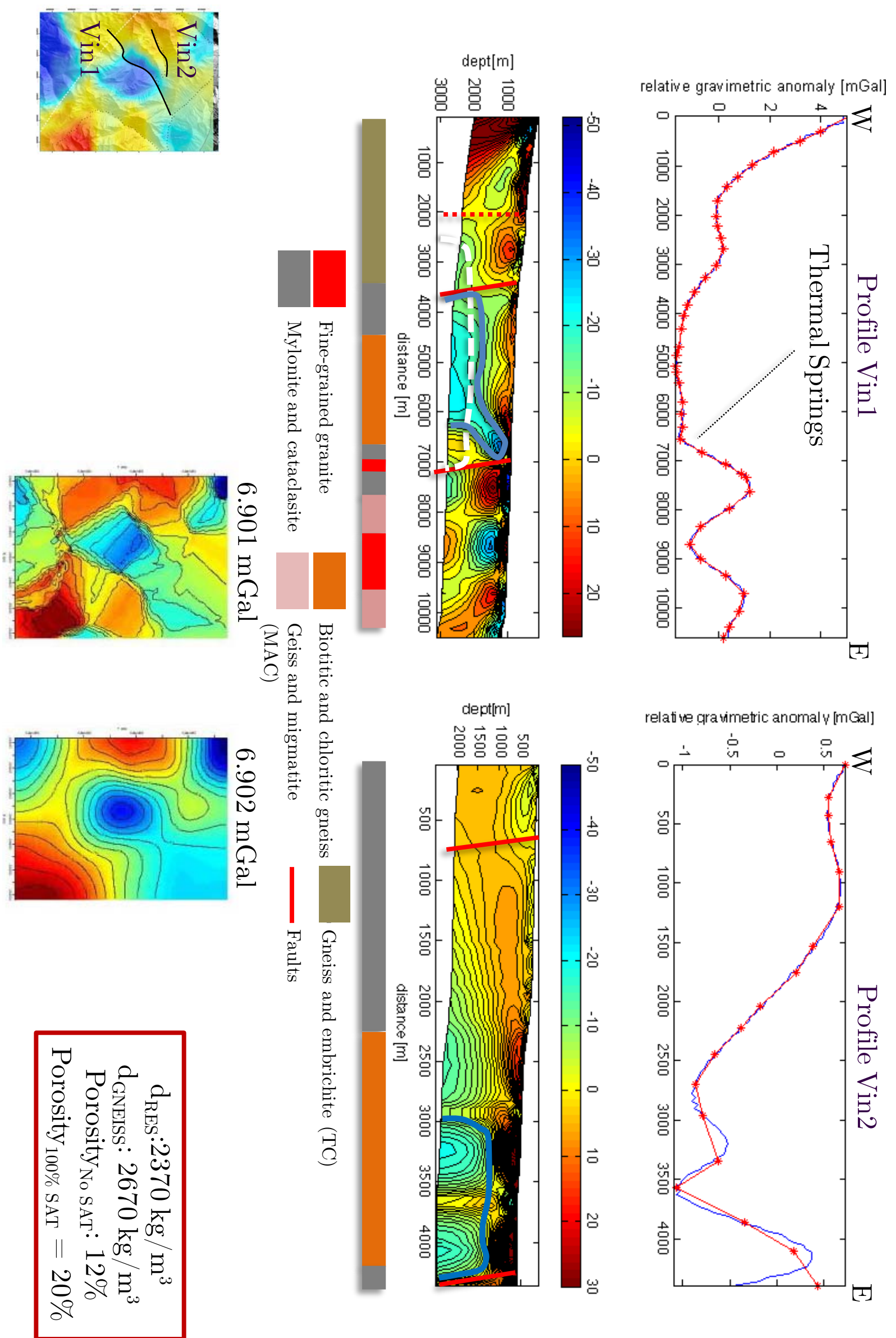


Figure 7-15 2D inversion models used to infer the geometry of the low density geological body and final gravity effect of the model. Dotted line: initial shape; full line: final shape

7.3.4.2. The Terme di Valdieri study area

In the Valdieri area the leucogranite of the Central Granite formation intrudes the Malinvern Argentera gneisses and is crossed by the Fremamorta Shear Zone in the southern part of the model. Moreover the amphibolitic agmatite outcrop North-West of the thermal springs. The observations were collected along 5 profiles following the main valleys. The topography in this region is very rough showing a range between 930 and more than 3200 m a.s.l.

As shown in Figure 7-16, a negative anomaly is located at the centre of the region, in correspondence of the thermal springs.

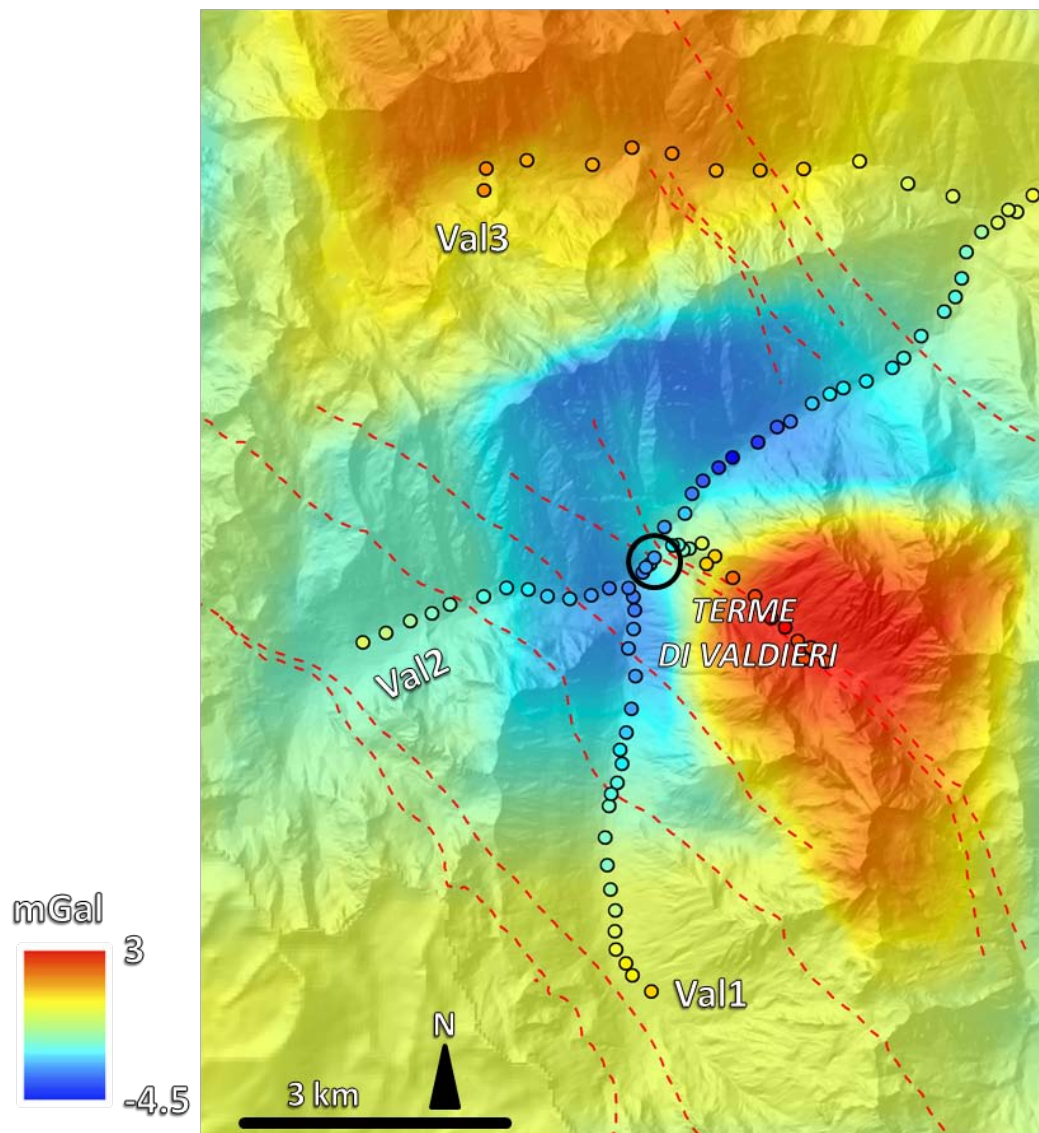


Figure 7-16 Residual gravity anomaly after a 10km filter in the Terme di Valdieri area

The densities initially set, according to the lab measurements, for these lithologies are listed in Table 7-5:

Table 7-5 Measured densities for the outcropping lithologies in the Valdieri region

| Rock Type | Density [g/cm ³] | | | | Porosity |
|-------------------------------|------------------------------|-------|-------|------|----------|
| | min | Max | AVG | SD | |
| Amphibolitic Agmatite | 2,63 | 2,901 | 2,749 | 0,14 | 0,02 |
| Biotitic Anatexite | 2,598 | 2,712 | 2,641 | 0,06 | 0,03 |
| Biotitic and Chloritic Gneiss | 2,655 | 2,795 | 2,717 | 0,07 | 0,01 |
| Embrichite | 2,638 | 2,809 | 2,731 | 0,05 | 0,02 |
| LeucoGranite | 2,578 | 2,673 | 2,613 | 0,05 | 0,03 |
| Mylonite | 2,617 | 2,794 | 2,682 | 0,03 | 0,02 |

Several simulations were carried out to evaluate the effects of the geological bodies taking into account the density range of each lithology. Figure 7-17 shows the gravity response of the models if considering the minimal, maximal and average density values in comparison to the residual anomalies computed on field observations.

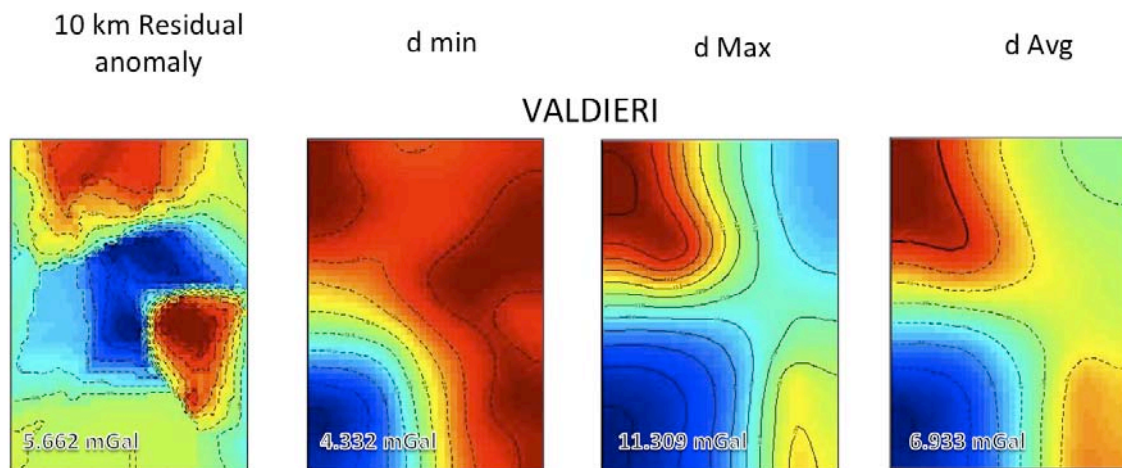


Figure 7-17 Comparison between the residual anomaly and three models calculated with different ranges of density

As for Vinadio a residual anomaly resulting from the application of a 10km high pass Butterworth filter was chosen as reference for the Valdieri area because best fitted the average gravity response of the model (Table 7-6).

Table 7-6 Comparison between gravity effect of the Valdieri 3D models computed according to different density ranges and the residual anomalies

| | | min | Max | Anomaly range | Anolay range average | Misfit |
|----------------------------------|-------|---------|---------|---------------|----------------------------|---------------|
| 3D model gravity effect | dmin | -15,049 | -10,717 | 4,332 | | |
| | dMax | 5,838 | 17,147 | 11,309 | 7,816 | |
| | davg | -7,070 | 0,737 | 7,807 | | |
| Calculated residual anomalies | Res50 | -7,682 | 6,338 | 14,020 | | 6,204 |
| | Res20 | -6,972 | 4,070 | 11,042 | | 3,226 |
| | Res10 | -5,707 | -0,085 | 5,622 | | -2,194 |

In the northern part of the area an amphibolitic body crops out. Amphibolite shows the highest values of measured densities and their effect is reflected in both the observed anomaly and the computed one. However the modelled body just partially covers the recorded positive anomaly. Moreover the negative at the centre of the region anomaly is well constrained around the thermal springs on the residual anomaly but it is not visible on the gravity response of the model.

Firstly the densities of the model were modified keeping the geometries of the formations unaltered until a solution having a good fit in terms of anomaly range was reached (Figure 7-18).

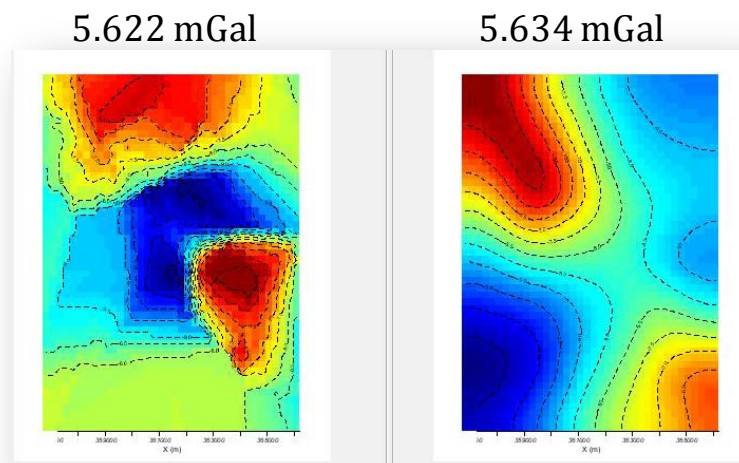


Figure 7-18 Resulting model for the Valdieri area after density modifications to reach a good anomaly range fit between the observed values and the 3D model

However, even though the anomaly range was comparable to the field observations, the negative anomaly was still concentrated in the SW corner of the model, the amphibolites still didn't constrained enough the positive anomaly in the Northern sector and the positive anomaly along the Lorusa valley was not fitted.

As for Vinadio, to exclude the possibility that the negative anomaly might originate from a superficial source such as unconsolidated deposits, these were modelled and their effect was then calculated. The thickness of the filling was set to be 200 m and the density to 2 g/cm³ down to 0.5 g/cm³. It has to be pointed out that the thickness of the alluvial deposits observed in the shallow wells drilled at the thermal spa was around 2 m, hence the modelled formation largely reproduced the real case. Even taking into account the quaternary deposits,

the model didn't show any negative significant variation in the gravity response anomaly (Figure 7-19).

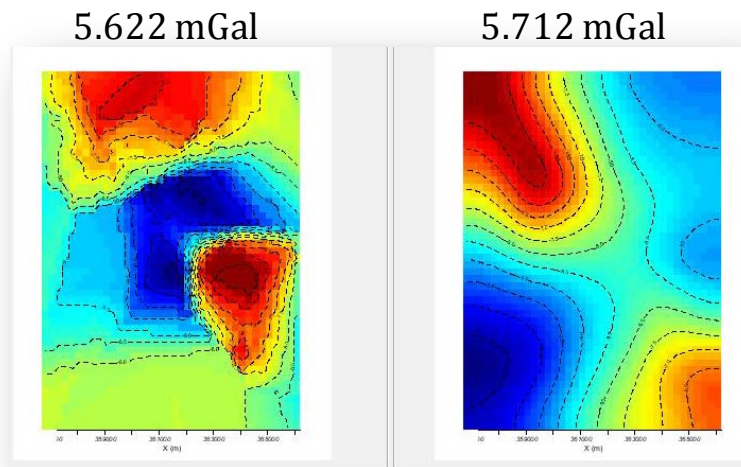


Figure 7-19 Gravity response of the 3D model which includes the Quaternary deposits in the thermal springs area having a density of 2 g/cm^3

Therefore the geological boundary of the amphibolite cropping out north of the springs was modified to cover a larger region towards NE. In addition a new body was created in correspondence of the negative anomaly to simulate the presence of a more fractured and fluid saturated granitic body and the gravity effect, setting a density of 2.4 g/cm^3 for the new body was calculated (Figure 7-20).

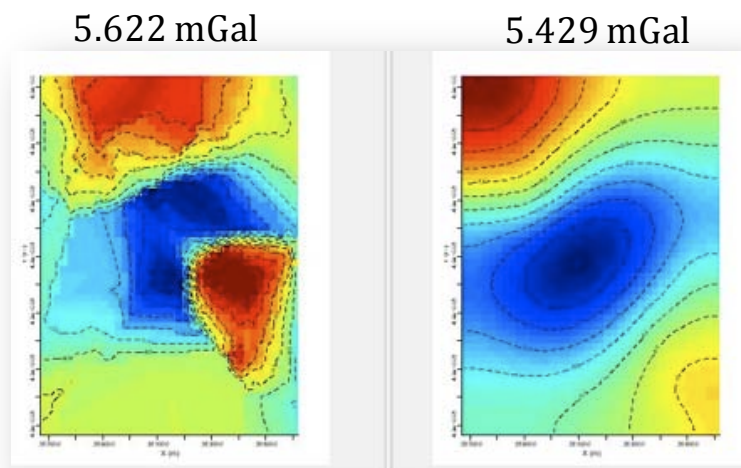


Figure 7-20 Gravity effect of the model after modifying the amphibolites formation and introducing a new body with lower density.

The new results have been more satisfying thanks to the modifications of the model. However to improve the accuracy and the fit with the real anomaly, 2D inversion models were calculated on the observation profiles. As shown in Profiles 1 and 2 in Figure 7-21, a less dense body resulting from the inversion is located at about 500m depth in correspondence of the negative anomaly, while on Profile 3 a denser body is located at the subsurface in the eastern part of the profile. In Profiles 1 and 2 the low density regions correspond to the saturated body previously introduced into the 3D model, whereas in Profile 3, the high

density volume might be interpreted as the amphibolitic body extending in the subsurface underneath the gneiss formation.

Therefore the geometry of the granitic and amphibolitic bodies were modified according to the inversion results as shown in Figure 7-21. This Figure highlights the negative anomaly, more constrained in the western part of the area, the positive values related to the amphibolitic body that is less extend towards NE. With these density values also the density contrasts between formations are more realistic. However the highly positive values in the Eastern part of the model are still affected by incertitude. It has to be marked that observations along this profile covered a very impervious trail in a very narrow valley, therefore some incertitude might be related both to the quality of the observation and to the of accuracy of the 10m DEM, employed to calculate the Bouguer anomaly, which probably wasn't able to totally reproduce the real topography.

The final results show a good fit reached for a density of 2365 kg/m^3 for the granitic body. The observed average density of the granite is 2610 kg/m^3 , hence a variation of 245 kg/m^3 corresponds to a porosity of 15% for the saturated granite with a 1000 kg/m^3 brine and a porosity of 10% in the case of unsaturated granite.

This comparison allows some interpretations. In fact as for Vinadio, the porosity related of the saturated granite seems too high to be realistic. However a 10% porosity might be more reasonable. However this latter value doesn't take into account the presence of water in the subsurface, hence a porosity of the highly fractured granite of about 11% can be legitimate if considering that the Central Granite formation is mainly a zone of widespread infiltration of the meteoric waters. In fact the upflow of the thermal waters is concentrated in the step-over area between the Lorusa and the Cougne strike-slip faults, which form typical flower structure. Moreover in this area the negative gravity anomaly seem to be more intense, in response to the combined effect observed enhanced fracture conditions and the presence of fluids.

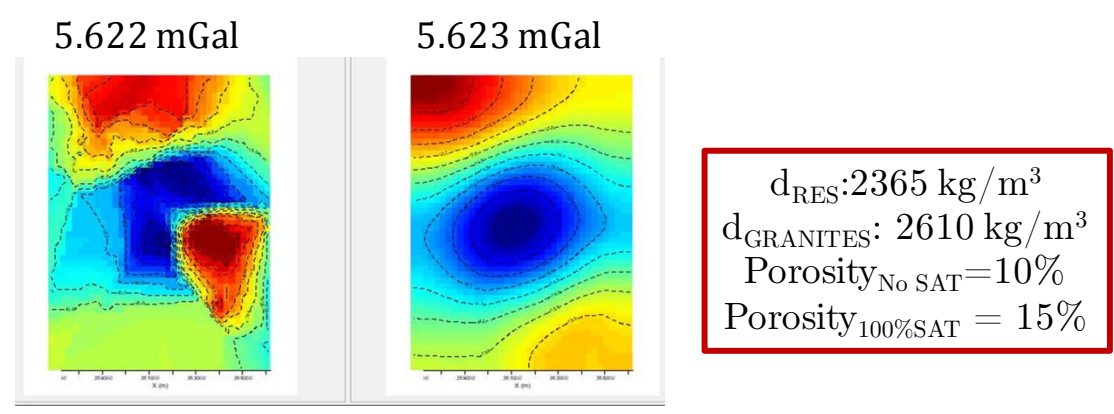
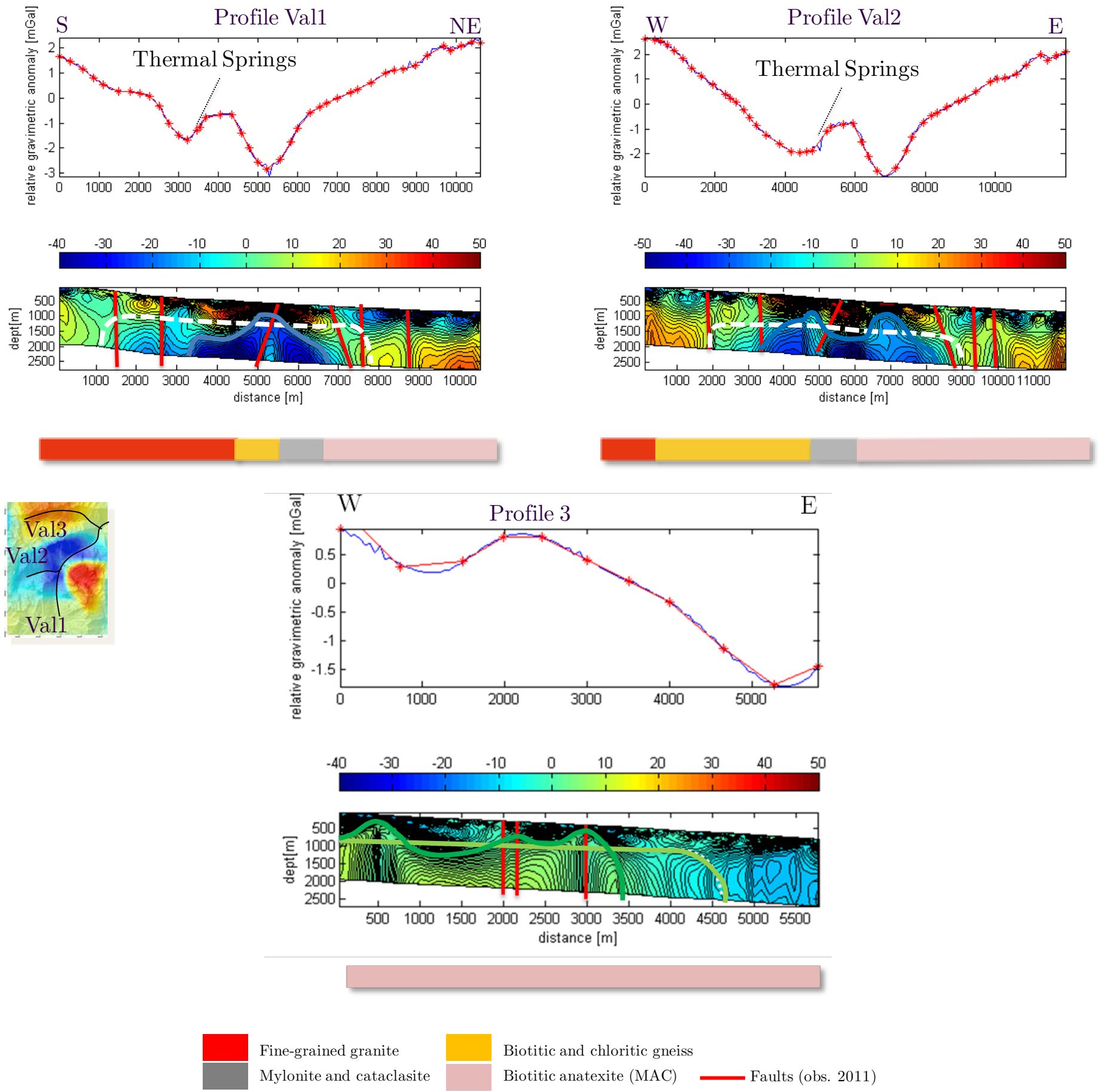


Figure 7-21 2D inversion models used to infer the geometry of the fractured geological body and the amphibolites in the subsurface and final gravity effect of the model. White dashed lines in 2D profiles: initial shape; solid line: final shape

7.4. The Magnetotelluric campaigns in the Argentera Massif

Two MT surveys were accomplished in summer 2010 and spring 2011 in the Italian side of the Argentera Massif (Figure 7-22). The surveys were intended to detect the electrical resistivity distribution up to 10 kilometres in depth and to figure out any relationship between resistivity variations and geological structures. The first campaign was in collaboration with the Institute of Geosciences and Georesources IGG of CNR (Centro Nazionale per le Ricerche) of Pisa and 29 measures were collected. The goal of this campaign was to cover as much as possible the study area. The second survey benefit from the collaboration with the Swiss Laboratory of Geothermics CREGE and The School of Engineering Geophysics EOST of the University of Strasbourg, which provided the instruments. This survey was planned to deepen the exploration of the subsurface in the proximities of the thermal sites.

Even more than the gravity survey, the complex topography prejudiced the amount and the location of the observations. In fact it has been difficult to find some almost flat areas covering a surface at least 600 m² (depending on the employed instrument that require 50 or 100 meter of distance between the electrodes), which were at the same time suitable for digging to bury the electrodes and coils and far enough (1-2 km at least) from villages to avoid the influence of stray currents related to power lines. Therefore the observations are hardly superposed to the gravity stations in the proximities of the thermal springs, where a gravity negative anomaly is evident. Magnetotelluric surveys in granitic areas are often affected by an increase of noise (TEUFEL, 1986). To reduce the noise of the recorded signal, synchronised data recordings were carried out, whether possible, for remote-reference estimation of MT transfer functions. However this procedure was applied only during the second campaign as the first was completed with only one instrument. In spite of these precautions, the signal-to-noise ratio was still high. One of the main causes is related to the topography as its variations in mountainous regions distort apparent resistivity curves and thus lead to artefacts in interpreted models. Moreover in populated areas, electricity power lines produce dominant highly polarised 50 Hz and 150 Hz electromagnetic fields, which can be easily, filtered during data treatment but might induce instrumental saturation. Furthermore field measurements are also susceptible to contamination from ground leakage currents arising from electric railways and electric fences having a broad span of frequencies, making filtering difficult. In the study area any railways is located but small villages, where electric fences and power generators are common.

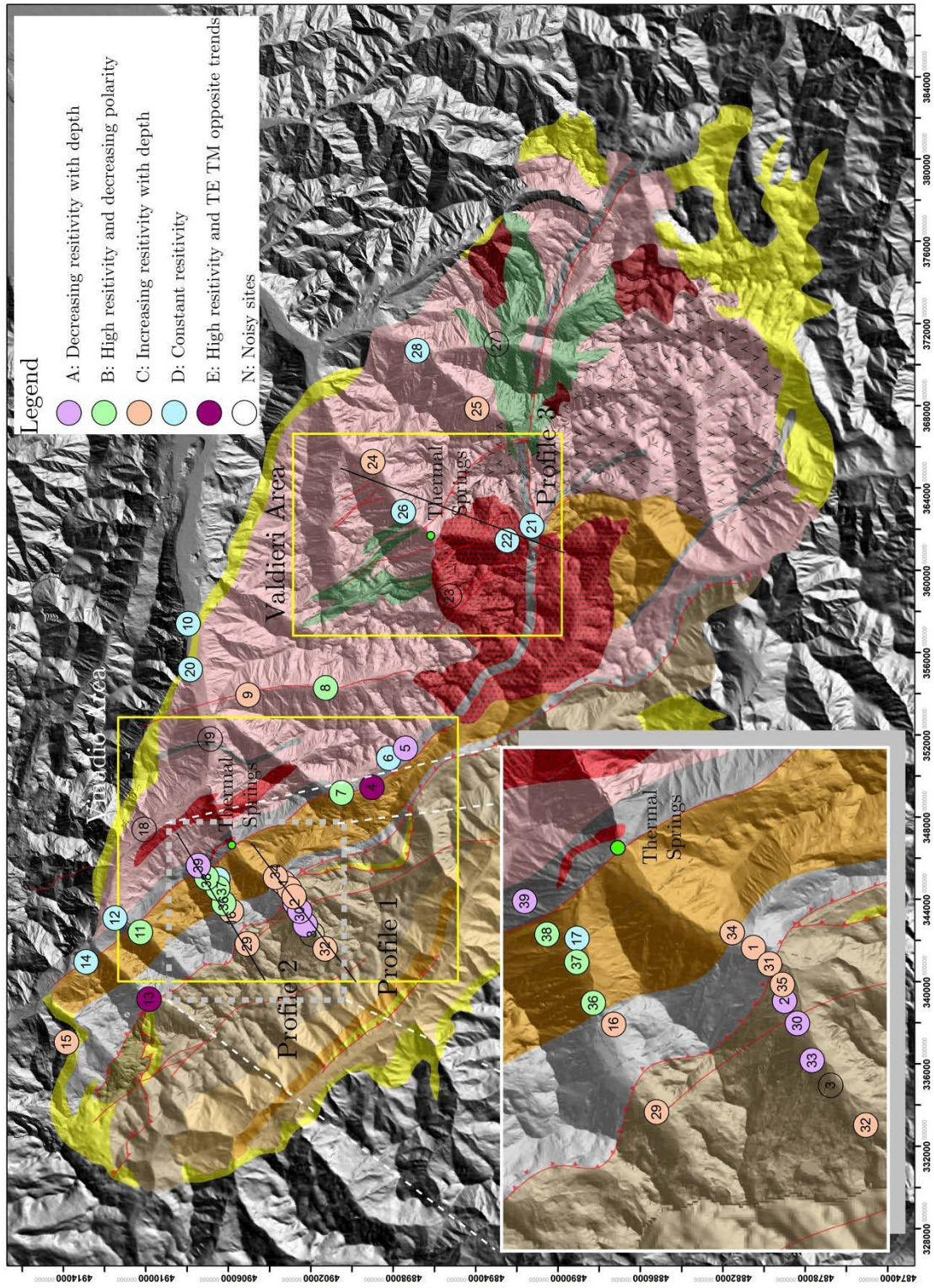


Figure 7-22 Location of the MT sites across the Argentera Massif

7.4.1. Data collection in the Argentera Massif

The first campaign was carried out using a Geometrics Stratagem AMT system. The employed instrument was a four-channels EMI-Stratagem coupled with two kinds of electrodes (non-polarizable and polarizable with a CuS solution) and two coils. This instrument is able to measure frequencies between 0.18 Hz e 96 kHz in five bands. Non polarized electrodes and two Schlumberger BF-6 coils were finally used. The four electrodes were placed at a distance of 50m along the NS and EW axes and the two coils were placed along the N and E direction. The acquired frequency bands were: 10 - 1000 Hz, 500 - 6000 Hz, and 750 Hz - 96 kHz. The sampling frequency for the first two bands was 12 kHz, while for the third was 192 kHz. The recording time was divided into segments (20-40) and each segment was 1 second long for the first two bands and 0.06 second for the third. Moreover the EMI-Stratagem instrument is equipped with real time data processing software, which works as follows:

- data recording of a segment
- the segment is divided in three intervals
- FFT (Fast Fourier Transform) calculation for each segment of each channel
- cross power calculation

These four steps are repeated for each segment and for the entire set of segments and the apparent resistivity values are calculated.

During the second campaign 13 measurements were collected in the Vinadio area using four Metronix GMS-07 systems. These systems include the ADU-07 datalogger (DC to 250 kHz frequency range, ten input channels with a 24 bit A/D converter). Synchronization is accomplished by a GPS clock with +/- 30 ns to satellite reference and positioning. Data are stored on an internal hard disk and are downloaded via TCP connection. Power is supplied by a 12 V external battery. Three magnetometers and two pairs of non-polarisable electrodes are connected to this five-channel data logger. For the registration of magnetic field variations in the range from 0.0001 Hz to 10 kHz broadband induction coil magnetometers MFS-06 are used. The electric field variations are registered by measuring potential inferences with non-polarizable Pb-PbCl-electrodes. The experimental set-up includes four electrodes, which are distributed at a distance of 100 m in north-south and east-west direction. They are buried at a depth of about 45 cm and coupling to the soil is improved using water. The ADU logger and magnetometers are located in the centre, whereas the three induction coils are oriented north-south, east-west and vertical at a distance of 10 m from the data logger and at least 1 m from electric field wires (Figure 7-23). The vertical coil was buried to 2/3 of its length and covered by a plastic tube in order to prevent recordings from the influence of wind. Configuration of the data logger was carried out using GMS207b software (Metronix Inc.). A self-test including internal calibration is carried out automatically upon starting the measurement. Three frequency bands have been measured at each site: The HF band (sample frequency 524 and 32 kHz, frequency range 500-20,000 Hz) were recorded for 30 s; for the LF1 band (sample frequency 4096 and 2048 Hz, frequency range DC-1000 Hz) a recording time of 30 min and for the LF2 (sample frequency 4-128 Hz, frequency range DC-30 Hz) band of 12 hours has been chosen.

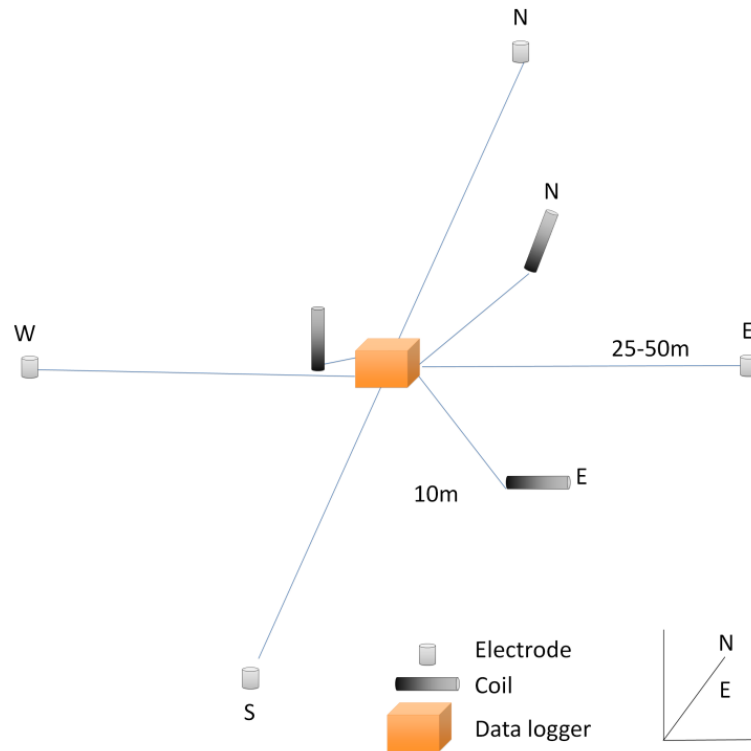


Figure 7-23 Typical set up for a MT sounding

7.4.2. Data treatment

The time series of each station were elaborated to come out with satisfying transfer functions using the tools from the processing software WinGLink[®] by Geosystem. First of all the 50 and 150 Hz frequencies were filtered to remove the known sources of noise and, where synchronized observations were available, remote referencing was applied to reduce the influence of uncorrelated noise. Then entire spectrum of frequencies was processed using WingLink processing tools applies cascade decimation (Wight and Bostick, 1980) to compute power spectra. At each level windows of 32 points are cosine tapered (von Hann-Window) and transformed into frequency domain by computing the 6th and 8th Discrete Fourier Transform (DFT). The estimation of transfer functions is carried out using a modified jack-knife method (Jones and Jödicke, 1984). Each site has been processed by maximizing coherency. Single site processing results could be improved by applying maximization of the multiple coherencies between one of the outputs and both inputs. Generally, remote referencing yields best results. A cross-power editor was used for manual rejection of elements from final stacking, in particular for the period range of 1 to 10 s. This was a crucial step in data improvement and resulted in more consistent apparent resistivity curve with respect to the phase curve.

MT data have been collected in the frequency range between 10^5 and 0.1 Hz using the Stratagem instruments and between 2048 and 2 Hz using the Metronix, frequencies which

assured in the first case a penetration depth of more than 1.5 km and in the second case up to more than 10km

Among the 41 stations 7 had to be rejected as the data resulted too noisy to be treated. Remaining sites still resulted noisy in particular in the lower frequencies and many sites from the first campaign showed a gap in the period range between $9 \cdot 10^{-3}$ and $8 \cdot 10^{-2}$ s as shown in Figure 7-24.

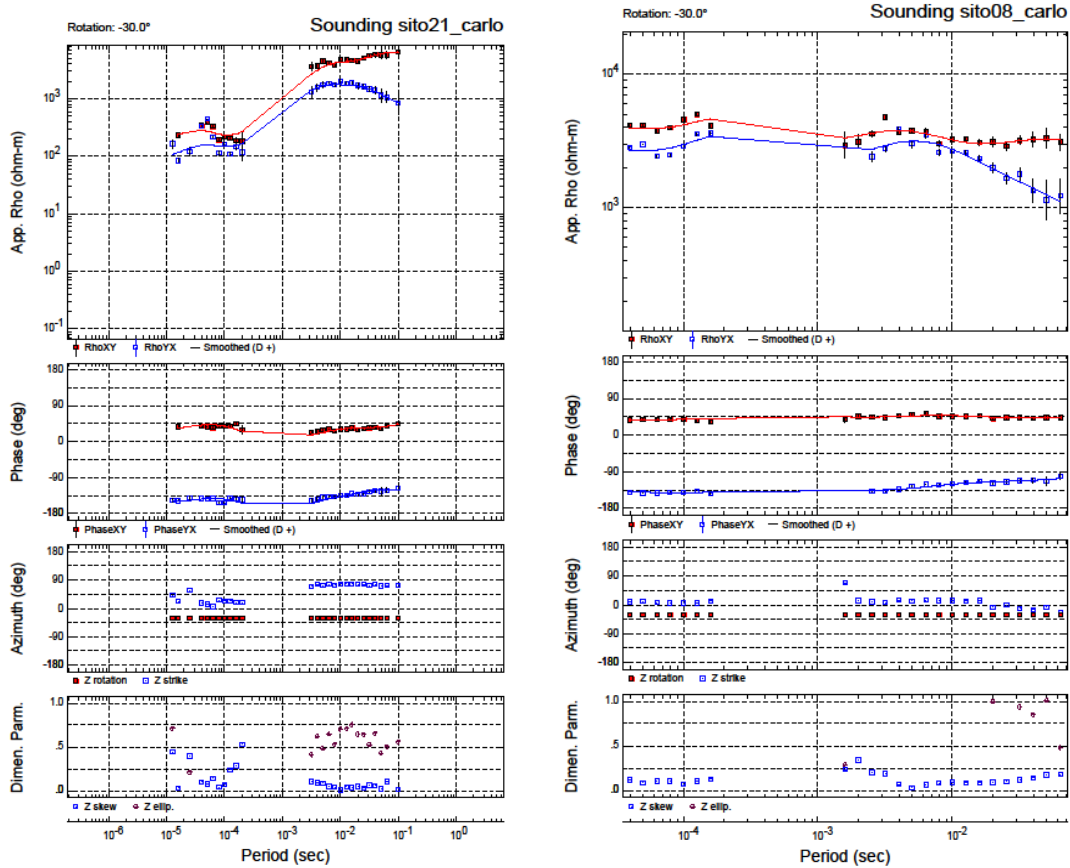


Figure 7-24 Example of MT station having recording issue in the medium period range

The MT data have been edited and modelled. Even though 2D inverted models have been obtained, they resulted poorly indicative for such complex and three-dimensional geologic context. Therefore the interpretations are limited to 1D profiles and the results of the interpolation between the 1D modelling are shown in 2D sections. Nevertheless some considerations can be expressed. For instance observations can be divided into five main groups (Figure 7-25):

- A. Sites where resistivity is high (more than 1000 Ω m) at high frequencies and it decreases with depth
- B. Sites showing a high resistivity and the TM polarity decreases with decreasing frequency
- C. Sites having increasing resistivity with decreasing frequencies. The low resistivity at the high frequencies, hence at the surface, might be due to the fillings of the valleys.
- D. Sites with constant resistivity
- E. Sites showing high resistivity but the polarity TE and TM shows two opposite trends, related to lateral variations of resistivity.

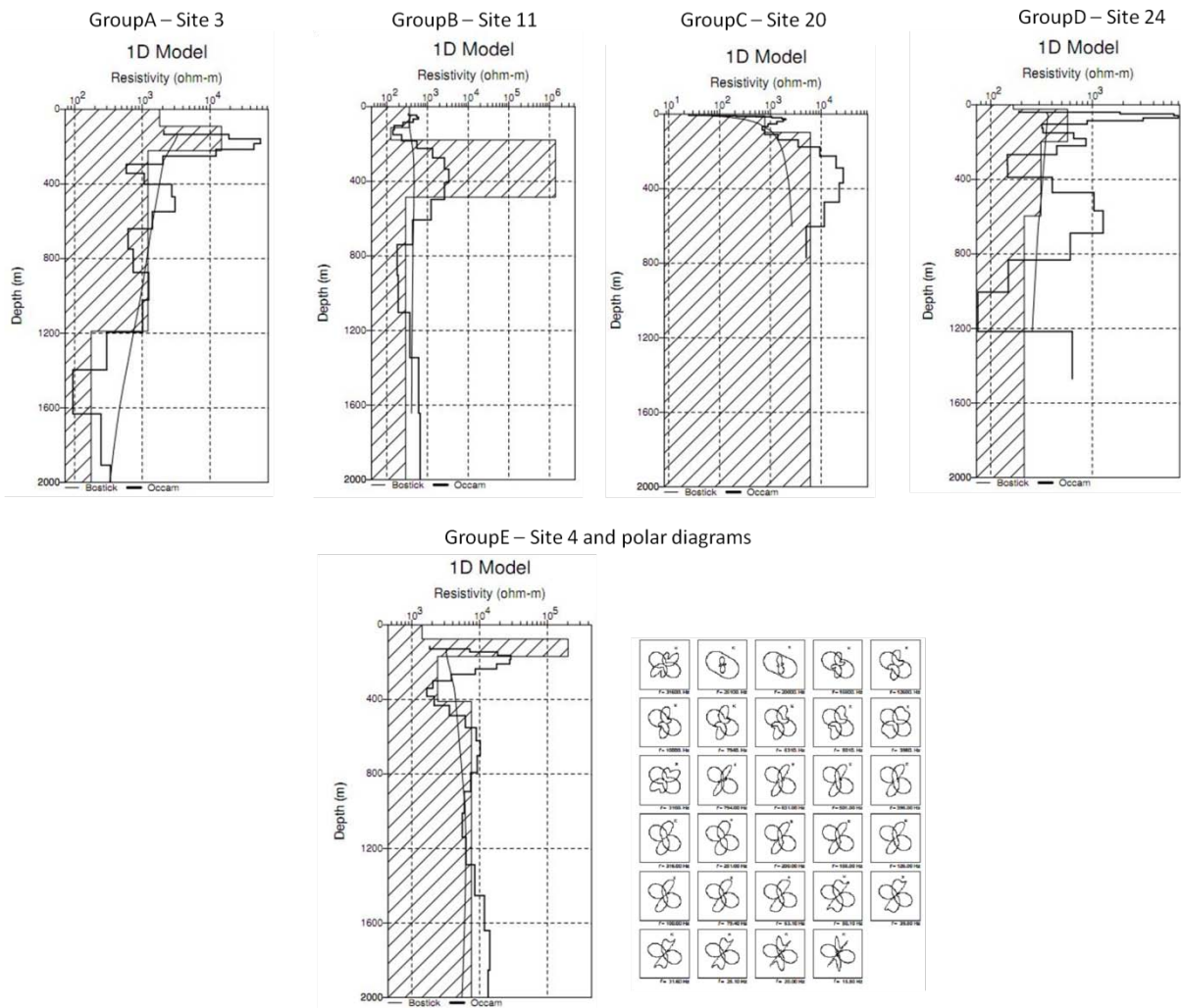


Figure 7-25 1D profiles of MT sites representative of each resistivity distribution

It is hard to correlate the single resistivity distributions to the geological conditions. In fact any

Two dimensional cross section were calculated on selected profiles in the proximities of the thermal site, interpolating the results of the 1D models.

- Profile 1 (Figure 7-26) runs west to east along the Corborant Valley, West of the Bagni di Vinadio Springs, and covers 7 MT stations. This profile crosses the Valletta Shear Zone in the western portion. The 1D profiles and the interpolation 2D section suggest the presence of a low resistivity ($<200 \Omega\text{m}$) zone in the western side of the Corborant Valley at a depth of about 1000m which seems to propagate towards East where a normal fault cuts the section in correspondence of a resistivity anomaly. A second negative anomaly is located at the centre of the section starting from a depth of about 3500 m. This anomaly is located in correspondence of the Valletta Shear Zone. In particular it is possible to see how the resistivity decreases with depth. If assuming that the lithological composition doesn't change, this decrease in resistivity might be associated to intense fracturing where water might circulate. The eastern sector of this section crosses the less fractured and altered gneiss, therefore the increase of resistivity might be justified by these geological conditions.

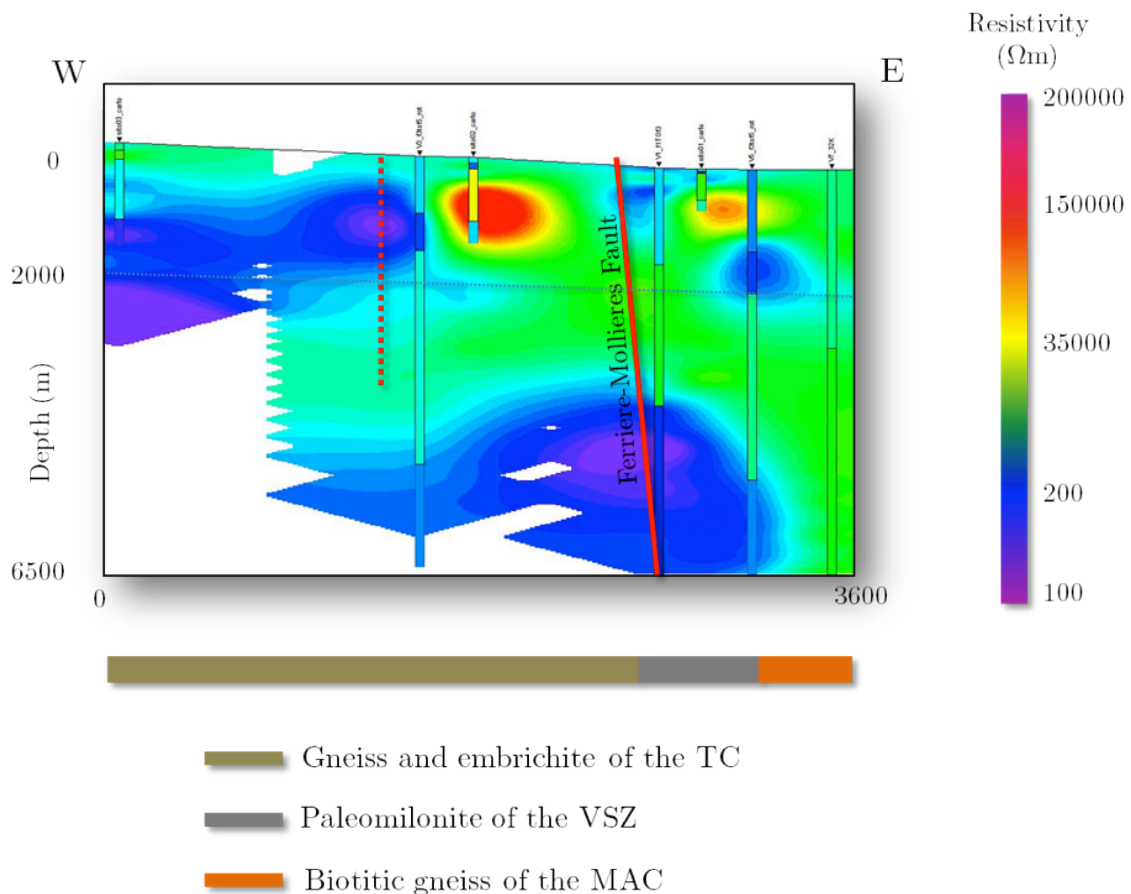


Figure 7-26 Profile 1 section showing the 1D profiles, the interpolated resistivity and the main geological features

- Profile 2, still in the Bagni di Vinadio area, covers 7 stations along the Ischiator Valley, north of the thermal springs. 1D profiles show a very low resistivity zone below the station at the extreme west. In this portion of the section quaternary deposits cover the crystalline formations. Moreover the Ischiator creek runs on these sediments, hence the unconsolidated deposit, coupled with widespread presence of water can be the cause of the low resistivity region at the surface. However another low resistivity region can be observed at about 500 m of depth, which can't be related to quaternary deposits as it's quite unlikely they are such thick. This anomaly is the same observed in Profile 1 and can be linked to the presence of a normal fault possibly linked to the Valletta Shear Zones, as show in Figure 7-27, hence to a zone of enhanced fracture density associated with fracture porosity. The two stations at the extreme East show an almost uniform low resistivity distribution ranging below 100 Ωm . These sites are located in the Bersezio Shear Zone which shows widespread evidences of pervasive cataclasis, which is composed by several sets of fractures

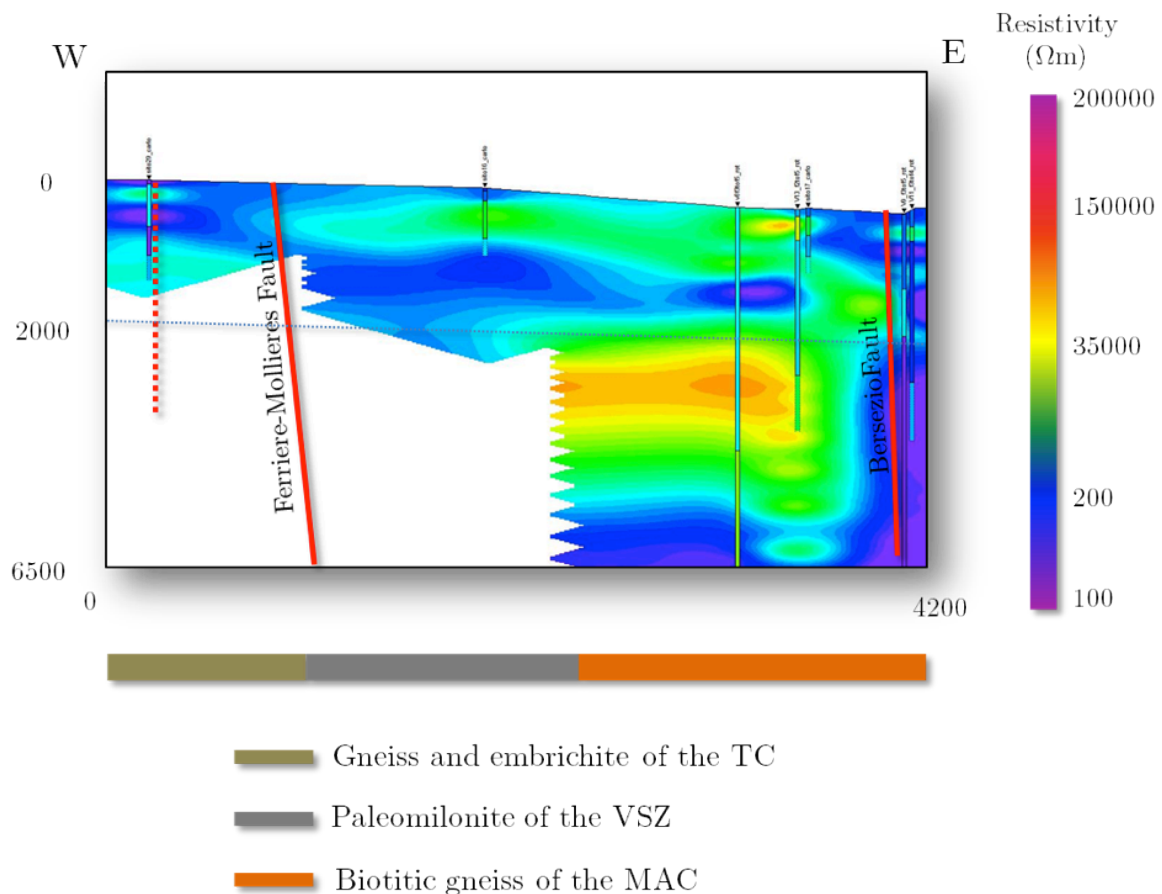


Figure 7-27 Profile 2 showing the 1D profiles, the interpolated resistivity and the main geological features

- Profile 3 (Figure 7-28) is located in the Valdieri area and crossed the Central Granite formations and reaches the Gesso valley, northeast of the thermal springs. Because of the rough topography any observation was carried out in the proximities of the thermal site. This profile connects two measures carried out in the Piano Casa del Re area, south of the thermal site in the Central Granite formation and two sites along the Gesso Valley, NE from the hot springs where amphibolites and gneiss crop out. The first two sites were noisy in the medium frequencies; hence the interpretation was split in two portions. The first reaching a depth of 250 m indicates low resistivity values, which can be indicative of the water saturated quaternary filling of this part of the Valletta valley. The deeper part starts from 1500 m of depth and shows a high resistivity region (100000-150000 Ωm). The two sites along the Gesso valley reveal constant resistivity values ranging between 35000 Ωm in the upper 2000 m and about 10000 Ωm in the second half of the sounding. Site 24 reaches a depth of about 3500m and shows a homogeneous low resistivity Ωm (<200 Ωm).

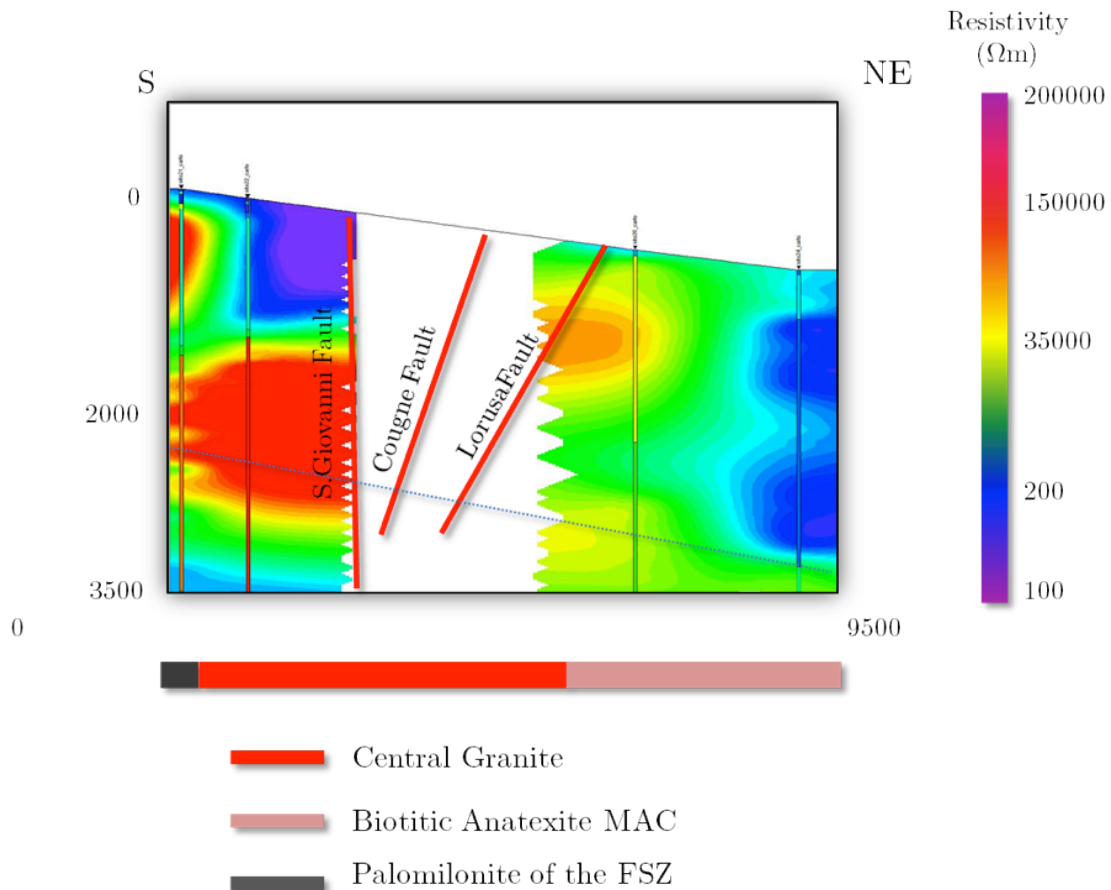


Figure 7-28 Profile 3 showing the 1D profiles, the interpolated resistivity and the main geological features

7.4.3. Joint interpretation with gravity models

Even though the results of MT soundings have been strongly affected by noise and their interpretation is strictly reduced to a description of the resistivity distribution with some link to the geological features modelled in 3D, a comparison between MT, gravity and geology was carried out to figure out if some correlation was possible. However it has to be pointed out that such comparison takes into account the results up to 2 km in depth as the 2D inversion model of gravity data reaches that depth.

- Profile 1 (Figure 7-29) shows correlations between density and resistivity anomalies in several regions. From west to east the decreasing resistivity trend can match to the density profile. Moreover the high resistivity region at the centre of the MT profile can be coupled to the high density region. Another correlation can be observed in the shallower region where a homogeneous medium to high density layer corresponds to an average resistivity portion crossing the entire profile and deepening for few hundred of meters (<300 m). However the formation modelled after the gravity interpretation to represent the “geothermal reservoir doesn’t seem to have a corresponding print in the MT profile.
- Profile 2 (Figure 7-30) shows a low resistivity region is located at about 1000m depth and, in particular in the eastern portion of the profile that seems to correspond to the low density area situated, at the same depth, on the gravity inversion profile, which

was interpreted as a potential area of enhanced fracture density and porosity where waters might circulate. Moreover the external western part of the profile where the resistivity section clearly shows negative anomalies in correspondence of a normal fault, the density distribution shows a superficial medium density that tends to increase with depth as the resistivity does as well. At shallow depth the density shows an increasing density trend from lower values at west to higher values at east. The same trend is shown in the resistivity distribution at about the same depth. However the strong negative resistivity anomaly at East, in association to the Bersezio Fault is not reflected in low-density values. The lack of gravity stations covering this portion of the profile affects the comparison between density and resistivity distribution.

- Profile 3 (Figure 7-31), in the Valdieri area, shows a good correlation with the gravity profile in correspondence at south where a high resistivity body is located at the same depth of a higher density region limited by the S.Giovanni Fault, which gradually switch to a lower resistivity and lower density sector towards the surface. However the lack of MT stations in the central part of the profile doesn't allow comparing the two methods and therefore validate the presence of a highly fractured and water filled formation in the subsurface of the thermal site as interpreted from the gravity data.

Density and resistivity variations can be correlated to porosity φ (expressed in %) variations assuming a saturation level of the rock. A simple equation can be used to estimate the porosity according to density values while the Archie's law is used to correlate the resistivity of a water saturated rock volume and its porosity. The results of these calculation were compared and listed in Table 7-7.

$$\Phi = 1 - (\delta_{RW} - \delta_R)$$

$$\delta_R \cdot x + (1 - x) \cdot \delta_W = \delta_{RW}$$

Where δ_R is the bulk density of the rock measured in the lab, δ_W is the density of water ($=1\text{g/cm}^3$), and δ_{RW} is the density of the fractured and water saturated volume of rock, estimated by 2D gravity inversion and 3D modelling.

Table 7-7 Comparison of the porosity estimated by means of gravity and resistivity parameters

| | Porosity (%) | |
|----------|--------------|-------------|
| | Gravity | Resistivity |
| Vinadio | 8 | 11 |
| Valdieri | 13 | 10 |

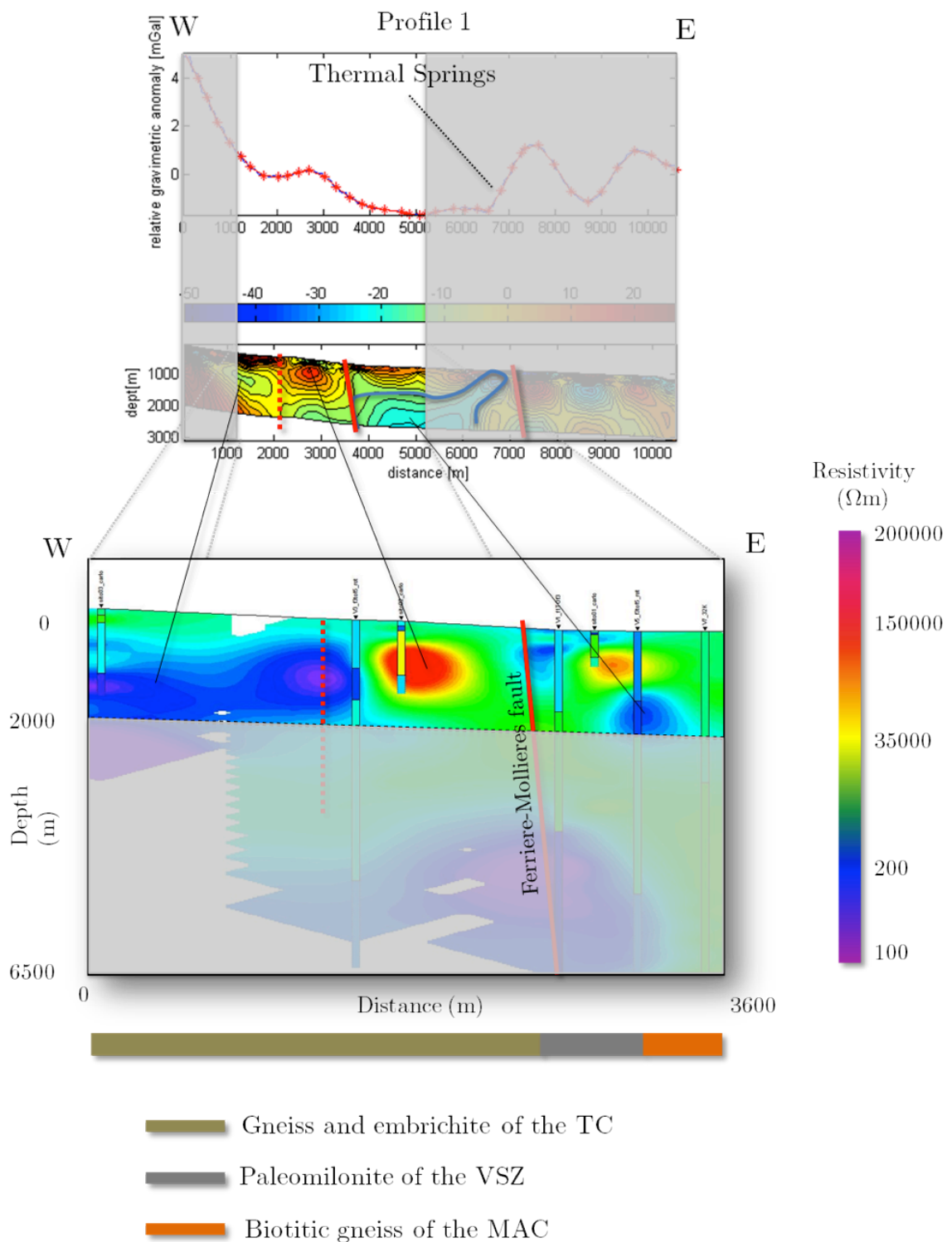


Figure 7-29 Comparison of gravity inversion and resistivity distribution along Profile 1 in the Vinadio area

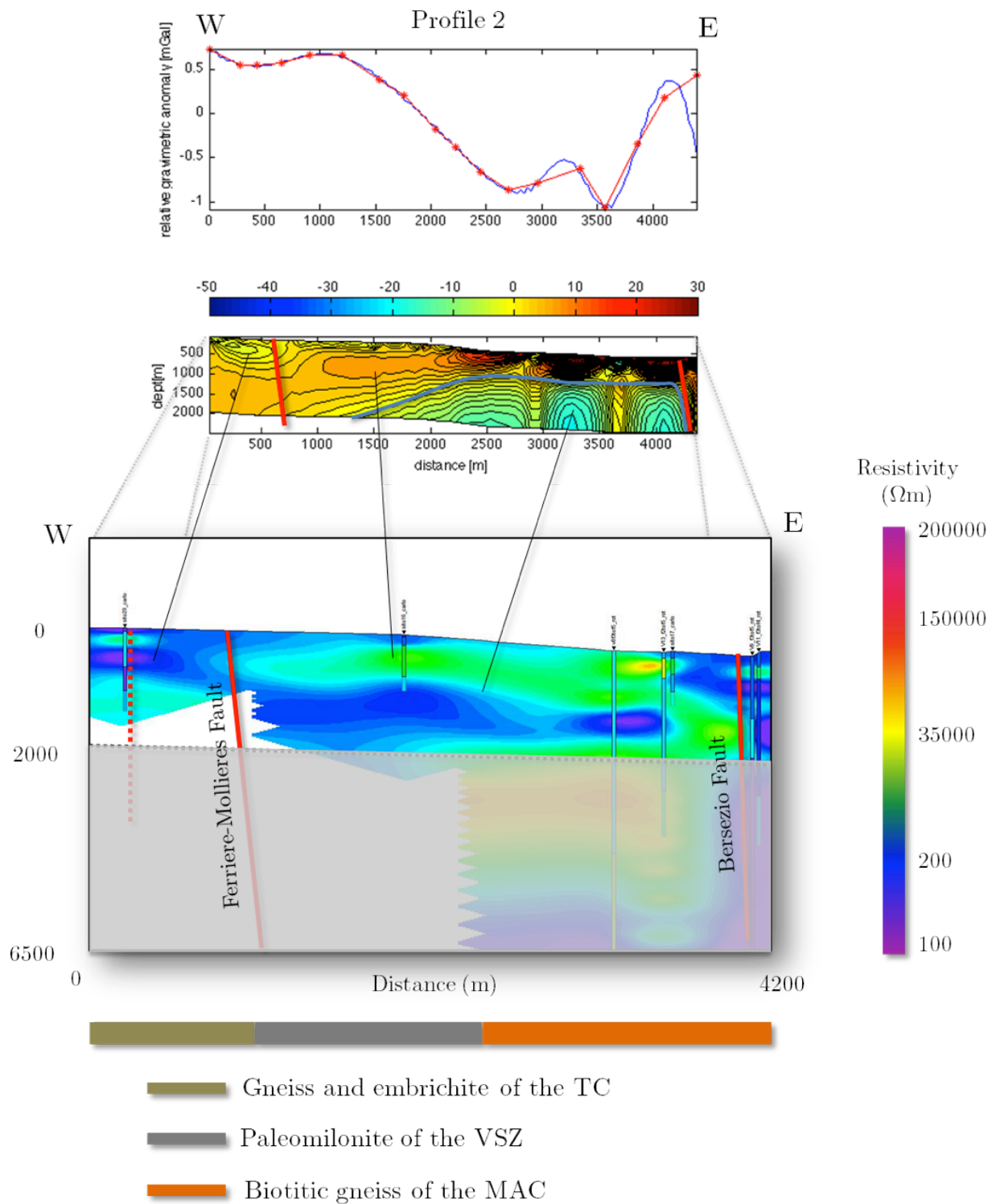


Figure 7-30 Comparison of gravity inversion and resistivity distribution along Profile 2 in the Vinadio area

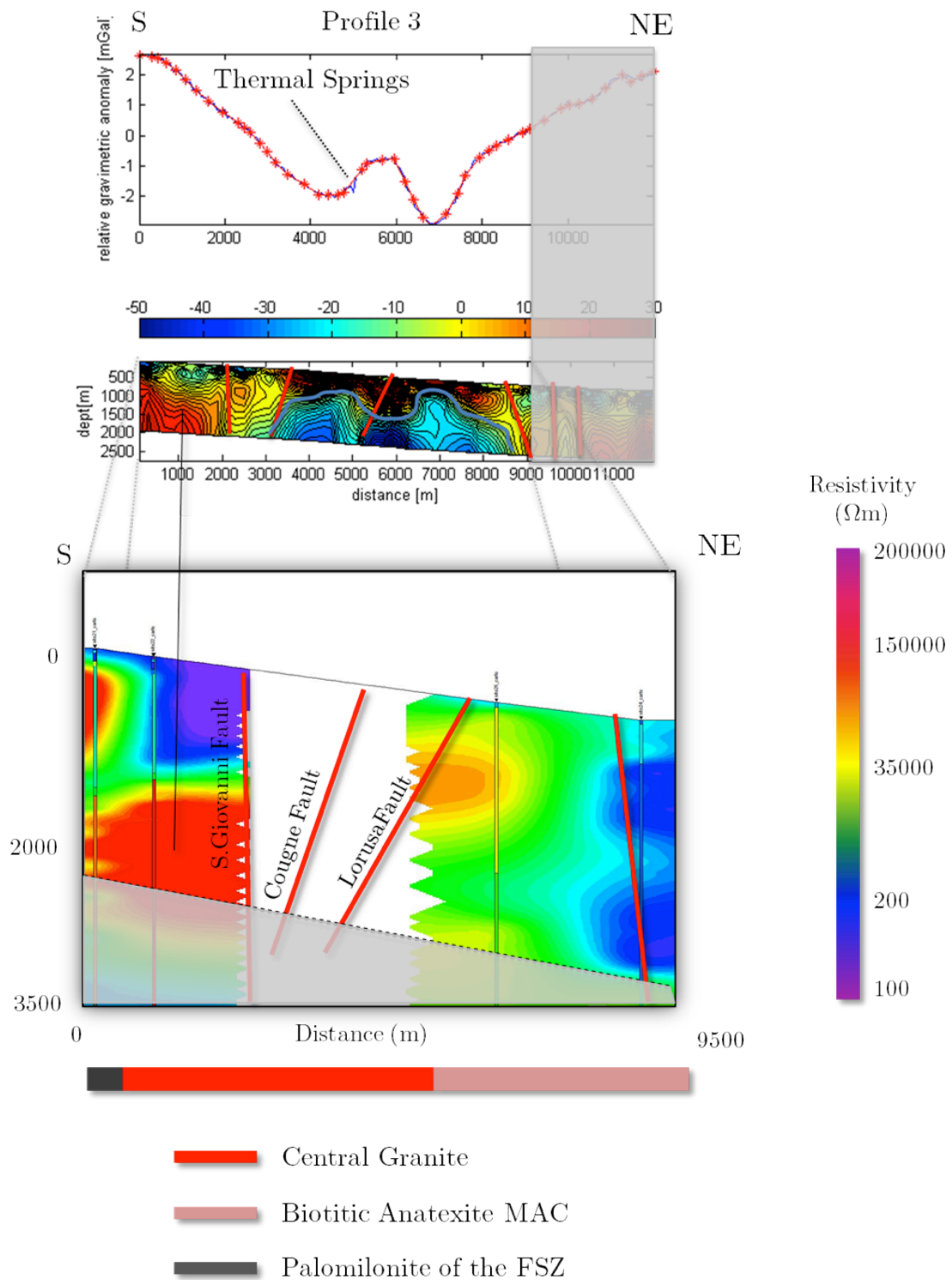


Figure 7-31 Comparison of gravity inversion and resistivity distribution along Profile 3 in the Vinadio area

8

EVALUATION OF THE GEOHERMAL POTENTIAL AND USAGE PROPOSALS

One of the main questions in geothermal resource assessment is the estimation of the quantity of resource that can be extracted and the duration of the exploitation at economical conditions. Low enthalpy fluids, such as those at Vinadio and Valdieri, are mainly exploited for thermal baths, but it is important to find out if more usages can be proposed to optimize the management of the resource. Moreover developments in binary power plant technology, using Organic Rankine Cycle (ORC) or Kalina Cycle, have led to electric power generation from systems with temperatures as low as 75° C, e.g. in Alaska at Chena Hot Springs (ANEKE et al., 2011; ERKAN et al., 2008) and lower temperatures is possible, if not always economically viable at the present time.

This part of the thesis deals with some estimations of energy production (heat or even electricity) and the utilization proposals of the thermal waters at Vinadio and Valdieri taking into account the available data resulting from the multidisciplinary approach described in previous chapters of this work. It should be noted that no economical consideration will be accounted as these aspects are not part of the main goal of this study but will be an interesting point to deepen in further studies.

8.1. Geothermal Potential Estimation Methods

The geothermal potential of a site can be divided into thermal energy and electrical power outputs, which can be extracted from the geothermal fluid. The former can be assessed using the *Surface Thermal Flux* (GRINGARTEN, 1978) and the *Volume* (MUFFLER and CATALDI, 1978) methods. The latter can be estimated using the *Net Electric Power* (DICKSON and FANELLI, 2005) and the *Exergy* (DI PIPPO, 2008) methods. Table 8-1 shows the parameters used to calculate the geothermal potential using the methods described in the following paragraphs.

Table 8-1 Parameters used to compute the geothermal potential

| Parameter | Unit | Parameter | Unit | | |
|------------------------------|---|----------------------|-----------------|--|----------------------|
| a | Surface occupied by the springs | km ² | q | Basal heat flux | W/m ² |
| ATP | Available Thermal Power | kW | q _R | Heat stored in the geothermal reservoir | W _{TH} |
| C _W | Heat capacity water | J/cm ³ °K | q _S | Conductive heat flow | W _{TH} |
| E | Exergy | W _{EL} | q _W | Heat recovered at the surface | W _{TH} |
| h _{WH} | Enthalpy of the produced fluid at the well head or at the surface | J/Kg | ρ | Density | kg/m ³ |
| h ₀ | Enthalpy at the dead-state temperature | J/Kg | ρC | Volumetric heat capacity | J/cm ³ °K |
| h _{IN} | Enthalpy of the plant inlet fluid | | R _G | Recovery Factor | |
| h _{OUT} | Enthalpy of the plant outlet fluid | J/Kg | s ₀ | Entropy at the dead state temperature | J/Kg °K |
| m _S | Extractable mass flow rate | kg/s | s _{WH} | Entropy of the produced fluid at the well head or at the surface | J/Kg °K |
| m _{WH} | Mass flow rate at the surface | kg/s | T _R | Temperature of the reservoir | °C |
| NEP | Net Electric Power | kW | T _W | Temperature of the extracted fluid | °C |
| η ₀ ^I | Overall plant efficiency based on the 1 st Law | | T ₀ | Dead-state temperature | °K |
| η ₀ ^{II} | Overall plant efficiency based on the 2 nd Law | | V | Volume of the reservoir | m ³ |
| Q | Maximum rate of heat transfer (thermal power) between the system and the surroundings | kW | | | |

8.2. Surface Thermal Flux method

The method of *Surface Thermal Flux* or *Heat in Place* is based on the calculation of thermal energy that can be transmitted from the subsurface to the surface by conductive heat flow. This method can be usually employed if the available information is limited to temperature and flow rate of thermal springs. The natural thermal power (P) is the obtained value from the equation:

c

Where the conductive heat flow is

$$q_s = a \cdot q$$

and the thermal energy contained in the fluids effluent is:

$$q_w = Q \cdot \rho C_w \cdot (T_w - T_0)$$

This method can be applied for a simple development scheme for heating project, consisting in producing geothermal water without reinjection at depth. In this case the water would be produced at constant temperature as long as the resource is available and the pressure conditions are sufficient for the production to be sustained.

8.2.1. The Volume method

The *volume method* is one of the key methods applied, e.g. by the USGS, as a standard approach, to assess the production potential of identified geothermal systems. The heat generation potential depends on the thermal energy present in the reservoir, its volume, temperature and physical conditions.

In the volume method, the thermal energy, also called *heat in place*, is calculated as:

$$q_R = \rho CV(T_R - T_0)$$

The USGS Open-File Report 2008-1296 (WILLIAMS et al., 2008) suggest some default parameters to estimate the reservoir volume. In fact, in some cases, information about a geothermal system is limited to the temperature and flow rate at the surface and to the geochemical composition of the hot springs discharging along fault damaged zones. Therefore the width of the fault zone constrains one horizontal extension of the reservoir, the default value along-strike extent ranges between 1 and 5 km, most likely 2 km, and the vertical extent is defined by the reservoir temperature relative to the average geothermal gradient of the study area.

The thermal energy that can be extracted at the wellhead is given by

$$q_s = m_s(h_{WH} - h_0)$$

where m_s can be approximated to Q in eq.1.

The wellhead thermal energy produced over a time span period of usually 30 years (KOHL et al., 2003), can be related to the total energy in the reservoir by the recovery factor, R_G , defined as:

$$R_G = q_S / q_R$$

8.2.2. Net Electric Power Method

For pre-feasibility studies aimed to estimate the electric power generation that can be derived using organic Rankine cycle to convert thermal energy from a flowing fluid source, the following equation can be used (DICKSON and FANELLI, 2005):

$$NEP = [(0.18T_R - 10) \cdot ATP] / 278$$

NEP is the Net Electric Power (kW) that can be generated by a binary plant using a low to medium enthalpy geothermal fluid. To calculate the ATP parameter, is the available heat from the geothermal flow and is conventionally calculated over a temperature 10°C higher than the bottom-cycle temperature, which is usually 40°C (DICKSON and FANELLI, 2005; GARG and COMBS, 2011). The member

$$(0.18T_R - 10) / 278$$

is the Net Conversion Efficiency, which corresponds to the rate between NEP and ATP and allows estimating the amount of thermal power which can be converted in to electric power.

8.2.3. The Exergy concept

One of the approaches to measuring the performance of an energy system is to use the Second Law of thermodynamics as the basis of the assessment because geothermal binary plants can be assumed as open systems operating in steady state. A system may receive or discharge from or to the surroundings and exchange heat and work with the surroundings. To seek the maximum output from the operation of the system, two thermodynamic conditions must be met:

- all processes taking place within the system must be reversible.
- the state of the fluids discharged from the system must be in thermodynamic equilibrium with the surroundings. It means that the discharged fluid has no more work to do relative to the surroundings. This allows defining the *dead state* temperature that is the temperature at which the fluid is in thermodynamic equilibrium with the surrounding, therefore there is no potential for doing work. Usually the dead state refers to the ambient temperature.

The Exergy E (DI PIPPO, 2008), can be determined as:

$$E = m_S \cdot [h_{WH} - h_0 - T_0 \cdot (s_{WH} - s_0)]$$

T_0 is expressed in °K.

Exergy can be defined as “*the maximum available work or power output that could theoretically be obtained from a substance at specific thermodynamic conditions relative to its surroundings*” (DI PIPPO, 2008).

In this approach the main questions regard on the definition of the volume of the reservoir and its physical parameters. Thanks to the geochemical, geological, geophysical data collected and the 3D modelling computed in the framework of this thesis, it was possible to estimate the volume of the reservoir and its porosity.

Although exergy is strongly related to the 2nd Law, it is also grounded to the 1st Law in which the mass is conservative in steady state open systems. The 1st Law approach allows understanding how geothermal binary plants are relatively poor converters of heat to work; therefore the choice of the most efficient working fluid is a crucial phase in designing such a power plant. The 1st Law efficiency is about 10%. However this plants might work with a higher 2nd Law exergetic efficiency where the motive fluids are at low temperature thanks to the design of the heat exchangers to minimize the loss of exergy during heat transfer process.

Therefore it is a simple approach comparing the conversion of Exergy to electric power to the conversion of heat in electric power by means of the 1st Law of thermodynamics:

$$Q = m_{WH} \cdot (h_{WH} - h_0)$$

The electrical power output, usually over a period of 30 years, is then calculated through multiplying the Exergy over an efficiency factor η_0 , which is averaged over the observed performances of several power plants at different thermodynamic conditions. For instance for temperature above 150°C, a value of 0.45 can be used {Lovekin, 2004 #113}. However the efficiency shows a linear decline down to 0.2 for temperature below 150°C, which can be exploited for power generation by means of binary power plants, as shown in Figure 8-1.

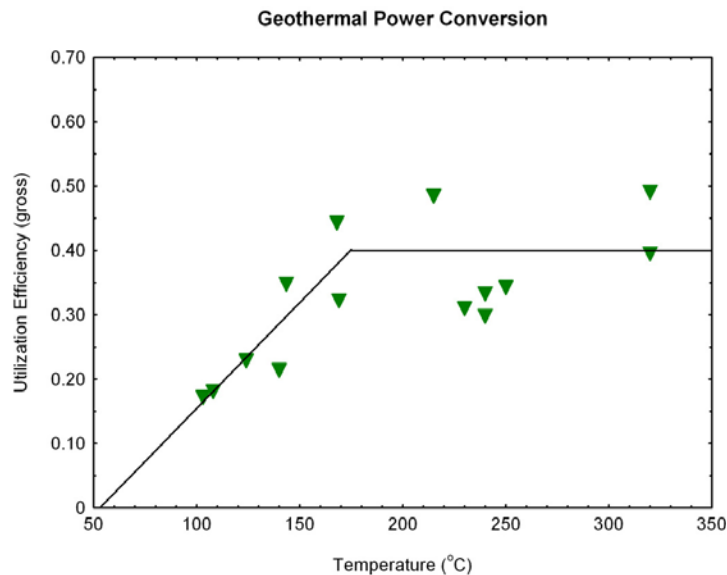


Figure 8-1 Utilization efficiency as a function of temperature for existing geothermal power plants studied by DiPippo (2005) (green triangles), along with the conversion relationship used in the new assessment (black line).

8.3. Estimations for the Study Areas

In the case of the Vinadio and Valdieri thermal areas all the above mentioned methods were applied and the results were compared to some real cases where the conditions are similar in terms of temperature and flow rate.

For the calculation some assumptions had to be taken into account:

- the available data of temperature, basal heat flux, reservoir volume, rock density and porosity were obtained from direct observations, 3D modelling or from previous studies carried out in the study area.
- the flow rate used is that measured at the surface. Any estimate has been taken in the case of new boreholes drilled to increase the production of thermal fluid. Therefore it is a conservative assumption as it is likely that part of the geothermal fluid flow is dispersed in the rivers and in the shallow sediments.
- as the measured flow rate is natural, any increased exploitation of the reservoir fluid has been forecast, therefore any reinjection of the fluid has been estimated.
- the geothermal gradient in paragraph 8.3.2 is the average regional gradient of the area (BAIETTO, 2006b), which only accounts for conductive heat transfer. It is plausible that the local gradient at the thermal sites might be much higher, due to the local and fast upflow of the thermal fluids and therefore to the consequent convective heat transfer. Convection might increase the gradient up to some hundreds of degree (°C) for kilometres, e.g. Lavey les Bains, where temperature of 62 °C were found at only 200 m in depth during drilling (SONNEY, 2011). However any data is available to confirm this hypothesis for the study sites.

8.3.1. Surface Thermal Flux

To calculate the Surface Thermal Flux (Table 8-2), the average of the temperature measured at springs and wells was considered. Moreover the surface covered by thermal springs is localized in a 100x100 m surface; the flow rate was estimated by direct measurements on the field during sampling campaigns and compared to those from previous studies. Temperature values refer to the average temperature of the thermal waters at the surface. The flow rate values, set to be 20 kg/s at Vinadio and 50 kg/s at Valdieri (BAIETTO, 2006b). These values refer to field observations and, as any data is available from deep wells, they are assumed to be representative for the deep conditions in the subsurface as well. The basal heat flux was set according to the thermal models proposed by Jaboyedoff & Pastorelli (1999). These authors pointed out that Alpine region showing an exhumation rate higher than 1mm/yr also might show a heat flow above 100 mW/m². A distinction between the two regions was chosen as the Valdieri area shows a higher exhumation rate (1.1-1.4 mm/y) than Vinadio (0.8-1 mm/y) (MUSUMECI et al., 2003; TRICART, 2004). Therefore the basal heat flux was set to be 80 mW/m² for the Vinadio area and 100 mW/m² at Valdieri.

Table 8-2 Surface thermal flux potential of the Vinadio and Valdieri area

| Site | Surface (m ²) | Basal Heat Flux (W/m ²) | Q (kg/s) | C _w (kJ/kg°C) | T _w (°C) | T ₀ (°C) | Heat in Place (kW _{TH}) | Heat in Place over 30 years (kW _{TH} ·10 ¹²) |
|----------|------------------------------|---|-------------|-----------------------------|------------------------|------------------------|--------------------------------------|---|
| Vinadio | 10 ⁴ | 0.08 | 20±5 | 4.1813 | 48.8 | 8 | 3420±853 | 3.2±0.9 |
| Valdieri | 10 ⁴ | 0.1 | 50±10 | 4.1813 | 49.1 | 7 | 8812±1760 | 8.3±1.8 |

8.3.2. Volume Method

The Volume method implies the estimation of the reservoir volume, which was inferred from the results of the integration between geochemical, geophysical investigations and 3D models. In both study areas several scenarios were considered to have a range of reservoir volumes to get the best, worst and average production scenarios. For Vinadio the reservoir volume according to the 3D model was interpreted to be the area between the Valletta and the Bersezio shear zone, while at Valdieri the area assumed to control the thermal water circulation was limited to the step-over between the Lorusa and S. Giovanni faults. These volumes estimations were considered as the best scenario configuration. The possibilities suggested by Williams (2008) were also considered to get a range of possible configuration and production estimations. The Bersezio Shear Zone and the Lorusa Fault Zone were considered as reservoirs for the Vinadio and Valdieri areas respectively. The Bersezio Zone is 500 m wide, while the Lorusa zone is 250 m thick. In both cases the maximal reservoir depth was estimated with respect to the average gradient of the area of 25°C/km (BAIETTO et al., 2008) and the reservoir temperature (130°C for Vinadio and 100°C for Valdieri) to be 5 km for Vinadio and 4 km for Valdieri. It is more likely that the local geothermal gradient is much higher due to the local convective heat transfer which can increase the gradient up to some hundreds of degree The horizontal extent of the reservoir was considered to be 0.1 (the area occupied by the thermal springs), 0.5, 1, 2.5 km² at Vinadio and 0.1, 0.25, 0.5, 1.25 km² at Valdieri assuming a horizontal extent of the fault zone involved in thermal water circulation to be 1, 2 and 5 km (WILLIAMS et al., 2008).

The fracture porosity of the reservoir was evaluated taking into account the density variation resulting from the integration of gravity, 3D model and estimate due to the Archie's law applied to the resistivity distribution resulting from MT surveys. Consequently, porosity at Vinadio was set to be 8% and 10% at Valdieri. The results are listed in Table 8-3:

Table 8-3 Heat potential q_R and recovery factor R_G over a time span of 30 years

| Site | Volumetric Heat Capacity (kJ/m ³ ·°K) | V _{RES} (m ³ ·10 ⁹) | Reservoir Temperature (°C) | Dead-state Temperature (°C) | q _R (kWth·10 ¹⁴) | Flow rate (kg/s) | T _{WH} (°C) | q _w 30 years (kWth·10 ¹²) | R _G 30 years |
|----------|--|--|----------------------------------|-----------------------------------|--|---------------------|-------------------------|---|----------------------------|
| Vinadio | 2253 | 41.5 | 130 | 8 | 114.1 | 20 | 48.1 | 3.17 | 0.0003 |
| | | 12.5 | | | 34.4 | | | | 0.0009 |
| | | 5 | | | 13.7 | | | | 0.002 |
| | | 2.5 | | | 6.9 | | | | 0.005 |
| Valdieri | 2234 | 24.8 | 100 | 7 | 68.2 | 50 | 49.1 | 8.32 | 0.0005 |
| | | 5 | | | 13.7 | | | | 0.002 |
| | | 2 | | | 5.5 | | | | 0.006 |
| | | 1 | | | 2.7 | | | | 0.01 |

8.3.3. Net Electric Power NEP method

The Net Electric Power (Table 8-4) was calculated taking the average fluid temperature calculated by geothermometers, saturation indexes and Giggenbach plots. Therefore for Vinadio it was set to be 130°C and 100°C for Valdieri. The Net Energy Conversion values estimates that only the 5% at Vinadio and the 3% at Valdieri of the heat power might be converted into electric power.

Table 8-4 Estimation of the electricity production by Net Electric Power NEP method

| Site | Q (kg/s) | C _w (kJ/kg°C) | T _R (°C) | T ₀ (°C) | q _R (kWth) | NEP kW _{EL} | Net Conversion Efficiency |
|----------|-------------|-----------------------------|------------------------|------------------------|-----------------------|-------------------------|------------------------------|
| Vinadio | 20±5 | 4.1813 | 130 | 50 | 6690±1673 | 322±81 | 0.05 |
| Valdieri | 50±10 | 4.1813 | 100 | 50 | 10453±2091 | 301±60 | 0.03 |

8.3.4. Exergy

Exergy was calculated (Table 8-5 and Table 8-6) setting the dead-state temperature at 8°C for Vinadio and at 7°C for Valdieri, according to the average air temperature observed by the ARPA observations. The efficiency of the ORC and Kalina cycle binary plants was taken into account according to the observations of Di Pippo* (2004; 2008).

Table 8-5 Exergy and electric power production estimates for ORC Cycle power plants

| Site | Flow rate (kg/s) | Reservoir T (°C) | Dead-state T (°C) | Exergy (kW) | η ORC Cycle* | Electric Power (kW _e) |
|----------|---------------------|---------------------|----------------------|----------------|-----------------|---|
| Vinadio | 20 | 130 | 20 | 1403 | 0.189 | 265 |
| Valdieri | 50 | 100 | 20 | 1947 | 0.189 | 368 |

Table 8-6 Exergy and electric power production estimates for Kalina Cycles power plants

| Site | Flow rate (kg/s) | Reservoir T(°C) | Dead-state T (°C) | Exergy (kW) | η Kalina Cycle* | Electric Power (kW _{EL}) |
|----------|---------------------|--------------------|----------------------|----------------|--------------------|---------------------------------------|
| Vinadio | 20 | 130 | 8 | 1746 | 0.231 | 403 |
| Valdieri | 50 | 100 | 7 | 2668 | 0.231 | 616 |

Moreover it is interesting to compare these results based on the second law of thermodynamics to the case of the First law of thermodynamics was applied (Table 8-7 and Table 8-8):

Table 8-7 1st Law application to power production estimation for ORC Cycle power plants

| Site | Flow rate (kg/s) | Reservoir T (°C) | T _{OUT} (°C) | Work (kW) | η ORC Cycle | Electric Power (kW _{EL}) |
|----------|---------------------|---------------------|--------------------------|--------------|----------------|---------------------------------------|
| Vinadio | 20 | 130 | 80 | 4028 | 0.099 | 399 |
| Valdieri | 50 | 100 | 80 | 3720 | 0.099 | 368 |

Table 8-8 1st Law application to power production estimation for Kalina Cycle power plants

| Site | Flow rate (kg/s) | Reservoir T (°C) | T _{OUT} (°C) | Work (kW) | η Kalina Cycle | Electric Power (kW _{EL}) |
|----------|---------------------|---------------------|--------------------------|--------------|-------------------|---------------------------------------|
| Vinadio | 20 | 130 | 80 | 4028 | 0.106 | 427 |
| Valdieri | 50 | 100 | 80 | 3720 | 0.106 | 394 |

8.4. Production Proposals

For the two thermal sites it was possible to estimate that, if the thermodynamic conditions of the geothermal fluid in the reservoir are confirmed, electric power production can be envisaged, in particular at Bagni di Vinadio, where the reservoir temperature might be more favourable. However, if a Kalina Cycle binary plant could be technically built at Valdieri, electricity might be produced as well without affecting the existing spa activities. In fact the fluid temperature in the subsurface of 100° is not favourable for a OCR binary plants, however if the amount of cooling fluid required for a Kalina cycle plant might be satisfied, this type of geothermal power plant can be ideal for the Valdieri case.

It is important to mention that any economical consideration has been taken into account.

On the basis of the results and keeping the usage of the fluids for thermal bath (temperature range 50-25°C) as a priority, it is possible to suggest two main scenarios for the exploitation of the resource.

1. the first scenario (Figure 8-2) involves the electricity production in the temperature range T_{RESERVOIR} - 50°C, then the returning fluid from the geothermal power plants can be used for thermal bathing (50-25°C) and finally the fluid can be used either for building heating and cooling by means of heat pumps all year round at the village of Bagni di Vinadio or for de-icing the roads during the winter season. Considering an average consumption of electricity per habitants of 4855 kW_h¹⁵, it could be possible to supply about 250 habitants at both sites with an average installed capacity of about 300 kW_{EL}. This estimation takes into account a total of 7800 hours, corresponding to the 90% of the hours in a year (DI PIPPO, 2008), of running activity for a binary geothermal plant.
2. the second (Figure 8-3) scenario doesn't involve power generation but is exclusively focused on heat production and direct uses. Therefore the fluid at temperature range T_{RESERVOIR} - 50°C can be exploited for district heating, to then be used at the thermal spa and finally for de-icing. The average energy consumption for heating and hot water for an apartment of 100 m² in Italy is about 50 kW_H¹⁶. Assuming that the heat production covers a time span of 6500 hours in an alpine region (October-June), it is possible to cover the need of about 150 apartments at Vinadio and 200 apartments at Valdieri.

¹⁵ Source Eurostat and IEA

¹⁶ Source ENEA

ENERGY PRODUCTION UTILIZATION POSSIBILITIES ELECTRIC POWER

| Vinadio | | Valdieri |
|---|------------------|---|
| <p>130-50°C (binary plant) ~ 300 kW_{EL}: Supply for ~ 250 habitants</p> | Power Generation | <p>100-50°C (binary plant) ~ 300 kW_{EL}: Supply for ~ 250 habitants</p> |
| <p>50-25°C Thermal baths with possible use of heat pumps</p> | Heat Production | <p>50-25°C Thermal baths with possible use of heat pumps</p> |
| <p>25-10°C Space heating and cooling or De-icing</p> | | <p>25-10°C De-icing</p> |

Figure 8-2 Cascade potential uses of geothermal fluids in case of power generation at Vinadio and Valdieri

ENERGY PRODUCTION UTILIZATION POSSIBILITIES HEAT

| Vinadio | | Valdieri |
|---|--|---|
| <p>130-50°C</p> <p>3.5 MW_{TH}: supply for about 300 habitants</p> | | <p>100-50°C</p> <p>9 MW_{TH}: supply for about 500 habitants</p> |
| <p>50-25°C Thermal baths with possible use of heat pumps</p> | | <p>50-25°C Thermal baths with possible use of heat pumps</p> |
| <p>25-10°C Space heating and cooling or De-icing</p> | | <p>25-10°C De-icing</p> |

Figure 8-3 Cascade potential uses of geothermal fluids in case of heat production at Vinadio and Valdieri

Table 8-9 Summary table of the geothermal potential at the study sites calculated by the methods proposed

| Site | Method | | | | | | | | | | | |
|----------|---------------------|--|------------------------------------|---------------------------|--|---|--|---|--|---|--|---|
| | Heat in Place | | NEP | | Volume Method | | | Exergy | | 1 st Law | | |
| | (MW _{th}) | | Electric Power (kW _{EL}) | Net Conversion Efficiency | Stored Heat q _R (MW _{TH}) | Recovery Factor R _G | Recovered Heat q _w (MW _{TH}) 30 years | Recovery Factor R _G 30 years | Electric Power ORC (kW _{EL}) | Electric Power Kalyna (kW _{EL}) | Electric Power ORC (kW _{EL}) | Electric Power Kalyna (kW _{EL}) |
| Vinadio | 3328 | | 322 | 0.05 | 1.38·10 ¹³ - 1.41·10 ¹⁶ | 3.3·10 ¹³ - 1.23·10 ¹⁰ | 3.17·10 ¹² | 3.1·10 ⁻⁴ - 0.23 | 265 | 403 | 399 | 427 |
| Valdieri | 8760 | | 301 | 0.03 | 1.04·10 ¹³ - 4.15·10 ¹⁵ | 1.7·10 ⁻¹² - 8.5·10 ⁻¹⁰ | 8.32·10 ¹² | 2·10 ⁻⁹ - 0.8 | 368 | 616 | 368 | 394 |

9

DISCUSSION AND FUTURE RESEARCH

9.1. Results

The presented work provided an example on how data from different sources can be integrated and jointly interpreted to come out with an overview of the general geological conditions controlling thermal water circulation in challenging areas such as the Alpine regions. Moreover it has been possible to gather the parameters in terms of flow rate, temperature at depth, reservoir volume, rock density and porosity, which have been used to calculate the geothermal potential.

Geological data can provide important information about the rock formations and the fracture conditions at the surface but the understanding of the thermal water flow paths coupled with the identification of the geothermal reservoir requires the comprehension of the geology and the physical conditions the subsurface. In fact structural and geomechanic conditions at the surface are usually different than those at the subsurface because of variations of the physical conditions in terms of temperature and lithostatic pressure.

Geochemical investigations allow understanding the water-rock interactions, to estimate the circulation path in terms of time, origin and depth of the flow path, the temperature of the reservoir and if phase changes occur at depth.

However the main sources of information to explore the subsurface are usually boreholes and seismic, which, however are not so often available, in particular in mountainous regions, because are cost effective and are technically complex. Therefore alternative methods have to be employed which are more handy in rough topography, which can investigate the subsurface at the required depth, which can interact between each other and which can count on the integration of the results. Hence starting from geological and geochemical data the next step has been to produce 3D geological models, which have been used as the crucial tool to the geophysical data deriving from gravity and MT surveys. In fact these two methods, broadly employed in geothermal exploration but never used for this task in the Alps before, allow improving geological models describing the underground distribution of density and electrical resistivity, which are very sensitive to fracture density variations and to the presence of circulating fluids. Carrying out such geophysical survey also highlighted the problems related to data collection in the study areas. In fact in mountainous regions collecting geological and geophysical data is often limited to some scattered observations, therefore integrating data from different sources become even more important to explore the subsurface.

The main results of the thesis can be resumed as follows:

The geological observations allowed understanding the complexity of the region in particular of the fault networks and their relations with the surrounding rock formations. Moreover detailed observations in the proximities of the springs showed that the final upflow of the thermal waters at both sites is strictly related to some sets of low angle minor fractures which are connected at depth to the major fault zones. Available geological data (field observations, geological maps and cross sections) were used as main data source for the starting geological model.

Geochemical data pointed out the differences in terms of chemical composition of the thermal waters discharging at Vinadio and Valdieri. These differences suggest that thermal

springs at two sites are recharged by two separate geothermal systems. At Vinadio the hot waters probably have a circulation path and residence time longer than those at Valdieri, as suggested by the increased salinity and the higher temperature of the reservoir. In particular the high salinity has been deepened as the concentration of Chloride in the waters of Vinadio is anomalous considering that they are supposed to entirely circulate within crystalline rocks. Therefore the Cl/Br molar ratio was applied and highlighted that the contribution of fluid inclusions which are rich in Chloride and that are a main feature of the rocks in the Vinadio area, can't be neglected but at the same time can't totally justify the high salinity. In fact the Cl/Br ratio values for Vinadio are characteristic of waters interacting with evaporite formations which, in the study area, entirely surround the Argentera Massif and are locally pinched in the thrust fault connected to the main shear zone which are located in the vicinities of the thermal springs. Moreover geochemical investigations provided the vertical extent of the model using the reservoir temperature coupled with the estimated geothermal gradient of the region.

The utilization of 3D models has been the core of the thesis. In fact 3D modelling allowed to group together all the scattered geological data coming from direct field observations and from maps and cross sections from previous studies. Even though creating 3D models implied some simplifications, the goal of the preliminary phase was to keep the geological complexity on the basis of strict interpretations but at the same time to produce models which can be used as the basic tool to integrate geology and geophysical data. The following phase has been to modify the geological model according to the results of the geophysical surveys. Both gravity and magnetotelluric provided important information about the physical properties at depth. In particular gravity enhanced the presence of low density areas in the proximities of both thermal sites. Thanks to the integration of forward modelling and inversion processing it has been possible to modify the geological models interpreting these anomalies as zones of increased porosity of the rock related to enhanced fracture density in the subsurface where the presence of deep fluid can be hypothesized. MT soundings were carried to find out if any relationship connected the density and the electrical resistivity anomalies. The comparison of the results of both methodologies on 2D cross sections suggested that the correlation between these two parameters and the modelled geology can be strong. However any MT observations were not carried out in the exact same areas of the density anomalies close to the thermal springs, hence it was not possible to compare the two methods on the most interesting zones.

Finally the integration of all these methodologies also allowed extracting the main parameters needed to estimate the geothermal potential of the study areas. In fact flow rate, temperature at the surface and at depth, rock density and porosity, reservoir volume were used to estimate the possible production of heat and electric power. The results showed that the geothermal resource is only partially exploited according to the present day usages of the thermal waters at both sites. In fact the discharging thermal fluids are in some measure used for thermal bathing and for heating the spa buildings during the winter. However the calculations carried out showed that, if the estimated thermal conditions in the subsurface can be confirmed by more detailed studies, the geothermal potential is much higher and can provide a wide spectrum of usages to optimize the management of the geothermal resource. In fact, keeping the thermal baths activity as a priority, the deep fluid at high temperature can be used for power generation, providing electricity to the surrounding buildings or for heat production, e.g. for the entire village of Bagni di Vinadio (composed by about 100

buildings). Then the fluids can be directly exploited for the spas and then they can be further exploited for heating building using heat pumps or de-icing the roads during the winter season, instead of being discharged in the rivers. In particular the site of Valdieri could benefit of this kind of approach as the thermal spa is open only during the summer season. In fact during the winter the road heading to the thermal bath is closed because of the snow covering the road, hence an accurate de-icing use might extend the opening period. A flexible scenario can be also predicted. In fact, for the higher temperature range, it could be possible to focus the exploitation of the resource for power generation during summer season and switch to heat production during the winter period when the need of heat is predominant.

9.2. Future Research

The present thesis provided an example of how some of the methodologies applied in geothermal exploration can be used in mountainous region to investigate the subsurface in crystalline geological conditions. However the complexity of the thermal fluid circulation was not totally explained and constrained during this work.

Therefore more data which can provide very useful results that can be integrated to those of this thesis might be:

- temperature measurements in the wells to obtain some temperature logs even in those wells which were not previously sampled
- accurate flow rate observations at both springs and wells
- residence time of the thermal fluids can be constrained with more accuracy by methods such as ^{14}C dating
- improve the characterization of fracture conditions, in particular of those formations supposed to control the thermal water circulation. Therefore it would be useful to carry out detailed geomechanic and geotechnic observations (e.g. scan lines) to picture the state of fracture at the surface
- photogrammetric observations could also provide a good source of information about the fracture conditions, in particular for those outcrops which are not accessible for direct observations
- geomechanic and photogrammetric surveys can be correlated to some geophysical methods such as seismic or Very Low Frequency VLF soundings which can sometimes reach a depth of few hundreds of meters. The investigation at this depth can be very useful to constrain the fracture condition controlling the final upflow the deep thermal waters
- interferometry could be a useful tool to monitor the movement at the surface not related to superficial geomorphologic processes. This method might highlight which tectonic structures are the most active in the Argentera Massif. In particular in the two thermal sites this technique might help to better constrain those structural features related to the thermal fluids circulation
- a correlation between interferometry and the study of the focal mechanisms of the earthquakes of the region can also allow understanding the stress conditions of the regions; hence the most active faults where hot waters might be located
- all these data can provide crucial results integrate the already available 3D geological models to carry out coupled thermal and chemical simulations and

reservoir modelling taking into account the complexity of the geological and structural conditions of the subsurface

- drilling deeper wells (up to 1-1.5 km in depth) at the thermal sites would be the most important source of information about the thermal and chemical processes occurring at depth and about the geological conditions in the subsurface. Planning a drilling campaign will enormously benefit from all the data resulting from the application of the methods mentioned above.

Geothermal exploration is multidisciplinary and needs to integrate data from a lot of sources. Hence geological field observations are crucial to understand the conditions at the surface but, to understand the circulation paths, geochemistry, geophysical methods and numerical modelling are the tools that need to be employed and jointly interpreted before drilling deep wells. Deep boreholes can be used as exploration wells during the exploratory phase and can be adapted into production wells whether the observed geothermal conditions are favourable for heat or power generation.

REFERENCES

- Alcala, F. and Custodio, E., 2008. Using the Cl/Br ratio as a tracer to identify the origin of salinity in aquifers in Spain and Portugal. *Journal of Hydrology* **359**, 189-207.
- Aneke, M., Agnew, B., and Underwood, C., 2011. Performance analysis of the Chena binary geothermal power plant. *Applied Thermal Engineering* **31**, 1825-1832.
- Archie, G. E., 1942. The electrical resistivity log as an aid in determining some reservoir characteristics. *T. Am. I. Min. Met. Eng.* **146**, 54-62.
- Árnason, K. and Eysteinnsson, H., 2010. Joint 1D inversion of TEM and MT data and 3D inversion of MT data in the Hengill area, SW Iceland. *Geothermics* **39**, 13-34.
- Arnorsson, S., Gunnlaugsson, and Svavarsson, 1983. The chemistry of geothermal waters in Iceland. III. Chemical geothermometry in geothermal investigations. *Geochimica et Cosmochimica Acta* **47**, 567-577.
- Arthaud, F. and Dazy, J., 1989. *Migration des saumures au front des chevauchements de l'arc alpin occidental*. CR Acad. Sci. Paris.
- Aug, C., 2004. Modelisation geologique 3D et caracterisation des incertitudes par la methode du champ de potentiel, Ecole des mines de Paris
- Axelsson, G. and Gunnlaugsson, E., 2000. Background: Geothermal utilization, management and monitoring. In: *Long-term monitoring of high- and low enthalpy fields under exploitation*, WGC 2000 Short Courses, Japan, 3-10
- Baietto, A., 2006a. Fault-related thermal water circulation in the Argentera Massif (South-Western Alps), University of Turin.
- Baietto, A., Cadoppi, P., and Martinotti, G., 2008. Assessment of thermal circulations in strike-slip fault systems: the Terme di Valdieri case (Italian western Alps). *Geological Society*.
- Baietto, A., Perello, P., Cadoppi, P., and Martinotti, G., 2009. Alpine tectonic evolution and thermal water circulations of the Argentera Massif (South-Western Alps). *Swiss Journal of Geosciences* **102**, 223-245.
- Baubron J.C., 1987. Compte rendu détaillé, Argentera (Alpes Italiennes) *Diffusion délégation Risques Majeurs*. BRGM.
- Bertani, R., 2010. Geothermal Power Generation in the World 2005–2010 Update Report *World Geothermal Congress*, Bali, Indonesia.
- Bhattacharyya, B. K., 1964. Magnetic anomalies due to prism-shaped bodies with arbitrary polarization. *Geophysics* **29**, 517-531.
- Bianchetti, G., 1993. Hydrogeologie et geothermie dans le tunnel du Rawyl. *Bull. CHYN Neuchatel* **12**, 87-109.
- Bianchetti, G. (1994). Hydrogéologie et géothermie de la région de Lavey-les-Bains (Vallée du Rhône, Suisse) [Hydrogeology and geothermal properties of the Lavey-les-Bains area (Rhône Valley, Switzerland)]. *Bull Centre d'Hydrogeol Neuchâtel*, **13** 3-32.
- Bianchi, A., Bovini, L., Botti, F., Doveri, M., Lelli, M., Manzella, A., Molli, G., Montanari, D., Pierotti, L., and Ungarelli, C., 2010. Multidisciplinary Approach to the Study of the Relationships Between Shallow and Deep Circulation of Geofluids. *World geothermal congress*, Bali, Indonesia.
- Bigot-Cormier, F., Braucher, R., Bourles, D., Guglielmi, Y., Dubar, M., and Stéphan, J., 2005. Chronological constraints on processes leading to large active landslides. *Earth and Planetary Science Letters* **235**, 141-150.
- Bigot-Cormier, F., Poupeau, G., and Sosson, M., 2000. Dénudations différentielles du massif cristallin externe alpin de l'Argentera (Sud-Est de la France) révélées par thermochronologie

- traces de fission (apatites, zircons). *Comptes Rendus de l'Académie des Sciences-Series IIA-Earth and Planetary Science* **330**, 363-370.
- Blakely, R., 1996. *Potential theory in gravity and magnetic applications*. Cambridge University Press.
- Blundell, D., 1993. *A continent revealed. The european geotraverse*. Cambridge University Press.
- Bogdanoff, S., 1986. Evolution de la partie occidentale du Massif cristallin externe de l'Argentera. Place dans l'arc Alpin. *Géologie de France* **4**, 433-453.
- Bogdanoff, S., Menot, R., and Vivier, G., 1991. Les Massifs Cristallins Externes des Alpes Occidentales françaises, un fragment de la zone interne varisque. *Science Géologique Bulletin* **44**, 237-285.
- Bogdanoff, S., Michard, A., Mansour, M., and Poupeau, G., 2000. Apatite fission track analysis in the Argentera massif: evidence of contrasting denudation rates in the External Crystalline Massifs of the Western Alps. *Terra Nova* **12**, 117-125.
- Bortolami, G. and Grasso, F., 1969. Osservazioni geologico-applicative sul cunicolo d'assaggio del traforo del Ciriegia e considerazioni sull'intero tracciato *Problemi tecnici nella costruzione di gallerie*, Turin.
- Bortolami, G. and Olivero, G., 1984. *Sistemi idrici profondi, geotermali e freddi, in Piemonte e Valle d'Aosta*. Mem. Soc. Geol. It.
- Bortolami, G., Ricci, B., and Susella, G., 1979. Isotope hydrology of the Val Corsaglia, Maritime Alps, Piedmont, Italy *International Symposium on Isotope Hydrology*. IAEA, Vienna (Austria), Neuherberg (Germany).
- Benderitter, Y. and Cormy, G., 1990. Possible approach to geothermal research and relative costs. In: Dickson, M.H. and Fanelli, M., eds., *Small Geothermal Resources: A Guide to Development and Utilization*, UNITAR, New York, pp. 59-69.
- Cagniard, L., 1953. Basic theory of the magnetotelluric method of geophysical prospecting. *Geophysics* **18**, 605-645.
- Calais, E., Galisson, L., Stéphan, J., Delteil, J., Deverchère, J., Larroque, C., Mercier de Lepinay, B., Popoff, M., and Sosson, M., 2000. Crustal strain in the southern Alps, France, 1948-1998. *Tectonophysics* **319**, 1-17.
- Calcagno, P., Chilès, J. P., Courrioux, G., and Guillen, A., 2008. Geological modelling from field data and geological knowledge Part I. Modelling method coupling 3D potential-field interpolation and geological rules. *Physics of the Earth and Planetary Interiors* **171**, 147-157.
- Campredon, R. and Giannerini, G., 1982. Le synclinal de Saint Antonin (arc de Castellane, chaînes subalpines méridionales). Un exemple de bassin soumis à une déformation compressive permanente depuis l'Eocène supérieur. *Géologie Alpine* **58**, 15-20.
- Chilès, J. P., Aug, C., Guillen, A., and Lees, T., 2005. Modelling the geometry of geological units and its uncertainty in 3D from structural data: the potential-field method. *Orebody Modelling and Strategic Mine Planning*
- Corsini, M. and Rolland, Y., 2009. Late evolution of the southern European Variscan belt: Exhumation of the lower crust in a context of oblique convergence. *Comptes Rendus Geosciences* **341**, 214-223.
- Corsini, M., Ruffet, G., and Caby, R., 2004. Alpine and late-hercynian geochronological constraints in the Argentera Massif (Western Alps). *Eclogae Geologicae Helveticae* **97**, 3-15.
- Darcy, J., 1997. La nouvelle liaison routiere Nice-Cuneo et le Tunnel du Mercantour. *Tunnels et ouvrages souterrains* **139**, 46-50.
- Debelmas, J., 1986. Intracontinental subduction and mountain upflow: the example of Western Alp. *Geologie Alpine* **62**, 1-10.
- Debelmas, J. and Kerckhove, C., 1980a. Le Alpes franco-italiennes, *Geologie Alpine*, Grenoble.

- Debon, F. and Lemmet, M., 1999. Evolution of Mg/Fe Ratios in Late Variscan Plutonic Rocks from the External Crystalline Massifs of the Alps (France, Italy, Switzerland). *Journal of Petrology* **40**, 1151–1185.
- Di Pippo, R., 2004. Second law assessment of binary plants generating power from low-temperature geothermal fluids. *Geothermics* **33**, 565-586.
- Di Pippo, R., 2008. *Geothermal power plants: principles, applications, case studies and environmental impact*. Butterworth-Heinemann, Elsevier, Oxford.
- Dickson, M. and Fanelli, M., 2005. *Geothermal energy: utilization and technology* 36-38. Earthscan, London.
- Epstein, S., 1953. Variation of O18 content of waters from natural sources. *Geochimica et Cosmochimica Acta*.
- Erkan, K., Holdmann, G., Benoit, W., and Blackwell, D., 2008. Understanding the Chena Hot Springs, Alaska, geothermal system using temperature and pressure data from exploration boreholes. *Geothermics* **37**, 565-585.
- Evans, J. P., Forster, C. B., and J.V., G., 1997. Permeability of fault-related rocks, and implications for hydraulic structure of fault zones. *Journal of Structural Geology* **19**, 1393-1404.
- Facello, A., 2011. Studio petrografico e micrometamorfico delle inclusioni fluide nel giacimento idrotermale a Pb-Zn_Florite di Rua (Vallone di Bagni di Vinadio, Massiccio dell'Argentera).
- Fancelli, R., 1978. *Studio geochimico delle sorgenti termali del Massiccio Cristallino dell'Argentera (Alpi Marittime)*. Boll. Soc. Geol. It. **97**, 115-130
- Faure-Muret, A., 1955. Etudes géologiques sur le massif de l'Argentera. In: BOILLOT, G. (Ed.), *Les Marges continentales actuelles et fossiles autour de la Mercantour et ses enveloppes sédimentaires. Mémoires pour servir à l'explication de la carte géologique détaillée de la France*. Imprimerie Nationale, Paris.
- Federici, P. R. and Pappalardo, M., 1991. Nota introduttiva alla morfologia glaciale della Valle del Gesso di Entracque (Gruppo dell'Argentera, Alpi Marittime). In: Geomorfologia, G. N. G. F. e. (Ed.), *Guida all'escursione primaverile 28–31 Maggio 1991*, Cuneo.
- Ferretti, A., Prati, C., and Rocca, F., 2001. Permanent scatterers in SAR interferometry. *IEEE Transactions on Geoscience and Remote Sensing* **1**, 8-20.
- FitzGerald, D. M., Reid, A. , 2003. Integrating Euler solutions into 3D geological models - automated mapping of depth to magnetic basement. *Geophysics* **23**, 3-6.
- Florinsky, I. V., 2000. Relationships between topographically expressed zones of flow accumulation and sites of fault intersection. *Environmental Modelling & Software* **15**, 87-100.
- Ford, M., 1996. Kinematics and geometry of early Alpine, basement-involved folds, SW Pelvoux Massif, SE France. *Eclogae Geol. Helv.* **89**, 269–295.
- Ford, M., Lickorish, W. H., and Kusznir, 1999. Tertiary foreland sedimentation in the Southern Subalpine Chains, SE France: a geodynamic appraisal. *Basin research* **11**.
- Fouillac, C., 1979. Un géothermomètre empirique: le rapport Na/Li des eaux. CR. Acad. Sci. Paris.
- Fouillac, C., G. Michard, 1981. Sodium/lithium ratio in water applied to geothermometry of geothermal reservoirs. *Geothermics* **10**, 55 – 70.
- Fournier, R., 1979. A revised equation for the Na-K geothermometer. *Geothermal Res. Council Trans.* **3**, 221-224
- Fournier, R., 1991. Water geothermometers applied to geothermal energy. *Application of Geochemistry in Geothermal Reservoir Development* (D'Amore F., Ed.), UNITAR/UNDP Center on Small Energy Resources, Rome, 37-69
- Fournier, R., Rybach, L., and Muffler, L., 1981. Application of water geochemistry to geothermal exploration and reservoir engineering. *Geothermal systems: principles and case histories*.

- Fréchet, J. and Pavoni, N., 1979. Etude de la sismicité de la zone briançonnaise entre Pelvoux et argentera (Alpes occidentales) à l'aide d'un réseau de stations portables. *Eclogae Geologicae Helvetiae* **72**, 763-779.
- Friedman, I., 1953. Deuterium content of natural waters and other substances. *Geochimica et Cosmochimica Acta* **4**, 89-103.
- Fry, N., 1989. Southwestward thrusting and tectonic so fthe western Alps. In: Coward, M. P., Dietrich, D., and Park, R. G. Eds.), *Alpine Tectonics*. Geological Society of London.
- Garg, S. and Combs, J., 2011. A reexamination of USGS volumetric "heat in place" method. *36th Workshop on geothermal reservoir engineering*, Stanford.
- Gat, J., 1981 Stable isotope hydrology. Deuterium and oxygen-18 in the water cycle. *Atomic Energy Agency, Vienna*.
- Giggenbach, W., 1988. Geothermal solute equilibria. Derivation of Na-K-Mg-Ca geoindicators. *Geochimica et Cosmochimica Acta* **52**, 2794-2765.
- Giggenbach, W., 1991. Chemical techniques in geothermal exploration. *Application of Geochemistry in Geothermal Reservoir Development* (D'Amore F., Ed.), UNITAR/UNDP Center on Small Energy Resources, Rome, 119-144
- Giggenbach, W., Gonfiantini, R., and Jangi, B., 1983. Isotopic and chemical composition of Parbati Valley geothermal discharges, north-west Himalaya, India. *Geothermics* **12**, 199-222.
- Giggenbach, W., Sheppard, D., and Robinson, B., 1994. Geochemical structure and position of the Waiotapu geothermal field, New Zealand. *Geothermics* **23**, 599-644.
- Glotzbach, C., Spiegel, C., Reinecker, J., Rahn, M., and Frisch, W. I. L. e.-., 111-124., 2009. What perturbs isotherms? An assessment using fission track thermochronology and thermal modelling along the Gotthard transect, Central Alps. In: Lisker, F., Ventura, B., and Glasmacher, U. Eds.), *Thermochronological methods: from paleotemperature constraints to landscape evolution models*. Geological Society of London, Special Publication.
- Gourlay, P., 1986. La déformation du socle et des couvertures delphinohelvétiques dans la région du Mont-Blanc (Alpes occidentales). *Bull. Soc. Géol. France* **8**, 159-169.
- Goy, L., Fabre, D., and Menard, G., 1996. Modelling of rock temperatures for deep alpine tunnel projects. *Rock mechanics and rock engineering* **29**, 1-18.
- Gringarten, A. C., 1978. Reservoir Lifetime and Heat Recovery Factor in Geotherma Aquifers used for Urban Heating. *Pure and Applied Geophysics* **117**, 297-308.
- Guillen A., C. G., Calcagno P., Lane R., Lees T., McInerney P., 2004. Constrained gravity 3D litho-inversion applied to Broken Hill ASEG, Sidney, Australia.
- Hammer, S., 1936. Terrain correction for gravity stations. *Geophysics* **4**, 184-194.
- Hochstein, M.P., 1990. Classification and assessment of geothermal resources. In: Dickson, M.H. and Fanelli, M., eds., *Small Geothermal Resources: A Guide to Development and Utilization*, UNITAR, New York, pp. 31—57.
- Horrenberger, J. C., Michard, A., and Werner, P., 1978. Le couloir de décrochement de Bersezio en Haute- Stura, Alpes externes, (Italie), structure de compression sub-méridienne. *Sci. Géol. Bull* **31**, 15-20.
- Hurter, S. and Schellschmidt, R., 2003. Atlas of geothermal resources in Europe. *Geothermics* **32**, 779-787.
- IAEA, 2007. GC(51)/5 - IAEA Annual Report 2006. 1-103.
- Jaboyedoff, M. and Pastorelli, S., 1999. The present therrnal state of the Alpine region: Influence of fluid circulation. *European Geothermal Conference* **2**, Basel
- Jamier, A. and Olive, P., 1977. Isotopic anche chemical data about deep waters in the crystalline massif of Mont Blanc. Proc. 2nd Intern. Symp. Water-Rock interaction.

- Kalina, A. I. and Liebowitz, H. M., 1989. Application of the Kalina cycle technology to geothermal power generation. *Geothermal Res. Council Trans.* **13**, 605-611
- Kalina, A. I. and Liebowitz, H. M., 1994. Applying Kalina cycle technology to high enthalpy geothermal resources. *Geothermal Res. Council Trans* **18**, 531-536.
- Kalina, A. I., Liebowitz, H. M., Lazzeri, L., and Diotti, F., 1995. Recent development in the application of Kalina cycle for geothermal plants *World Geothermal Congress*, Florence **3**, 2093-2096.
- Kearey, P., Brooks, M., and Hill, I., 2009. *An Introduction to Geophysical Exploration*. Blackwell Science.
- Kerckhove, C., 1969. La zone du Flysch dans les nappes d'Embrunais- Ubaye. *Géol. Alpine* **45**, 5-204.
- Kharaka, Y., 1989. Chemical geothermometers and their application to formation waters from sedimentary basins. *Thermal history of sedimentary basins*. Edited by: Naeser, N.D. and McCulloh, T.H. 99-117. New York, USA: Springer-Verlag.
- Kohl, T., Andenmatten, N., and Rybach, L., 2003. Geothermal resource mapping--example from northern Switzerland. *Geothermics* **32**, 721-732.
- Kohl, T., Signorelli, S., and Rybach, L., 2001. Three-dimensional (3-D) thermal investigation below high Alpine topography. *Physics of the Earth and Planetary Interiors* **126**, 195-210.
- Kohl, T., 1999. Transient thermal effect at complex topographies. *Tectonophysics* **306**, 311-324
- L L Thatcher, V. J. J. K. W. E., 1977. Techniques of Water-Resources Investigations of the United States Geological Survey. 1-94.
- Labaume, P., Ritz, J.-F., and Philip, H., 1989. Failles normales récentes dans les Alpes sud-occidentales: leurs relations avec la tectonique compressive. *C.R. Acad. Sciences Paris Sér II* **308**, 1553-1560.
- Lajaunie, C., Courrioux, G., and L, M., 1997. Foliation fields and 3D cartography in geology: principles of a method based on potential interpolation. *Mathematical Geology* **29**.
- Lane, R., 2007. GeoModeller information model: a description from a geoscience perspective.
- Lane, R., Fitzgerald, D., Guillen, A., Seikel, R., and McInerney, P., 2007. Lithologically constrained inversion of magnetic and gravity data sets *Australian Society of Exploration Geophysicists*.
- Larroque, C., Béthoux, N., Calais, E., Courboux, F., Deschamps, A., Déverchère, J., Stéphan, J. F., Ritz, J. F., and Gilli, E., 2001. Active deformation at the junction between southern French Alps and Ligurian basin. *Netherlands Journal of Geosciences/Geologie en Mijnbouw* **80**, 255-272.
- Larroque, C., Delouis, B., Godel, B., and Nocquet, J.-M., 2009. Active deformation at the southwestern Alps-Ligurian basin junction (France-Italy boundary): Evidence for recent change from compression to extension in the Argentera massif. *Tectonophysics* **467**, 22-34.
- Last, B. J. and Kubik, K., 1983. Compact gravity inversion. *Geophysics* **48**, 713-721.
- Le Bel, L. and Chery, C., (2012). Low-Bin: de l'électricité avec une ressource à 76°C. *La géothermie en France* **7**.
- Legmann, H. and Legmann (2003). The Bad Blumau geothermal project: a low temperature, sustainable and environmentally benign power plant. *Geothermics* **32**(4-6): 497-503.
- Li, Y., 2006. Calculation of sulfur isotope fractionation in sulfides. *Geochimica et Cosmochimica Acta* **70**, 1789-1795
- Lund, J. W. and Boyd, T., 1999. Small geothermal power projects examples. *Geo-Heat Center Quarterly Bulletin* **20**, 9-26.
- Madeddu, B., Bertoux, N., and Stephan, J. F., 1996. Champ de contrainte post-plioce et deformation récentes dans les Alpes sud-occidentales *Bulletin Societe Geologique de France* **8**, 797-810.

- Malaroda, 1970. Carta geologica del Massiccio dell'Argentera alla scala 1:50.000 *Memorie Società Geologica Italiana*.
- Malaroda, R., 1999. L'Argentera meridionale - Memoria Illustrativa della «Geological Map of the southern Argentera Massif (Maritime Alps) 1: 25.000
- Maréchal, J. and Perrochet, P., 1999. Long-term simulations of thermal and hydraulic characteristics in a mountain massif: The Mont Blanc case study, French and Italian Alps. *Hydrogeology Journal* **7**, 341-354
- Maréchal, J. C., 1998a. Les circulation d'eau dans les massif cristallins alpins et leurs relations avec les ouvrages souterrains, EPFL.
- Maréchal, J. C., 1998b. Observations des massifs cristallins alpins au travers des ouvrages souterrains. Caracterisation de la conductivité hydraulique a l'echelle du massif. *Hydrogeologie* **1**, 21-32
- Maréchal, J. C. and Etcheverry, D., 2003. The use of 3H and 18O tracers to characterize water inflows in Alpine tunnels. *Applied Geochemistry* **18**, 339-351.
- Marquer, D., 1990. Structures et déformation alpine dans les granites hercyniens du massif du Gothard (Alpes centrales suisses). *Eclog. Geol. Helv* **83**, 77-97.
- Martelet, G., 2004. Integrated 3D geophysical and geological modelling of the Hercynian Suture Zone in the Champtoceaux area (south Brittany, France). *Tectonophysics* **382**, 117-128.
- Masson, F., Gal, F., and Leloup, P., 2002. Une carte gravimétrique haute résolution du massif du Mont-Blanc: implications structurale. *C.R. Geosciences* **334**, 1011-1019.
- Masson, F., Verdun, J., Bayer, R., and Debeglia, N., 1999. Une nouvelle carte gravimétrique des Alpes occidentales et ses conséquences structurales et tectoniques. *Comptes Rendus de l'Académie des Sciences Series IIA Earth and Planetary Science*, **329**, 865-871.
- Maxelon, M. and Mancktelow, N. S., 2005. Three-dimensional geometry and tectonostratigraphy of the Pennine zone, Central Alps, Switzerland and Northern Italy. *Earth-Science Reviews* **71**, 171-227.
- McInerney, G., Courioux, Calcagno, Lees, 2005. Building 3D geological Models directly from the data? A new approach applied to Broken Hill, Australia.
- McInerney, L., Seikel, Guillen, Gibson, FitzGerald, 2007. 3D GeoModeller Forward modelling and inversion.
- Michard, G., 1990a. Behaviour of major elements and some trace elements (Li, Rb, Cs, Sr, Fe, Mn, W, F) in deep hot waters from granitic areas. *Chemical geology* **89**, 117-134.
- Michard, G., Grimaud, D., D'Amore, F., and Fancelli, R., 1989b. Influence of mobile ion concentrations on the chemical composition of geothermal waters in granitic areas. Example of hot springs from piemonte (italy). *Geothermics* **18**, 729-741.
- Mlcak, H. A., 2002. Kalina cycle[®] concepts for low temperature geothermal. *Geothermal Resource Concl* **26**, 707-712
- Morelli, M., Mallen, L., G, N., Piana, F., and Fioraso, G., 2008. Il contributo dell'interferometria PS-InSARTM satellitare nella valutazione della mobilità tettonica in Piemonte. *Memorie descrittive della Carta Geologica d'Italia* **XC**, 1-4.
- Muffler, P. and Cataldi, R., 1978. Methods for regional assessment of geothermal resources. *Geothermics* **7**, 53-89.
- Muñoz, G., Bauer, K., Moeck, I., and Schulze, A., 2010. Exploring the Groß Schönebeck (Germany) geothermal site using a statistical joint interpretation of magnetotelluric and seismic tomography models. *Geothermics* **39**, 35-45
- Musumeci, G. and Colombo, F., 2002. Late Visean mylonitic granitoids in the Argentera Massif (western Alps, Italy): age and kinematic constraints on the Ferrière-Mollières shear zone. *Comptes Rendus Geosciences* **334**, 213-220.

- Musumeci, G., Ribolini, A., and Spagnolo, M., 2003. The effects of late Alpine tectonics in the morphology of the Argentera Massif (Western Alps, Italy-France). *Quaternary International* **101**, 191-201.
- Newman, G., Gasperikova, E., Hoversten, G., and Wannamaker, P., 2008. Three-dimensional magnetotelluric characterization of the Coso geothermal field. *Geothermics* **37**, 369-399.
- Nicholson, K., 1993. *Geothermal fluids Chemistry and exploration techniques*. Springer-Verlag, Berlin, Germany.
- Ohmoto, H., 1997. *Sulfur and carbon isotopes*. Geochemistry of hydrothermal ore deposits. 517-542
- Paces, T., 1975. A systematic deviation from Na-K-Ca geothermometer below 75 °C and above 10⁻⁴ atm PCO₂. *Geochimica et Cosmochimica Acta* **39**, 541-544.
- Parasnis, D., 1999. Principles of applied geophysics. Chapman & Hall.
- Parkhurst, D., 1999. User's guide to PHREEQC (Version 2) - a computer program for speciation, batch-reaction, one-dimensional transport, and inverse geochemical calculations.
- Pastorelli, S. and Marini, L., 2001. Chemistry, isotope values (δD , $\delta^{18}O$, δS_{SO_4}) and temperatures of the water inflows in two Gotthard tunnels, Swiss Alps. *Applied Geochemistry* **16**, 633-649
- Paventa, F., 1873. Le sorgenti termiche minerali di Vinadio in Val di Stura presso Cuneo, 56-58. Cuneo.
- Pearson, F. J., Jr., and Truesdell, A.H., 1978. Tritium in the waters of the Yellowstone National Park. 4th International Conference, Geochronology, Cosmology, Isotope Geology 327-329. U.S. Geological Survey Open-File Report 78-701, Washington DC
- Perello, P., Marini, L., Martinotti, G., and Hunziker, J., 2001. The thermal circuits of the Argentera Massif (western Alps, Italy): an example of low-enthalpy geothermal resources controlled by Neogene alpine tectonics. *Eclogae Geologicae Helvetiae* **94**, 75-94.
- Pernecker, G. and S. Uhlig (2003). Low enthalpy power generation with ORCTurbogenerator The Altheim Project, Upper Austria. *International Summer School*. 1-7
- Pfeifer, H. and Sanchez, A., 1992. Thermal springs in granitic rocks from the Grimsel Pass (Swiss Alps): The late stage of a hydrothermal system related to Alpine Orogeny. 7th international Symposium on Water-Rock interactions, Park City, Balkema, Rotterdam, 1327-1331
- Reynolds, J., 1997. An introduction to applied and environmental geophysics. 785-796.
- Ribolini, A. and Spagnolo, M., 2008. Drainage network geometry versus tectonics in the Argentera Massif (French-Italian Alps). *Geomorphology* **93**, 253-266.
- Ritz, J. F., 1992. Tectonique récente et sismotectonique des Alpes du sud: Analyses en termes de contraintes. *Quaternaire* **3**, 111-124.
- Rosselli, A., 2001. Modélisation gravimétrique bi et tridimensionnelle du substratum rocheux des vallées alpines, Lausanne.
- Sauret, B. and Terrier, M., 1987. Compte rendu de mission Argentera. BRGM note BS/GR 87, 175.
- Schill, E., Geiermann, J., and Kummritz, J., 2010. 2-D Magnetotellurics and Gravity at the Geothermal Site at Soultz-sous-Forêts *World Geothermal Congress*, Bali, Indonesia.
- Schmid, S., Fugenschuh, B., Kissling, E., and Schuster, R., 2004. Tectonic map and overall architecture of the Alpine orogen. *Eclog. Geol. Helv* **97**, 93-117.
- Schreiber, D., Lardeaux, J., Martelet, G., Courrioux, G., and Guillen, A., 2010. 3-D modelling of Alpine Mohos in Southwestern Alps. *Geophysical Journal International* **180**, 961-975.
- Simpson, F. and Bahr, K., 2005. Practical magnetotellurics. Cambridge University press. 24-35
- Sonney, R., 2010a. Remobilisation of deep Na-Cl waters by a regional flow system in the Alps: Case study of Saint-Gervais-les-Bains (France). *Comptes Rendus Geosciences* **341**, 151-161

- Sonney, R., 2010b. Use of Cl/Br Ratio to Decipher the Origin of Dissolved Mineral Components in Deep Fluids from the Alps Range and Neighbouring Areas *World Geothermal Congress 2010*, Bali, Indonesia.
- Sonney, R., 2011. Groundwater flow, heat and mass transport in geothermal systems of a Central Alpine Massif, Univeristy of Neuchatel, Switzerland.
- Sonney, R. and Vuataz, F., 2008. Properties of geothermal fluids in Switzerland: a new interactive database. *Geothermics* **37**, 496-509.
- Sonney, R. and Vuataz, F., 2010. Validation of Chemical and Isotopic Geothermometers from Low Temperature Deep Fluids of Northern Switzerland. *Proceedings World Geothermal Congress*.
- Spichak, V., Zakharova, O., and Rybin, A., 2007. Estimation of the sub-surface temperature by means of magnetotelluric sounding. *32nd Workshop on Geothermal Reservoir Engineering*, Stanford University, Stanford, California.
- Steinhauser, P., Meurers, B., and Ruess, D., 1990. Gravity investigations in mountainous areas. *Exploration Geophysics* **21**, 161-168
- Stober, I. and Bucher, K., 2007. Hydraulic properties of the crystalline basement. *Hydrology Journal* **15**, 213-224.
- Stocco, S., Godio, A., and Sambuelli, L., 2009. Modelling and compact inversion of magnetic data: A Matlab code. *Comput. Geosci.* **35**, 2111-2118.
- Strzeczynski, P., Guillot, S., Courrioux, G., and Ledru, P., 2005. Modélisation géométrique 3D des granites stéphaniens du massif du Pelvoux (Alpes, France). *Comptes Rendus Geosciences* **337**, 1284-1292.
- Sturani, C., 1962. Il complesso sedimentario autoctono all' estremo nord-occidentale des Massicio dell' Argentera (Alpi Marittime), Padova.
- Telford, W., Geldart, L., and Sheriff, R., 1990. Applied geophysics. Cambridge University Press. 6-62
- Teufel, U., 1986. Die Verteilung der elektrischen Leitfähigkeit in der Erdkruste unter dem Schwarzwald, ein Beispiel für Möglichkeiten und Grenzen der Interpretation von AudioMagnetotellurik, Magnetotellurik, Erdmagnetischer Tiefensondierung Ludwig-Maximilian-Universität.
- Thomas, R. P., Chapman, R. H., and Dykstra, H., 1981. A reservoir assessment of The Geysers Geothermal field. *Journal of Petroleum Technology* **36**, 2137-2159
- Thouvenot, F., Paul, A., Fréchet, J., Béthoux, N., Jenatton, L., and Guiguet, R., 2007. Are there really superposed Mohos in the south-western Alps? New seismic data from fan- profiling reflections. *Geophysical Journal International* **170**, 1180-1194.
- Tikhonov, A. N., 1950. The determination of the electrical properties of deep layers of the Earth's crust. *Dokl. Acad. Nauk* **73**, 295-297
- Tikhonov, A. N., 1986. On determining electrical characteristics of the deep layers of the Earth's crust. In: Vozoff, K. (Ed.), *In Magnetotelluric Methods*. Society of Exploration Geophysicists, Tulsa.
- Tricart, P., 2004. From extension to transpression during the final exhumation of the Pelvoux and Argentera massifs, Western Alps. *Eclogae Geologicae Helvetiae* **97**, 429-439.
- Truesdell, A., 1976. Geochemical techniques in exploration. *Proceedings of the Second United Nations Symposium on the Development and Use of Geothermal Resources*, San Francisco, California, United States, 20-29 May.
- Vernon, A., Van Der Beek, P., Sinclair, H., and Rahn, M., 2008. Increase in late Neogene denudation of the European Alps confirmed by analysis of a fission-track thermochronology database. *Earth and Planetary Science Letters* **270**, 316-329.
- Volpi, G., Manzella, A., and Fiordelisi, A., 2003. Investigation of geothermal structures by Magnetotellurics (MT): an example from the Mt. Amiata area, Italy. *Geothermics* **32**, 131-145.

- Vuataz, F.-D., 1982. Hydrogeologie, geochemie et geothermie des eaux thermales de Suisse et des regions alpines limitrophes. [Hydrogeological, geochemical and geothermal properties of thermal waters from Switzerland and neighbouring regions]. *Matér. Géol. Suisse, sér. Hydrol.*, 29, 174 p
- Williams, C., Reed, M., and Mariner, R., 2008. A review of methods applied by the US Geological Survey in the assessment of identified geothermal resources. *Open-File Report* 1296.
- Zanchi, A., Francesca, S., Stefano, Z., Simone, S., and Graziano, G., 2009. 3D reconstruction of complex geological bodies: Examples from the Alps. *Computers & Geosciences* **35**, 49-69.
- Zanolla, C., Braitenberg, C., Ebbing, J., Bernabini, M., Bram, K., Gabriel, G., Gotze, H.-J., Giammetti, S., Maurers, B., Nicolich, R., and Palmieri, F., 2006. New gravity maps of the Eastern Alps and significance for the crustal structures. *Tectonophysics* **414**, 127-143.
- Zuppi, G., Novel, J., Dray, M., Darmendrail, X., Fudral, S., Jusserand, C., and Nicoud, G., 2004. Eaux fortement minéralisées et circulations profondes dans le socle. Exemple des Alpes franco-italiennes. *Comptes Rendus Geosciences* **336**, 1371-1378.